NORTHWESTERN UNIVERSITY

Atomic-Scale Studies of the Self-Assembly of Pi-Conjugated Molecules on Silicon Surfaces

A DISSERTATION

SUBMITTED TO THE GRADUATE SCHOOL
IN PARTIAL FULLFILLMENT OF THE REQUIREMENTS

for the degree

DOCTOR OF PHILOSOPHY

Field of Materials Science and Engineering

By

Jui-Ching (Phillip) Lin

EVANSTON, ILLINOIS

December 2009

ABSTRACT

Atomic-Scale Studies of the Self-Assembly of Pi-Conjugated Molecules on Silicon Surfaces

Jui-Ching (Phillip) Lin

A variety of surface-sensitive characterization tools together with density functional theory (DFT) modeling have been applied to study the atomic-scale structures of the self-assembly of pi-conjugated molecules on silicon surfaces. Through the studies of covalently bound *p*-bromostyrene (BrSty)-, *p*-(4-bromophenyl)styrene (BPS)-, *p*-(4-bromophenylethynyl)styrene (BPES)-, (4-bromophenyl)acetylene (BPA)-, (*p*-(4-bromophenyl)phenyl)acetylene (BPPA)-, and (*p*-(4-bromophenylethynyl)phenyl)acetylene (BPEPA)- based self-assembled monolayers (SAMs) on H-Si(111), and BrSty- and BPA- based SAMs on H-Si(001), a structure characterization strategy for SAMs/Si was developed. In each case DFT calculations predicted several possible atomic-scale models from which the most correct structure was experimentally determined by the characterization package using atomic force microscopy (AFM), X-ray photoelectron spectroscopy (XPS), X-ray reflectivity (XRR), X-ray fluorescence (XRF), and X-ray standing wave (XSW). The XSW determined atomic density maps, in conjunction with the coarser-length-scale XRR analysis and DFT modeling, provided the atomic-scale structure of a SAM on Si.

The comparisons of the three alkyl SAMs/Si(111) with the three alkenyl SAMs/Si(111) show a higher degree of order for the alkenyl SAMs relative to the alkyl SAMs in the AFM and 111 XSW analyses. In addition, DFT shows that a sp^2 alkenyl C=C bond at the surface will azimuthally align over the sp^3 Si-Si bond from the substrate, whereas the sp^3 alkyl C-C bond at the surface will azimuthally bisect two sp^3 Si-Si bonds. With this hypothesis, the (2 x 1) periodic DFT, where the linear packing of molecules on Si(111) is approximated by a periodic attachment to every other surface silicon, was found to best simulate the structures of the SAMs on Si(111).

In addition to the studies of SAMs on Si, the characterization package was successfully applied in the development of the microwave-assisted Sonogashira coupling chemistry. The microwave-assisted Sonogashira coupling reaction provides a strategy to extend the conjugated organic structures on Si surfaces and tailor the electronic property of the hybrid materials.

Approved:

Professor Michael J. Bedzyk

Department of Materials Science and Engineering

Northwestern University

Evanston, Illinois

ACKNOWLEDGEMENTS

First, I would like to give huge thanks to my advisor, Prof. Michael Bedzyk, for guiding and supporting me throughout my graduate studies. I am also grateful to the members of my qualifier and thesis committees: Prof. Mark Hersam, Prof. SonBinh Nguyen, Prof. Kenneth Shull, and Prof. Jiaxing Huang. I especially like to show my appreciation to Prof. Hersam and Nguyen for guiding me in my research.

I am very grateful to my collaborators Rajiv Basu, Mathew Schmitz, Josh Keller, and Michael Walsh for the sample preparations. I am also thankful to Dr. Jun-Hyun Kim for the syntheses of the novel molecules and the guidance in organic chemistry. I also want to show my great appreciation to Kirk Bevan and Nathan Yoder for doing a great amount of DFT calculations for me. My research is a closely collaborative project and I enjoyed working with my collaborators and solving the puzzles together.

I would also like to acknowledge the funding support from the National Science Foundation (through the Northwestern University Nanoscale Science and Engineering Center). Use of the Advanced Photon Source was supported by the U. S. Department of Energy. I also thank the DND-CAT and XOR/UNI staff and Jerry Carsello of the NU X-ray Diffraction Facility for technical assistance. I especially appreciate Dr. Denis Keane at the DND-CAT for helping me developing new techniques, including EPICS and 2D detector systems, for my research.

I am grateful to many past and present members of the Bedzyk research group. I thank Joseph Libera and Zhan Zhang for showing me the path to doing computer programming. I especially like to thank Zhan Zhang for also assisting me setting up the experiments at APS. I would also like to acknowledge Dr. Chang-Yong Kim for his guidance of X-rays techniques. I

am grateful to Steve Christensen, Jeff Klug, Yuan-Chieh Tseng, Vaibhav Kohli, Brent Fiedler, Zhenxing Feng, and Jon Emery for providing various forms of help along the way.

I am grateful to my friends Wei-Wen Tsai and Chun-Yi Sung respectively for sharing the research experience in organic chemistry and DFT calculation. I also like to thank the many friends I met at NU who have enriched my life in US in so many ways.

Last, but not least, I want to give an enormous thanks to my parents. Their love and support throughout my graduate studies are invaluable.

TABLE OF CONTENTS

LIST OF FIGURES

LIST OF TABLES

Chaper 1 : Introduction

Functionalization of inorganic surfaces with organic molecules has been widely studied for tailoring the electrical properties of hybrid materials.[1-4] Aromatic molecules, in contrast with aliphatic, have delocalized electrons contributing to a π-conjugated structure and gain special interests for the development of molecular electronics.[2,5,6] With different choices for the terminal end groups, aromatic molecules can be attached to metal,[7,8] oxide[6], or semiconductor[9] surfaces. Hydrosilylation of unsaturated alkenes or alkynes have been widely explored and high-quality self-assembled monolayers (SAMs) of aromatic molecules have been successfully used.[10-12] Since the properties of a organic/inorganic material are greatly affected by the configurations of the molecules,[6] resolving the details of the bonding configuration, molecular orientation, and molecular packing within the film are critical to the utilization of SAMs in real devices.

In contrast with the more weakly bonded monolayers grown with van der Walls force (spin-coating) or thiol-Au chemistry,[13] covalently bonded alkenyl or alkyl SAMs on Si single crystal surfaces suffer from lower coverage (typically < 0.6-monolayers) and lack lateral long-range-order. Because of the low coverage and lack of long-range-order, structural analyses employing in-plane diffraction (LEED, SXRD, etc) are ineffective. This thesis focuses on the exploration of Si surfaces functionalized with aromatic molecules. The employed strategy is to use X-ray standing wave (XSW), X-ray reflectivity (XRR), and X-ray photoelectron spectroscopy (XPS) measurements together with density functional theory (DFT) to provide atomic-scale structural analysis of SAMs on Si. The direct growth of the monolayer and the

secondary modification of the organic structure, using hydrosilylation and Sonogashira coupling chemistries, respectively, are studied step-by-step in this thesis work.

Chaper 2 : Background

2.1 Self-assembled monolayers on Si(111)

Since Linford and Chidsey presented covalently bound, densely packed alkyl monolayers on Si(111) and Si(001) surfaces by the pyrolysis of diacyl peroxides in the presence of hydrogen-terminated silicon,[14] covalent linkage of organic molecules with Si surfaces has become a subject of great interest and an incredible diversity of approaches have been developed. The reaction mechanisms can be categorized as: (A) Hydrosilylation involving radical initiator, (B) Thermally induced hydrosilylation, (C) Photochemical hydrosilylation, (D) Hydrosilylation mediated by metal complexes, (E) Reaction of alkyl/aryl carbanions with hydride- and halide-terminated surfaces, (F) Electrochemical grafting, and (G) Mechano-chemical functionalization.[15]Among all, the photochemical hydrosilylation method has gained a special interest because the process can take place in an ambient environment and at room temperature without thermal input. A range of alkenes and alkynes monolayers on Si(111) is succeeded by UV-induced hydrosilylation process[15-17] and a saturated coverage of about one-half monolayer (ML) was reported (Fig 2.1). The authors proposed a radical chain reaction mechanism, shown in Fig 2.2, and the reaction scheme is experimentally confirmed by their ATR-FTIR and XPS measurements.[16] The self-avoiding, random walk chain reaction results to the growth of the molecular islands on Si(111)–1x1 surfaces (Fig 2.3). [18,19]

2.2 Self-assembled monolayers on Si(001)

In contrast to the molecular islands on Si(111), it has been shown that alkenes can be grown one dimensionally along the dimer rows on Si(001)-2x1 surfaces (Fig 2.4).[20] The dimer rows are orientated along either [110] or [$\bar{1}$10] directions and the two types of domains are separated by atomic step-edges. The growth of molecules on the dimer rows are initiated by Si dangling bonds, where the creation of the dangling bonds can be precisely controlled on the surfaces using STM tips, and the reaction stops at a defect site. By using feedback-controlled lithography (FCL), the growth of the molecular rows can be further manipulated (Fig 2.5).[21]

The proposed chain reaction chemistry for unsaturated molecules on mono-hydride Si(111) surfaces illustrated in Fig 2.2 has also been shown to be valid for growing alkenes molecules, e.g. styrene, on a mono-hydride Si(001)–2x1 surface. The growth of alkynes molecules on monohydride Si(001)–2x1 surfaces, compared to that on monohydride Si(111)–1x1 surface, is expected to follow the identical chain reaction mechanism. However, a first-principle DFT study of the surface reaction of acetylene with di-hydride Si(001)–1x1 also shows that after the acetylene molecules reacting to the surface Si and forming the alkenyl structure, it is possible that the C=C double bond at the root may be broken and may in addition react with a neighboring unoccupied Si site.[22] If this reaction happens, the linkage between acetylene molecules and the Si substrate will no longer be fully conjugated.

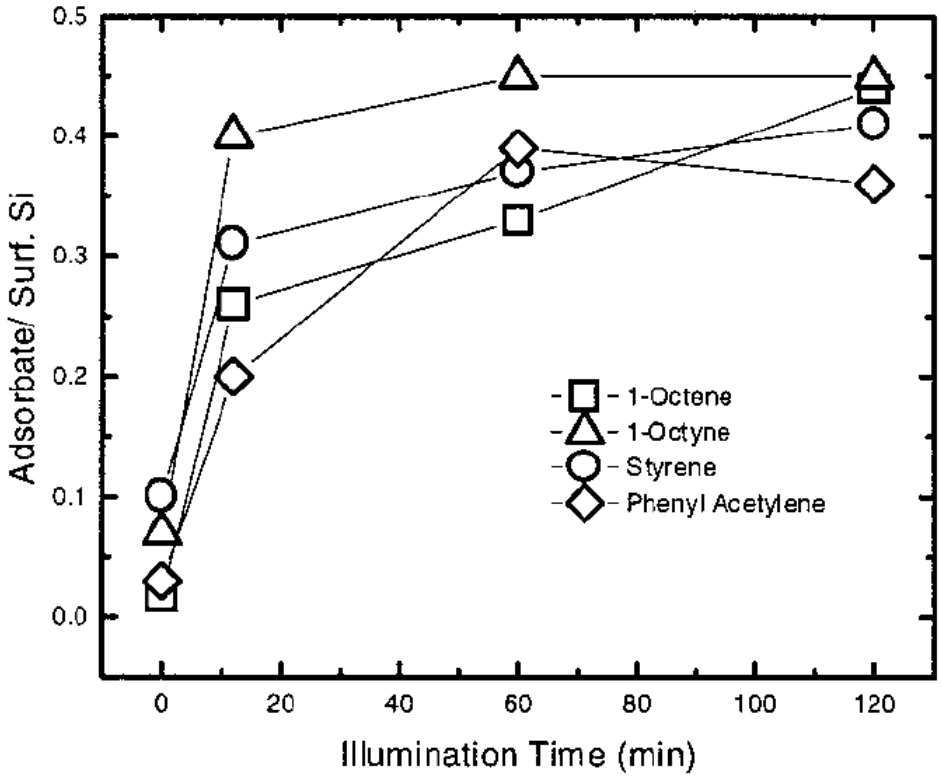

Figure 2.1 The growth of 1-octene, 1-octyne, styrene, and phenyl acetylene molecules on H-Si(111) versus UV illumination time. All four molecules approach a 1/2 ML saturated coverage after 2 h of illumination. The figure is reproduced from Ref. [16].

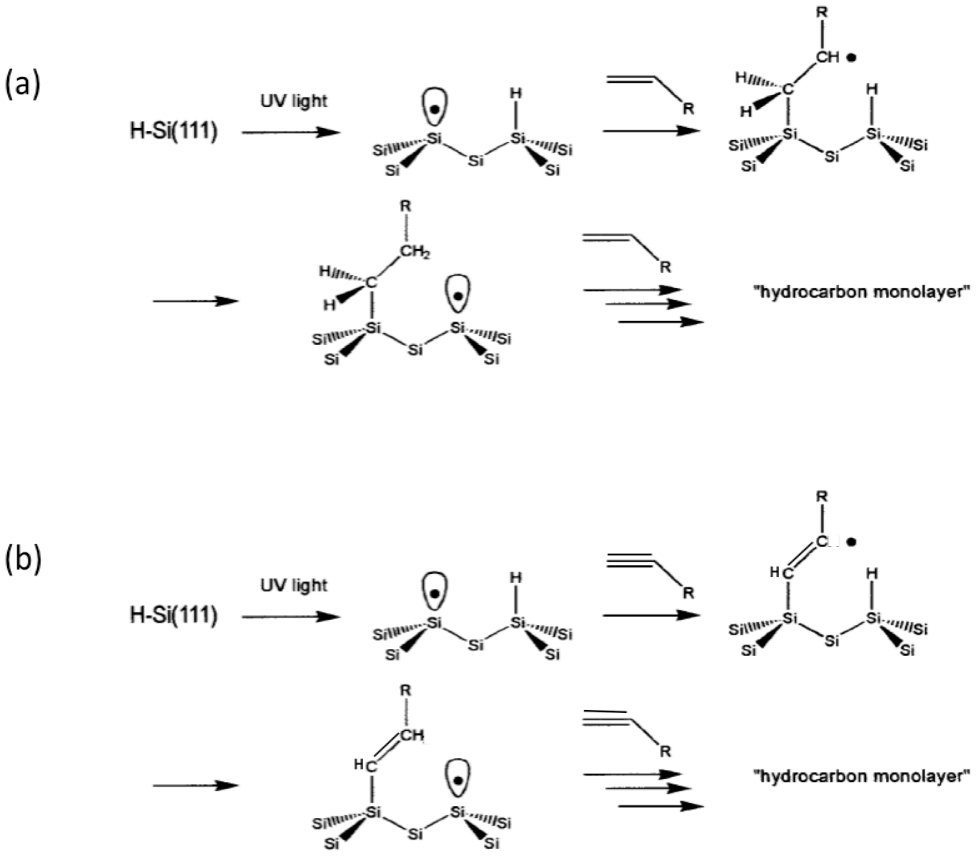

Figure 2.2 Mechanism for UV induced hydrosilylation growth of (a) alkenes and (b) alkynes on H-Si(111). (a) is reproduced from Ref. [19]. (b) is a modified reaction from (a).

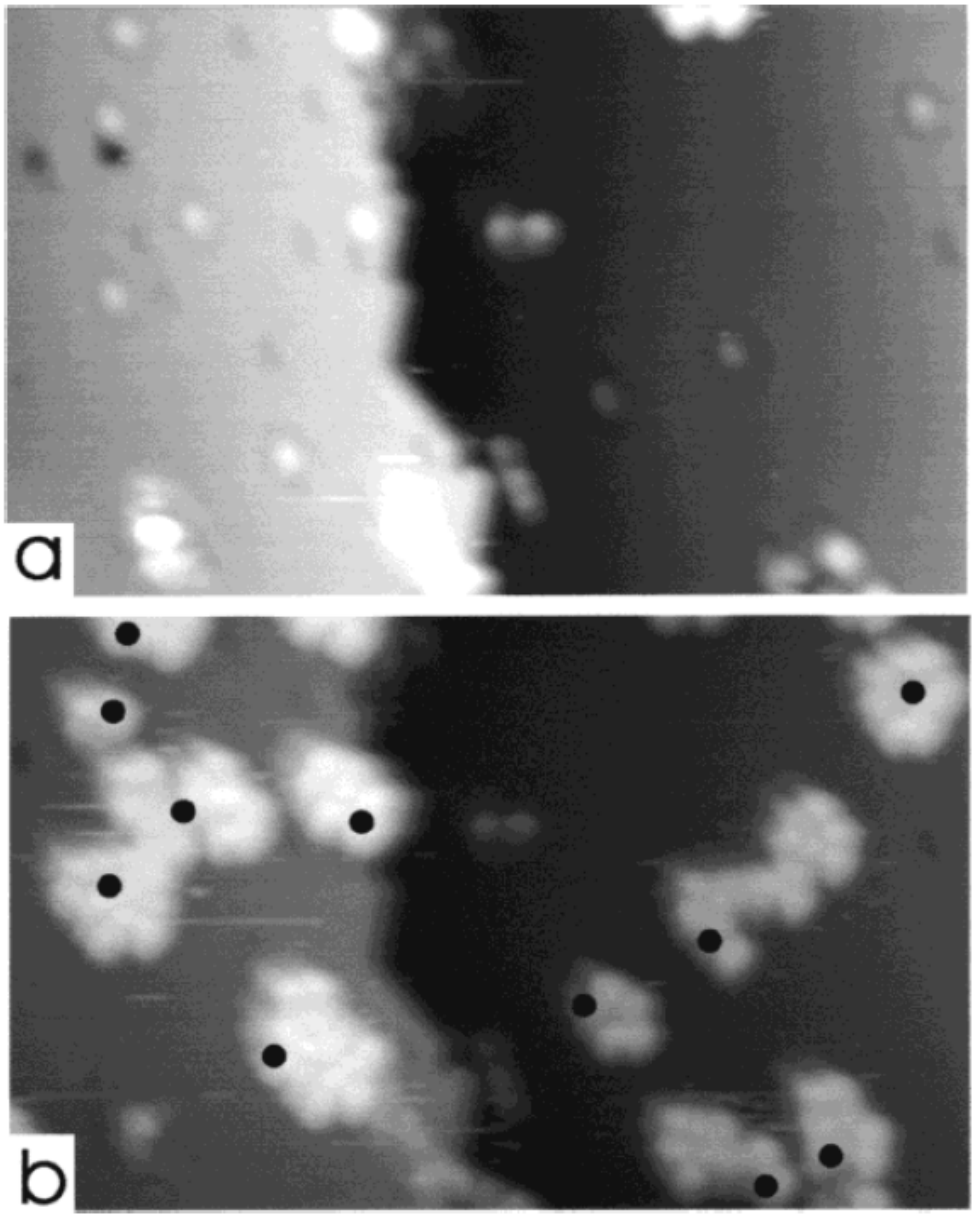

Figure 2.3 STM images (a) before and (b) after the hydrosilylation growth of styrene on a H-terminated Si(111). The black dots in (b) mark the positions of the initial dangling bonds, showing that these sites serve to nucleate the growth of styrene islands. The figure is reproduced from Ref. [19].

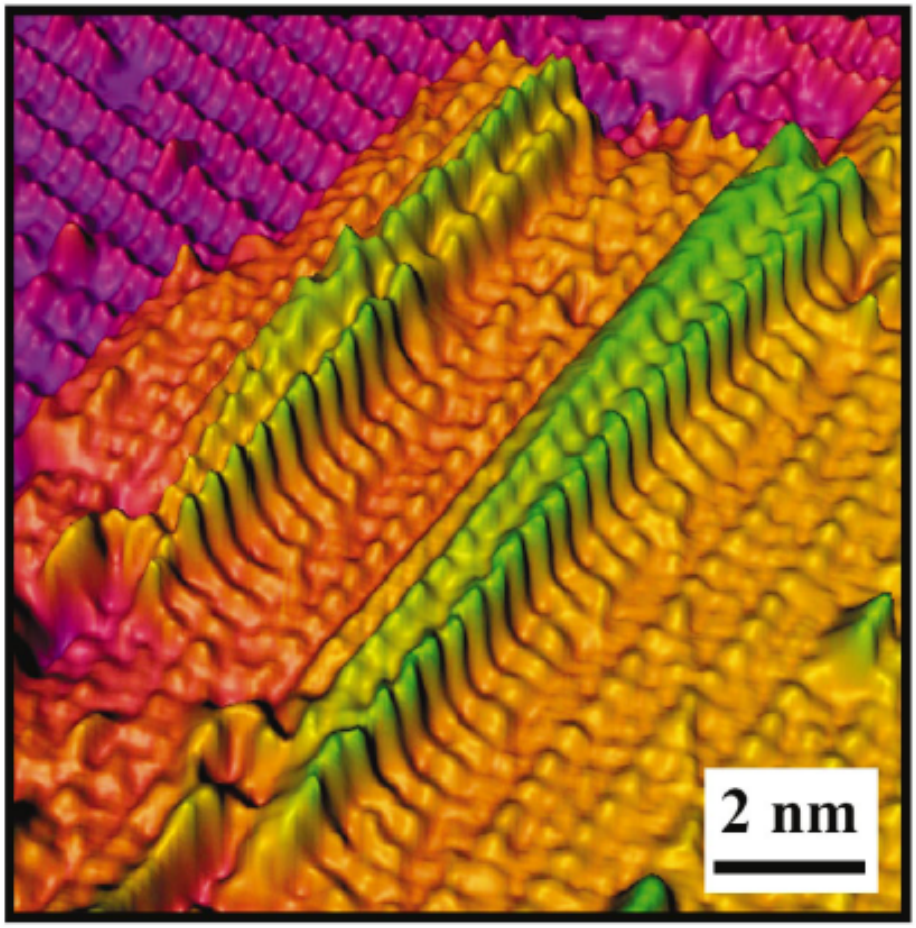

Figure 2.4 An unoccupied states UHV STM image of styrene chains on a H-Si(001)–2x1 surface. The figure is reproduced from Ref. [21].

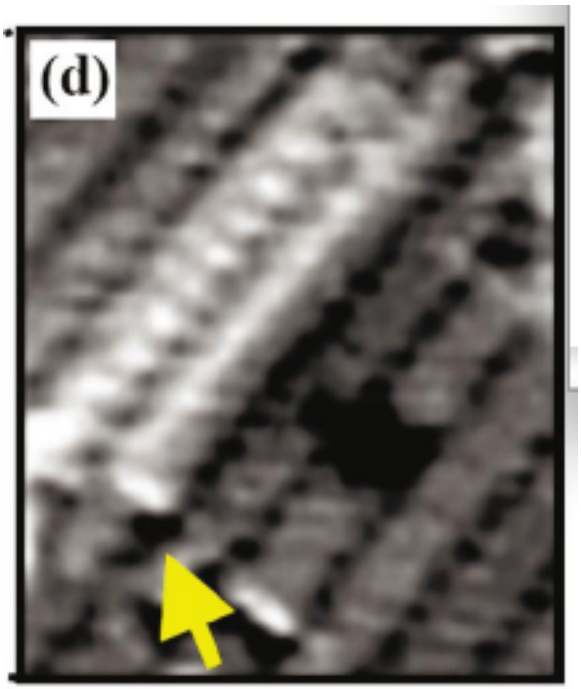

Figure 2.5 Unoccupied states UHV STM image of the resulting heteromolecular nanostructure following styrene chain growth. The resulting styrene chain is bounded by the originally patterned TEMPO (2,2,6,6-tetramethyl-1-piperidinyloxy) molecule that is indicated with a yellow arrow. The figure is reproduced from Ref. [21].

Chaper 3 : Sample Preparation

3.1 The vinyl- and acetylene- terminated aromatic molecules

Six brominated aromatic molecules were studied in this thesis: (a) *p*-bromostyrene (BrSty), (b) *p*-(4-bromophenyl)styrene (BPS), (c) *p*-(4-bromophenylethynyl)styrene (BPES), (d) (4-bromophenyl)acetylene (BPA), (e) (*p*-(4-bromophenyl)phenyl)acetylene (BPPA), and (f) (*p*-(4-bromophenylethynyl)phenyl)acetylene (BPEPA). The six molecules are shown in Fig 3.1. The first three molecules, with "=CH2" vinyl terminal end groups, are aromatic alkenes; where the last three molecules, with the "≡CH" acetylene terminal end groups, are aromatic alkynes. The syntheses of the vinyl- and acetylene- terminated aromatic molecules are detailed in appendix A.

3.2 Preparation of SAMs on H-Si(111)

The procedure for preparing a monohydride terminated Si(111) surface is detailed in appendix B. A 254 nm UV pen lamp (Spectroline 11SC-1Short Wave UV Lamp) was used to photochemically grow self-assembled monolayers (SAMs) on the hydrogen terminated Si(111) surface inside the inert atmosphere (N_2) glove box. H-Si(111) wafers were immersed in a petri dish containing 0.2 M benzene solutions of the styrene/acetylene derivatives (except for the case of BrSty-based SAMs, where a neat BrSty liquid (Sigma-Aldrich, 98%) was used) and the monolayer growths were achieved by irradiating this reagent-covered surfaces with the UV pen lamp from a distance of 1 cm for a measured amount of time, which varied with the choice of solution. The typical thickness of the reagent layer covering the surface during the

photochemical process was 2 mm. The samples were then brought out of the glove box, sonicated in chloroform for ~5 min. Sample surfaces were then examined with AFM to make sure that no significant physisorption or polymerization occurred on the surfaces (Fig 3.2). More sonication would be applied if surfaces were not clean. As shown in Fig 3.2, even extensive sonication cannot recover the atomic steps of Si for the alkyl SAMs (after the attachment of the molecules) except BrSty/Si(111). This is due to the non-rigid C-C single bond at the root, as compared to the more rigid C=C double bond at the roots for the alkenyl SAMs, and the greater molecular structure. This issue will be discussed in detail later. Because of the non-uniformity of BPS- and BPES- based SAMs on Si(111), no periodic DFT calculations and XRR measurements were performed on these samples. The samples were stored in the glove box when not being used in any experiment.

In-house X-ray photoelectron spectroscopy (XPS) measurements were performed on the SAM/Si samples before further X-ray reflectivity and X-ray standing wave experiments to verify the Br bonding state. XPS was also used to confirm that no oxidation of the silicon substrate had occurred. XPS analysis was performed at the Keck Interdisciplinary Surface Science Center of Northwestern University using an Omicron ESCA Probe. A monochromated 1486.6 eV Al $K\alpha$ beam was made incident on the sample surface that was oriented such that the emitted photoelectrons had a take-off angle of 45º from the sample surface to the hemispherical analyzer. The energy calibration of the spectra was referenced with respect to that of the adventitious C_{1s} peak fixed at 284.8 eV. All the brominated SAMs in the study have clear XP spectra with a single Br 3d spin doublet at 70.5 and 71.5 eV, which is the expectation for carbon-bound

bromine (Fig 3.3a) as opposed to Si bound Br. The results legitimated the use of Br as the marker for structural characterization.

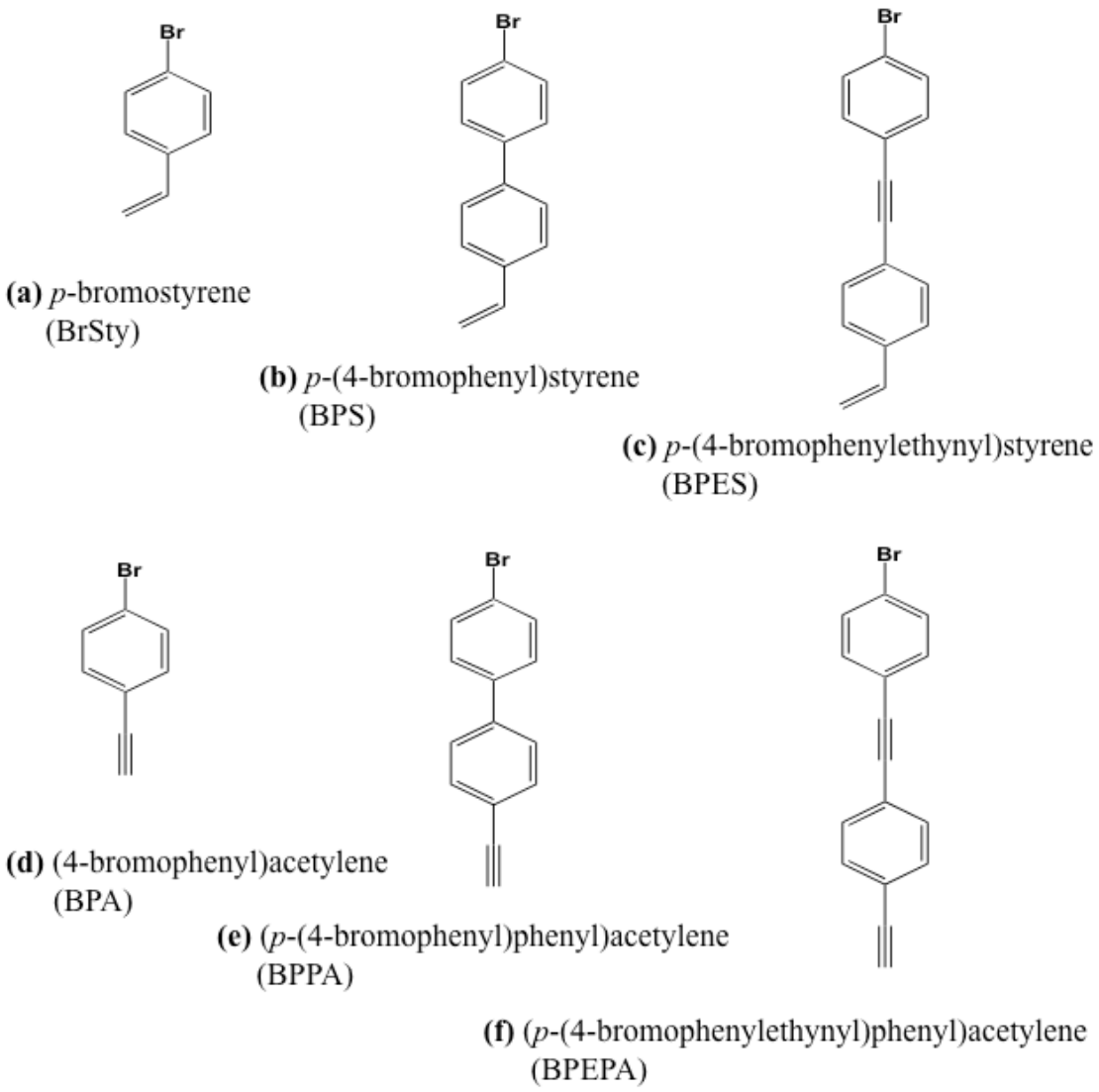

Figure 3.1 Chemical schematics for the three aromatic alkenes (a to c) and three aromatic alkynes (d to f) used in this study.

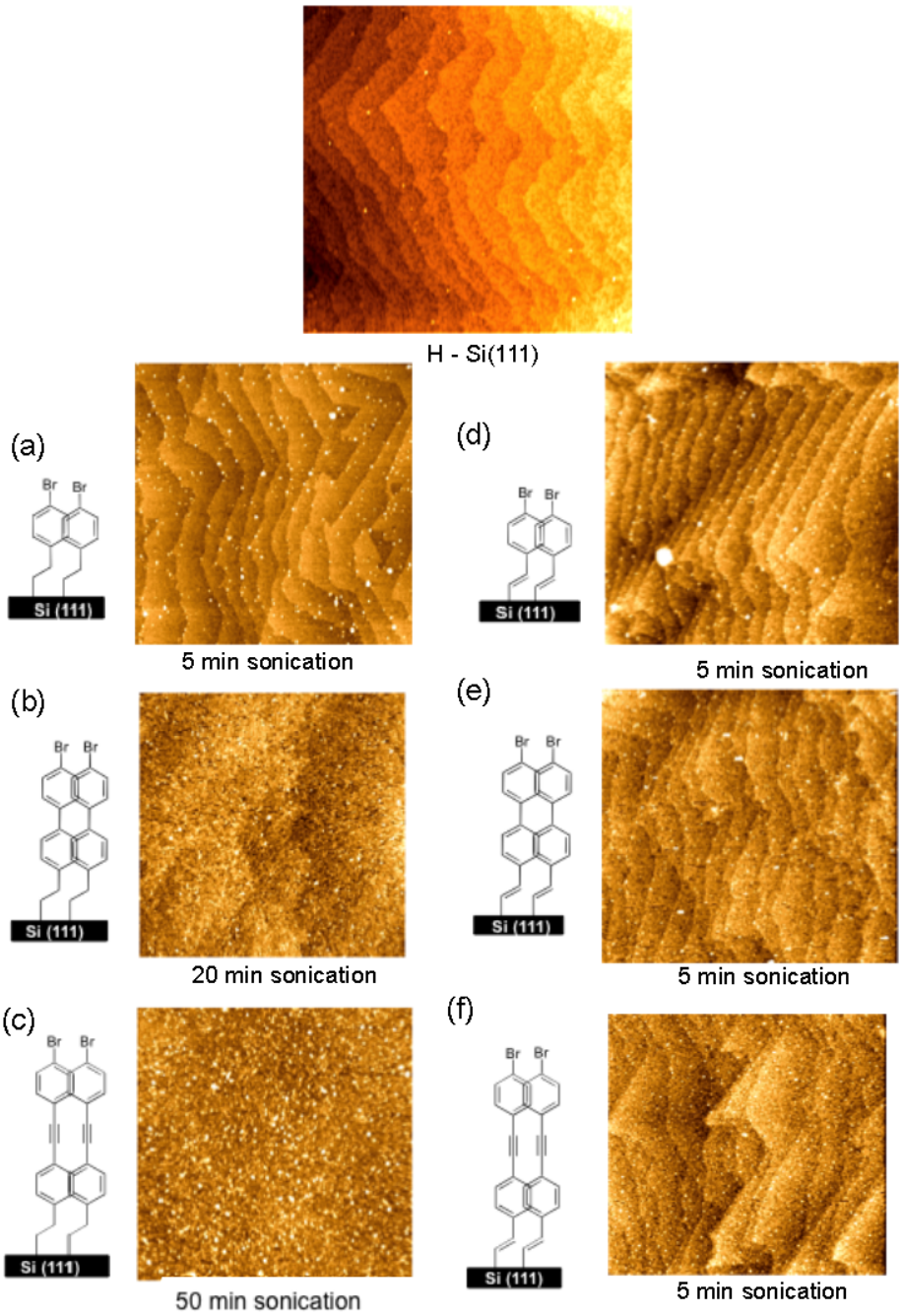

Figure 3.2 AFM intermittent contact mode images of a H-Si(111) surface and surfaces of (a) BrSty/Si(111), (b) BPS/Si(111), (c) BPES/Si(111), (d) BPA/Si(111), (e) BPPA/Si(111), and (f) BPEPA/Si(111). The AFM images are from J. Kellar in the Hersam group.

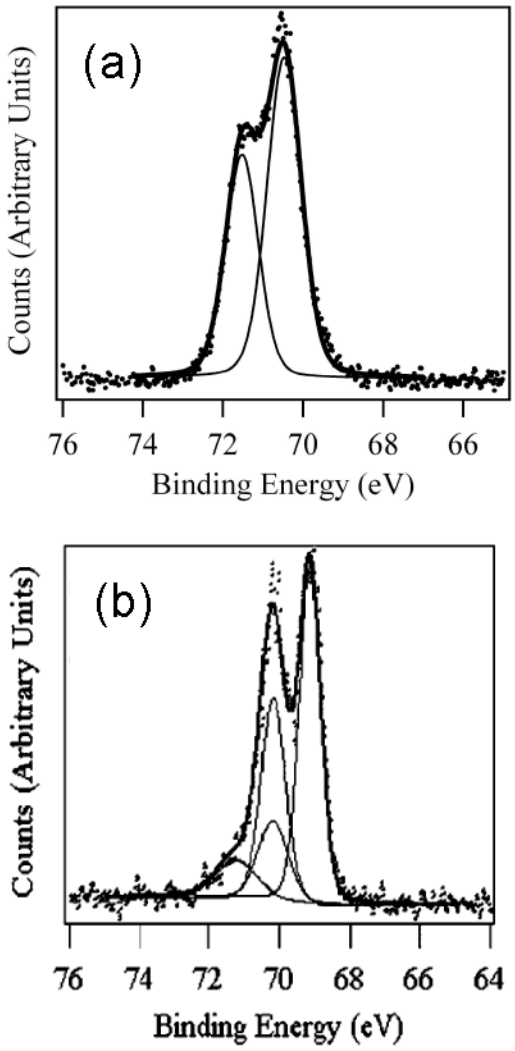

Figure 3.3 Br 3d XP spectra for (a) BrSty/Si(111) (b) Undec-10-enoic acid 2-bromo-ethyl ester /Si(111).[23] Figure (a) is from Rajiv Basu in the Hersam group. In contrast to the (a) spectrum, which has a clear single spin doublet with peaks located at 71.5 and 70.5 eV that is assigned to carbon-bound bromine, the (b) spectrum shows an additional spin doublet at 69.1 and 70.2 eV and that is assigned to silicon-bound bromine.

3.3 Sonogashira coupling

The Sonogashira coupling between the BPA and an iodophenyl acetylene- derived monolayer on Si(111) surfaces was carried out by using a microwave reactor (Biotage Initiator, SW Version) in the Nguyen group. In an N_2-filled glovebox, TEA (5 mL), $(PPh_3)_2PdCl_2$ catalyst, and CuI co-catalyst were combined in a 5-mL microwave vial. The iodide-terminated organic layer on Si(111) wafer was then submerged in this mixture, followed by the addition of BPA (0.2 M). The vial was capped, taken out of the glovebox, and sonicated for 1 min before being placed in the microwave reactor (~30 W) at 40 ˚C for 120 min. After cooling to room temperature, the final wafer was rinsed with methylene chloride (~5 mL), sonicated (room temperature methylene chloride x ~30 min and diethyl ether x ~20 min; ~50˚C THF x ~5 min and diethyl ether x ~30 min), dried with N_2 gas, and stored in the glovebox before analysis. The sonication cleaning is extensive in order to remove the physisorbed BPA molecules from the surface. The remaining liquid after the microwave reaction was also collected to evaluate the purity of the unreacted precursors and/or determine the formation of possible side products.

3.4 Preparation of SAMs on Si(001)

The growths of SAMs on Si(001) were performed by Michael Walsh in the Hersam group. The procedure is summarized in the following:

Step1: The Si(001) sample was annealed at 1250°C via resistive heating, with a base pressure < 5.0×10^{-11} Torr.

Step 2: Monohydride passivation is achieved by heating the sample to 375°C and exposing it to 1000 L (1 L = 1.0 x 10^{-6} Torr-s) of molecular hydrogen cracked on a hot tungsten filament (1400°C) located 6 cm from the sample.

Step 3: H-Si(001) is heated up to around 400°C to increase the dangling bond concentration.

Step 4: The H-Si(001)–2x1 sample is then brought into the UHV analysis chamber to confirm the surface quality with STM.

Step 5: The surface of H-Si(001) is exposed to between 60 L – 450 L of molecules via a precision leak valve.

3.5 Coverage determination by X-ray fluorescence

After the growth of the brominated or iodated SAMs on the Si surfaces, the coverage of the organic adlayers was determined using X-ray fluorescence (XRF) analysis. In the analysis, the direct comparison of the x-ray fluorescence yield from the sample with that from a calibrated reference standard provides the atomic coverage of the sample. The coverage of iodine is measured by comparing the I $L\beta_1$ XRF yield to the Ba Lα yield from a Ba implanted standard. While the bromine coverage is determined by comparing the Br Ka XRF yield to the As Kβ yield from an As-implanted standard. At 7 keV, the I $L\beta_1$ to Ba Lα cross-sectional ratio is 0.36. While at 16 keV the Br Kα to As Kβ cross-sectional ratio is 8.41. Both Ba and As coverages for the implanted standards were calibrated by Rutherford backscattering. For a 1x1 bulk-like terminated Si(111) or Si(001) surface, a coverage of 1 monolayer (ML) corresponds to 7.83 or 6.78 molecules/nm^2 , respectively.

Chaper 4 : The X-ray Standing Wave Method

4.1 Introduction

A couple of decades after Batterman's discovery of generating an XSW field within a bulk crystal,[24] the XSW technique was developed by Golovchenko and co-workers[25,26] as a powerful tool for locating surface adatoms with respect to the substrate lattice. The details for XSW analysis can be found elsewhere.[27-30] Basically, the XSW method combines X-ray diffraction and X-ray spectroscopy, thereby solving the phase problem that is common to most diffraction methods. Under the 2-beam dynamical Bragg condition from a "perfect' single crystal (in a Bragg-Bragg geometry) the coherently–coupled incident and Bragg reflected plane waves superimpose to form a well-defined standing wave.[31] Advancing in incident angle through the strong Bragg condition causes the phase between the two plane waves to change by π-radians, which causes the XSW antinodes to shift inward by one-half of a d-spacing, which induces characteristic modulations in the atomic XRF signals. The modulation of the fluorescence yield is sensitive to the distribution of the fluorescence species with respect to the substrate lattice. For many surface science techniques, it is difficult to exclusively separate the signal originated from the atoms on the surface from signal that is from the appreciable number of atoms in the bulk substrate. However, it is easy to distinguish the spectroscopic response of the surface atoms from the bulk atoms in XSW analysis and gains the surface sensitivity. In a XSW analysis, the reflected plane wave can be attributed to single crystal Bragg diffraction, or total external reflection (TER), or reflection from a periodic layered-synthetic-microstructure (LSM) mirror. The length-scale for each of these three XSW methods matches the XSW period, which is

expressed as $D = 2\pi/Q = \lambda/(2\mathrm{Sin}\theta)$. This is 10 - 100 nm for the TER-XSW, 2 – 20 nm for the LSM-XSW, and 0.1 - 1 nm for the single crystal Bragg reflection XSW case. The single crystal XSW case has the added bonus of providing atom location in 3D via the use of specular and off-normal reflections. Whereas, the TER and LSM cases are strictly generated by a specular reflection condition and are thereby constrained to only give 1D profiles along the surface normal direction. The single crystal XSW method determines the *h k l* Fourier amplitudes and phases for the XRF selected atomic distribution, which can be combined to produce a 3D real-space map of the fluorescence selected species.[32-34] The atomic density maps can then be combined with theoretically calculated structures providing the atomic-scale structures of the systems.

4.2 Experimental setup

The XSW measurements presented in this thesis work were carried out at the APS (Advanced Photon Source, Argonne National Laboratory) 5ID-C, 12ID-D, and 33ID-D undulator stations or at the Northwestern University X-ray Diffraction Facility. The basic experimental setups are shown in Fig 4.1. At the undulator stations, the incident photon energy was tuned by the undulator-gap and by the high-heat-load monochromator (HHLM) to E = 15.50 - 17.00 keV for the Br XSW experiments or E = 7.00 keV for the I XSW experiments. The HHLMs at 5ID-C and 12ID-D use L-N_2 cooled Si(111) crystals, while the HHLM at 33ID-D uses water-cooled diamond(111) crystals. At 5ID-C, a pair of horizontally deflecting mirrors with Pt and Rh stripes in the beamline was used after the HHLM for 1:1 horizontal focusing and higher order harmonic rejection. The vertically focusing beamline mirrors at 12ID and 33ID

were not used to avoid degradation of the source brightness in the vertical plane for these single crystal XSW measurements. At NU, the XSW measurements were performed on a Ragaku 18 KW rotating anode with a Mo target operating at 50 kV and 240 mA. An Osmic MaxFlux parabolic multilayer mirror was used to defocus the line source X-rays into a parallel beam. The multilayer in conjunction with a slit also excludes the continuous bremsstrahlung radiation and Mo Kβ characteristic X-rays.

After the HHLM or the parabolic multilayer mirror, one of the two-bounce Si(hhh), (hh0) or (00h) channel-cut crystals was used to create a nondispersive reflection from the sample. The selected channel-cut crystal was chosen to match the d-spacing of the sample crystal. By using a feedback controlled piezoelectric actuator (monochromator stabilizer, MOSTAB), the channel-cut angle is continuously adjusted with sub-microradian resolution to maintain a constant ratio between incident and reflected X-ray intensity. The MOSTAB unit is not required for the XSW experiments in NU X-ray Diffraction Facility.

A XSW experiment simultaneously measures the X-ray diffraction and X-ray fluorescence while scanning through an $\mathbf{H} = h\ k\ l$ Bragg diffraction. The XSW measurements at NU were limited to *111* reflections from Si(111) samples due to the use of a Huber 2-circle diffractometer on the XSW machine. In order to have enough statistic for the data, a typical XSW measurement for a ~0.3 ML brominated SAM on Si(111) will take ~5 min at APS, but ~8 hours at the NU X-ray Diffraction Facility because of the difference of the X-ray intensity. Ionization chambers and NaI scintillator detectors are used to record the flux of X-rays at the undulator stations at APS and at the NU X-ray Diffraction Facility, respectively.

For the collection of X-ray fluorescence with a solid-state energy dispersive detector, either a Canberra UltraLEGe or Vortex Si drift-diode (SDD) detector was used. Because the polarization of X-rays at APS is almost 100% in the horizontal direction, we could choose the preferred σ-polarization geometry by reflecting in the vertical plane. In this case the XRF detector is placed beside the samples with take off angle normally ~5˚. In contrast, the XRF detector for the XSW setup at NU is directly facing the sample with take off angle ~ 90˚ due to the non-polarized X-rays from the rotating anode. The threshold energy for the detectors was carefully adjusted so Si Kα fluorescence (E = 1.74 keV) from the substrate is always collected and used as a reference. Typical spectra from a brominated SAM and an iodated SAMs on Si are shown in Fig 4.2. SiKα, Ar Kα and the TDS (thermal diffuse scattering) peaks are usually used for the calibration of energy. The TDS energy is essentially the incident beam energy.

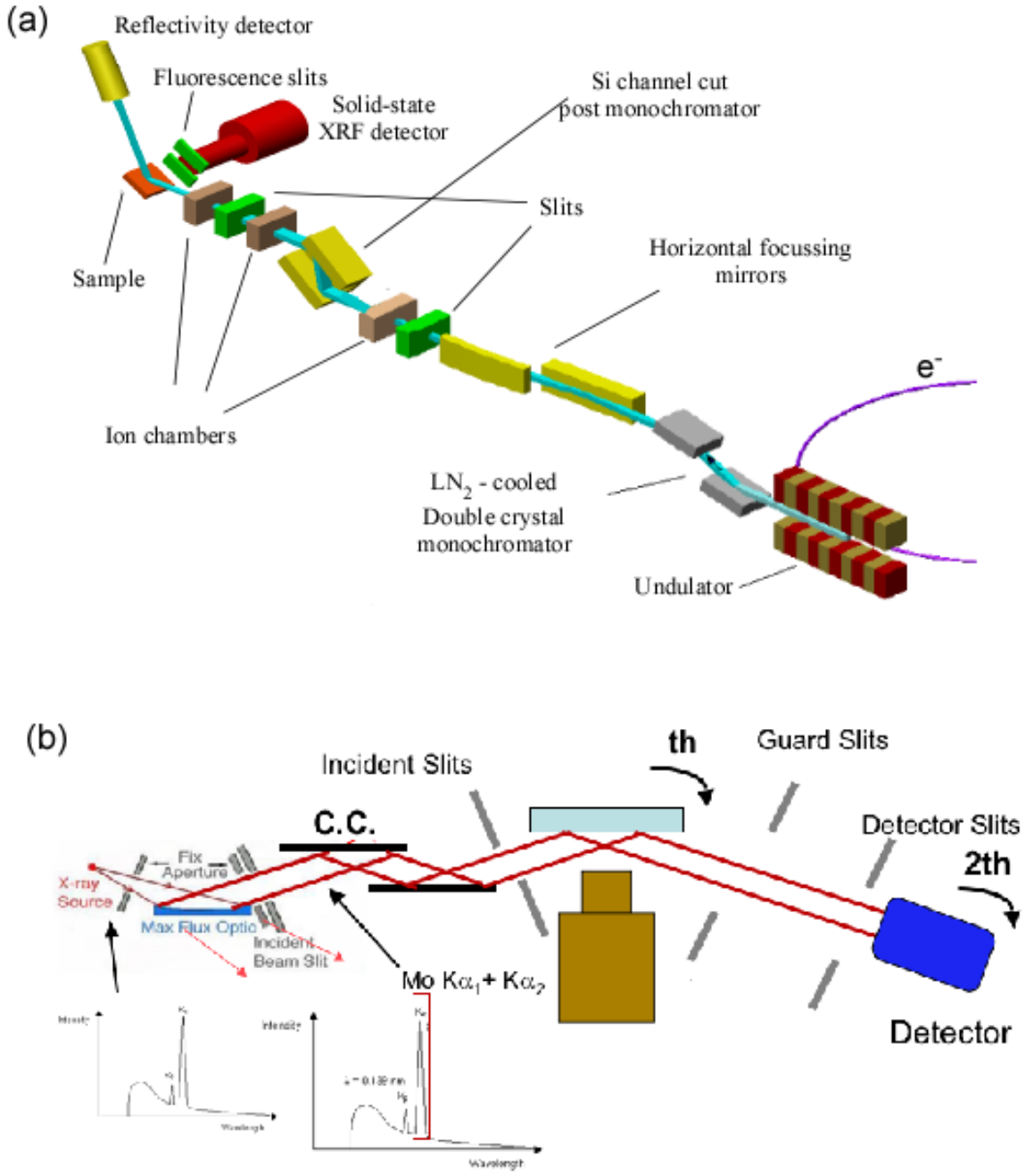

Figure 4.1 Schematic diagrams showing (a) the XSW setup at the APS 5ID-C station and (b) top-view of the XSW setup at the Northwestern University X-ray Diffraction Facility.

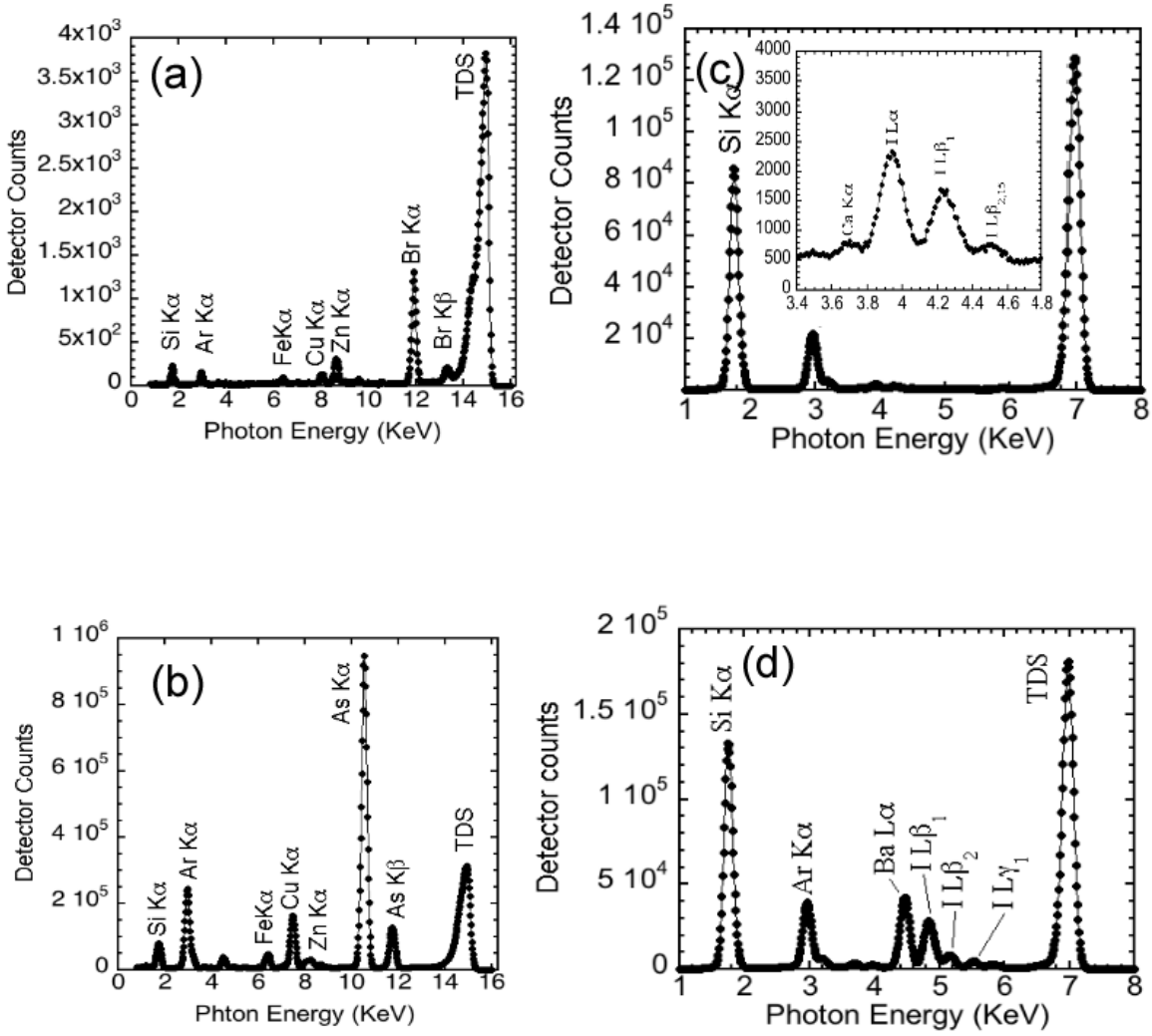

Figure 4.2 XRF spectra for (a) BPA/Si(111), (b) As implanted Si(111) standard, (c) IPA/Si(111), and (d) Ba implanted Si(111) standard. The As standard and Ba standard are used as calibrated references for the XRF coverage measurements for brominated SAMs and iodated SAMs, respectively. Each of these spectra were collected at the APS 5ID-C station with a Vortex SDD detector at take off angle ~5°. The energy, flux, and incident angle for the incident X-rays are 15.00 keV, 1 x 10^{11} p/s and 7° for (a) and (b), and 7.00 keV, 5 x 10^{9} p/s and 4° for (c) and (d).

4.3 Dynamical diffraction

For a **H** = *h k l* Bragg reflection from a thick single crystal, the diffracted X-ray plane wave interferes with the incident wave forming an X-ray standing-wave field. Based on two-beam dynamical diffraction theory,[31] the amplitude ratio of the coherently diffracted X-ray plane wave (E_H) to the incident plane wave (E_0) can be expressed as

$$\frac{E_H}{E_0} = -\sqrt{|b|}\frac{|P|}{P}\sqrt{\frac{F_H}{F_{\bar{H}}}}(\eta \pm \sqrt{\eta^2 - 1}) \qquad \textbf{(4.1)}$$

where b is the asymmetry factor of the crystal, P is the polarization constant, F_H is the structure factor for the **H** Bragg reflection and η is a normalized angular parameter. P = 1 for the σ polarization case, where the electric field $\mathbf{E_0}$ is perpendicular to the scattering plane. P = Cos(2θ) for the π polarization case, where $\mathbf{E_0}$ is parallel to the scattering plane. The crystal asymmetry factor b is defined as

$$b = -\frac{\sin(\theta_B - \phi)}{\sin(\theta_B + \phi)} \qquad \textbf{(4.2)}$$

where ϕ is the miscut angle between the optical surface and the diffraction planes of the crystal. The structure factor F_H and F_{-H} are the H^{th} and $-H^{th}$ order Fourier coefficients for the electron density ρ(r), which can be expressed as

$$F_H = \int_{V_c} \rho(\vec{r}) \exp(i\vec{H} \bullet \vec{r}) dV \qquad \textbf{(4.3)}$$

For a periodic crystal structure with N atoms within the unit cell, it can also be written as

$$F_H = \left|F_H\right| \exp(i\phi_H) = \sum_{j=1}^{N} [f_0(H) + \Delta f'(\lambda) + i\Delta f''(\lambda)]_j S_j(H) D_j(H) \qquad \textbf{(4.4)}$$

where $S_j(\mathbf{H}) = \exp(i\mathbf{H} \bullet \mathbf{r_j})$ is the geometrical phase factor for the j^{th} atom locating at r_j.

$$D_j(\vec{H}) = \exp(-\frac{2\pi^2 \left\langle u^2{}_H \right\rangle_j}{d^2{}_H}) \qquad \textbf{(4.5)}$$

is the Debye-Waller factor for the j^{th} atom. $\langle u^2{}_H \rangle_j$ is the mean square vibrational amplitude of the i^{th} atom along the direction of **H**. $d_H = 2\pi/|H|$ is the diffraction-plane spacing. A higher temperature will produce a smaller $D_i(H)$.

The normalized angle parameter η is a function of the relative incident angle $\Delta\theta = \theta - \theta_B$ where

$$\eta = \frac{b\Delta\theta \sin(2\theta_B) + \frac{1}{2}\Gamma F_0(1-b)}{\Gamma|P|\sqrt{|b|}\sqrt{F_H F_{\bar{H}}}} \qquad \textbf{(4.6)}$$

$$\Gamma = \frac{r_e \lambda^2}{\pi V_c} \qquad \textbf{(4.7)}$$

$r_e = 2.818 \times 10^{-5}$ Å is the classical electron radius and V_c refers to the volume of the unit cell. When η changes from +1 to -1, the relative phase (υ) of E_H and E_0 decreases by π radians (see Fig 4.3) and the corresponding angular difference $\omega = \theta_{\eta=-1} - \theta_{\eta=1}$, defined as Darwin width, can be expressed as:

$$\omega = \frac{2\Gamma\sqrt{F'_H F'_{\overline{H}} + F''_0{}^2 - F''_H F''_{\overline{H}}}}{\sqrt{|b|}\sin 2\theta_B} \qquad \textbf{(4.8)}$$

The center of the Bragg reflection ($\eta = 0$) is offset from the geometrical Bragg angle θ_B by

$$\Delta\theta_{\eta=0} = \frac{\Gamma F'_0}{\sin 2\theta_B}\left(\frac{1+|b|}{2|b|}\right) \qquad \textbf{(4.9)}$$

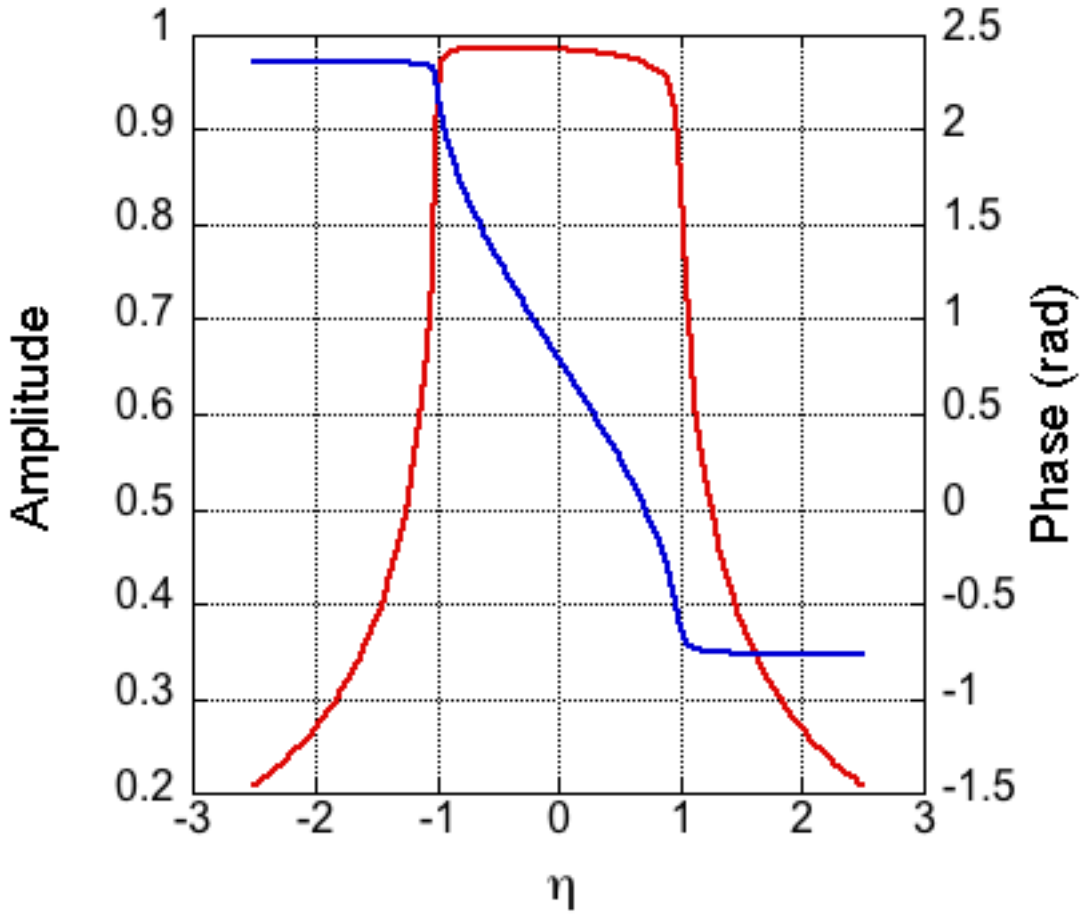

Figure 4.3 Calculated amplitude and phase of the complex E-field amplitude ratio (Eq. 4.1) for a Si *111* Bragg diffraction at 16.00 keV with b = 1 and P =1. For this calculation, the unit cell origin was chosen to coincide with a Si atom in the top of the Si(111) bilayer.

4.4 Photoexcitation from X-ray standing waves

In the two-beam plane-wave case of a dynamical X-ray Bragg diffraction, the total E-field intensity, as the sum of the incident and diffracted plane waves, has the form of

$$I_{Tot} = |\mathcal{E}_0 + \mathcal{E}_H|^2 = |E_0 \exp[-i(K_0 \bullet r - \omega t)] + E_H \exp[-i(K_H \bullet r - \omega t)]|^2$$

$$= |E_0|^2 [1 + \left|\frac{E_H}{E_0}\right| + 2P\left|\frac{E_H}{E_0}\right| \cos(v - \vec{H} \bullet \vec{r}] \times e^{-\mu_z Z} \qquad \textbf{(4.10)}$$

$$= I(\theta, \vec{r}) = [1 + R(\theta) + 2\sqrt{R(\theta)} Cos(\upsilon(\theta) - \vec{H} \bullet \vec{r})] \times \{ \begin{matrix} 1; \textit{above the surface} \\ e^{-\mu_z(\theta) Z}; \textit{at Z below surfce} \end{matrix}$$

where we have set the incident intensity $|E_0|^2 = 1$ and where μ_z is the effective liner absorption coefficient defined as

$$\mu_z(\theta) = \frac{\mu_0}{Sin(\theta_B)} [1 + \frac{F'_{\bar{H}}}{F''_0} (\frac{E_H}{E_0})'' + \frac{F''_{\bar{H}}}{F''_0} (\frac{E_H}{E_0})'] \qquad \textbf{(4.11)}$$

$$\mu_0 = \frac{2\pi}{\lambda} \Gamma F''_0 \qquad \textbf{(4.12)}$$

and μ_0 is the linear absorption coefficient. The X-ray penetration depth $\Lambda \equiv \mu_z^{-1}$ is minimized at $\eta' = 0$ to a value known as the extinction depth:

$$\Lambda_{ext} = \frac{V_c}{4 d_H r_e (F''_0 + \sqrt{|F_H \| F_{\bar{H}}|})} \qquad \textbf{(4.13)}$$

When the incident X-ray energy is greater than the binding energies of the core electron, the atom can undergo the photoelectric effect and emit photoelectrons. The excited ion can transit to its ground state via Auger electron and X-ray fluorescence emission. Based on the dipole approximation for the photoelectric effect, the XRF yield from an atom will be proportional to the E-filed intensity at the center of that atom and therefore the XSW induced X-ray fluorescence yield can be expressed as

$$\begin{aligned} Y(\theta) &= \int I(\theta,\vec{r})\rho(\vec{r})e^{-\mu_f(\alpha)Z}d\vec{r} \\ &= Y_{OB}\{1 + R(\theta) + 2\sqrt{R(\theta)}\int_{V_c}\rho(\vec{r})Cos[\upsilon(\theta) - \vec{H}\bullet\vec{r}]e^{-\mu_f(\alpha)Z}d\vec{r}\} \end{aligned} \quad \textbf{(4.14)}$$

where the off-Bragg Yield (Y_{OB}) is proportional to the coverage of the fluorescent species. In Eq. 4.14, the absorption coefficient $\mu_f(\alpha)$ accounts for the attenuation of the out going fluorescent X-rays and varies as a function of take-off angle α

$$\mu_f(\alpha) = \frac{2\sqrt{2}\pi}{\lambda_f}[\sqrt{(2\delta - \alpha^2)^2 + 4\beta^2} + 2\delta - \alpha^2]^{1/2} \quad \textbf{(4.15)}$$

where $$\delta = \frac{\Gamma F_0'}{2} \quad , \quad \beta = \frac{\Gamma F_0''}{2} \quad \textbf{(4.16)}$$

are related to the index of refraction $n = 1 - \delta - i\beta$ and are calculated for the substrate material at the energy of the emitted fluorescent X-ray.

If we define the amplitude and phase of the H^{th} order Fourier coefficient of the distribution function for the fluorescence selected species as coherent fraction f_H and coherent position P_H, respectively, then

$$\mathcal{F}_H[\rho(\vec{r})] = \int_{V_c} \rho(\vec{r}) e^{i\vec{H}\bullet\vec{r}} d\vec{r} = f_H \exp(2\pi i P_H) \tag{4.17}$$

and the fluorescence yield can be simplified as

$$Y(\theta) = Y_{OB}[1 + R(\theta) + 2\sqrt{R(\theta)} f_H Cos(v(\theta) - 2\pi P_H)]Z(\theta) \tag{4.18}$$

where the effective-thickness factor Z(θ) accounts for the absorption of both the incident X-ray beam and the emitted X-rays. Z(θ) = 1 if the fluorescence selected species are located on or above the crystal surface. Z(θ) can also be approximated as 1 if the fluorescence species are below the surface but $Z << \Lambda_{ext}$. If the fluorescing atoms are distributed evenly throughout the crystal, then[30]

$$Z(\theta) = \frac{\mu_0[Sin(\theta_B)]^{-1} + \mu_f(\alpha)}{\mu_z(\theta) + \mu_f(\alpha)} \tag{4.19}$$

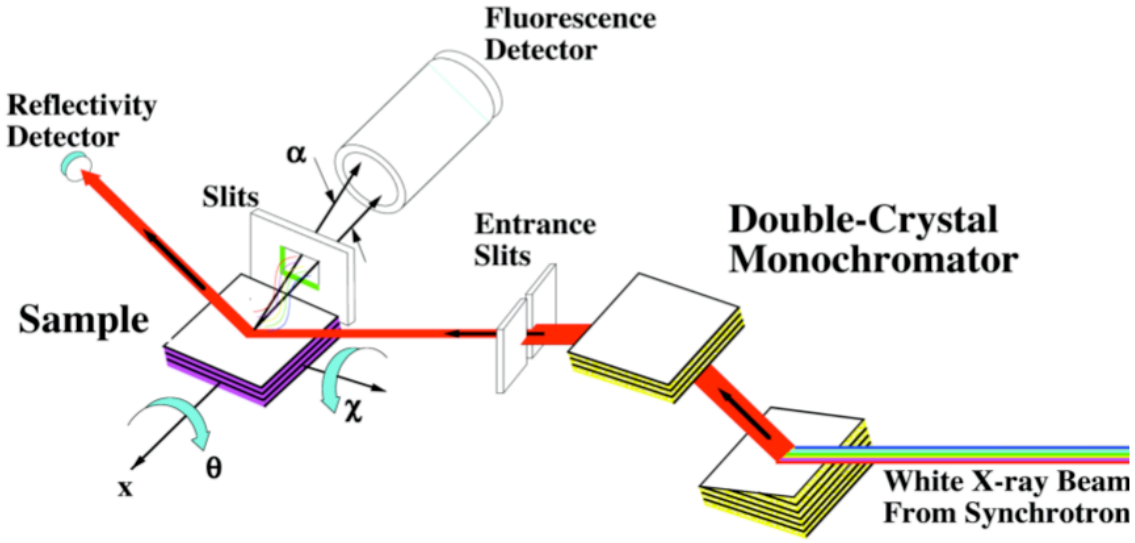

Figure 4.4 Depiction of a typical XSW experimental setup. The beam from a synchrotron beamline is monochromated by a double crystal monochromator. While stepping the incident angle θ of the sample through the reflection, the reflected intensity and fluorescence spectrum are simultaneously collected by two separate detector systems. The figure is reproduced from Ref. [30].

As was shown in Fig 4.4, the reflectivity R(θ) and the fluorescence yield Y(θ) are simultaneously collected while scanning in θ through a **H** = *h k l* Bragg reflection in a XSW measurement. For each XSW data set, a rocking curve, calculated as the convoluted result from the emittance and acceptance functions from the upstream monochromator and the sample crystal, respectively, is fitted to the experimentally measured R(θ) to obtain the absolute angle scale. This is then used in the fitting of Eq. (4.18) to the measured Y(θ) to determine Y_{OB}, f_H and P_H.

4.5 Structural analysis using the coherent fraction and coherent position

In a XSW analysis, the coherent position P_H is related to the location of the atoms relative to the diffraction planes. The coherent fraction f_H, on the other hand, not only senses the geometric configuration of the atoms but also the order of the distribution. The coherent fraction can be considered as the combination of three factors:

$$\boldsymbol{f_H = C\, a_H\, D_H} \qquad \textbf{(4.20)}$$

where C is the ordered fraction, a_H is the geometrical factor and D_H is the Debye-Waller factor. In a general case of a discrete distribution having the identical atoms located at N different sites $\mathbf{r_i} = x_i\,\mathbf{a} + y_i\,\mathbf{b} + z_i\,\mathbf{c}$, i = 1 to N that are in the unit cell, plus some randomly distributed same

atoms. The ordered fraction C is the fraction of the total n_{Tot} atoms that are coherent to the substrate crystal lattice

$$C = \sum_{i=1}^{N} \frac{n_i}{n_{Tot}} = \sum_{i=1}^{N} c_i \qquad \textbf{(4.21)}$$

where n_i is the number of the atoms at r_i. Since a_H is the modulus of the normalized geometrical structure factor S_H for the coherent atoms from the N lattice sites,

$$S_H = \frac{1}{C} \sum_{i=1}^{N} [c_i \exp(i 2\pi \vec{H} \bullet \vec{r}_i)] \qquad \textbf{(4.22)}$$

$$\boldsymbol{a_H = |S_H|} \qquad \textbf{(4.23)}$$

Comparing Eq. (4.18) to (4.22), one can derive

$$\boldsymbol{P_H = \mathrm{Arg}[S_H] \,/\, 2\pi} \qquad \textbf{(4.24)}$$

In Eq. (4.20), the Debye-Waller factor D_H is identical to that defined in Eq. (4.5). However, the distribution width $\langle u^2_H \rangle$ is generalized to the overall width of the displacement field attributed to the effects of time- and domain- averaging.

4.6 3D atomic density map reconstruction

As was shown in Eq. (4.18), the XSW measured coherent fraction f_H and coherent position P_H are the amplitude and phase, respectively, of the H^{th} Fourier coefficient of the fluorescence selected species. As the result, with an inversed Fourier transformation, the distribution function of the selected atoms ρ(r) can be calculated as

$$\rho(\vec{r}) = \sum_{\vec{H}} \exp[i(2\pi P_H - \vec{H} \bullet \vec{r})] = 1 + 2 \sum_{\substack{\vec{H} \neq -\vec{H} \\ H \neq 0}} f_H Cos[(2\pi P_H - \vec{H} \bullet \vec{r})] \quad \textbf{(4.25)}$$

the simplified form of the equation makes use of $f_0 = 1$ and the symmetry relationship analogous to Friedel's law that makes $f_{-H} = f_H$ and $P_{-H} = - P_H$.

Since the Fourier summation in Eq. (4.25) includes both amplitude and phase of each Fourier coefficient, the XSW technique resolves the common "phase problem" in diffraction techniques. Ideally, with infinite number of Fourier components for the summation, any distribution of the fluorescence species can be unambiguously determined. However, because the available Fourier components in a XSW analysis are limited to the allowed reflections from the single crystal substrate, a XSW method produced density map is influenced by the crystallographic structure of the substrate and the symmetry of the crystal. More details are discussed in chapters 4.7 and 4.8.

4.7 XSW imaging and substrate crystallography

Since X-ray standing waves are originated from the Bragg reflections of the substrate crystal, the Fourier components available in a XSW analysis are limited to the allowed reflections determined by the crystal structure of the substrate. For an example, a $\mathbf{H} = h\ k\ l$ reflection is not allowed for a face-centered cubic (FCC) crystal if $h\ k\ l$ is a mix of odd and even integers. On the other hand, a XSW reflection is allowed for a body-centered cubic (BCC) only if $h + k + l$ equals to an even number. The distribution of atoms, produced by the Fourier summation of the available XSW reflections, will therefore be projected within the bulk primitive unit cell depending on the substrate crystal structure.

For example, considering "one" atom locating at (X, Y, Z) = (0.37, 0.18, 0.18) within a cubic unit cell where the lattice constant |a| = |b| = |c| = 5.431 Å and $\alpha = \beta = \gamma = 90^{\circ}$. The values of the 21 sets of a_H and P_H are calculated accordingly using Eq. (4.20) to (4.24) and the numbers are listed in the inset table of Fig 4.5. Three atomic density maps using three different selections of the 21 reflections, based on the forbidden reflection rules for (a) simple cubic, (b) FCC, and (c) BCC structure, are also constructed and shown in Fig 4.5. Although one atom commonly shows up in all three density maps at (X, Y, Z) = (0.37, 0.18, 0.18), map (b) has an additional atom at the face center and (c) has an additional atom at the body center. The XSW images have the intrinsic periodicities of the substrate crystals. For the case of (b) or (c), the XSW analysis itself cannot exclude the subsidiary pseudo hot spot in the density map. However, since the heights for the different hot spots are normally different, an independent measurement of the atom height such as XRR analysis will help determining the correct location.

Form	{004}	{022}				{131}								{123}							
hkl	004	022	202	0 $\bar{2}$2	$\bar{2}$02	131	311	3 $\bar{1}$1	1 $\bar{3}$1	$\bar{1}$ $\bar{3}$1	$\bar{3}$ $\bar{1}$1	$\bar{3}$11	$\bar{1}$31	123	213	2 $\bar{1}$3	1 $\bar{2}$3	$\bar{1}$ $\bar{2}$3	$\bar{2}$ $\bar{1}$3	$\bar{2}$13	$\bar{2}$13
a_H	1	1	1	1	1	1	1	1	1	1	1	1	1	1	1	1	1	1	1	1	1
P_H	0.74	0.74	0.10	0.00	0.63	0.10	0.47	0.10	0.00	0.26	0.90	0.26	0.37	0.29	0.47	0.10	0.55	0.82	0.63	0.00	0.55
(a)	√	√	√	√	√	√	√	√	√	√	√	√	√	√	√	√	√	√	√	√	√
(b)	√	√	√	√	√	√	√	√	√	√	√	√	√								
(c)	√	√	√	√	√									√	√	√	√	√	√	√	√

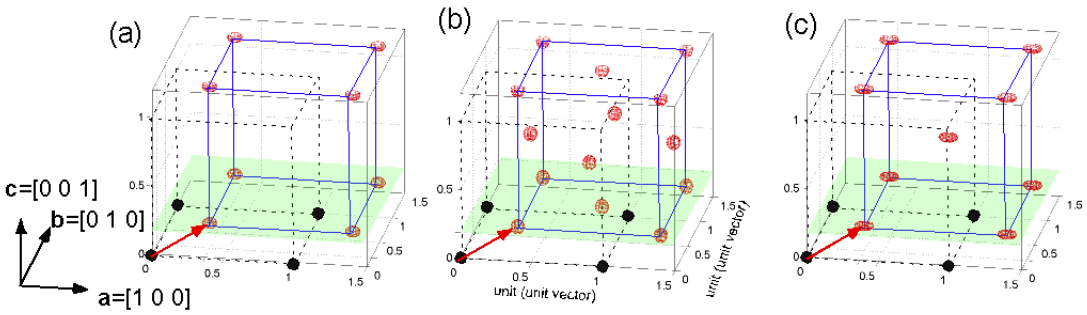

Figure 4.5 Tabulated XSW a_H and P_H values for 21 *h k l* reflections based on the assumption that the XRF-selected atom occupies one symmetry inequivalent position (X, Y, Z) = (0.37, 0.18, 0.18) within the unit cell. Three 3D atomic-density maps based on Fourier summations (Eq. 4.25) of the allowed reflections for (a) simple cubic, (b) face-centered cubic (FCC), and (c) body-centered cubic (BCC) are generated accordingly. The selections of the reflections are indicated by the "√" mark in the Table. The black-dashed-lines and the blue-solid-lines represent the volumes of the cubic unit cells. All three maps commonly have one atom at (X, Y, Z) = (0.37, 0.18, 0.18), indicated by the red arrows, but maps (b) and (c) have one additional atom at the face center and the body center, respectively, due to the missing *h k l r*eflections within the summation. In other words, each occupied symmetry inequivalent site will generate an infinite 3D periodic image with the translation symmetry of the primitive unit cell.

4.8 XSW imaging and plane group symmetry on Si surfaces

A crystalline surface, in contrast to a non-crystalline surface, has a specific 2D-symmetry due to the lattice structure, the cut of the crystal and the environment (e.g. different temperature will induce different surface reconstructions). Multiple atoms at different locations on a surface may be chemically equivalent because of the surface symmetry. For an example, atoms locating at (X, Y, Z) = (1, 2, 3), (1, -2, 3), (-1, 2, 3), and (-1, -2, 3) on a Si(001)-2x1 surface with the origin at one of the bulk-terminated Si are essentially equivalent due to the P4mm symmetry (the P2mm symmetry and the equally populated two domains). Since a typical X-ray beam has an area of mm^2 and is much greater than the μm^2 scale domain size, a XSW measurement result is often an ensemble-averaged result of the symmetry equivalent configurations. Cases for Si(111)–1x1 and Si(001)–2x1 surfaces are discussed in the following.

4.8.1 Si(001)–2x1

Fig 4.6 and 4.7 show the [001] projection of a two-domain dimerized Si(001)-2x1 surface. In Fig 4.6, the domain consisting of dimer rows oriented parallel to the atomic step is referring to as “A domain”, and the domain with dimer rows orientated perpendicular to the atomic step is referring to as “B domain”. The (2 x 1) unit cell for the reconstructed surface is illustrated together with the plane group symmetry, the (1 x 1) surface unit cell (green-dashed-lines) for the bulk-terminated surface, and the surface unit cell for the (2 x 1) reconstructed surface (blue-dashed-lines). For a XSW measurement on a Si(001)-2x1 surface, because the footprint of X-ray is much greater than the domain size, the XSW E-field interacts with atoms from both A- and B- type of domains and the measurement therefore shows the ensemble-

averaged result. When the two perpendicular P2mm (2x1) unit cells overlap, the ensemble-averaged surface will have a P4mm plane group symmetry (Fig 4.8). The atoms at (x,y,z), (x,-y,z), (-x,y,z), (-x,-y,z), (y,x,z), (y,-x,z), (-y,x,z), and (-y,-x,z) are symmetry equivalent and need to be considered together in a XSW analysis (x, y = 0, 0 at the 4-fold symmetry axis).

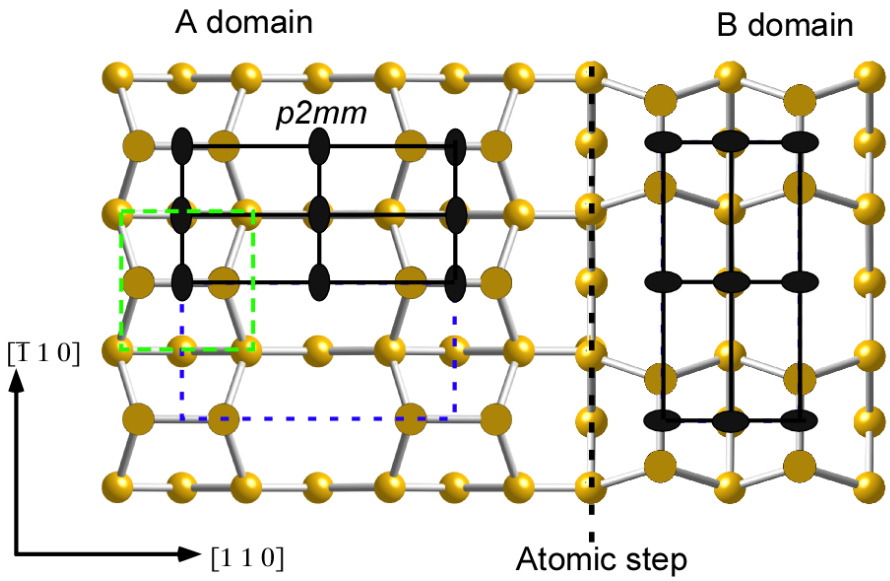

Figure 4.6 The [001] projection of a two-domain Si(001)-2x1 surface. The B domain is one atomic step lower than the A domain. The (2 x 1) and (1 x 2) surface unit cells for both domains belong to the P2mm plane group. The green dashed lines show the (1 x 1) surface unit cell for the bulk-like Si surface termination. The blue dashed lines indicate the reconstructed (2 x 1) surface unit cell.

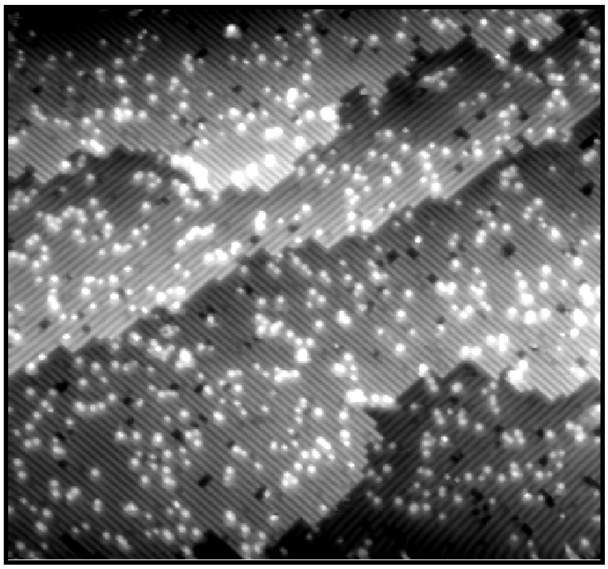

Figure 4.7 An STM image for a Si(001)–2x1 surface with Si dangling bonds (bright spots). This image is from Michael Walsh in the Hersam group.

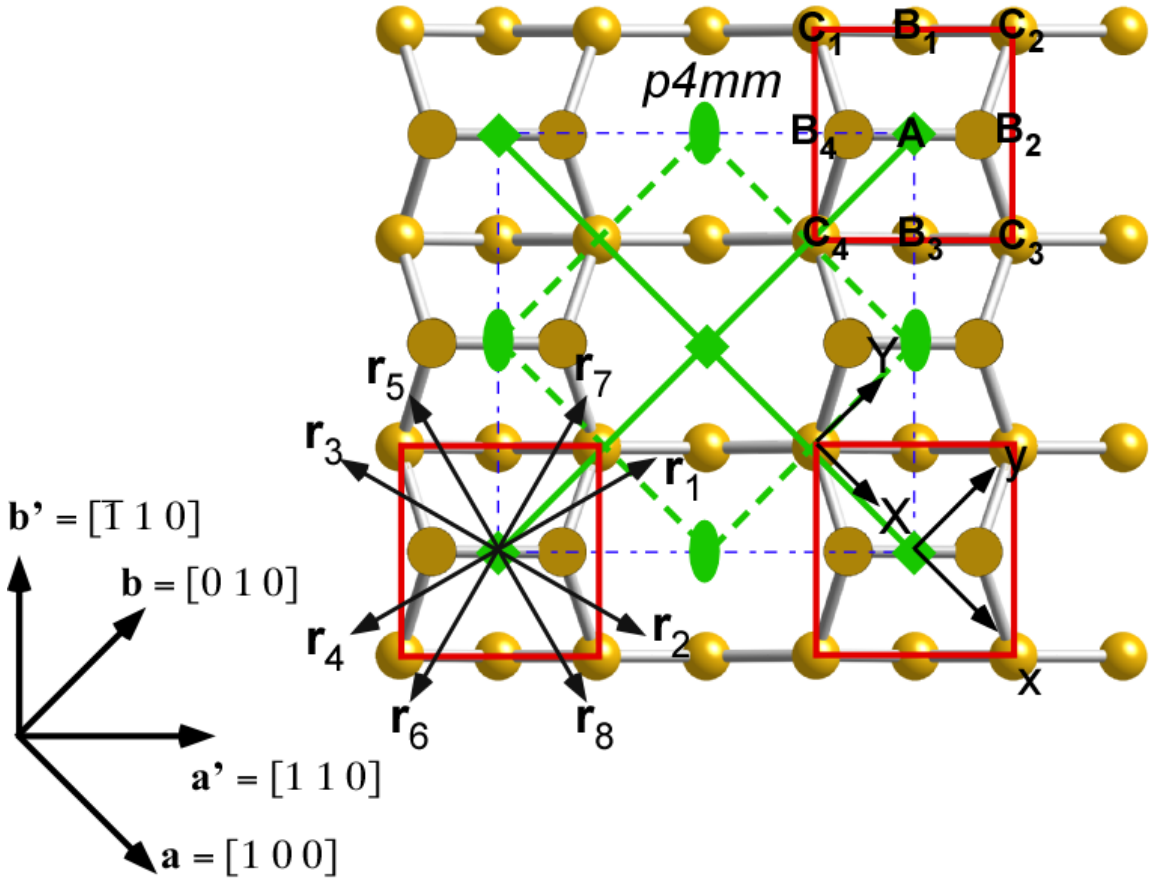

Figure 4.8 The domain-averaged (2 x 2) unit cell on Si(001)-2x1 surfaces. The unit cell has P4mm symmetry.

If we use the lattice constant of Si as the unit and move the origin from the center of the (1 x 1) unit cell to a bulk-terminated Si atom (x, y coordinate -> X, Y coordinate in Fig 4.8), the (0, 0, 0) in the old coordinate becomes (1/2, 0, 0) in the new coordinate and (X, Y, Z) = (x, y, z) + (0.5, 0, 0) and the normalized geometrical structure factor S_H becomes:

$$
\begin{aligned}
S_H &= \frac{1}{8}\sum_{i=1}^{8}\exp[2\pi i(\vec{H}\bullet\vec{r}_i)] = \frac{1}{8}\sum_{i=1}^{8}\exp[2\pi i(hX_i + kY_i + lZ_i)] = \frac{1}{8}\sum_{i=1}^{8}\exp[2\pi i(h/2 + lz)]\exp[2\pi i(hx_i + ky_i)] \\
&= \frac{1}{8}\exp[2\pi i(h/2 + lz)]\{[e^{2\pi i(hx+ky)} + e^{-2\pi i(hx+ky)}] + [e^{2\pi i(-hx+ky)} + e^{-2\pi i(-hx+ky)}] + [e^{2\pi i(-hy+kx)} + e^{-2\pi i(-hy+kx)}] + [e^{2\pi i(-hy-kx)} + e^{-2\pi i(-hy-kx)}]\} \\
&= \frac{1}{4}\exp[2\pi i(h/2 + lz)]\times\{Cos[2\pi(hx + ky)] + Cos[2\pi(hx - ky)] + Cos[2\pi(hy - kx)] + Cos[2\pi(hy + kx)]\} \\
&= \frac{1}{2}\exp[2\pi i(h/2 + lz)]\times\{Cos[2\pi hx]Cos[2\pi ky] + Cos[2\pi hy]Cos[2\pi kx]\}
\end{aligned}
\qquad \textbf{(4.26)}
$$

Based on Eq. (4.26):

1. Symmetry equivalent XSW reflections will have the identical a_H and P_H because of the **H•r** in the calculation of S_H. Eight reflections, *h k l*, *h -k l*, *-h k l* , *-h -k l* , *k h l* , *k -h l* , *-k h l, and –k -h l* are symmetry equivalent.

2. The XSW phase P_H will always be either (h/2 + lz) or (h/2 + lz + π/2) depending on the sigh of the term "Cos[2π*h*x] Cos[2π*k*y] + Cos[2π*h*y] Cos[2π*k*x]"

3. If an atom at (X, Y, Z) = ($x_0 + \delta x_0$, $y_0 + \delta y_0$, z) and both δx_0 and δy_0 are small enough that from (x_0, y_0, z) to ($x_0 + \delta x_0$, $y_0 + \delta y_0$, z) does not change the sign of [Cos[2π*h*x] Cos[2π*k*y] + Cos[2π*h*y] Cos[2π*k*x]], P_H for ($x_0 + \delta x_0$, $y_0 + \delta y_0$, z) will be identical to that for (x_0 ,y_0 ,z).

4. Four high symmetry sites that will degenerate the total number of symmetry equivalent locations, A(0,0), B(1/2,0), C(1/4,1/4), and D(1/4,0), are on a Si(001)–2x1 surface. The XSW

results for atoms at one of the four high symmetry sites are very distinctive. The corresponding values of the four sets of a_H and P_H are calculated and listed in Table 4.1

		A	B	C	D
(x,y) unit = Si lattice constant a_{Si}	(a,b) (a-b) (-a,b) (-a,-b) (b,a) (b-a) (-b,a) (-b,-a)	(0,0)	(1/2,0) (-1/2,0) (0,1/2) (0,-1/2)	(1/4,1/4) (-1/4,1/4) (1/4,-1/4) (-1/4,-1/4)	(1/4,0) (-1/4,0) (0,1/4) (0,-1/4)
Tot. Num. atoms	8	1	4	4	4
h, k are odd	a_H =0.5x {Cos[2π*h*α]Cos[2π*k*β]] + Cos[2π*h*β]Cos[2π*k*α] } P_H = +/-(h/2 + lz), 0	a_H = 1 P_H = h/2 + lz	a_H = 1 P_H = -(h/2 + lz)	a_H = 0 P_H = N/A	a_H = 0 P_H = N/A
h, k are even h/2 + k/2 = 2n+1		a_H = 1 P_H = h/2 + lz	a_H = 1 P_H = (h/2 + lz)	a_H = 1 P_H = -(h/2 + lz)	a_H = 0 P_H = N/A
h, k are even h/2 + k/2 = 2n		a_H = 1 P_H = h/2 + lz	a_H = 1 P_H = (h/2 + lz)	a_H = 1 P_H = (h/2 + lz)	a_H = 1 P_H =+/-(h/2 + lz)

Table 4.1The XSW a_H and P_H values for an atom located at a general position (a, b) or at one of the four high symmetry sites (A, B, C, D).

With the consideration of the P4mm symmetry, the density function in Eq. (4.25) can be written as:

$$\rho(\vec{r}) = \sum_{\vec{H}} f_H \exp[i2\pi(P_H - \vec{H}\bullet\vec{r})]$$

$$= 1 + \sum_{h^2+k^2=0} f_H \exp[i2\pi(P_H - \vec{H}\bullet\vec{r})] + \sum_{\substack{h^2+k^2\neq 0 \\ hk=0 \text{ or } |h|=|k|}} f_H \exp[i(2\pi(P_H - \vec{H}\bullet\vec{r})] + \sum_{\substack{h^2+k^2\neq 0 \\ hk\neq 0 \text{ and } h\neq k}} f_H \exp[i(2\pi(P_H - \vec{H}\bullet\vec{r})] \quad use\ \vec{r} = (X,Y,Z) = (0.5a_{Si},0,0) + (x,y,z)$$

$$= 1 + \sum_{h^2+k^2=0} f_H \exp[i2\pi(P_H - lz)] + \sum_{\substack{h^2+k^2\neq 0 \\ hk=0 \text{ or } |h|=|k|}} f_H \exp[i2\pi(P_H - \frac{h}{2} - (hx+ky+lz))] + \sum_{\substack{h^2+k^2\neq 0 \\ hk\neq 0 \text{ and } h\neq k}} f_H \exp[i2\pi(P_H - \frac{h}{2} - (hx+ky+lz))]$$

$$= 1 + \sum_{h=k=0} f_H \exp[i2\pi(P_H - lz)] + \sum_{\substack{h^2+k^2\neq 0 \\ hk=0 \text{ or } |h|=|k|}} f_H \{\exp[i2\pi P_H] \times 2\exp[-i2\pi(\frac{h}{2} + lz)] \times (Cos[-2\pi hx]Cos[-2\pi ky] + Cos[-2\pi hy]Cos[-2\pi kx])\}$$

$$+ \sum_{\substack{h^2+k^2\neq 0 \\ hk\neq 0 \text{ and } h\neq k \\ 0\leq h\leq k}} f_H \{\exp[i2\pi P_H] \times 4\exp[-i2\pi(\frac{h}{2} + lz)] \times (Cos[-2\pi hx]Cos[-2\pi ky] + Cos[-2\pi hy]Cos[-2\pi kx])\}$$

$$let \quad a = Cos[2\pi hx]Cos[2\pi ky] + Cos[2\pi hy]Cos[2\pi kx], b = \frac{h}{2} + lz + \pi \times (\frac{1}{2} - \frac{a}{|2a|})$$

$$= 1 + 2\sum_{\substack{h=k=0 \\ H\neq \bar{H}}} f_H Cos[2\pi(P_H - lz)] + 4 \sum_{\substack{h^2+k^2\neq 0 \\ hk=0 \text{ or } |h|=|k| \\ 0\leq h\leq k, H\neq \bar{H}}} f_H |a| Cos[2\pi(P_H - b)] + 8 \sum_{\substack{h^2+k^2\neq 0 \\ hk\neq 0 \text{ and } h\neq k \\ 0\leq h\leq k, H\neq \bar{H}}} f_H |a| Cos[2\pi(P_H - b)]$$

(4.28)

An example of the calculation of a_H, P_H and the corresponding density maps assuming one atom at (X, Y, Z) = (0.37, 0.18, 0.18) on a Si(001)–2x1 surface with and without the consideration of surface symmetry is illustrated in Table 4.2 and Fig 4.9

Form	h k l	No symmetry		P4mm symmetry	
		a_H	P_H	a_H	P_H
0 0 4	(0 0 4)	1	0.21	1	0.21
0 2 2	(0 2 2)	1	-0.16	0.06	0.10
	(0 -2 2)	1	0.37	0.06	0.10
	(-2 0 2)	1	-0.26	0.06	0.10
	(2 0 2)	1	0.47	0.06	0.10
1 3 1	(1 3 1)	1	-0.16	0.46	0.05
	(3 1 1)	1	0.47	0.46	0.05
	(3 -1 1)	1	-0.26	0.46	0.05
	(1 -3 1)	1	-0.37	0.46	0.05
	(-1 -3 1)	1	0.26	0.46	0.05
	(3 -1 1)	1	-0.37	0.46	0.05
	(-3 1 1)	1	0.37	0.46	0.05
	(-1 3 1)	1	0.47	0.46	0.05

Table 4.2 Calculated a_H and P_H values for $H = (004), \{0\ 2\ 2\}, \{1\ 3\ 1\}, and \{1\ 2\ 3\}$ assuming a single-site occupation of an atom at (X, Y, Z) = (0.37, 0.18, 0.18) on a P4mm Si(001)–2x1 surface. Also shown is the case for "No surface symmetry". **a** = [1 0 0], **b** = [0 1 0], **c** = [0 0 1].

Because Si is a FCC type crystal, the XSW atomic-maps in Fig 4.9 have the FCC periodicity. However, with the further consideration of the P4mm surface symmetry, the origin of the markers' unit cell is shifted from (X, Y, Z) = (0.37, 0.18, 0.18) to (0.5, 0, 0.18) on one of the high symmetry sites.

It shows that the lateral location of the hot spot in an XSW-generated atomic-map does not always directly correspond to the true location of the atom. A complementary technique, such as DFT, will be needed for determining the absolute coordinates of the atoms.

4.8.2 Si(111)–1x1

A [111] projection of a Si(111)-1x1 surface with its plane group symmetry are shown in Fig 4.10.

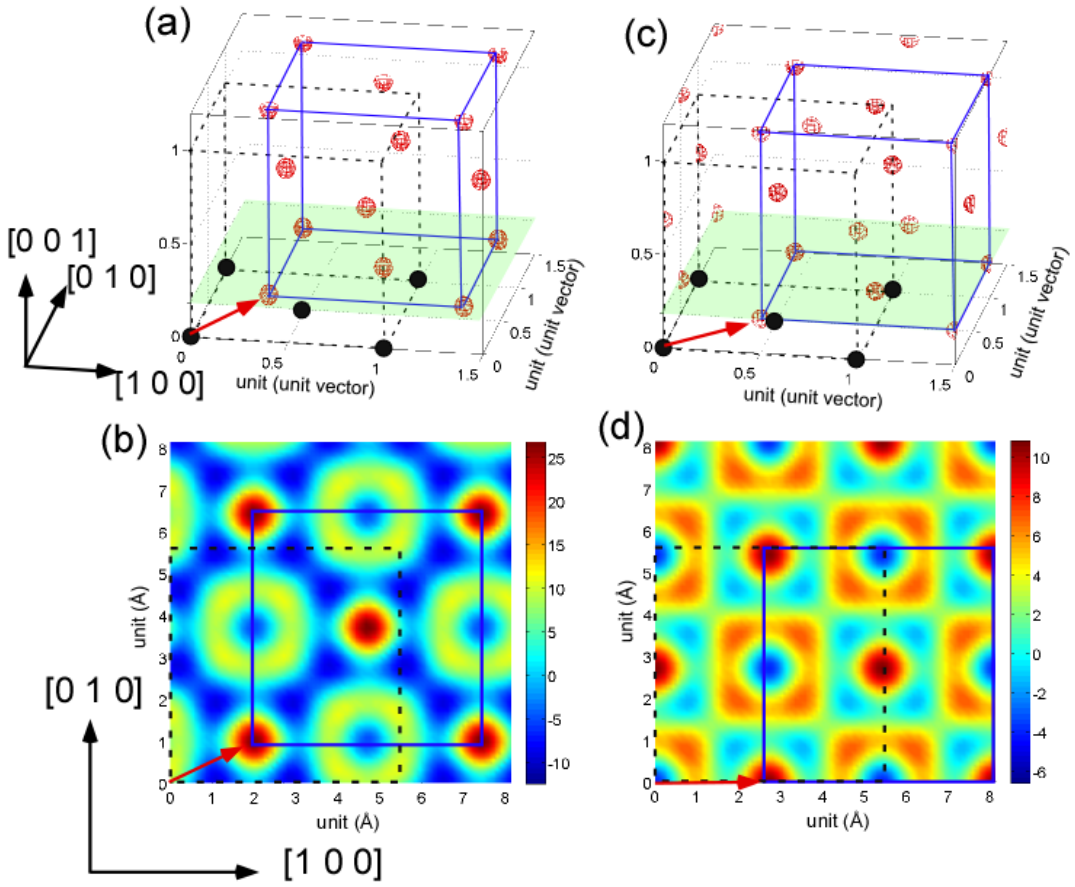

Figure 4.9 (a) and (c) are the 3D XSW-generated atomic maps based on the calculated a_H and P_H values from Table 4.2. Image (a) corresponds to the case where no surface symmetry is being considered, while image (c) corresponds to the case with P4mm surface symmetry. (b) and (d) are the 2D cuts through the 3D maps of (a) and (c), respectively, at 1 Å above the bulk-terminated Si atomic layer. Although for both cases the atom is assumed to be at (X, Y, Z) = (0.37, 0.18, 0.18) = (2Å, 1Å, 1Å), the XSW atomic map for the case with P4mm surface symmetry has the hot spots laterally shifted to their nearest high symmetry sites.

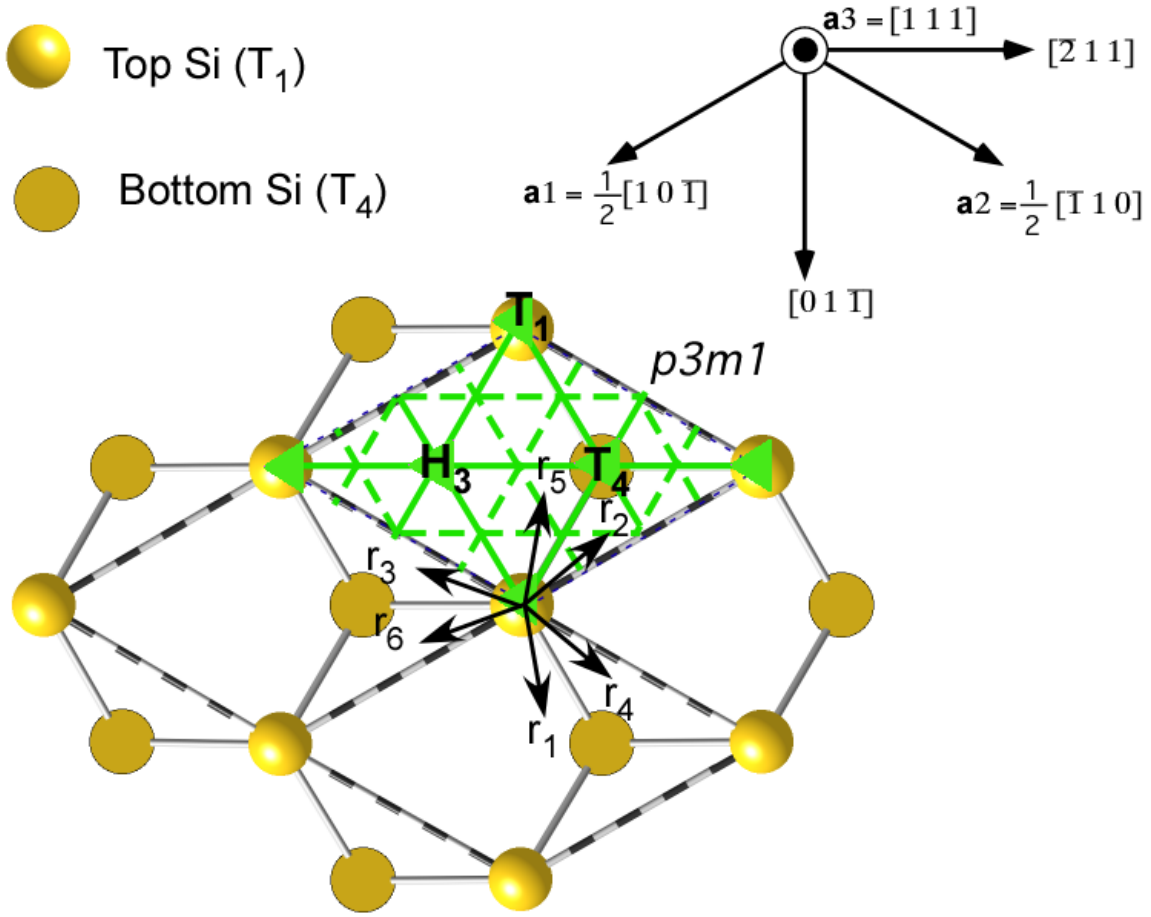

Figure 4.10 The [111] projection of a Si(111)-1x1 surface. The surface has the P3m1 plane group symmetry. For the purpose of clarity, only the top-most bilayer is shown. The T_1, T_4, and H_3 symmetry sites are labeled.

In Fig 4.10, the unit vectors $a_1 = ½[a_{Si}, 0, -a_{Si}]$, $a_2 = ½[-a_{Si}, a_{Si}, 0]$, and $a_3 = [0, 0, a_{Si}]$ are chosen for the hexagonal coordinate for the convenience of discussion. The three 3-fold high symmetry sites, T_1, T_4, and H_3, are labeled in the figure as well. If an atom is tethered to a T_1 site but locates at $\mathbf{r_1}$ = (a1, a2, a3) = (x, y, z), it is expected to have five other symmetry equivalent atoms at $\mathbf{r_2}$(-y, x-y, z), $\mathbf{r_3}$(y-x, -x, z), $\mathbf{r_4}$(-y, -x, z), $\mathbf{r_5}$(-x+y, y, z), and $\mathbf{r_6}$(x, x-y, z). The corresponding normalized geometrical structure factor S_H becomes:

$$
\begin{aligned}
S_H &= \frac{1}{6}\sum_{i=1}^{6}\exp[2\pi i(\vec{H}\bullet\vec{r}_i)] = \frac{1}{6}\sum_{i=1}^{6}\exp[2\pi i(hX_i + kY_i + lZ_i)] \\
&= \frac{1}{6}\exp[2\pi ilz]\{[e^{2\pi i(hx+ky)} + e^{2\pi i[-hy+k(x-y)]} + e^{2\pi i[h(y-x)-kx]}] + [e^{2\pi i(-hy-kx)} + e^{2\pi i[h(y-x)+ky]} + e^{2\pi i[hx+k(x-y)]}]\} \\
&= \frac{1}{6}\exp[2\pi ilz]\{[e^{2\pi i(hx+ky)} + e^{2\pi i[kx-(h+k)y]} + e^{2\pi i[-(h+k)x+hy]}] + [e^{2\pi i(-kx-hy)} + e^{2\pi i[-hx+(h+k)y]} + e^{2\pi i[(h+k)x-ky]}]\}
\end{aligned}
\qquad \textbf{(4.29)}
$$

Based on the normalized geometrical structure factor S_H in Eq. (4.29):

1. The 3m symmetry equivalent reflections, *h k l* = a b c, -b -(a+b) c, -(a+b) a c, -b –a c, -a (a+b) c, and (a+b) –b c, have the identical XSW a_H and P_H.

2. For (X, Y, Z) at one of the three high symmetry sites:

T_1: $\mathbf{r}$ = (0, 0, z) => $S_H = \exp[2\pi ilz]$

=> a_H =1, P_H = lz regardless of h, k

T_4: $\mathbf{r}$ = (1/3, 2/3, z),

$$S_H = \frac{1}{6}\sum_{i=1}^{6}\exp[2\pi i(\vec{H}\bullet\vec{r}_i)] = \frac{1}{6}\sum_{i=1}^{6}\exp[2\pi i(hX_i + kY_i + lZ_i)]$$

$$= \frac{1}{6}\exp[2\pi ilz]\{[e^{2\pi i\frac{1}{3}(h+2k)} + e^{2\pi i\frac{1}{3}(-2h-k)} + e^{2\pi i\frac{1}{3}(h-k)}] + [e^{2\pi i\frac{1}{3}(-2h-k)} + e^{2\pi i\frac{1}{3}(h+2k)} + e^{2\pi i\frac{1}{3}(h-k)}]\}$$

$$= \frac{1}{3}\exp[2\pi ilz]\{[e^{2\pi i\frac{1}{3}(h+2k)} + e^{2\pi i\frac{1}{3}(-2h-k)} + e^{2\pi i\frac{1}{3}(h-k)}]\}$$

$$\because \quad e^{i2\pi\frac{1}{3}\alpha} = (e^{i2\pi\frac{1}{3}})^{\alpha} = (e^{i2\pi\frac{-2}{3}})^{\alpha}$$

$$S_H = \frac{1}{3}\exp[2\pi ilz]\{[e^{2\pi i\frac{1}{3}(h+2k)} + e^{2\pi i\frac{1}{3}(h+2k)} + e^{2\pi i\frac{1}{3}(h+2k)}]\} = \exp[2\pi i(lz + \frac{1}{3}(h+2k)]$$

$$= \exp[2\pi i(lz + \frac{1}{3}(h-k)] \qquad \textbf{(4.30)}$$

=> a_H =1, P_H = lz + (h-k)/3

H_3: **r** = (2/3, 1/3,z),

$$S_H = \frac{1}{6}\sum_{i=1}^{6}\exp[2\pi i(\vec{H}\bullet\vec{r}_i)] = \frac{1}{6}\sum_{i=1}^{6}\exp[2\pi i(hX_i + kY_i + lZ_i)]$$

$$= \frac{1}{6}\exp[2\pi ilz]\{[e^{2\pi i\frac{1}{3}(k+2h)} + e^{2\pi i\frac{1}{3}(-2k-h)} + e^{2\pi i\frac{1}{3}(k-h)}] + [e^{2\pi i\frac{1}{3}(-2k-h)} + e^{2\pi i\frac{1}{3}(k+2h)} + e^{2\pi i\frac{1}{3}(k-h)}]\}$$

$$= \frac{1}{3}\exp[2\pi ilz]\{[e^{2\pi i\frac{1}{3}(k+2h)} + e^{2\pi i\frac{1}{3}(-2k-h)} + e^{2\pi i\frac{1}{3}(k-h)}]\} = \exp[2\pi i(lz + \frac{1}{3}(2h+k)]$$

$$= \exp[2\pi i(lz + \frac{1}{3}(k-h)] \qquad \textbf{(4.31)}$$

=>a_H =1, P_H = lz + (k-h)/3

3. If (x, y, z) = (x_0 + dx, y_0 + dy, z) where (x_0, y_0) in on one of the three high symmetry sites (T_1, T_4, or H_3) and dx, dy are relatively small,

$$S_H = \frac{1}{6}\sum_{i=1}^{6}\exp[2\pi i(\vec{H}\bullet\vec{r}_i)] = \frac{1}{6}\sum_{i=1}^{6}\exp[2\pi i(hX_i + kY_i + lZ_i)]$$

$$= \frac{1}{6}\exp[2\pi ilz]\{[e^{2\pi i(hx+ky)} + e^{2\pi i[-hy+k(x-y)]} + e^{2\pi i[h(y-x)-kx]}] + [e^{2\pi i(-hy-kx)} + e^{2\pi i[h(y-x)+ky]} + e^{2\pi i[hx+k(x-y)]}]\}$$

$$= \frac{1}{6}\exp[2\pi ilz]\{[e^{2\pi i[h(x_0+\delta x)+k(y_0+\delta y)]} + e^{2\pi i[k(x_0+\delta x)-(h+k)(y_0+\delta y)]} + e^{2\pi i[-(h+k)(x_0+\delta x)+h(y_0+\delta y)]}]$$

$$+[e^{2\pi i[-k(x_0+\delta x)-h(y_0+\delta y)]} + e^{2\pi i[-h(x_0+\delta x)+(h+k)(y_0+\delta y)]} + e^{2\pi i[(h+k)(x_0+\delta x)-k(y_0+\delta y)]}]\}$$

$$= \frac{1}{6}\exp[2\pi ilz]\{[e^{2\pi i[hx_0+ky_0]}e^{2\pi i[h\delta x+k\delta y]} + e^{2\pi i[kx_0-(h+k)y_0]}e^{2\pi i[k\delta x-(h+k)\delta y]} + e^{2\pi i[-(h+k)x_0+hy_0]}e^{2\pi i[-(h+k)\delta x+h\delta y)]}]$$

$$+[e^{2\pi i[-kx_0-hy_0]}e^{2\pi i[-k\delta x-h\delta y]} + e^{2\pi i[-hx_0+(h+k)y_0]}e^{2\pi i[-h\delta x+(h+k)\delta y]} + e^{2\pi i[(h+k)x_0-ky_0]}e^{2\pi i[(h+k)\delta x-k\delta y)]}]\}$$

$$= \frac{1}{6}\exp[2\pi i(hx_0 + ky_0 + lz)]\times\{[e^{2\pi i[h\delta x+k\delta y]} + e^{2\pi i[k\delta x-(h+k)\delta y]} + e^{2\pi i[-(h+k)\delta x+h\delta y)]}] + e^{2\pi i[-k\delta x-h\delta y]} + e^{2\pi i[-h\delta x+(h+k)\delta y]} + e^{2\pi i[(h+k)\delta x-k\delta y)]}]\}$$

$$\because\quad e^{i\alpha} = 1 + \frac{i\alpha}{1!} - \frac{\alpha^2}{2!} - \frac{i\alpha^3}{3!} + \ldots \sim 1 + \frac{i\alpha}{1!} - \frac{\alpha^2}{2!} \quad when\ \alpha << 1$$

$$\Rightarrow S_H \sim \frac{1}{6}\exp[2\pi i(hx_0 + ky_0 + lz)]$$

$$\times\{2\pi i\{[h\delta x + k\delta y] + [k\delta x - (h+k)\delta y] + [-(h+k)\delta x + h\delta y)] + [-k\delta x - h\delta y] + [-h\delta x + (h+k)\delta y] + [(h+k)\delta x - k\delta y)]\}$$

$$+ 2\pi^2\{[h\delta x + k\delta y]^2 + [k\delta x - (h+k)\delta y]^2 + [-(h+k)\delta x + h\delta y)]^2 + [-k\delta x - h\delta y]^2 + [-h\delta x + (h+k)\delta y]^2 + [(h+k)\delta x - k\delta y)]^2\}\}$$

$$= \frac{1}{6}\exp[2\pi i(hx_0 + ky_0 + lz)]\times F(h,k,\delta x,\delta y)$$

$$where\quad F(h,k,\delta x,\delta y) = 2\pi^2\{[h\delta x + k\delta y]^2 + [k\delta x - (h+k)\delta y]^2 + [-(h+k)\delta x + h\delta y)]^2 + [-k\delta x - h\delta y]^2 + [-h\delta x + (h+k)\delta y]^2 + [(h+k)\delta x - k\delta y)]^2\}$$

(4.32)

Because $a_H = |S_H|$ and $P_H = \mathrm{Arg}(S_H)/2\pi$, a_H and P_H for (x_0 + dx, y_0 + dy,z) are identical to that for (x_0, y_0, z). It also shows that a_H is more sensitive to (dx, dy) than P_H. Similar to that of a Si(001)-2x1 surface, an XSW-derived atomic map will also have the center of each hot spot locating at one of the high symmetry sites.

Chaper 5 : The X-ray Reflectivity Method

5.1 Introduction

The scattering of electromagnetic waves is used in many fields to probe surfaces and interfaces of materials. The wavelength covers a great length-scale from meter (radio wave), micron (laser) to angstrom (X-ray, electrons), and the scattering problem can be treated as solving Maxwell's equations. Particularly, for the angstrom scale wavelength X-ray, the index of refraction is slightly smaller than unity for most materials and the penetration as well as the scattering of X-rays at an air/solid interface can be limited to the near surface region when the incident angle is near the critical angle therefore enhancing the sensitivity at the surface. For the case of a specular X-ray Reflectivity (XRR) measurement for a SAM/Si, the wave-vector transfer Q is perpendicular to the surface and the measurement is sensitive to the electron density distribution perpendicular to the surface. The measured electron density profile can therefore be used to determine the thickness of the film, the roughness at the interfaces and the packing density of the molecules. The analysis can also be used to determine the height of the XRF selected markers hence solving the ambiguity in XSW analysis as described in the previous chapter. XRR analysis can be done by either using Kinematical scattering method or Parratt's recursion method and the methods will be discussed in Chapter 5.3 and 5.4.

5.2 XRR measurements

Most of the XRR experiments presented in this thesis were performed at NU X-ray Diffraction Facility while other experiments were done at 33BM-C, 5BM-D, or 5ID-C station at

APS. Different than the 5ID-C undulator beamline, both 33BM-C and 5BM-D stations are bending magnet beamlines. At the NU X-ray Diffraction Facility, the XRR measurements were performed on a Rigaku ATX-G rotating anode four-circle diffractometer with a Cu target and a multilayer parabolic mirror (Cu $K\alpha_1$ energy = 8.05 keV) operating at 50 kV and 240 mA. The XRR experiment setup at APS is identical to the XSW setup without the XRF detector and the Si channel-cut. The channel-cut was removed to improve the incident beam intensity.

In a XRR measurement, the reflectivity signal is distinguished from the background signal by measuring the reflectivity at and away from the specular reflection condition. The traditional method is to do a rocking scan, i.e. measuring the reflectivity as a function of incident angle, at each Q vector (Fig 5.1). However, it typically takes 10 - 20 data points to resolve the profile of a rocking scan so a complete XRR measurement, with 50 - 100 Q data points along the rod, will take a great amount of time. On the other hand, for a sub-monolayer organic film, a long X-ray exposure time will change the structures of the organic film. Therefore, an alternative three-points measurement, including a measurement on the peak (I_{Peak}) and measurements at each side of the background (I_{LBG}, I_{RBG}), was used in our study (see Fig 5.1b). The reflected intensity is calculated as $I_{Refl} = I_{Peak} - (I_{LBG} + I_{RBG})/2$. The background subtracted net scattering intensity is then normalized by the straight-through beam intensity, becoming reflectivity, and used in the XRR analysis. However, in order to do this, the detector slits and the guard slits have to be wide enough so the full-width-half-maximum (FWHM) of the rocking scans does not change as a function of Q. Both sets of slits should not be too big to include the scattering background as well. More details of a XRR measurement can be found in Ref. [35].

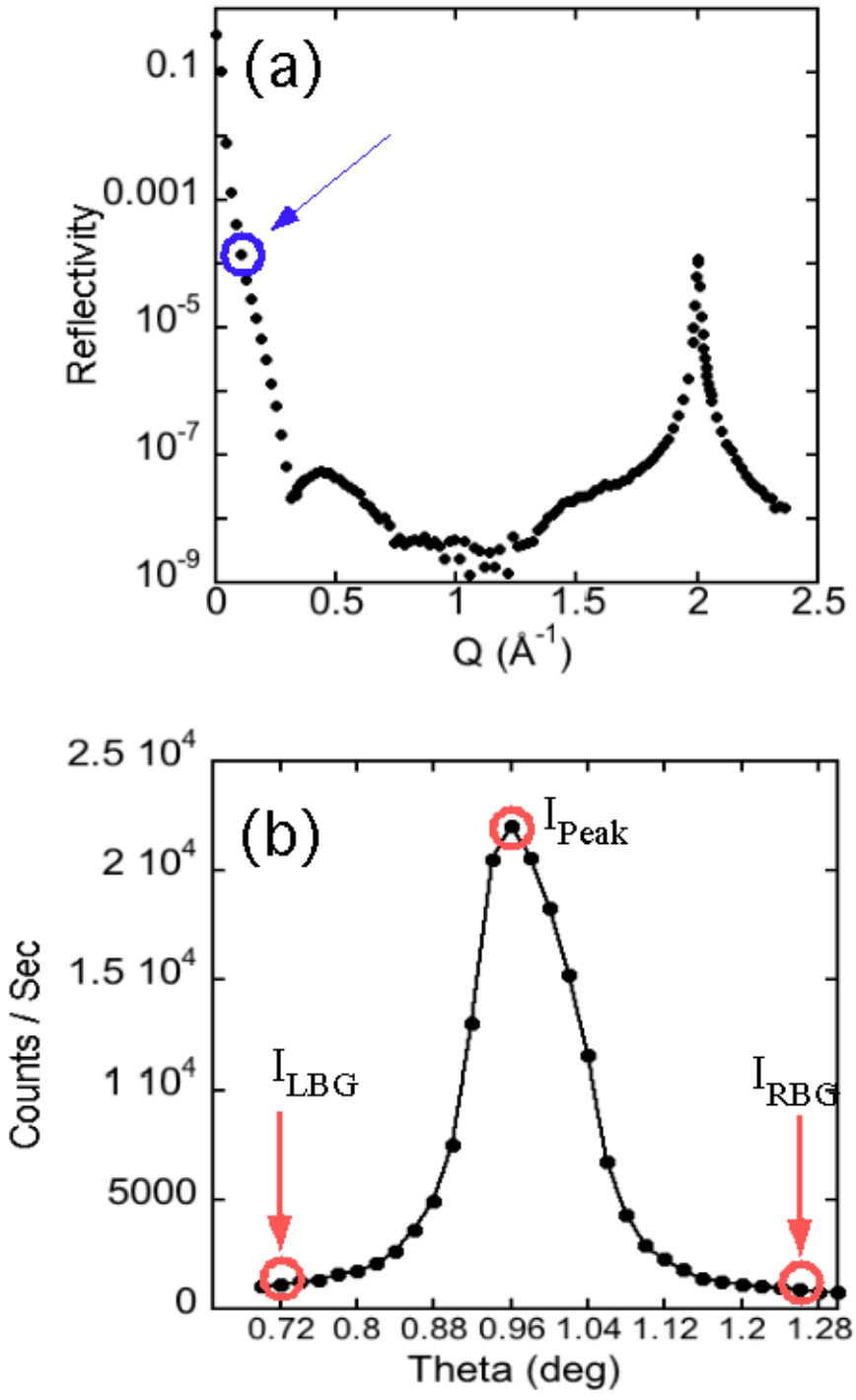

Figure 5.1 (a) The specular XRR scan for a BPA-derived SAM on Si(111). (b) A transverse rocking scan at the Q indicated by the arrow in (a).

5.3 Kinematical scattering method

Since the scattering of X-rays from a single electron is almost isotropic, the angular variation of scattering intensities observed in experiments is due to interference phenomena attributed to the non-uniform distribution of electron density within the radiated sample. The scattered total intensity I(q), which is proportional to the square of the total E-field intensity, is related to the electron density function ρ(**r**):

$$\mathbf{I(q)} \propto |\textstyle\sum \boldsymbol{\varepsilon}_i|^2 = |\,\mathbf{F(q)}\,|^2 \tag{5.1}$$

$$F(\vec{q}) = \int \rho(\vec{r})\, e^{i\vec{q}\bullet\vec{r}}\, d^3\vec{r} = \sum_{i=1}^{N} f_i(\vec{q})\, e^{i\vec{q}\bullet\vec{r}_i} \tag{5.2}$$

$$\mathbf{f\,(q,E) = f_0\,(q) + f'\,(E) + i\,f''(E)} \tag{5.3}$$

The structure factor F(q) is the Fourier transform of the overall electron density within the unit cell. f_i is the atomic form factor of i^{th} atom and r_i is the location of the i^{th} atom within the unit cell. $f_0(q) = \int \rho(r) e^{i\mathbf{q}\cdot\mathbf{r}} dr$ approximates the atomic electrons as a charge cloud freely surrounding the nucleus with density ρ(r). For computational convenience, f_0 can be analytical approximated as:

$$f_0(q) = \sum_{j=1}^{4} a_j e^{-b_j (\frac{q}{4\pi})^2} + c \tag{5.4}$$

where a_j, b_j, c are fitting parameters. A list of a_j, b_j, c is shown in Table 5.1. The energy dependent dispersion correction factor *f' + if"* is considered in Eq. (5.3) to account for the "bound" state of the electrons.

	a_1	a_2	a_3	a_4	b_1	b_2	b_3	b_4	c
Si	6.29	3.04	1.99	1.54	2.44	32.33	0.68	81.69	1.14
C	2.31	1.02	1.29	0.87	20.84	10.21	0.57	51.65	0.22
Br	17.18	5.24	5.64	3.99	2.17	16.58	0.26	41.43	2.96

Table 5.1 Coefficients of the Eq. 5.4 analytical approximation for the atomic form factor f_0 for a selection of elements. (Source: International Tables of Crystallography)

For the case of organic film on a single crystal Si substrate, the total structure factor is the sum of the structure factors from the Si substrate (F_{Sub}) and the organic film (F_{film}). Based on the derived absolute specular reflectivity from Fenter,[35] the specular reflectivity for an organic thin film on a substrate, where the transmission correction ~ 1 for thin organic film, can be written as

$$R(q) = [\frac{4\pi r_e}{qa_{uc}}]^2 |B(q)|^2 |F_{Sub} + F_{Film}|^2 \quad \textbf{(5.5)}$$

where r_e is the classical e^- radius, a_{uc} is the area of the surface unit cell and B(q) is the roughness factor. If the atoms in the structure distributed like a Gaussian function (e.g. due to the thermal vibration), $|B(q)|^2 = e^{(q\sigma)^2}$ where σ is the distribution width. For a rough surface attributed to the terraces on the substrate surface, $|B(q)|^2 = \frac{(1-\beta)^2}{[1+\beta^2 - 2\beta Cos(qd)]}$ where β is the occupation fraction

of the first terrace and β^n is the occupation fraction of the n^{th} layer.[36] $\sigma = 0$ and $\beta = 0$ for a perfectly flat surface.

For a semi-infinite crystal substrate with X-ray absorption per atomic layer, ε, below the surface, the structure factor F_{Sub} can be expressed as

$$F_{Sub}(q) = \frac{\sum f_{Si}(q,E)e^{iqz}}{[1 - e^{(-iqz-\varepsilon)}]} \qquad \textbf{(5.6)}$$

Simulations of XRR for a covalently bound 4-bromo-phenylacetylene (BPA) self-assembled monolayer (SAM) on Si(111) are shown in Fig 5.2. The energy of X-rays is 8.04 keV (identical to CuKα radiation). The intensity oscillations between the 0 and 1^{st} order Bragg peaks in the figure are due to the constructive interference of X-rays attributed to the organic film and are referred to as Kiessig fringes. The shape of the oscillations is related to the coverage (Fig 5.2a) and roughness (Fig 5.2c), while the periodicity of the oscillations is determined by the film thickness affected by the tilting of the molecules (Fig 5.2b).

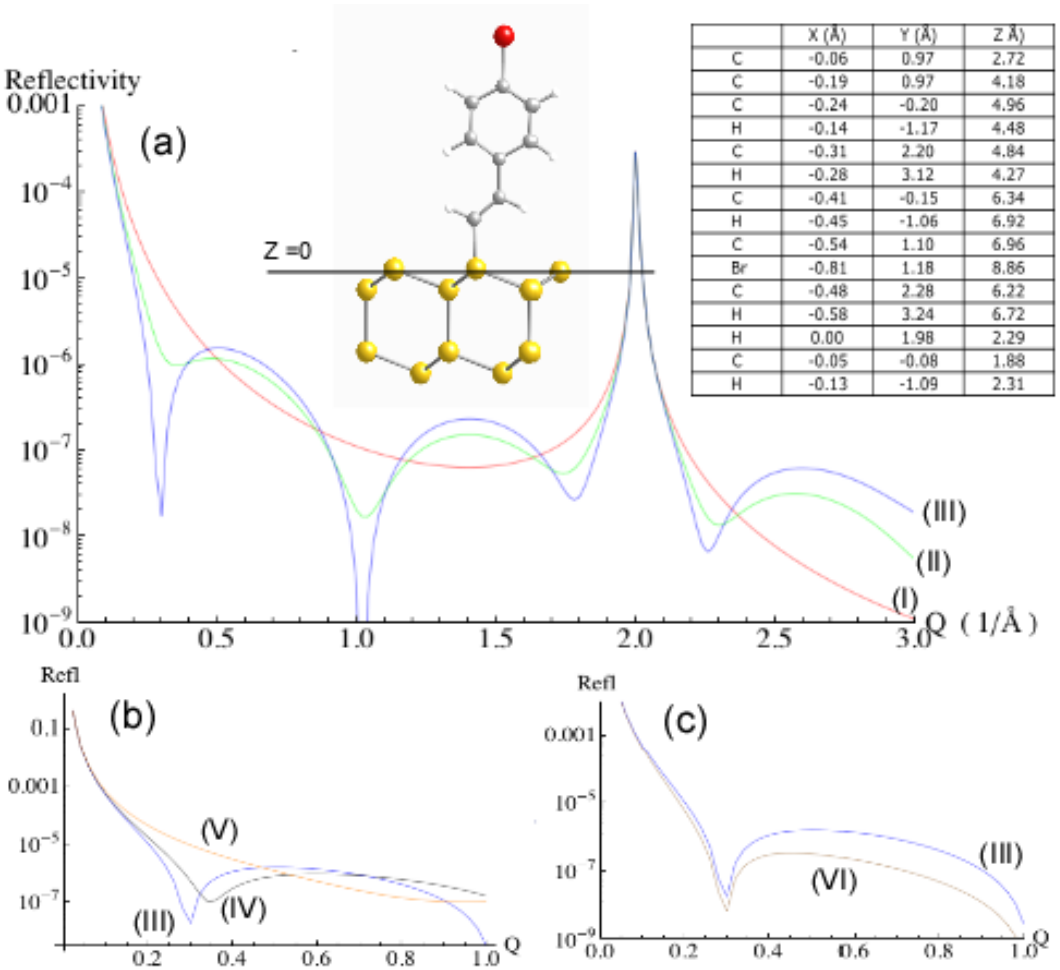

	X (Å)	Y (Å)	Z Å)
C	-0.06	0.97	2.72
C	-0.19	0.97	4.18
C	-0.24	-0.20	4.96
H	-0.14	-1.17	4.48
C	-0.31	2.20	4.84
H	-0.28	3.12	4.27
C	-0.41	-0.15	6.34
H	-0.45	-1.06	6.92
C	-0.54	1.10	6.96
Br	-0.81	1.18	8.86
C	-0.48	2.28	6.22
H	-0.58	3.24	6.72
H	0.00	1.98	2.29
C	-0.05	-0.08	1.88
H	-0.13	-1.09	2.31

	(I)	(II)	(III)	(IV)	(V)	(VI)
Cov.(ML)	0	0.3	0.5	0.5	0.5	0.5
Tilt (deg)	—	0	0	30	60	0
β	—	0	0	0	0	0.5

Figure 5.2 Six XRR simulations based on six different sets of structural parameters listed in the Table. The tabulated coordinates shown in (a) correspond to the ball-and-stick model shown in the figure based on a single-molecule cluster DFT calculation of BPA/Si(111). The model is used as the reference structure for which the molecular tilt angle is defined as 0. Height Z = 0 is at the topmost Si of the 1st bilayer. See text for a discussion for (b) and (c).

5.4 Parratt's recursion method

In chapter 5.3, the scattering process is studied as the interaction between X-rays and individual atoms. The scatter process, on the other hand, can also be treated as the change of the propagation of the wave when passing through an interface. For a wave passing through an interface between the i^{th} and $(i+1)^{th}$ layers of the material, the ratio of the reflected and incident waves' amplitudes, $r_i = |E_r| / |E_i|$, and the ratio of the amplitudes of the transmitted and incident waves, $t_i = |E_t| / |E_i|$, can be expressed as:

$$r_i = \frac{k_{i,z} - k_{i+1,z}}{k_{i,z} + k_{i+1,z}}$$
$$t_i = \frac{2k_{i,z}}{k_{i,z} + k_{i+1,z}} \qquad \textbf{(5.7)}$$

where the wave vector $k_{i,z} = k(n_i^2 - Cos^2\alpha_i)^{1/2}$. k is the incident wave vector, n_i is the index of refraction for the i^{th} layer and α_i is the incident angle. This is the well-known Fresnel formula.

For the example given in Fig 5.2, the BPA-derived SAM on Si(111) can also be treated as an air/Br/hydrocarbon/Si four-layer material. With the known incident angle (α_0), n_{air} and n_{Si}, the XRR data can be fitted with the recurring formula determining the n_{Br}, thickness of the Br layer, $n_{hydrocarbon}$, the thickness of the hydrocarbon layer and the roughness at each interface. The determined electron density profile can then be used to derive the film thickness and the packing density accordingly.

An open source IGOR PRO package for XRR analysis developed by the Nelson's group, Motofit, is used in this thesis for its intuitive interface and powerful analytical fitting. The program calculates the specular reflectivity using the Abeles formulation, (identical to the

Parratt's recursion formula). The data input/output is handled via a graphical user interface (GUI) and the genetic optimization method allows the program to find the global minimum solution. More details about the program can be found at http://motofit.sourceforge.net/wiki/index.php/Main_Page.

Chaper 6 : Density Functional Theory Modeling

Density functional theory (DFT), which is based on quantum mechanics, is widely used to investigate the structure of many-body systems.[37] The popularity of DFT is related to the fact that the relatively simple local density approximation to the energy functional is in many respects a good approximation for typical many body systems.[37] In our study, DFT is used to provide model structures for self-assembled monolayers on Si. Because the SAM/Si hybrid system is a complex system and a calculation of many molecules together with a semi-infinite substrate simultaneously is almost impossible due to the computational limit, some approximations/assumptions are necessary in the calculations in order to improve the computational efficiency. In our study, a SAM/Si system is first simulated as a cluster including one single molecule and a finite size of the Si substrate. Although the "Single Molecule" assumption prevents the intermolecular interaction from being considered in the computation (and therefore the model may not accurately describe the system), it can be used to describe a low coverage SAM/Si (assuming the local packing density of the molecules is low as well), which is a typical case for a SAM at the early stage of the growth. Because such a calculation emphasizes the molecule-substrate interaction, it can also be used to study the reaction pathway of the growth.[22]

In addition to studying the SAMs/Si systems using single molecule cluster DFT, a periodic DFT method, which many molecules systems are achieved by periodically repeating surface unit cells two dimensionally, is also used in our research to understand the effect of molecule-molecule interaction in SAMs. The single molecule cluster DFT work was done by

Nathan Yorder (for SAMs on Si(111)) and Michael Walsh (for SAMs on Si(001)) in the Hersam group, while the periodic DFT work was done by Kirk H. Bevan in the Datta group at Purdue University.

6.1 Single molecule cluster DFT

A $Si_{26}H_{30}$ and a Si_9H_{12} cluster is respectively used for the SAMs/Si(111) and SAMs/Si(001) to approximate the silicon surfaces in the vicinity of the adsorption site of the molecule as well as the underlying silicon substrate. A molecule is bonded to a silicon atom in the top layer, and all other silicon atoms are passivated with hydrogen. The cluster was constructed using HyperChem Release 7 (Hypercube, Inc., Gainesville, FL) and optimized using molecular mechanics. The cluster was further optimized using DFT within the Q-Chem electronic structure package. The B3LYP density functional was chosen to account for electron exchange and correlation effects, and a 6-31G* all-electron basis set with polarization functions was employed for all atoms. The cluster was allowed to optimize its geometry without constraint. The β carbon radical of the molecule was capped with hydrogen to mimic the structure of a single molecule following abstraction of a hydrogen atom from the H-Si surfaces.[16]

6.2 Periodic DFT

While a cluster DFT calculation can yield insight into the binding geometries for SAMs/Si,[11] it does not account for effects resulting from molecule-molecule interactions within the organic adlayer. Consequently, periodic DFT calculations, which many molecules systems are achieved by periodically repeating surface unit cells two dimensionally, are performed to simulate the SAMs/Si structures. Due to the computation limit, (1 x 1) and (2 x 1) periodicities,

where (1 x 1) case has one molecule bonded to each surface silicon site and the (2 x 1) case has every other surface silicon being bounded, were considered in the study for SAMs/Si(111). For SAMs/Si(001), only the (2 x 1) case is considered. The local density approximation was used and geometry was converged to 0.01 eV/Å on a real-space grid corresponding to an energy cutoff of 300 Ryd. A double polarized local atomic orbital basis set was employed. Both unit cells were relaxed on slabs eight layers deep through the conjugate gradient method.

Chaper 7 : Structural characterization of Brominated SAMs on Si(111)

The self-assembled monolayer (SAM) structures formed by six brominated molecules on H-Si(111), includes SAMs derived from *p*-bromostyrene (**BrSty**), *p*-(4-bromophenyl)styrene (**BPS**), *p*-(4-bromophenylethynyl)styrene (**BPES**), (4-bromophenyl)acetylene (**BPA**), (*p*-(4-bromophenyl)phenyl)acetylene (**BPPA**), and (*p*-(4-bromophenylethynyl)-phenyl)acetylene (**BPEPA**). These were studied using a characterization package, including single molecule cluster DFT, periodic DFT, X-ray reflectivity (XRR), X-ray fluorescence (XRF), and X-ray standing wave (XSW). Because BPS- and BPES- derived SAMs are not as order as the others based on the (111) XSW measurement results, the studies for the two SAMs are limited to single molecule cluster DFT and (111) XSW.

7.1 Single molecule cluster DFT

Ball-and-stick models for covalently bound isolated BrSty, BPS, BPES, BPA, BPPA, and BPEPA molecules on H-Si(111) surfaces, based on the single molecule cluster DFT calculation results, are shown in Fig 7.1. The coordinates for the six structures are shown in appendix C.1 and the heights for the covalently bound molecules are summarized in Table 7.1. The starting configurations for the six DFT calculations had the bottom C=C bond (sp^2) of the alkenyl molecule aligned directly over Si T_1-T_4 (sp^3) bond direction, and the bottom C-C bond (sp^3) of the alkyl molecule aligned directly over Si T_1-H_3 (bisect two sp^3) direction. (On a (111) Si surface, a Si-Si sp^3 bond links the T_1 and T_4 sites. T_1 site is the 1-fold coordinated site directly

above the top Si at the surface bilayer, T_4 site is the 4-fold coordinated site directly above the bottom Si at the surface bilayer, and H_3 site is the 3-fold coordinated hollow site (Fig 7.1a)). The two different types of the lateral orientations assumed in the starting configurations were based on the rotation study results shown in Fig 7.2.

	BrSty	BPS	BPES	BPA	BPPA	BPEPA
Height (Å)	8.86	13.13	15.58	8.86	13.21	15.79

Table 7.1 The heights of the terminal Br atoms in Fig 7.1. Height Z = 0 corresponds to the T_1 Si site.

In Fig 7.2, the three alkenyl structures (propene, BPA/Si(111), BPPA/Si(111)) and two alkyl structures (propane, BrSty/Si(111)) were rotated about their C-X axes (X = C or X = Si). The DFT calculated energy changes for each orientation are shown in Fig. 7.2f and 7.2g. At a rotation angle of $\phi = 0$, the C=C bond in Fig. 7.2a – 7.2c or C-C bond in Fig. 7.2d – 7.2e is aligned with the sp^3 bond (i.e. C-H bond for propene and propane, and Si-Si bond for the three SAMs/Si). From Fig. 7.2f all three alkenyl structures have the lowest energy at $\phi = 0^\circ$. In contrast, the alkyl molecule and SAM structure (BrSty/Si(111)) become energetically most stable at $\phi = 60^\circ$, where the C-C bond bisects two sp^3 bonds. Each of these calculated energy barriers is greater than the k_BT thermal energy at room temperature. This result suggests that the interaction at the molecule-silicon interface is directly attributed to the sp^2 and sp^3 hybridization and is

confirmed by the rotation of propene and propane molecules. Since the total energy change of both rotated propene and propane can be qualitatively matched by the change of HOMO energy (Fig. 7.2f and 7.2g), the alignment of the molecules on Si(111) surface may also change the HOMO level and affects the electric property of SAMs. Further study is necessary for better understanding the mechanism.

The six models in Fig 7.1 are the DFT calculation results under the assumption that each molecule only reacts to one surface Si site after the hydrosilylation reaction. However, for the three acetylene molecules originally having two pi-bonds at the terminals before surface reaction, besides the alkenyl type of bonding proposed by Linford and Chidsey[14] (Fig 7.3a) it is also possible that each molecule reacts to two neighboring surface Si sites, forming a double-bridge (Fig 7.3b) or single-bridge (Fig 7.3c) configuration.[22] To explore these possibilities, the SAM structure for BPA, the smallest acetylene molecule in our study, is further explored using DFT with the consideration of the three possible types of bonding, and the corresponding results are shown in Fig 7.3. The coordinates for the three relaxed structures are listed in appendix C.1. (For the comparison purpose, a cluster DFT calculation using a bigger Si substrate, $Si_{38}H_{45}$, was also performed but showed no significant difference in the calculation. The coordinates for the relaxed structures are listed in appendix C.2). Because of the differences of the Br heights, a XRR analysis, which is sensitive to the thickness of the monolayer, will be able to determine the correct structure. The details of combining XRR with DFT to study BPA SAM will be later given in the XRR analysis section.

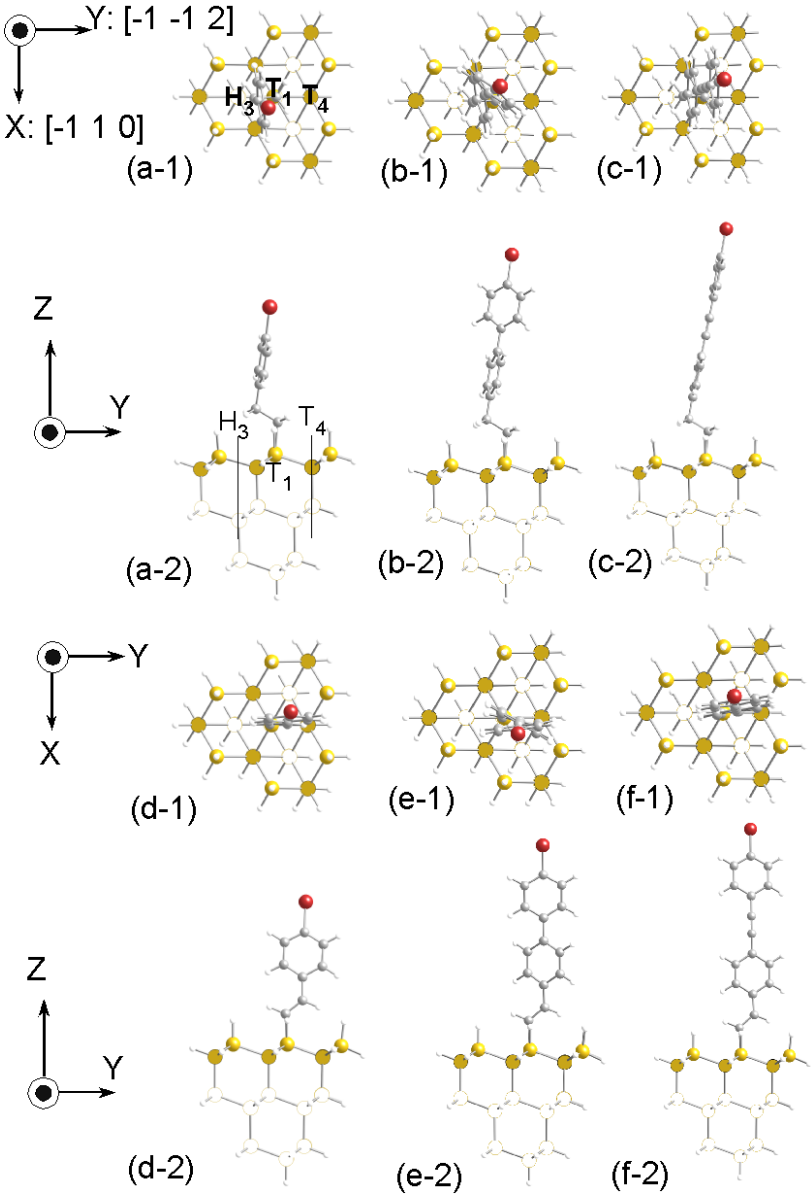

Figure 7.1 DFT optimized models for $Si_{26}H_{30}$ cluster covalently bonded to: (a) *p*-bromostyrene (BrSty), (b) *p*-(4-bromophenyl)styrene (BPS), (c) *p*-(4-bromophenylethynyl)styrene (BPES), (d) (4-bromophenyl)acetylene (BPA), (e) (*p*-(4-bromophenyl)phenyl)acetylene (BPPA), and (f) (*p*-(4-bromophenylethynyl)phenyl)acetylene (BPEPA). For purposes of clarity, the Si atoms at the top of the surface bilayer are made brighter than those below. The coordinates for the DFT structures are listed in appendix C.1.

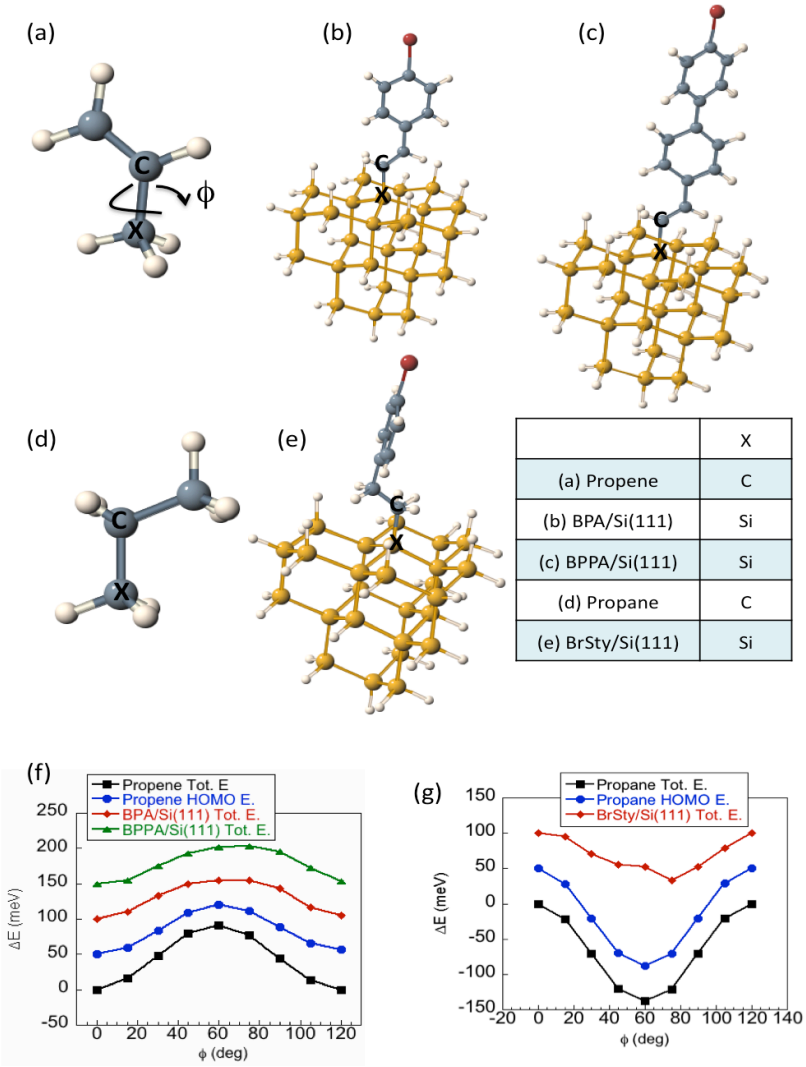

	X
(a) Propene	C
(b) BPA/Si(111)	Si
(c) BPPA/Si(111)	Si
(d) Propane	C
(e) BrSty/Si(111)	Si

Figure 7.2 Illustration of the rotation of (a) propene, (b) BPA/Si(111), (c) BPPA/Si(111), (d) propane, and (e) BrSty/Si(111) at the C-X axes. The DFT calculated energies (periodic DFT model with a great vacuum to avoid molecule-molecule interaction) at various rotational orientations are plotted in (f) and (g) for alkenyl and alkyl structures, respectively. Due to the limit of using DFT for the orbital hybridization between molecules and surfaces in SAM/Si case, the HOMO energy calculations were only performed for the rotations of propene and propane molecules. For purposes of clarity each curve is given a 50 meV vertical offset. At a rotation angle of $\phi = 0$, the C=C bond in (a) – (c) or C-C bond in (d) – (e) is aligned with the sp^3 bond.

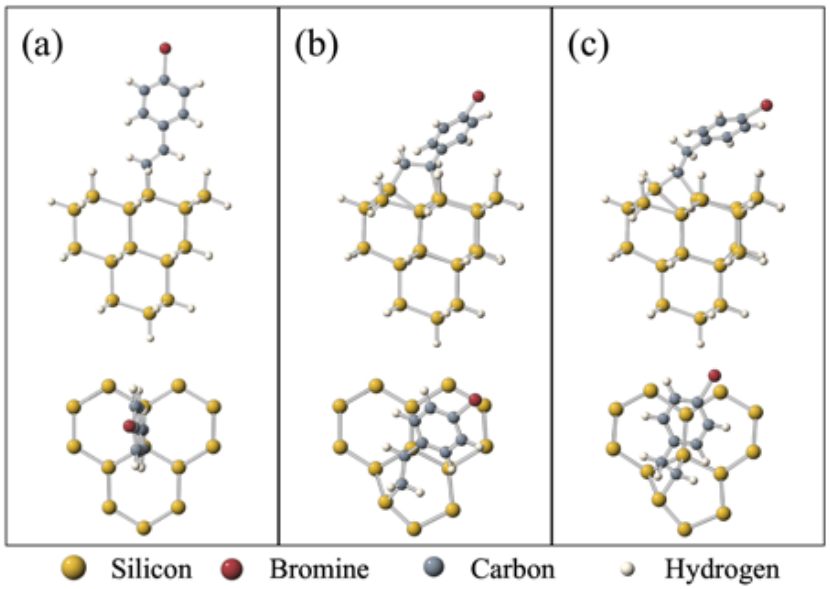

Figure 7.3 Binding geometry configurations for isolated-molecule cluster DFT calculations, showing a side view and top-down view of the BPA molecule on a $Si_{26}H_{31}$ cluster. (a) Configuration based on a proposed model by Linford and Chidsey,[14] showing the BPA molecule after reacting with a single silicon atom and extracting one hydrogen atom from the surface. (b) "Double-bridge" configuration, showing the two end-carbons bonded to two neighboring silicon T_1 sites. (c) "Single-bridge" configuration, showing the terminal carbon bonded with two neighboring T_1 sites. In (b) and (c), the molecule has extracted two hydrogen atoms from the surface. The coordinates for the DFT structures are listed in appendix C.1. The figure is reproduced from Ref. [11].

7.2 Periodic DFT

7.2.1 BrSty/Si(111)

Two different periodicities were considered for the periodic DFT study for BrSty SAM on Si(111): a (1 x 1) case, where there is a BrSty molecule bonded to each T_1 silicon site, and a (2 x 1) case, where one-half of the silicon T_1 sites have a molecule attached. For the (1 x 1) packing, eight initial configurations that are azimuthally rotated in steps of 15˚ are considered (Fig 7.4a) and the results are shown in Fig 7.4b. The coordinates for the unit-structures before and after the relaxation are listed in appendix C.4. The DFT determined total energies and the terminal Br heights are summarized in Table 7.2.

In Fig 7.4, the results for orientation 3 and 7 are not available because such orientations cause every molecule directly overlapping with a neighboring molecule. Since the differences of the total energies in Table 7.2 are smaller than the thermal energy at room temperature (k_BT = 25 meV), the six relaxed configurations are equally possible. The six configurations also have the almost identical heights for the terminal Br despite the difference of the lateral orientations. Comparing the six relaxed configurations with that from the single molecule DFT, the terminal Br in the former is set further away from the Si(111) surface than that in the latter, 8.87 Å to 9.07 Å, due to the molecule-molecule interaction.

	Or1	Or2	Or3	Or4	Or5	Or6	Or7	Or8
E(eV)	-2608.698	-2608.700	N/A	-2608.698	-2608.697	-2608.697	N/A	-2608.700
z	9.07 Å	9.08 Å	N/A	9.07 Å	9.07 Å	9.07 Å	N/A	9.07 Å

Table 7.2 Periodic DFT calculated total energies and the heights of the terminal Br atoms for the eight orientations shown in Fig 7.4 for BrSty/Si(111). Z = 0 is height of the T_1 Si that is bonded to the BrSty molecule .

As was shown in the earlier single molecule DFT study, alkyl and alkenyl molecules are azimuthally orientated over T_1-H_3 and T_1-T_4 directions on Si(111) surfaces, respectively, due to the molecule-substrate interaction. For comparison purposes, two (2 x 1) packed BrSty-derived monolayers on Si(111), T_1-H_3 and T_1-T_4 orientated, are explored using periodic DFT and the results are shown in Fig 7.5. The coordinates for the unit-structures before and after the relaxation are also listed in appendix C.4. It shows that the heights of the terminal Br atoms in the (2 x 1) case are both smaller than that in the (1 x 1) case. Because the total energy for the T_1-H_3 orientated structure (Fig 7.5a) is 74 meV smaller than that for the T_1-T_4 orientated structure (Fig 7.5b), the former is thermodynamically more favorable and the result is consistent with that found in the rotation study in chapter 7.1.

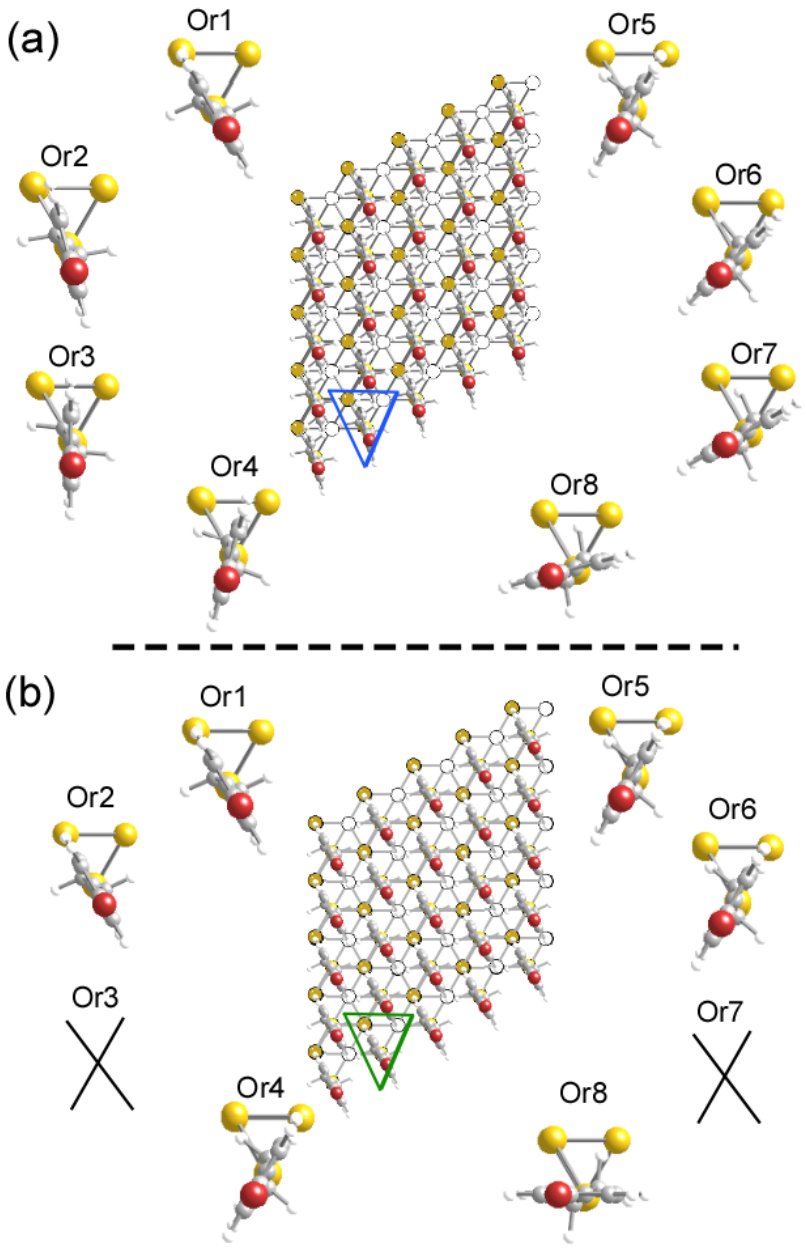

Figure 7.4 **BrSty/Si(111) 1x1 periodic DFT results:** (a) Eight unit-structures with different azimuthal orientations for the molecules used as the starting configurations in the (1 x 1) periodic DFT study for BrSty–derived SAM on Si(111). The center is the super-cell created using Or1 unit-structure. (b) The relaxed structures for the eight orientations from (a). The center is the super-cell created using the relaxed Or1 unit-structure. The coordinates for the DFT structures are listed in appendix C.4.

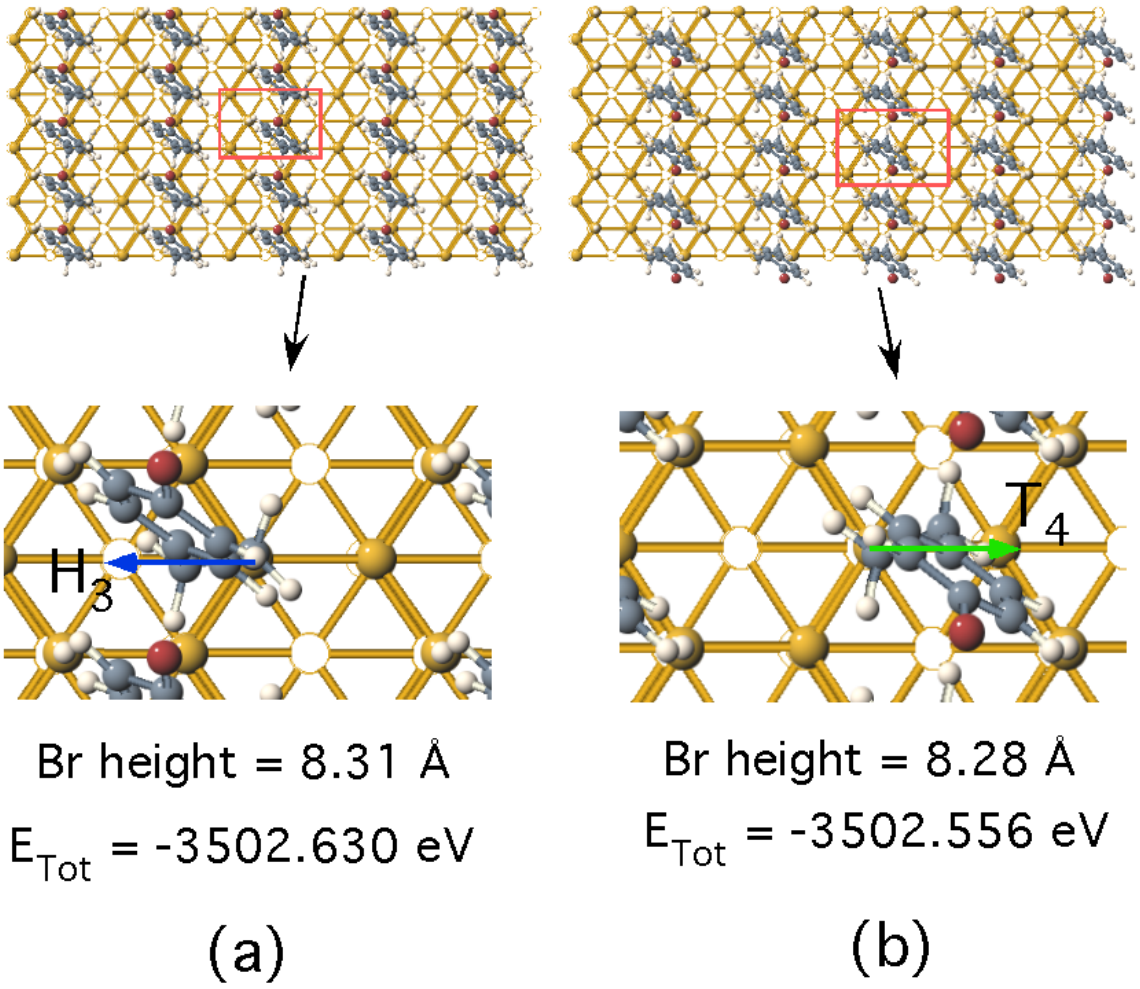

Figure 7.5 **BrSty/Si(111) 2x1 periodic DFT results:** Top views of the relaxed (2 x 1) periodic super-cells for BrSty-derived SAMs on H-Si(111) surfaces that are (a)T_1-H_3 orientated and (b) T_1-T_4 orientated. The Br heights are measured with respect to the tethered Si site. For purposes of clarity, the Si atoms at the surface bilayer are made brighter than those below. The coordinates for the DFT structures are listed in appendix C.4.

7.2.2 BPA/Si(111)

Following the same strategy used in the study of BrSty/Si(111), (1 x 1) and (2 x 1) packed BPA–derived monolayers are studied using periodic DFT. Since the covalently bound molecules in Fig 7.1 are either T_1-T_4 or T_1-H_3 orientated, the study is limited to both the orientations. The results for the (1 x 1) and (2 x 1) packing are respectively shown in Fig 7.6 and Fig 7.7 - 7.10. The coordinates for the unit-structures before and after the relaxation are listed in appendix C.5. Different than the (1 x 1) packed BrSty/Si(111), the total energy for the T_1-T_4 orientated BPA–derived monolayer is 70 meV lower than that for the T_1-H_3 orientated monolayer. However, a lower energy for T_1-T_4 orientation was not observed in the (2 x 1) periodic DFT calculations. If we compare the (2 x 1) packed BrSty–derived SAMs in Fig 7.5 with the (2 x 1) packed BPA-derived SAMs in Fig 7.7 - 7.10, it shows that both the studied T_1-T_4 and T_1-H_3 orientated BrSty-derived SAMs (Fig 7.5), and the studied T_1-H_3 orientated BPA-derived SAMs (Fig 7.9 and 7.10) have the aromatic rings perpendicular to the molecular rows, but the T_1-T_4 orientated BPA–derived SAMs (Fig 7.7 and 7.8) do not. As a result, the T_1-T_4 orientated BPA-derived SAMs have smaller inter-molecular interaction than that in the T_1-H_3 orientated BPA/Si(111) configurations, therefore the two cases could not be directly compared. The result suggests that the relative orientation of the molecules to the molecular rows is critical in a (2 x 1) periodic DFT study.

Although the relaxed structures are very different in Fig. 7.9 and 7.10, each structure belongs to a local minimum energy result. It suggests that a global minimum energy structure may not be obtained if a wrong starting configuration is chosen.

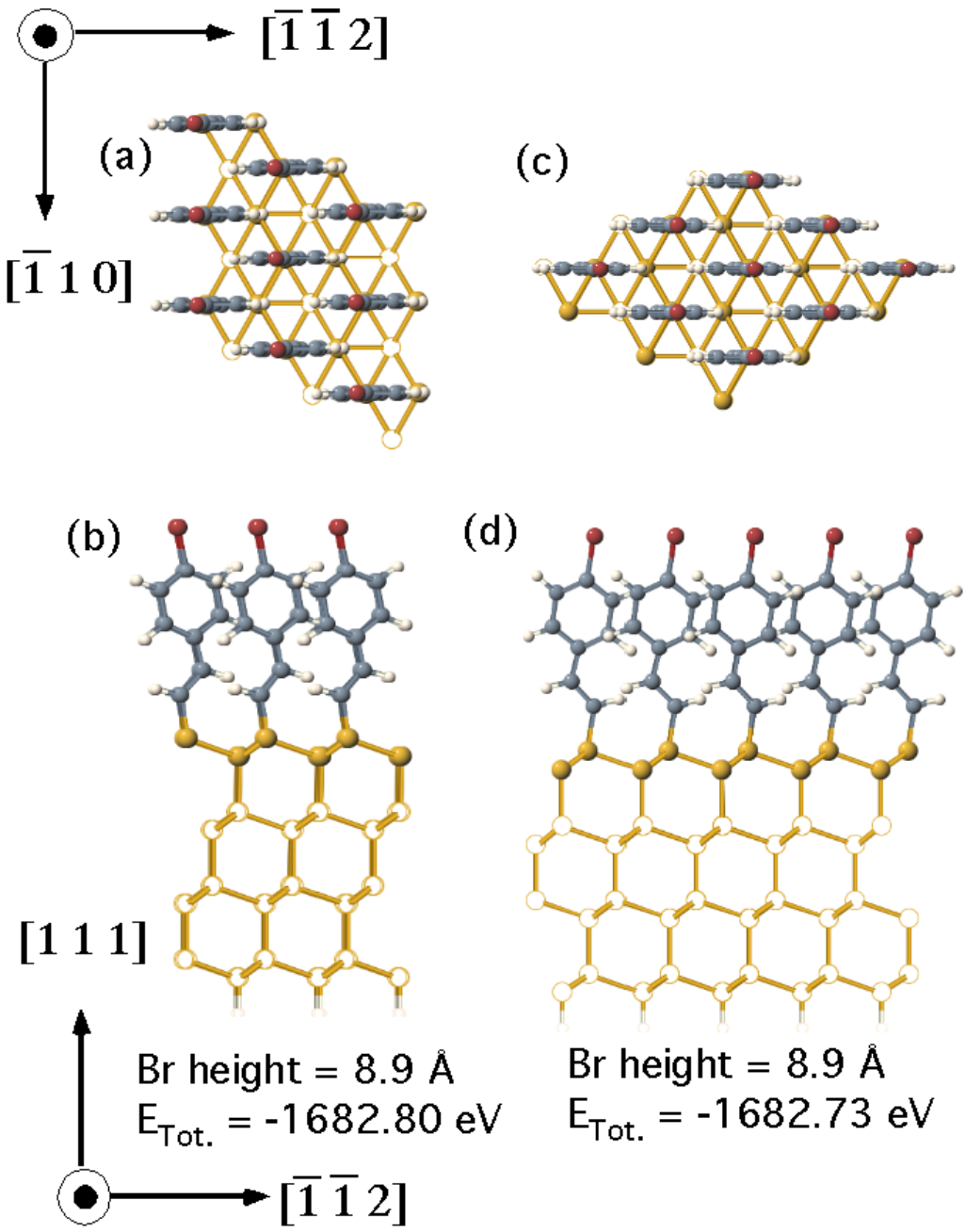

Figure 7.6 Top views (upper images) and side views (lower images) of the relaxed (1 x 1) periodic unit cells for the BPA/Si(111) calculated within SIESTA. (a) and (b) are the T_1-T_4 orientated configurations while (c) and (d) are the T_1-H_3 orientated configurations. For purposes of clarity, the Si atoms at the surface bilayer are made brighter than those below. The coordinates for the DFT structures are listed in appendix C.5.

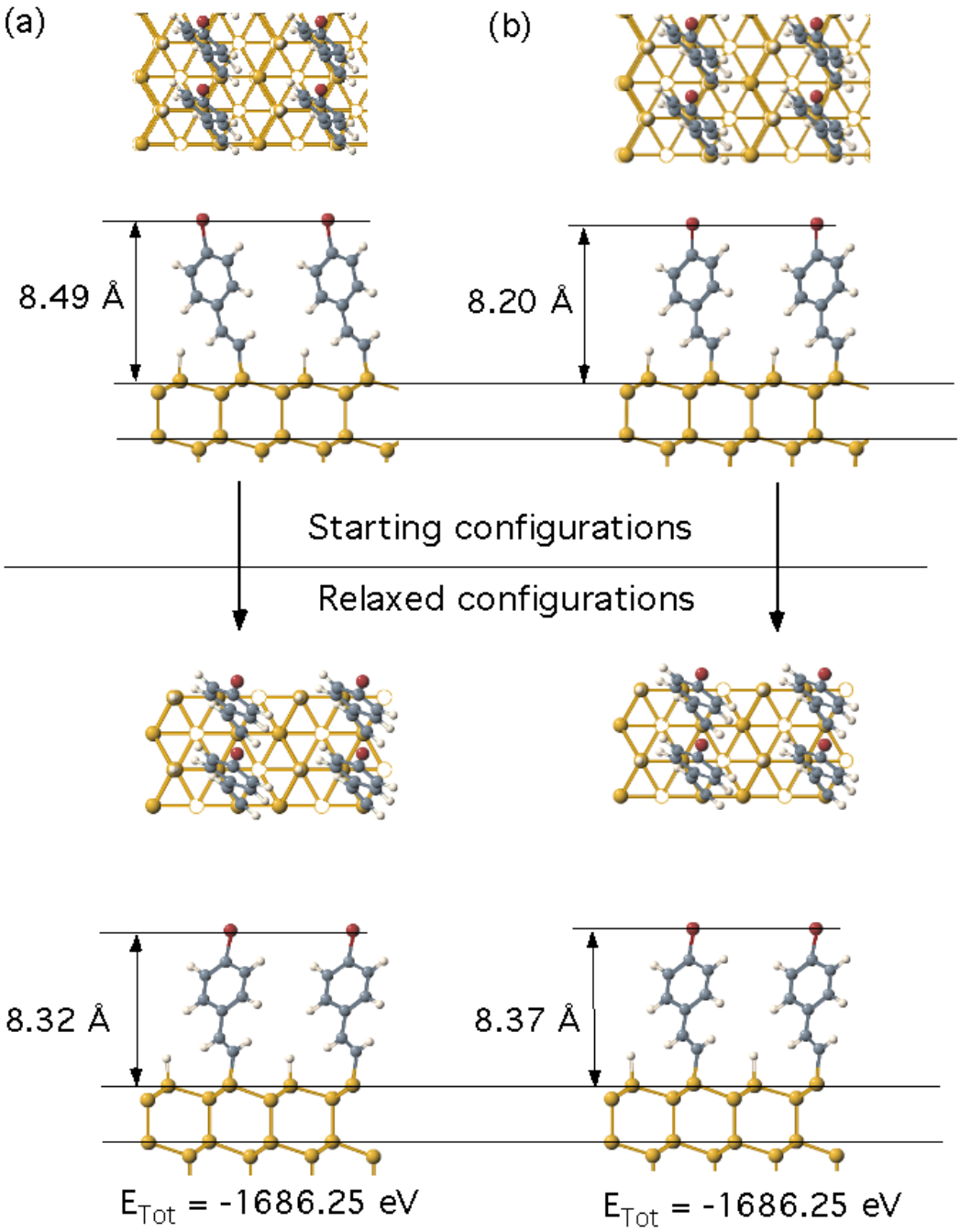

Figure 7.7 Top views and side views of the T_1-T_4 orientated (2 x 1) packed BPA–derived SAMs on Si(111) before and after structure relaxation in DFT calculations. The tilting of the BPA molecules for (b) is initially greater than that in (a). For purposes of clarity, the Si atoms at the surface bilayer are made brighter than those below in the top views. The coordinates for the structures are listed in appendix C.5.

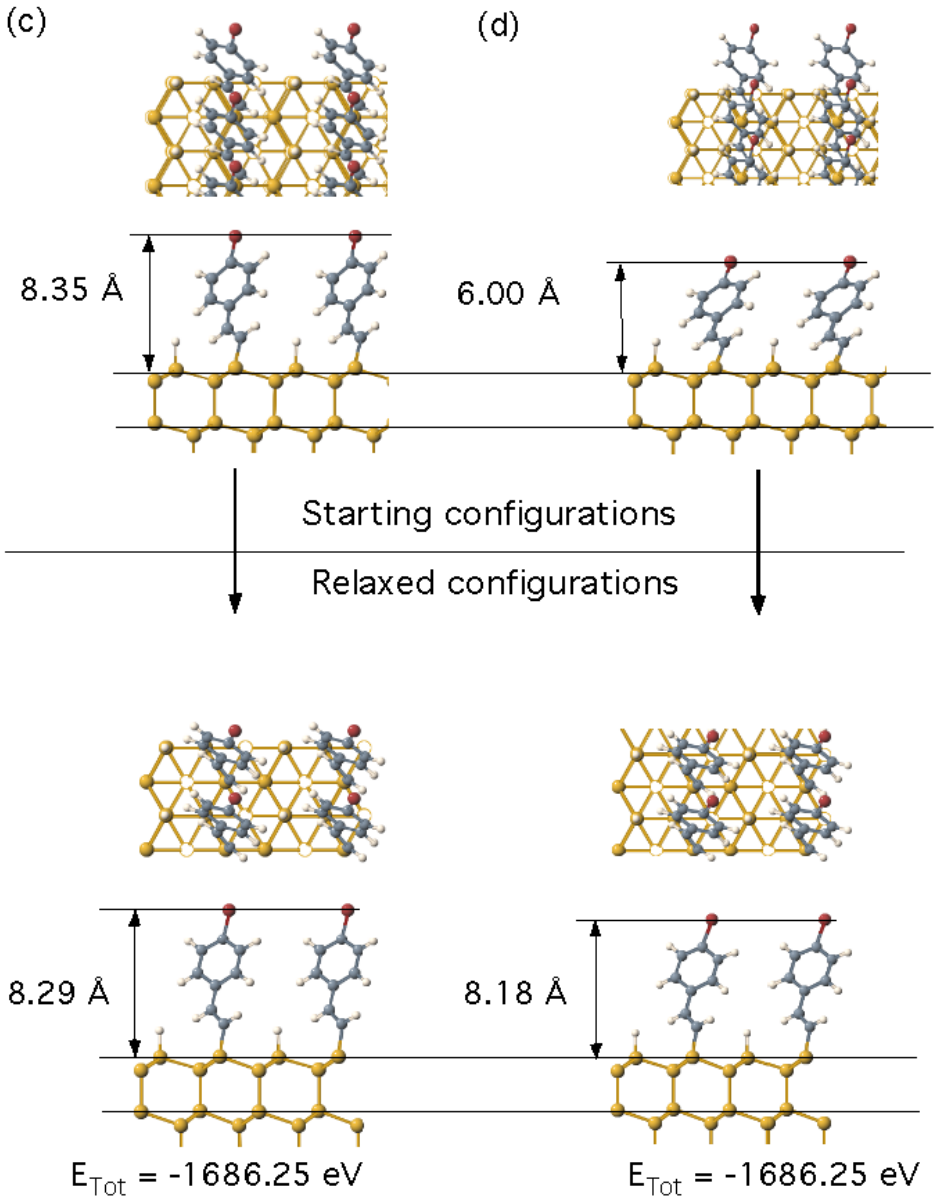

Figure 7.8 Top views and side views of the T_1-T_4 orientated (2 x 1) packed BPA-derived SAMs on Si(111) before and after structure relaxation in DFT calculations. The tilting of the BPA molecules for (c) is initially smaller than that in (d) but greater than that in Fig 7.7(a). For purposes of clarity, the Si atoms at the surface bilayer are made brighter than those below in the top views. The coordinates for the structures are listed in appendix C.5.

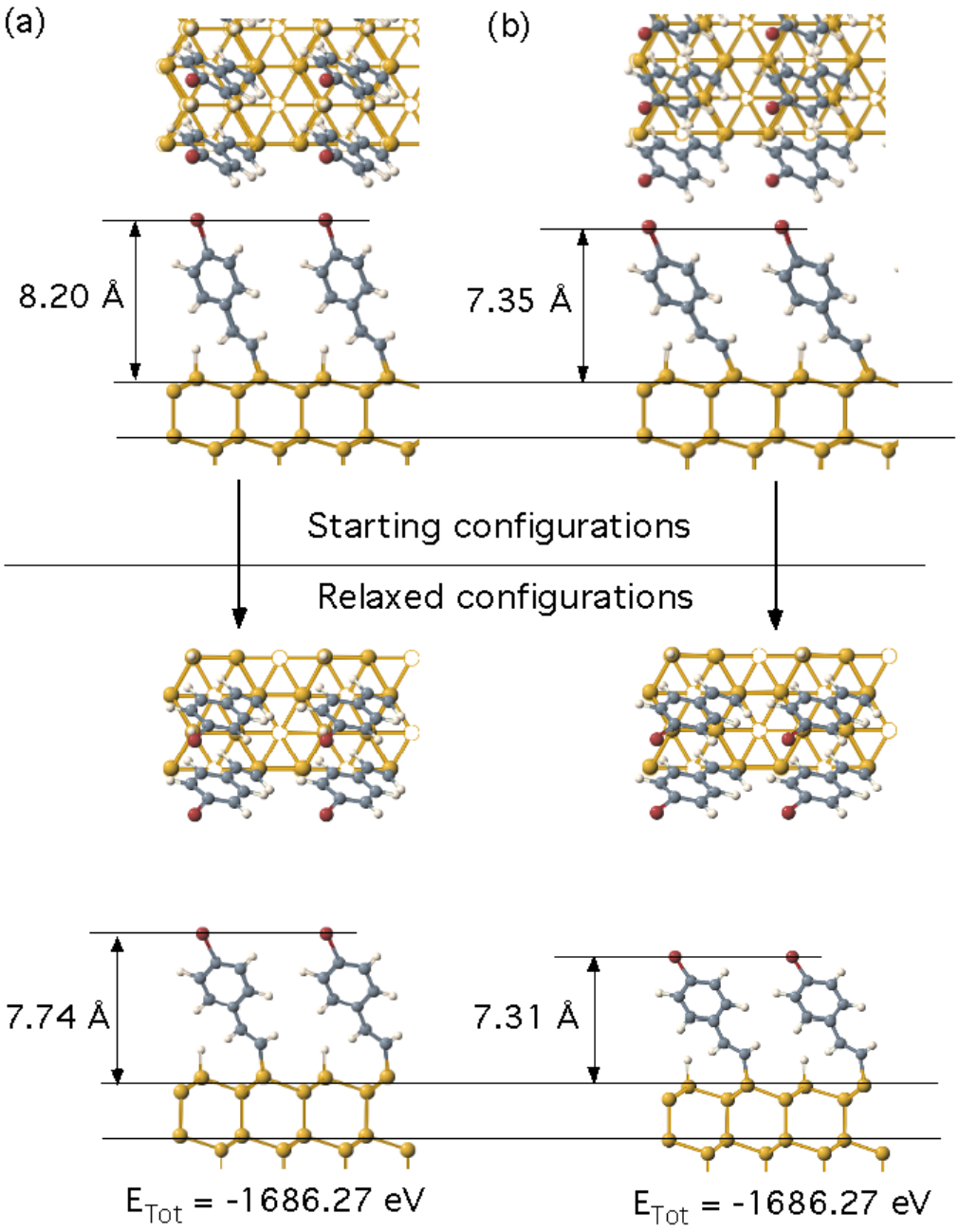

Figure 7.9 Top views and side views of the T_1-H_3 orientated (2 x 1) packed BPA-derived SAMs on Si(111) before and after structure relaxation in DFT calculations. The tilting of the BPA molecules for (b) is initially greater than that in (a). For purposes of clarity, the Si atoms at the surface bilayer are made brighter than those below in the top views. The coordinates for the structures are listed in appendix C.5.

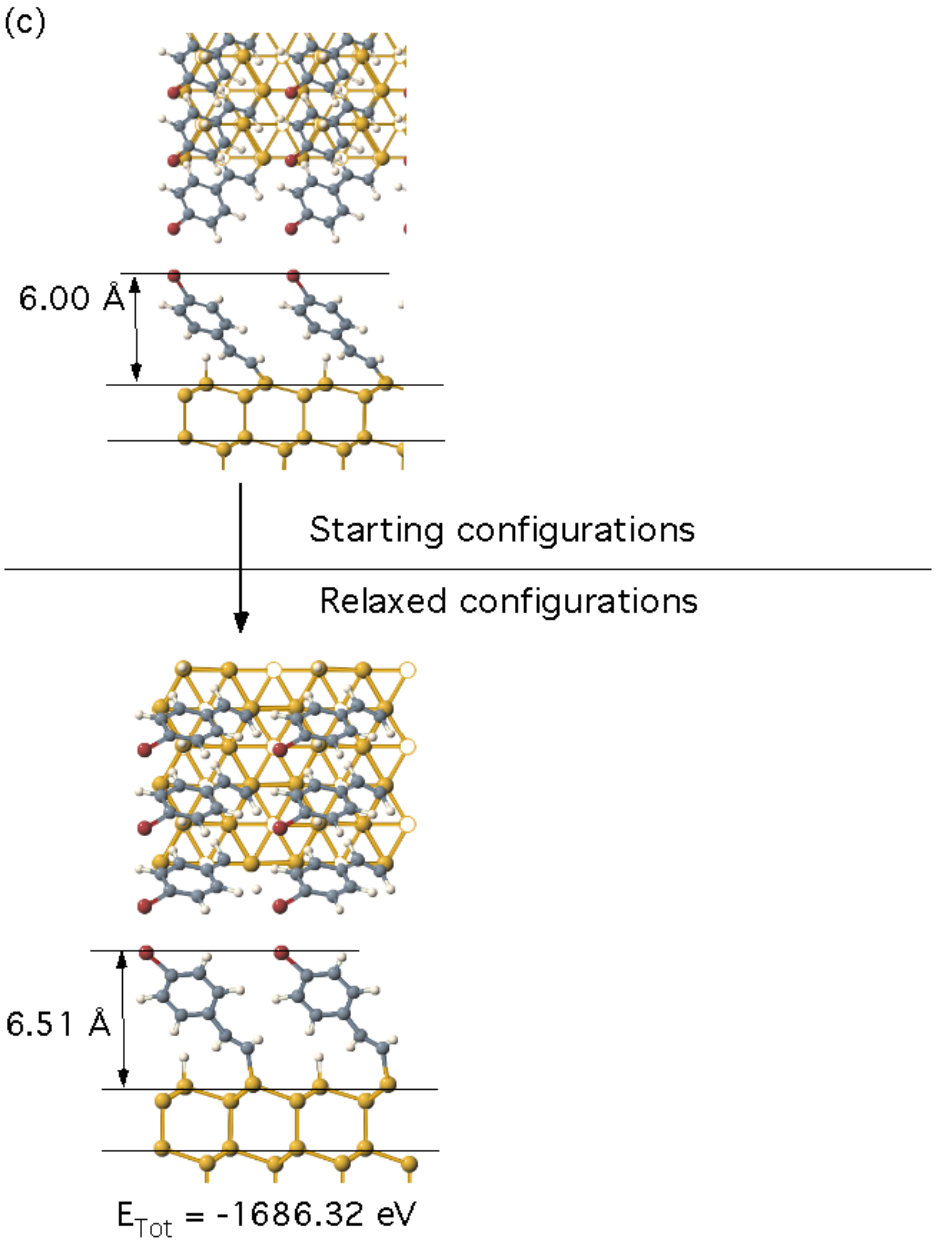

Figure 7.10 Top view and side view of a T_1-H_3 orientated (2 x 1) packed BPA-derived SAMs on Si(111) before and after structure relaxation in a DFT calculation. The tilting of the BPA molecules is initially greater than that in Fig 7.9(b). For purposes of clarity, the Si atoms at the surface bilayer are made brighter than those below in the top views. The coordinates for the structures are listed in appendix C.5.

7.2.3 BPPA/Si(111)

In the (1 x 1) periodic DFT study for BPPA SAM on Si(111), two orientations for the bottom aromatic ring, i.e. T_1-T_4 and T_1-H_3 directions, were considered in conjunction with three relative rotations between the two rings (0˚, -60˚, and 60˚) (Fig 7.11). After the relaxations of the structures, only three out of the six configurations are energetically converged and the results are shown in Fig 7.12. The parallel two-ring structure of the Or0 and Or3 configurations in Fig 7.12, which is attributed to the strong molecule-molecule interaction in the (1 x 1) type packing, is suspicious because the hindering effect between the hydrogen atoms from the two aromatic rings is expected to push the both rings to be not aligned. The dense (1 x 1) packing is also questionable because the coverage of our BPPA SAM is always less than half monolayer.

According to the earlier discussions for BrSty- and BPA- based SAMs on Si(111), the molecule-molecule interaction as well as the molecule-substrate interaction affects the configuration of a monolayer on a Si (111) surface. For a (2 x 1) packed monolayer, the relative rotation of the molecules with respect to the molecular rows is also critical to the determination of the final structure. For a monolayer consisting of “two-ring” BPPA, such effect is expected to be greater than that in a BrSty- or BPA- based monolayer because of the stronger pi-pi interaction attributed to the additional phenyl ring. In order to fully explore the possible configurations for the SAM, seven starting models with BPPA molecules azimuthally rotated in steps of 30˚ (Fig 7.13) are studied using (2 x 1) periodic DFT. Or0, Or1, and Or2 are respectively symmetry equivalent to Or4, Or5, and Or6, and the difference is the relative rotation of the

molecules with respect to the molecular rows. The relaxed structures and the corresponding Br heights, in conjunction with the total energies, are shown in Fig 7.14.

In Fig 7.14, those (2 x 1) relaxed configurations possessing sp^2 C=C bond alignment over an sp^3 Si-Si substrate bond were the most energetically favorable. The alkenyl C=C in the relaxed structures of Or1, Or2, and Or5 are aligned toward the nearest Si T_1 site (and *not* along a sp^3 Si-Si bond) thereby are energetically unfavorable. This result is consistent with the DFT study discussed in chapter 7.2. Therefore, we conclude that the intermolecular interactions do not overwhelm the substrate-molecule interaction. In the pre-relaxed structures for Or2 and Or6, although both the BPPA molecules are aligned over the sp^3 Si-Si substrate bonds, the molecules in Fig 7.14c are 30˚ rotated from the molecular rows while the molecules in Or6 are 90˚ rotated from the molecules rows. The relaxed structure of Or2 places the Br markers laterally over the nearest neighbor Si T_1 sites at a height of 12.3 Å while the molecules in the relaxed Or6 structure are further tilted with the Br markers located over the next nearest neighbor Si T_1 site across the long diagonal of the unit cell and consequently ~1Å lower than that of Or2. Therefore, though intermolecular interaction does not drastically influence the rotational orientation of the molecule, it does however play a substantial role in determining the height and lateral position of the molecule. The result underscores the need to include intermolecular interaction in the calculations of SAMs' structures. The Or2 structure, although is the second lowest energy structure, is later experimentally confirmed to be the correct configuration for BPPA SAM/Si. The details will be stated in the XSW analysis.

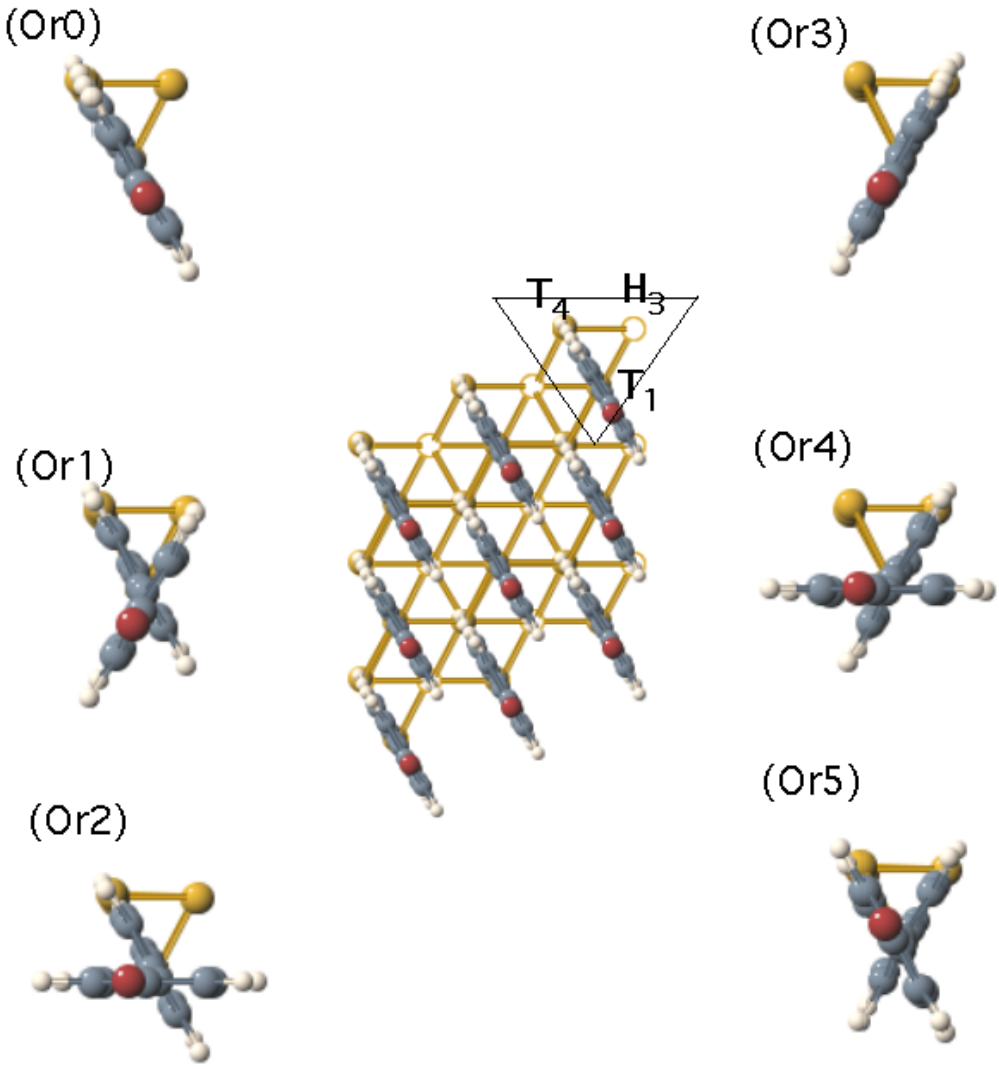

Figure 7.11 Top views of the six triangle unit structures created by the combination of T_1-T_4 and T_1-H_3 root orientations, with 0˚, -60˚, and +60˚ relative rotations for the two aromatic rings, for the (1 x 1) periodic DFT calculations for BPPA SAM. The center is a super-cell created using Or1 unit structure. The coordinates for the DFT structures are listed in appendix C.6.

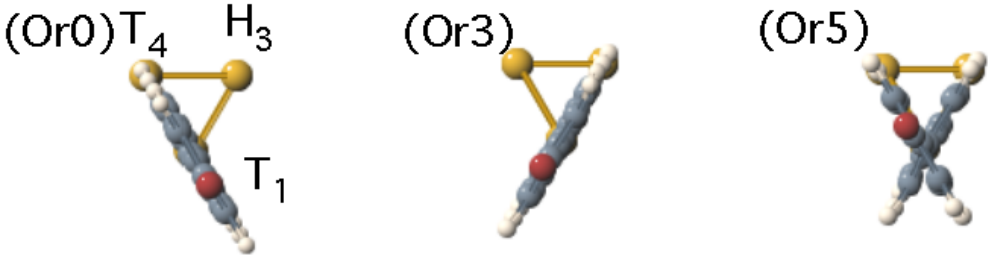

	Type	Br height (Å)	E_{Tot}
Or0	T_1-T_4	13.26	-3567.486
Or3	T_1-H_3	13.32	-3567.017
Or5	T_1-H_3	13.27	-3567.446

Figure 7.12 The relaxed structures that energetically converge for BPPA/Si(111) in the (1 x 1) periodic DFT calculations. The coordinates for the DFT structures are listed in appendix C.6.

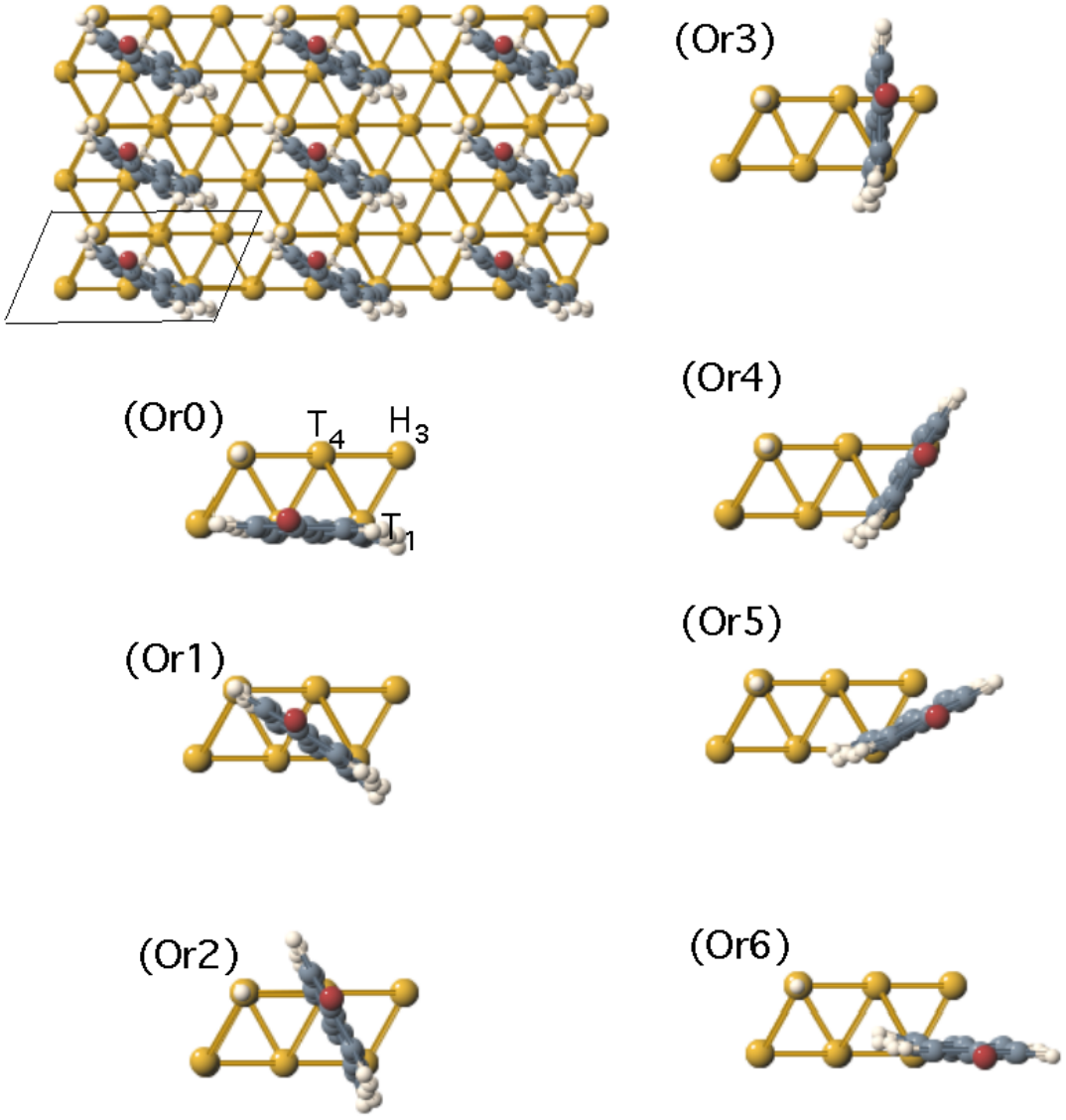

Figure 7.13 Top views of the seven unit structures used in the (2 x 1) BPPA periodic DFT calculations. The coordinates for the models are listed in appendix C.6.

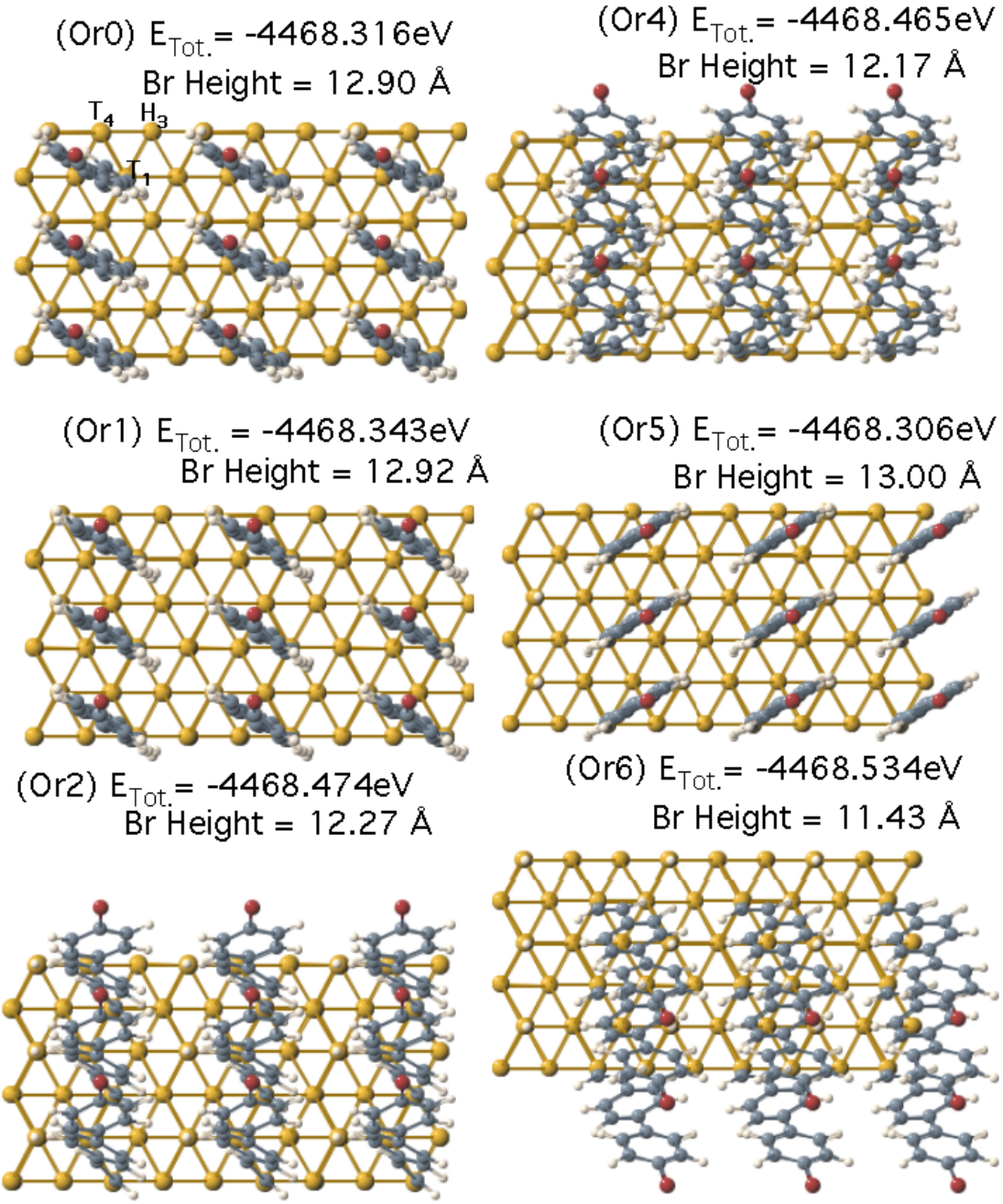

Figure 7.14 Top views of the relaxed BPPA/Si(111) super-cells based on the (2 x 1) periodic DFT results. The calculations were based on the initial configurations shown in Fig 7.11. Or3 configuration is not feasible due to the direct overlap of the molecules. The coordinates for the unit structure of each super-cell are listed in appendix C.6.

7.2.4 BPEPA/Si(111)

Following the same strategy used in the study for BPPA SAM on Si(111), seven rotations of the BPEPA molecules with respect to the Si substrate (Fig 7.15) are explored in (2 x 1) periodic DFT and the relaxed structures are shown in Fig 7.16. (1 x 1) periodic DFT for BPEPA SAM on Si(111) was not performed because such molecular packing overemphasizes the intermolecular interaction as was discussed previously in the BPPA/Si(111) case. Besides Or0, all the relaxed structures shown in Fig 7.16 have the root alkenyl C=C double bound aligned over one of the three T_1-T_4 Si-Si bonds and the result is consistent with the earlier study of the rotation of alkenyl structures on Si(111). The relaxed structures for Or2, Or3, and Or4 have the lowest total energies and are equally possible because the difference of energy is <= 25 meV. However, the height of the terminal Br for each configuration is different due to the tilting of the molecules. Experimental measurements will be needed in order to determine the correct structure.

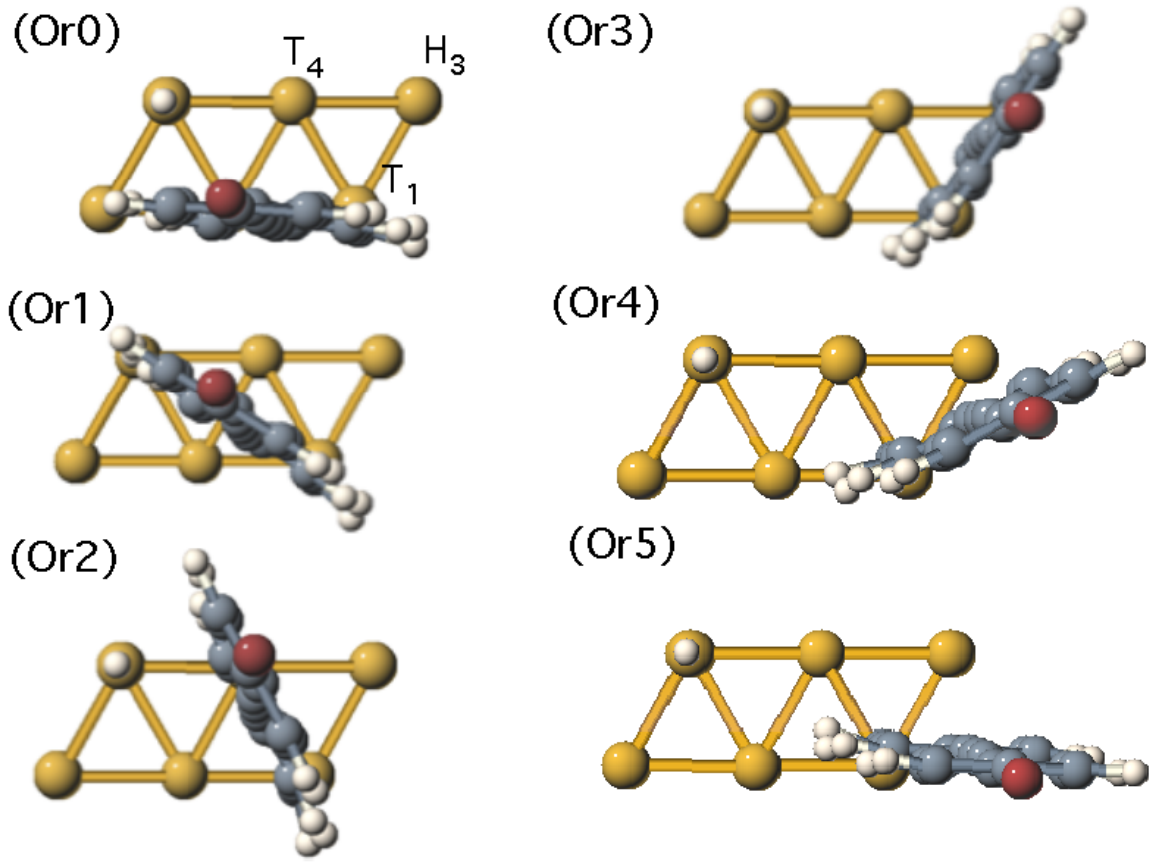

Figure 7.15 Top views of the six unit cells used in the (2 x 1) BPEPA periodic DFT calculations. The orientation where the molecule bisects the T_1-T_4 and T_1-H_3 directions is not considered because it will result in a direct overlap of the molecules. The coordinates for the structures are listed in appendix C.7.

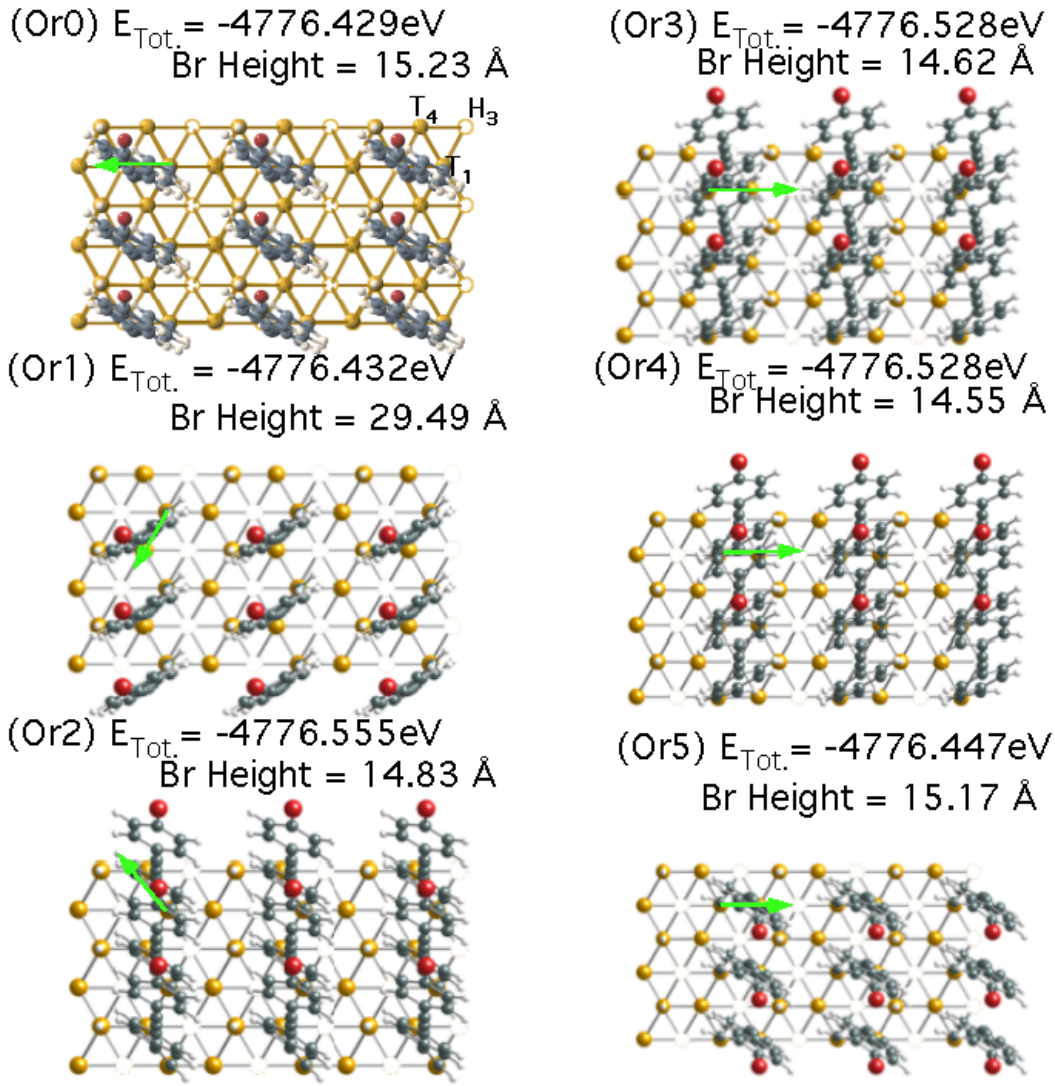

Figure 7.16 Top views of the relaxed BPEPA/Si(111) structures after the (2 x 1) periodic DFT calculations based on the starting configurations shown in Fig 7.15. The green arrows indicate the directions for the root alkenyl C=C bonds. For purposes of clarity, the Si atoms at the surface bilayer are made brighter than those below. The coordinates for the unit structure for each super-cell are listed in appendix C.7.

7.3 XRR analysis

The X-ray reflectivity (XRR) data and analysis for the three alkenyl SAMs, BPA-, BPPA-, and BPEPA- based monolayers on Si(111), are shown in Fig 7.17. The best fits are based on using Parratt's recursion formulation[38] with a Br / hydrocarbon / Si multilayer model. The normalized electron density profiles determined from the XRR analysis are shown as an inset in the figure. The XRR measured Br heights are 9.1 Å, 12.4 Å, and 14.6 Å for BPA-, BPPA-, and BPEPA- based SAMs, respectively. The analysis illustrates the sensitivity of XRR measurement to the thickness of an organic film on Si surface.

Additional information for a SAM/Si can be acquired by combing XRR analysis with DFT modeling. An example is given in Fig 7.18, which the XRR data for BPA/Si(111) are compared to three model calculations based on the three different bonding configurations discussed in Fig 7.3. For the model calculations, a packing density of 0.67 monolayers is commonly assumed because such coverage is independently measured by XRF experiment. The result in the figure clearly shows that the alkenyl type structure of Fig 7.18a is the correct bonding configuration for BPA/Si(111). The alkenyl C=C bond is also confirmed in a SUM Frequency Generation (SFG) study.[11]

A XRR analysis for a SAM/Si is sensitive to the coverage of the film, the tilting of the molecules, and the roughness at each interface (substrate surface[36] and the film/air interface). An example is given in Fig 7.19, which the XRR data for BrSty SAM/Si(111) is compared to six different model calculations. Referring to the DFT calculated structure shown in Figure 7.1a, the film thickness (t) is allowed to vary by changing the tilt-angle (η) to the molecule about the T_1 Si

site from its nominal DFT determined configuration. The DFT predicted film thickness (with η = 5°) is t = 8.9 Å. The best-fit curve to the data is labeled A1, which has: (1) the molecule tilted further inward to η = 17° (corresponding to t = 8.5 Å), (2) the molecular packing at a coverage of Θ = 0.46 ML, (3) a static Gaussian vertical displacement distribution for all atoms in the molecule characterized by a width σ = 1.0 Å, and (4) the interface roughness parameter at β = 0.47 for the Si surface. The XRR sensitivity to molecular packing density is demonstrated by the accompanying curves labeled A2 and A3, where the coverage has been changed to 0.52 and 0.40 ML, respectively. As can be seen, the strength of the anti-reflection dip at Q = 0.32 $Å^{-1}$ changes with coverage. Curves B1 and B2 illustrate the sensitivity to changing the film thickness by changing the molecular tilt angle to 5° and 53°, respectively. Curve B1 corresponds to the DFT model shown in Fig 7.1a (t = 8.9 Å) and curve B2 corresponds to t = 5.3 Å. The shift in Q of the dip is quite sensitive to the height of the Br layer. (All other parameters in models A2, A3, B1, and B2 are identical to those described above for model A1).

Although XRR analysis can be used to confirm the DFT predicted models of SAMs/Si, a XRR analysis only senses the electron density profile along the surface normal direction and is not sensitive to the lateral structure. To obtain the lateral information, we further combine DFT, XRR with XSW analysis.

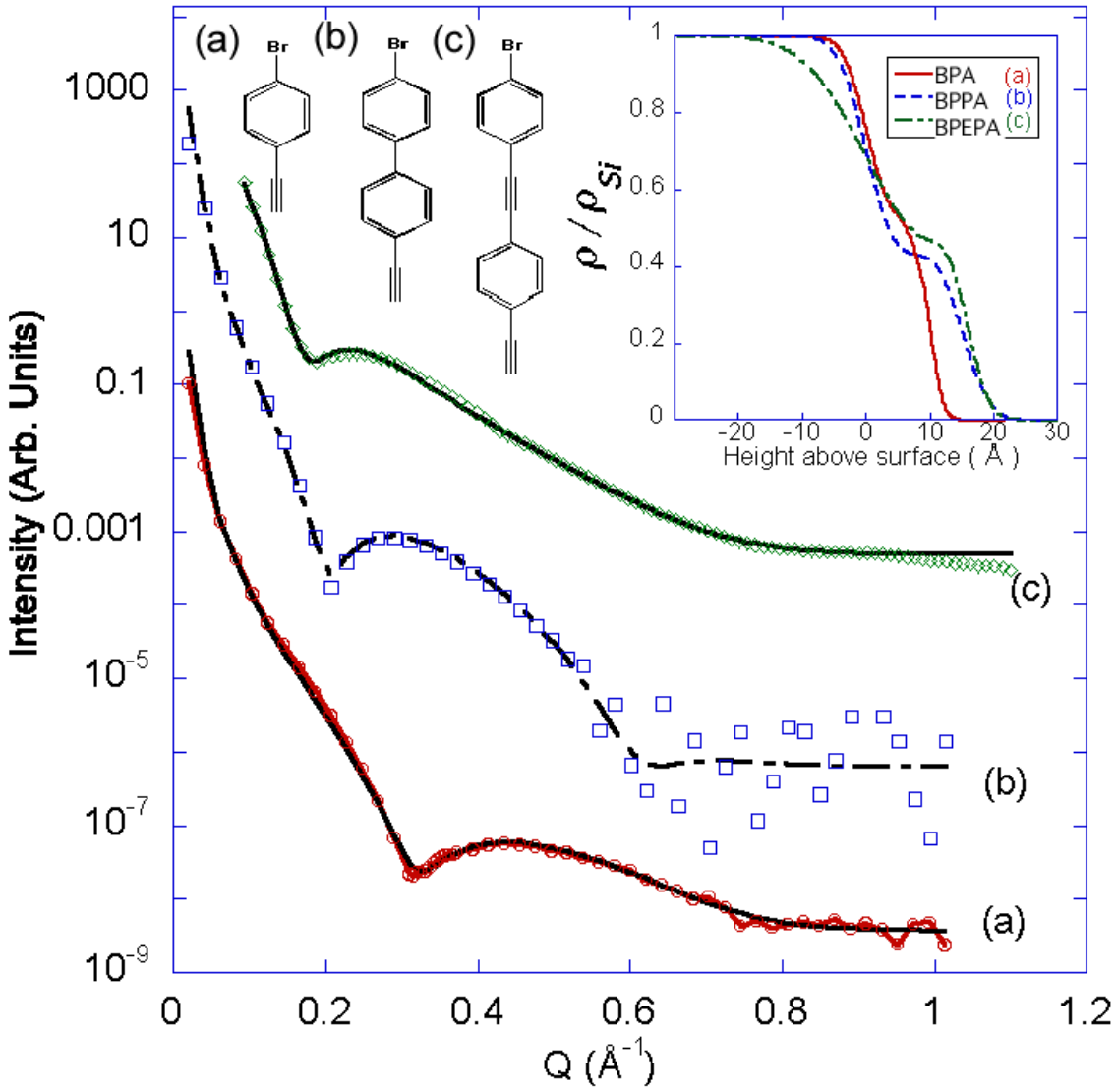

Figure 7.17 X-ray reflectivity data and 3-layer model fits for (a) BPA-, (b) BPPA-, and (c) BPEPA- based SAMs grown on Si(111). The normalized electron density profiles for the best fits are shown in the inset. The XRR curves (b) and (c) are vertically offset by $x10^2$ and $x10^4$, respectively.

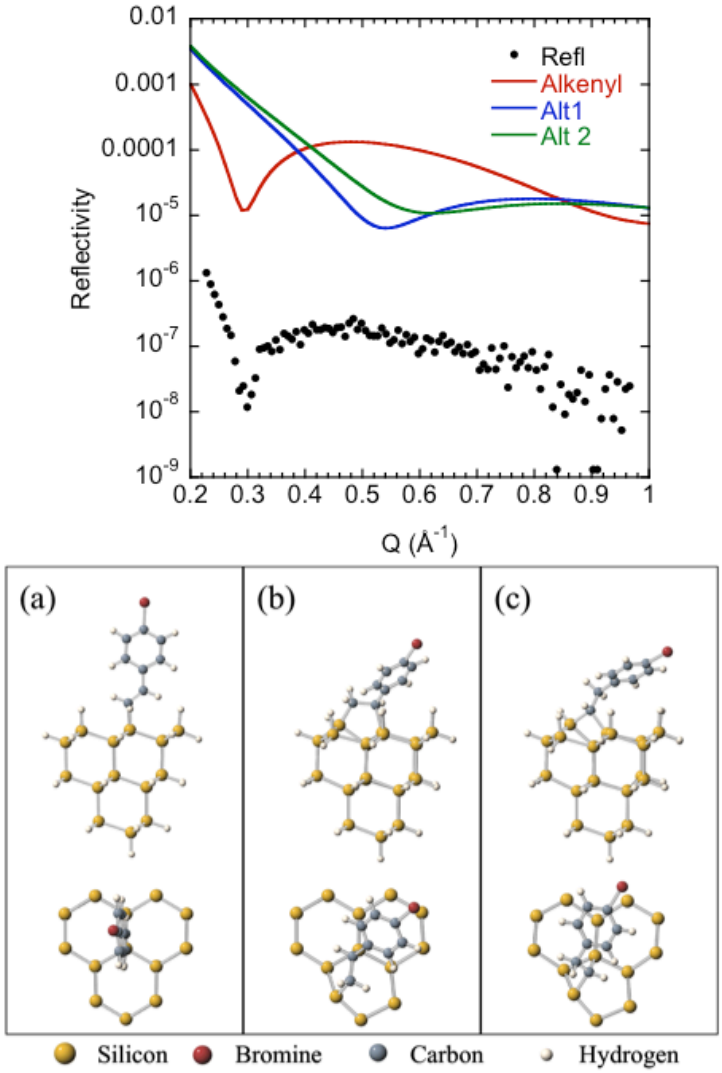

Figure 7.18 Specular XRR data (filled circles) for the BPA-derived SAM on Si(111) and model simulations using a molecular structure factor with atomic coordinates based on the cluster DFT calculation results in Fig. 7.3. The DFT predicted models are again shown in the lower image. The theoretical XRR from the alkenyl structure (a) best fits the data. Alt1 depicts the double-bridge configuration (b) and Alt2 the single-bridge configuration (c). 0.67 monolayers and 2 Å roughness are assumed in the XRR calculations. For purposes of clarity, the three model simulations are vertically offset by 10^2.

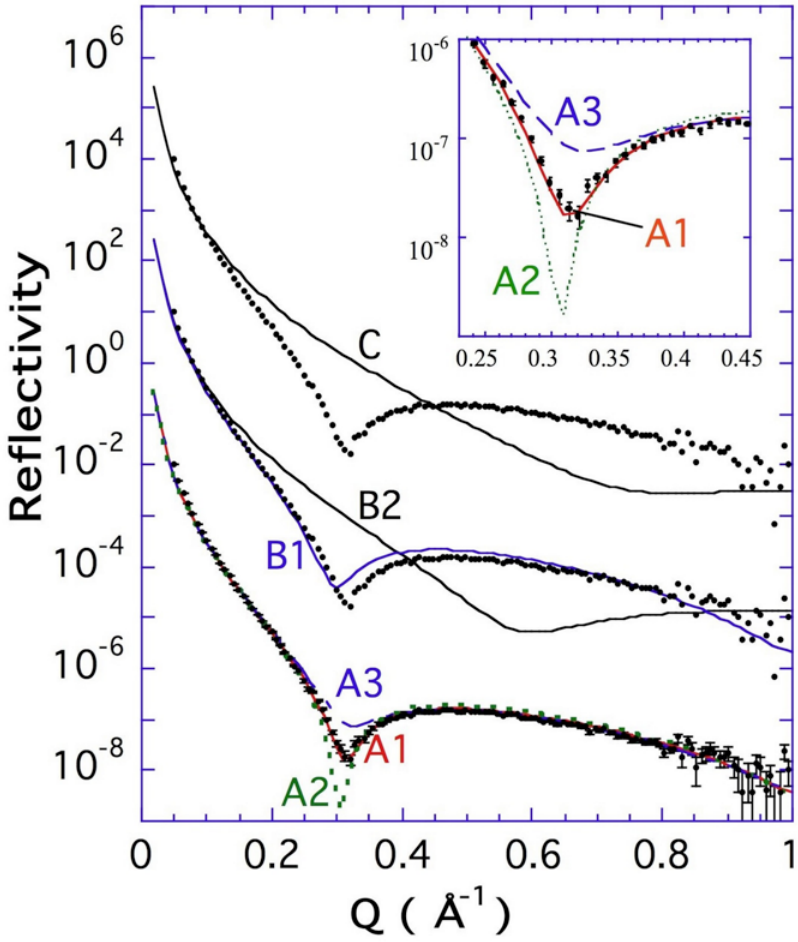

Figure 7.19 Specular XRR data (filled circles) for the BrSty-based SAM on Si(111) and model simulations using a molecule structure factor with atomic coordinates based on the DFT calculation of Fig 7.1a. The best-fit simulation is labeled A1. The A1 model has a molecular coverage of Θ = 0.46 ML, an inward molecular tilt of η = 17° (t = 8.5 Å), a Si surface roughness parameter of β = 0.47, and a σ = 1.0 Å Gaussian distribution to the vertical displacements of the atoms in the molecule. Model A2: same as A1, except Θ = 0.52 ML. A3: same as A1, except Θ = 0.40 ML. B1: same as A1, except η = 5° tilt (t = 8.9 Å). B2: same as A1, except η = 53° tilt (t = 5.3 Å). C: same as A1, except Br removed from styrene and attached directly to Si at the T_1 site. For purposes of clarity the vertical offsets are: x10^3 for B1 and B2, and x10^6 for C.

7.4 XSW analysis

7.4.1 XRF coverage measurement and 111 XSW

Specular and off-specular *h k l* XSW data and theoretical fits (from Eq. 4.18, Z(θ) = 1 because Br is on the substrate surface) for the six brominated SAMs on Si(111) are shown in Fig 7.20 -7.25. Besides the XSW data for BPEPA/Si(111), which were taken at 33ID-D station, all the other XSW data shown in this chapter were taken at 5ID-C station. The Br coverage, the coherent fractions f_H and the coherent positions P_H for all the samples are summarized in Table 7.3. Because the measured f_{111} for BPS- and BPES- derived SAMs are smaller than 0.1, the distributions of the Br atoms within the both SAMs are expected to be more random than the others therefore no off-normal XSW were performed on them.

	Cov (ML)	*h k l*	111	333	11-1	220	311	31-1
BrSty	0.5	f_H	0.33(2)	0.09(2)	0.23(2)	0.10(2)		
		P_H	0.70(1)	0.10(6)	0.36(2)	0.08(3)		
BPS	0.4	f_H	0.05(1)					
		P_H	0.03(4)					
BPES	0.6	f_H	0.03(1)					
		P_H	0.39(9)					
BPA	0.2	f_H	0.64(2)	0.23(2)	0.18(2)	0.12(2)		
		P_H	0.77(2)	0.35(2)	0.32(2)	0.13(2)		
BPPA	0.2	f_H	0.46(2)	0.04(3)	0.27(6)	0.13(2)		
		P_H	0.11(1)	0.38(8)	0.34(2)	0.12(3)		
BPEPA	0.2	f_H	0.20(2)	0.16(4)	0.27(3)	0.21(3)	0.31(2)	0.19(4)
		P_H	0.65(1)	0.95(4)	0.28(1)	0.03(3)	0.93(1)	0.67(3)

Table 7.3 XSW measured Br coherent fractions (f_H) and coherent positions (P_H) for the listed set of $\boldsymbol{H}$ =*h k l* reflections. The origin is chosen at the bulk-like Si position in the top of the surface bilayer. P_H is ambiguous if $f_H <$ 0.1 .

Qualitatively, f_{111} measures the spatial spread in the Br distribution relative to the (111) standing wave period (d_{111} = 3.135Å). The value of f_{111} is directly proportional to the non-random fraction

C, which is the fraction of Br atoms at specific locations. A larger distribution spread relative to the periodicity will result in a smaller f_{111}. The measured f_{111} (BrSty) > f_{111} (BPS) > f_{111} (BPES) and f_{111} (BPA) > f_{111} (BPPA) > f_{111} (BPEPA) are consistent with the fact that the Br atoms are set further away from the Si surfaces with the increase of the lengths of the hydrocarbon backbones (Fig. 7.1). In addition, although BPA-, BPPA-, and BPEPA- derived SAMs have the similar structures as BrSty-, BPS-, and BPES– derived SAMs, respectively, each one of the three alkenyl SAMs, with the C=C double bonds at the root after the reaction, has a higher f_{111} than its corresponding alkyl SAM, which has the alkyl C-C bond at the root. The result suggests an overall improvement of the vertical order from the more rigid C=C bond at the molecule/substrate interface.

The effect of having a C=C double bond or a C-C single bond at the molecule/substrate interface is further studied by comparing BrSty- and BPA- derived SAMs. Assuming that the up-right configuration is the only conformation for both the SAMs, the vertical spread of Br can be analytically determined by the comparison of f_{111} with f_{333}. f_H can be expressed as the product of non-random fraction C, geometrical factor a_H and the Debye-Waller D_H. $D_H = \exp(-2\pi^2\sigma^2_H/d^2_H)$ treats the averaged displacement field of the Br atoms as a Gaussian distribution with width σ_H. Using the f_{111} and f_{333} values, and assuming $a_{111} = a_{333} = 1$ (i.e., a single Br height), we compute that $C = 0.8$ and $\sigma_{111} = 0.26$ for the BPA/Si(111), whereas $C = 0.4$ and $\sigma_{111} = 0.30$ for the BrSty/Si(111). The greater non-random fraction and smaller distribution spread of Br in the BPA-derived SAM suggests that this overall improvement to the vertical order can be accredited to the more rigid C=C bond at the bottom of BPA-based monolayer in contrast to the C−C bond for BrSty-based monolayer.

7.4.2 Br density maps

Since a XSW measurement senses the distribution of the XRF selected atoms in the direction perpendicular to the diffraction plane, a combination of specular and off-specular XSW results can therefore be used to three-dimensionally triangulate the site of the XRF selected atoms relative to the Si lattice (Fig 7.26). Using Eq. 4.25, the XSW-measured Fourier components listed in Table 7.3 (and their 3-fold symmetry equivalents) are summed to produce Br 3D atomic density maps with 2D cuts shown in Fig 7.27.

The multiple maxima in the density maps are due to the truncation of the Fourier summation (missing terms in the infinite sum). Since the Br density maps are produced by allowed Si reflections with the use of 3-fold symmetry of Si(111) surface, the hot spots have the same periodicities as the Si primitive unit cell (rhombohedral) appearing at one of the three horizontal high symmetry sites, i.e. T_1, T_4, or H_3. The XSW measurement by itself cannot discriminate among these possibilities. However, in conjunction with the longer-length scale XRR measurements (Fig 7.17 and 7.19), the hot spots for the Br atoms are determined and indicated by the horizontal lines. The XSW and XRR determined heights and the lateral positions for the Br markers are listed in Table 7.4. After comparing the experiments measured heights with the predicted models based on single molecule cluster DFT calculations (Fig 7.1), additional tilting for the molecules in the cluster models is suggested. If using periodic DFT to simulate the molecule-molecule interaction and comparing the (1 x 1) and (2 x 1) DFT calculation results with the density maps, good agreements between the BPPA Br atomic map with Or2 structure in Fig 7.14, and the BPEPA Br atomic map with Or4 structure in Fig 7.16, are observed and shown in Fig 7.28. Both best fitting models are based on (2 x 1) periodic DFT.

Since locally lines of molecules within molecular islands were both experimentally observed in high resolution STM images[39] and theoretically predicted by a Monte Carlo simulation,[40] it could be the reason why a (2 x 1) periodic packing, where the molecular rows are formed by periodically tethering every other surface silicon to one molecule, better simulate the SAMs/Si(111) structure. Because not all azimuthal orientations were considered in the (2 x 1) periodic DFT computations for BrSty and BPA, good matches did not observed for both the SAMs. A better fitting should be available if repeating the DFT calculations using the strategy developed in the study of BPPA/Si(111) and BPEPA/Si(111).

SAMs	BrSty	BPA	BPPA	BPEPA
Br height (Å)	8.50	8.68	12.5	14.58
Lateral location	T_4	T_4	T_1	H_3

Table 7.4 The vertical heights and the lateral positions of the Br markers for the BrSty, BPA, BPPA, and BPEPA XSW density maps shown in Fig 7.27. The origin is at the T_1 Si .

In the direct comparison of the BPPA (2 x 1) periodic DFT calculated structures with its XSW measured Br density map in Fig 7.27, all three energetically most stable structures, Or2, Or4, and Or6, have the calculated Br atoms laterally above Si T_1 sites and match the map. However, even though the energy of Or6 relaxed structure is ~60 meV and ~70 meV lower than that of Or2 and Or4, respectively, the predicted Br height in the relaxed Or2 configuration,

instead of Or6, better agrees with the XSW & XRR measurement. This is possibly due to the improper assumption in the Or6 pre-relaxed structure. According to the proposed growth kinetics,[40] the structural change of C≡C to C=C at the interface results in radical-chain reaction and is responsible for the growth of alkenyl monolayers on Si. Thereby, molecules should grow along the direction of the C=C· radicals, which can be approximated by the directions of the alkenyl C=C bonds. In Or6, the perpendicular arrangement of the individual molecules to the molecular rows in the pre-relaxed configuration contradicts to the chain reaction mechanism and hence the result does not match the experiment result. The better prediction of the Or2 than Or6 is consistent with the radical chain reaction theory.

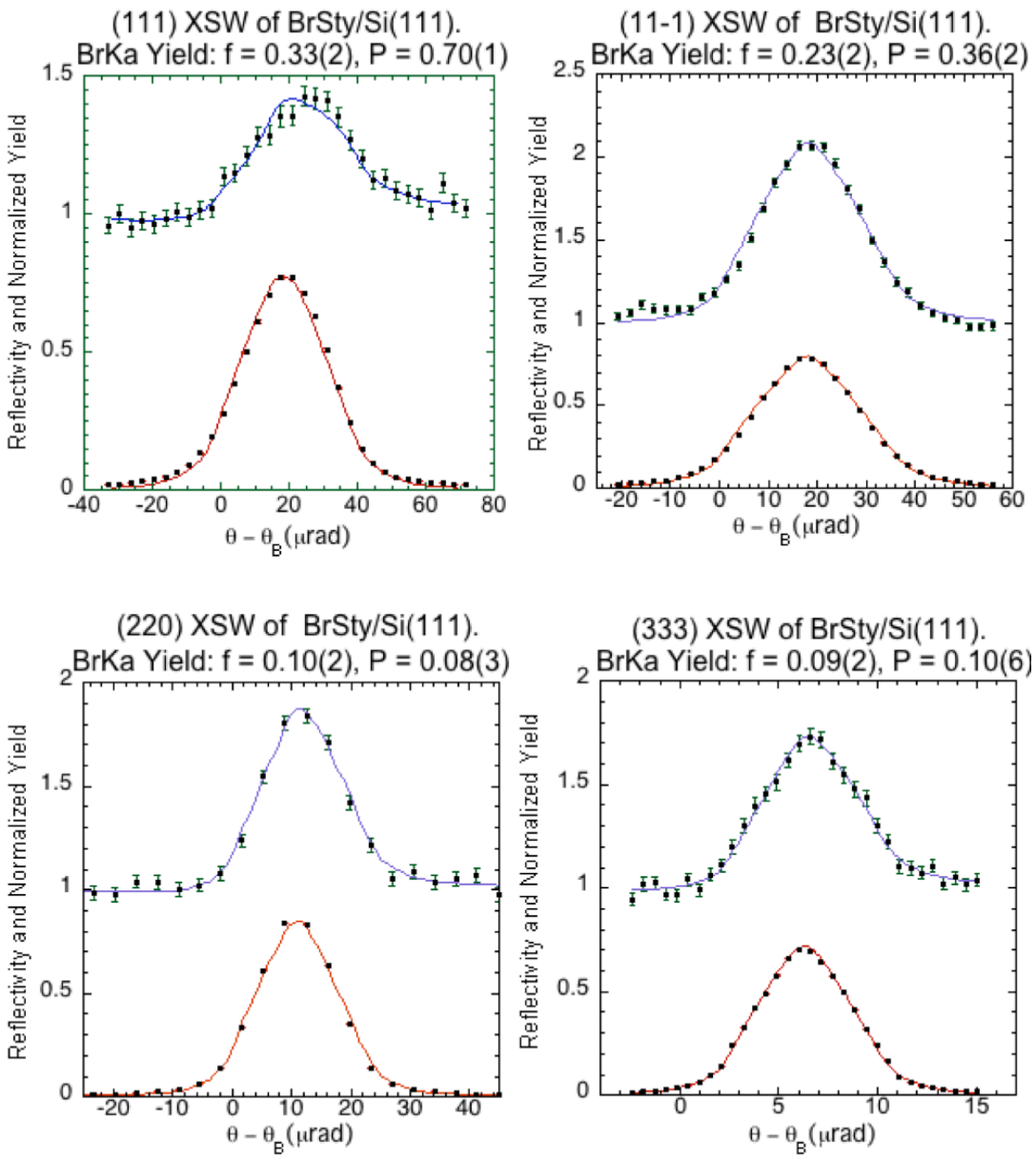

Figure 7.20 The single-crystal XSW results for the *p*-bromostyrene (**BrSty**)-derived SAM on Si(111). Shown are the angle dependences of the *h k l* Si Bragg reflectivity (bottom) and the Br Kα XRF yield data (top). Symbols are measured data, and solid lines are the best-fits of theory to the data.

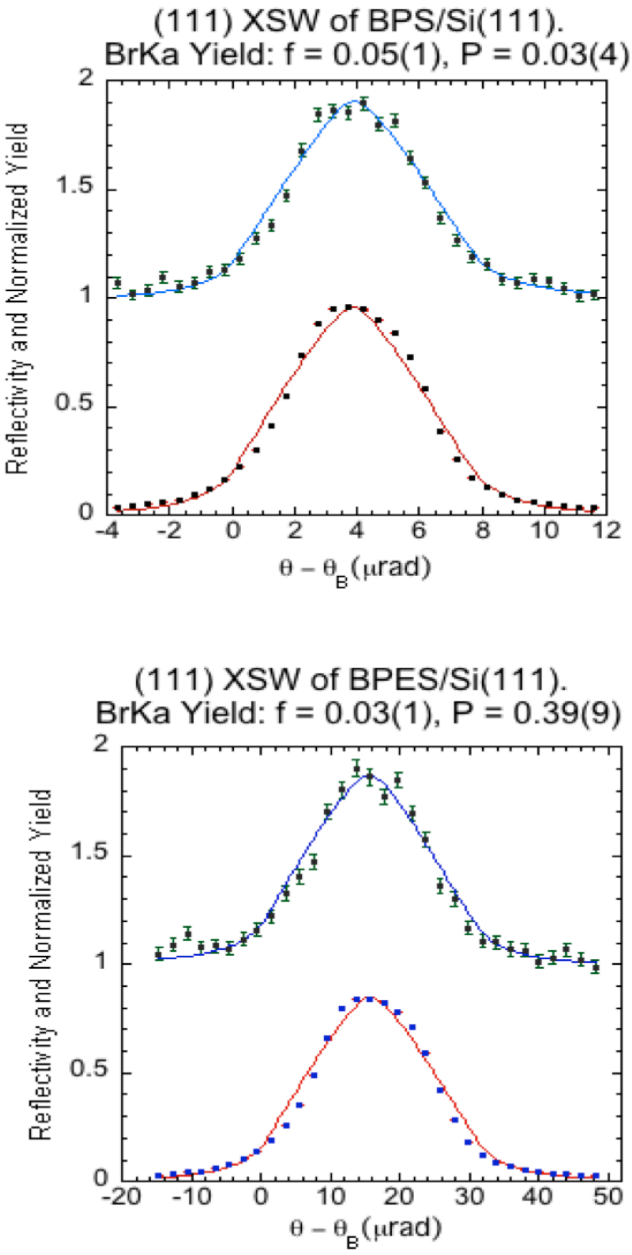

Figure 7.21 The 111 XSW results for *p*-(4-bromophenyl)styrene (**BPS**)- and *p*-(4-bromophenylethynyl)styrene (**BPES**)- derived SAMs on Si(111). Symbols are measured data, and solid lines are the best-fits of theory to the data.

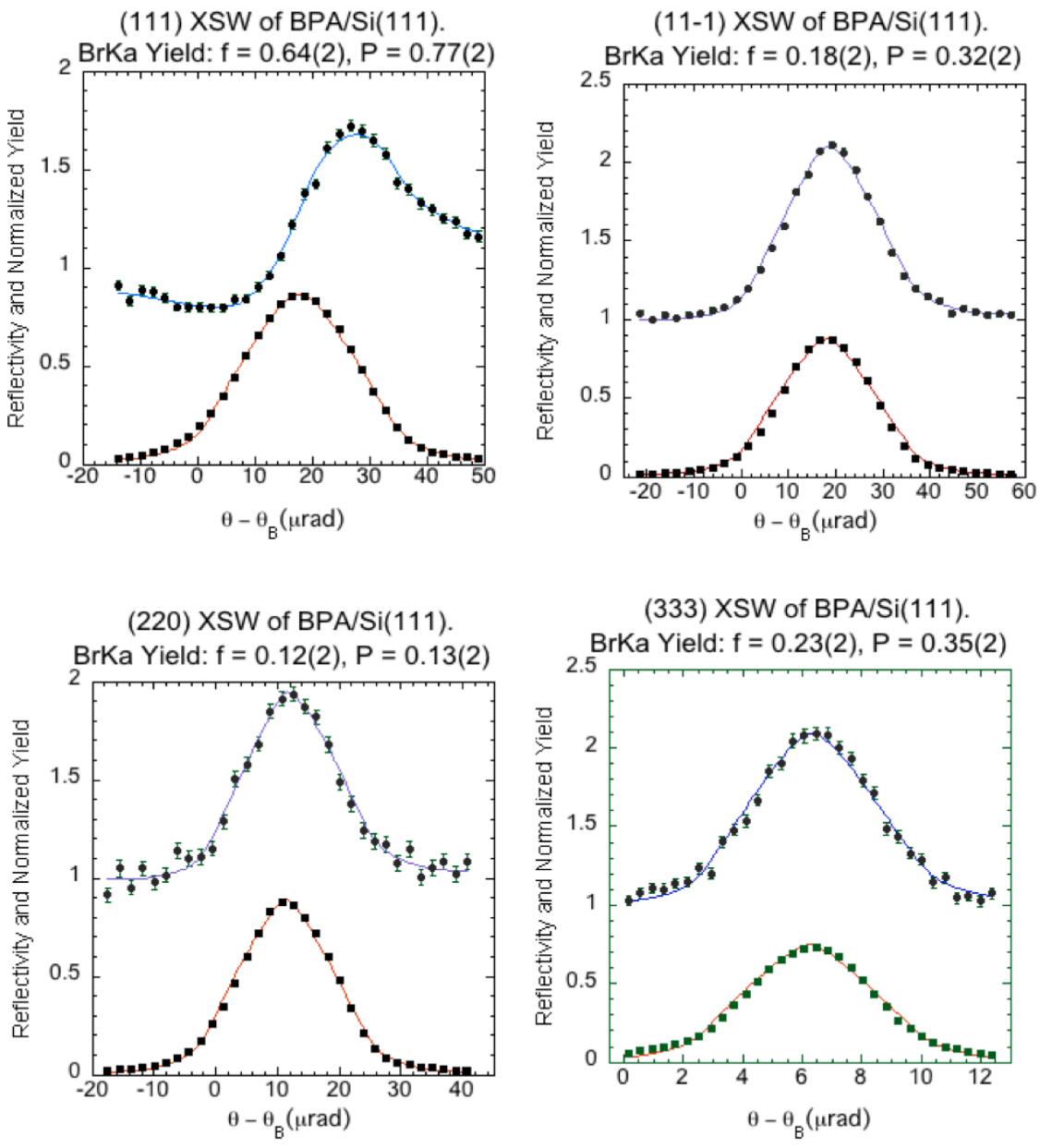

Figure 7.22 The single-crystal XSW results for the (4-bromophenyl)acetylene (**BPA**)-derived SAM on Si(111). Shown are the angle dependences of the *h k l* Si Bragg reflectivity (bottom) and the Br Kα XRF yield data (top). Symbols are measured data, and solid lines are the best-fits of theory to the data.

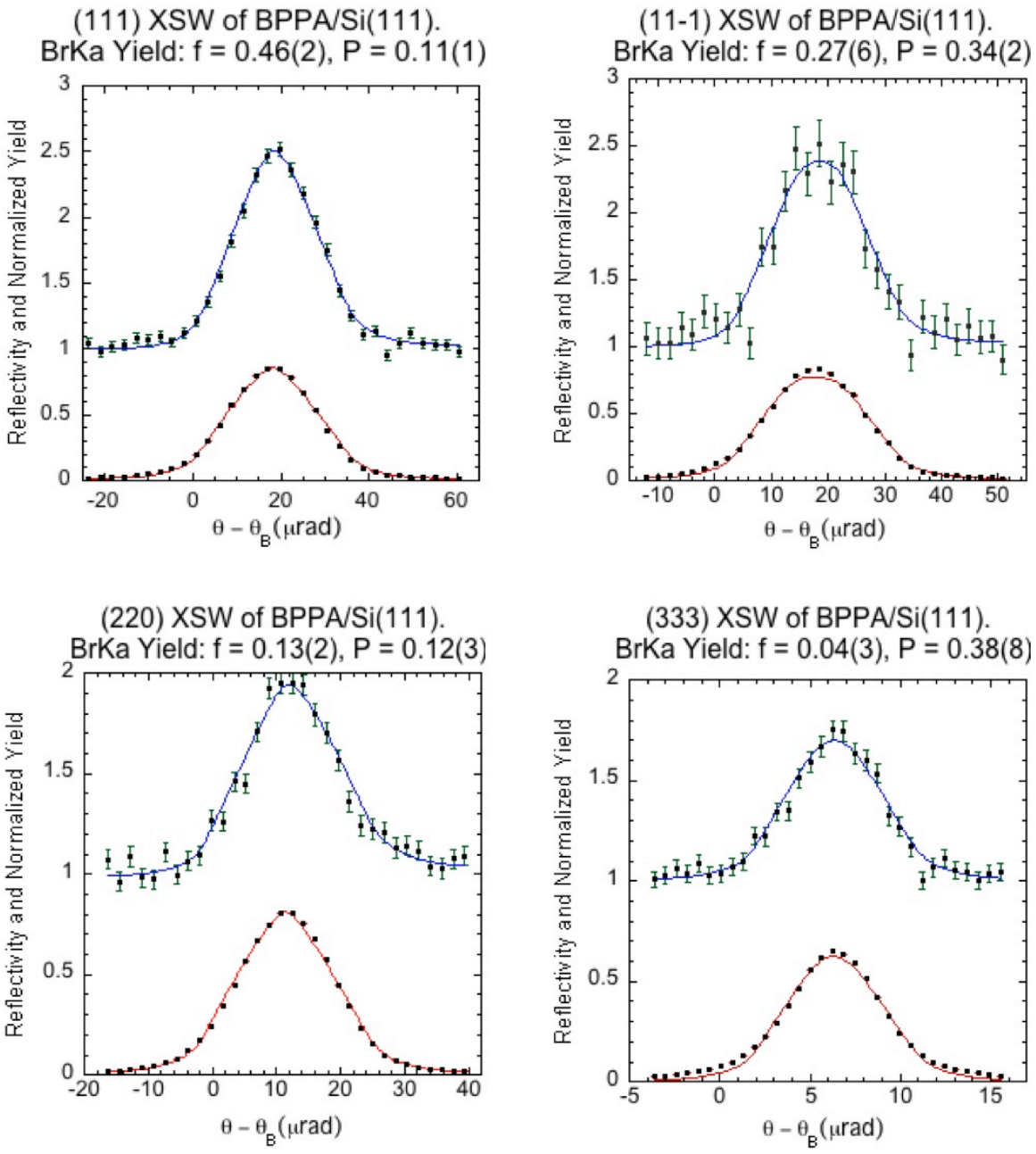

Figure 7.23 The single-crystal XSW results for the (*p*-(4-bromophenyl)phenyl)acetylene (**BPPA**)-derived SAM on Si(111). Shown are the angle dependences of the *h k l* Si Bragg reflectivity (bottom) and the Br Kα XRF yield data (top). Symbols are measured data, and solid lines are the best-fits of theory to the data.

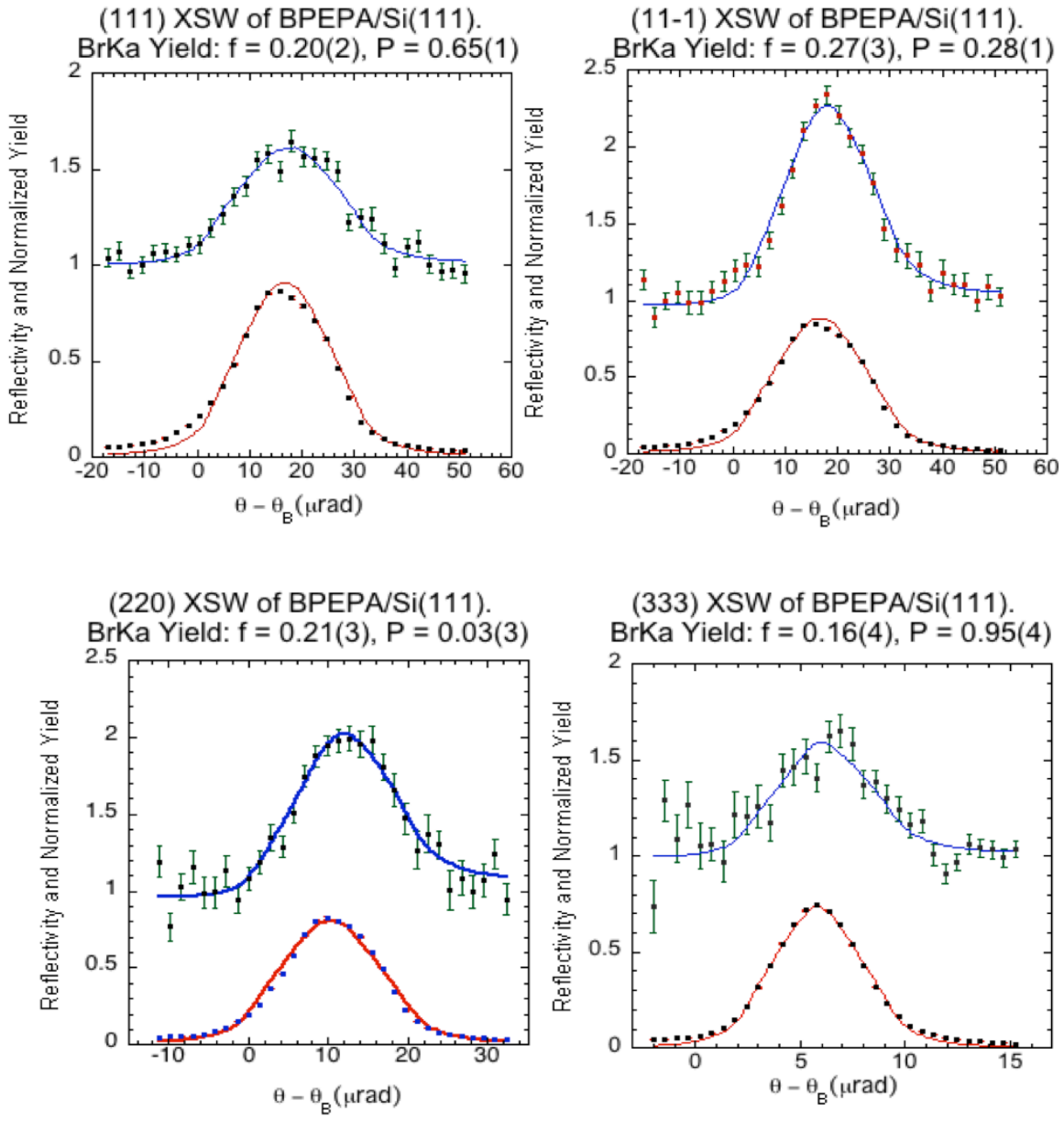

Figure 7.24 The single-crystal XSW results for the (*p*-(4-bromophenylethynyl)-phenyl)acetylene (**BPEPA**)-derived SAM on Si(111). Shown are the angle dependences of the *h k l* Si Bragg reflectivity (bottom) and the Br Kα XRF yield data (top). Symbols are measured data, and solid lines are the best-fits of theory to the data.

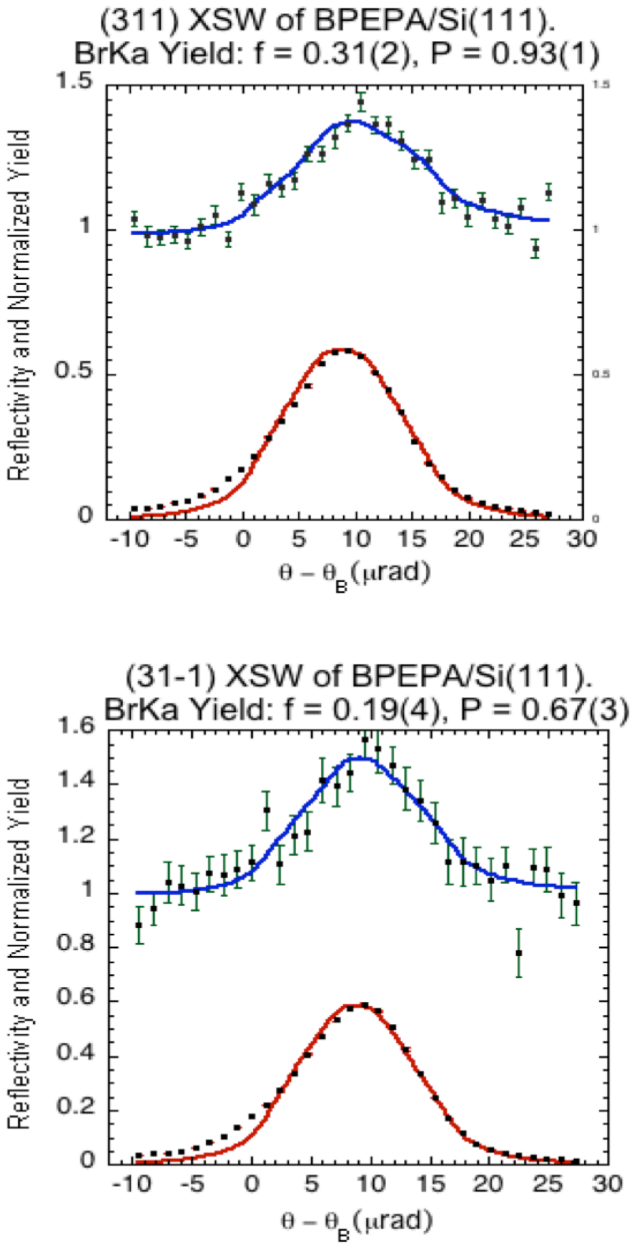

Figure 7.25 Additional two off-normal single-crystal XSW results for the (*p*-(4-bromophenylethynyl)-phenyl)acetylene (**BPEPA**)-derived SAM on Si(111).

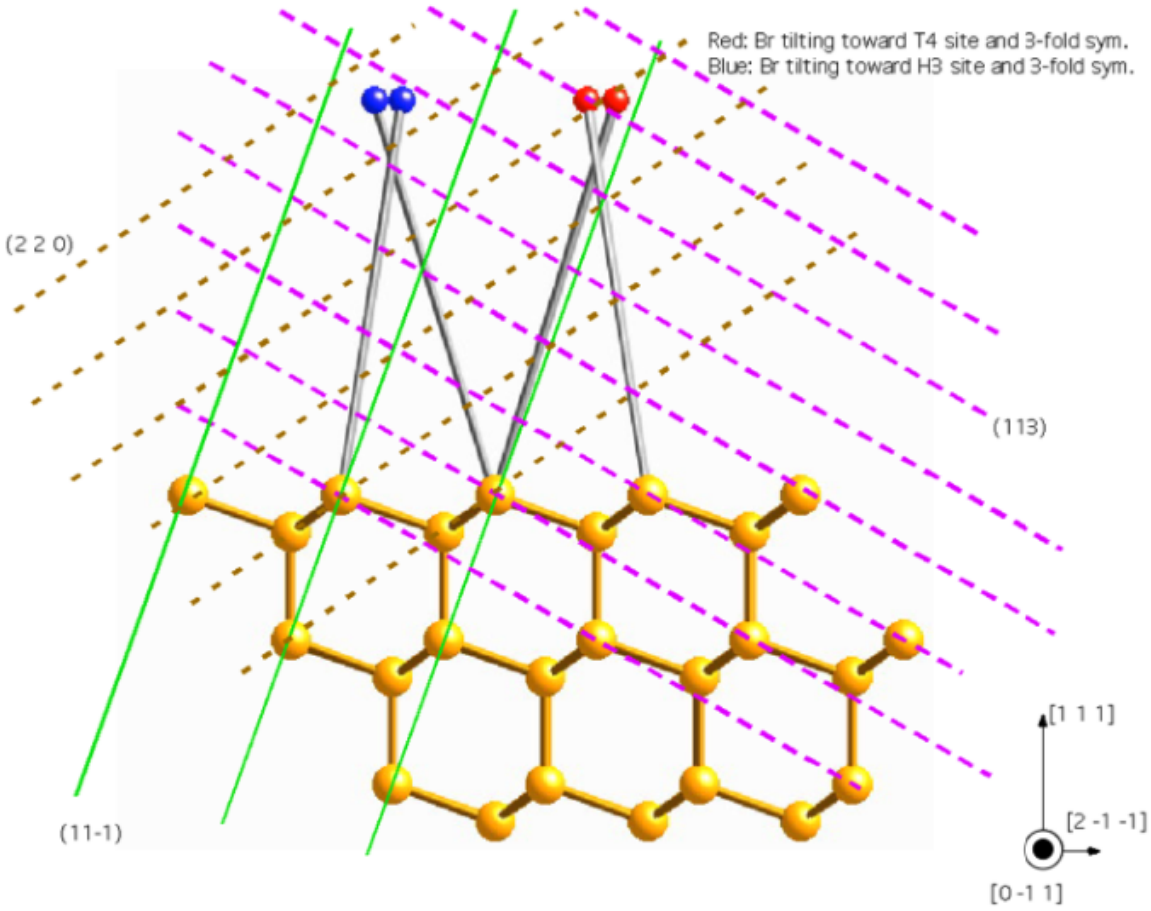

Figure 7.26 A schematic drawing of (11-1), (220), and (113) diffraction planes on a (111) Si crystal. The red atoms, tethered to the Si T_1 sites, are tilted toward the T_4 sites. The blue atoms, on the other hand, are tilted toward the H_3 sites. All the blue atoms are symmetry equivalent (likewise for the red atoms). Since the red and blue atoms have the same height above the Si surface, they cannot be distinguished in a 111 XSW measurement. However, they may be distinguished in off-specular XSW measurements.

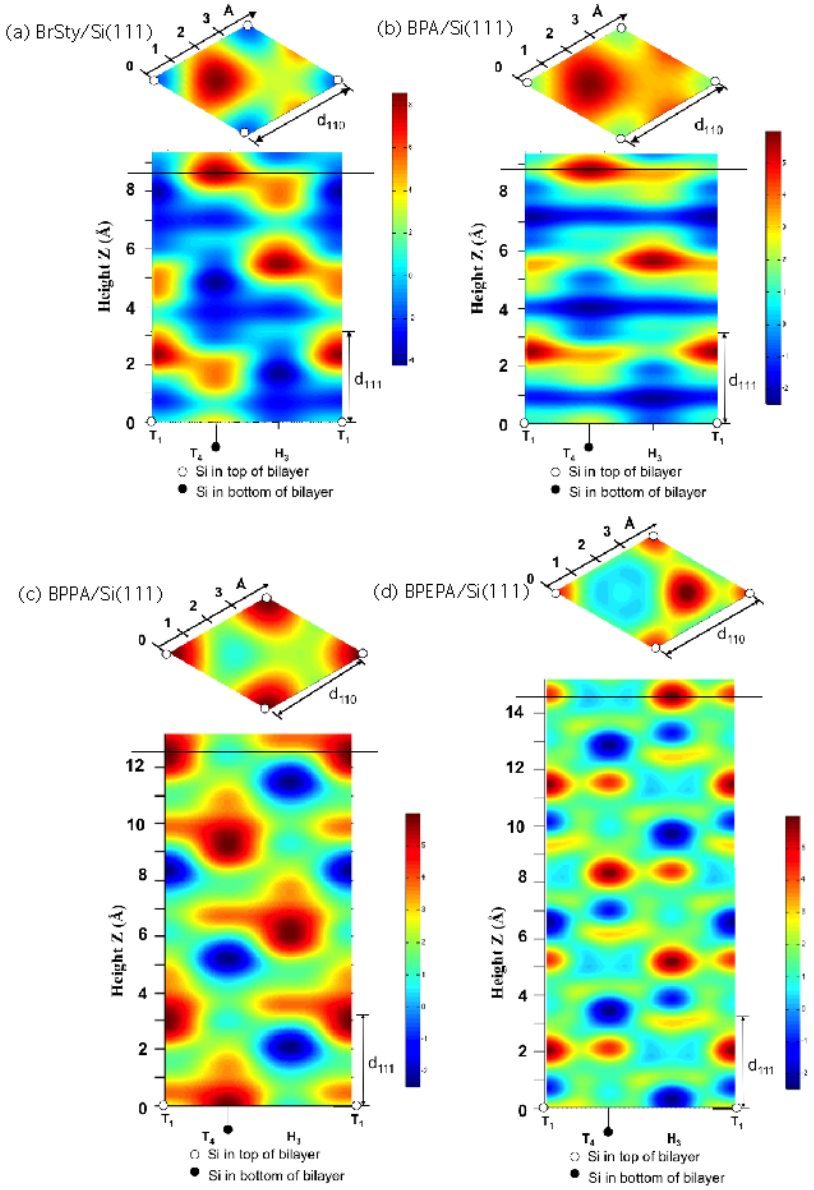

Figure 7.27 XSW generated Br atomic maps for (a) BrSty-, (b) BPA-, (c) BPPA-, and (d) BPEPA- based SAMs on Si(111) with respect to the hexagonal unit cell of the Si(111)-1x1 surface. The 2D cuts through the measured 3D Br atomic density maps coincide with the Br maxima in the 3D maps. The upper images are top-view cuts parallel to the (111) surface at the center of the hotspots that best match the XRR measured Br heights (indicated by the horizontal lines). The lower images are side-view cuts perpendicular to the (111) surfaces that coincide with the T_1, T_4, and H_3 high symmetry sites of the Si(111)-1x1 surface.

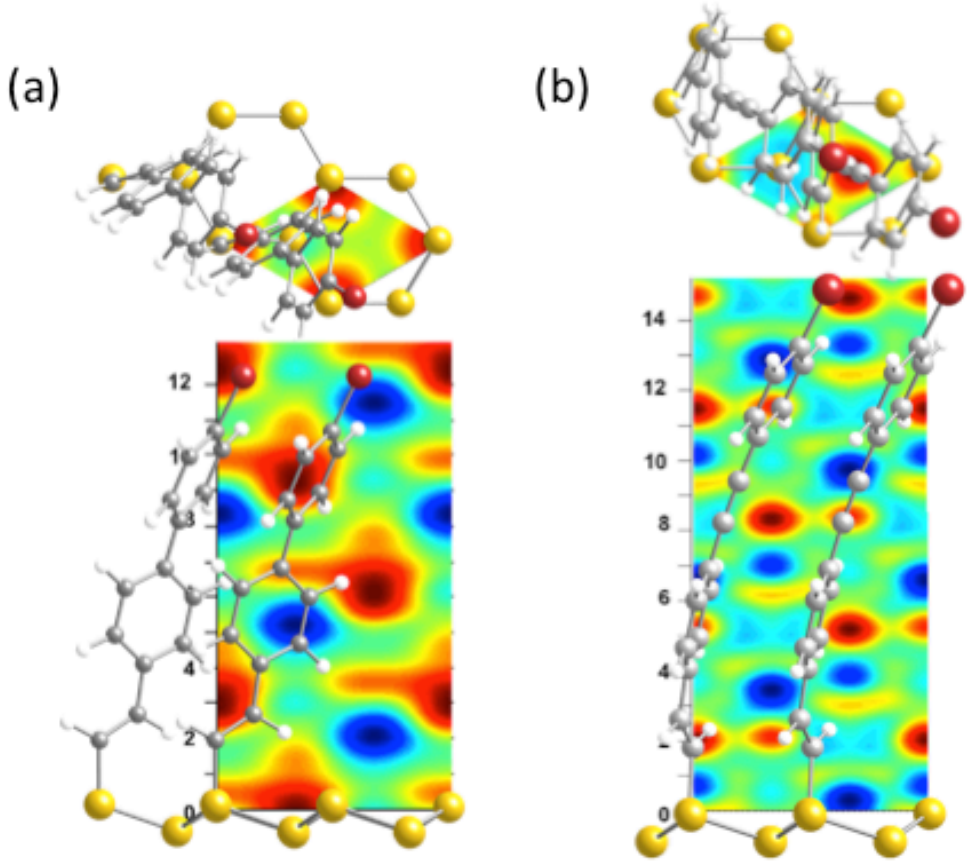

Figure 7.28 Projected ball-and-stick models for (a) BPPA- and (b) BPEPA- based SAMs on Si(111) superimposed on top of cuts through the XSW measured Br atomic maps. The lower images are side-view cuts that coincide with the T1, T4, and H3 high-symmetry sites of the Si(111) 1x1 surface. The upper images are top-view cuts parallel to the (111) surfaces at the measured Br heights indicated by the horizontal lines. The superimposed models of BrSty- and BPA- based SAMs are the (2 x 1) periodic DFT calculation results. The models for (a) and (b) are Or2 in Fig. 7.14 and Or4 in Fig 7.16, respectively.

7.5 Growth kinetics

Fig. 7.29 shows the XRF measured Br total coverage (Θ_T) for a series of BPA-derived SAMs that were grown with different UV reaction times (t). Also shown in Fig. 7.29 are the corresponding XSW measured coherent positions, P_{111}. The observation that P_{111} and f_{111} are invariant to the SAM coverage indicates that the local molecular configuration of the SAM is independent of the globally averaged coverage. The result agrees with the islands nucleation growth mechanism[39] of SAMs on Si(111) where the growth of the coverage increases the number of the molecular islands but not the size of the islands. It also suggests that the growth of the monolayer increases the number of molecules laterally but not vertically (because the vertical distribution of Br does not change). We also show in Fig. 7.29 the variation in the Br ordered coverage, defined as $\Theta_O = C\ \Theta_T$. While Θ_T is a tally of all BPA molecules adsorbed on the surface (physisorbed and chemisorbed), Θ_O only includes BPA molecules that are covalently bonded to the surface as depicted in the inset of Fig. 7.29. The growth kinetics for Θ_T and Θ_O can be approximated by a simple exponential function with a time constant of 34 hours (for our particular growth conditions). The non-zero coverage at t = 0 points to a faster reaction step at the beginning of the hydrosilylation process. The growth kinetics in Fig. 7.29 predicts saturation coverage for Θ_O *at* 0.7 ML.

7.6 Summary

By combing XPS, XRR, XRF, and XSW experiments with DFT structure modeling, the atomic-scale structures of SAMs on Si(111) can be determined. The characterization package can be used to study the growth kinetics of SAMs on Si as well. For a DFT study, the choice of the starting configuration is critical to the relaxed result. Single molecule cluster DFT can

provide insights of the structures and be used to study the reaction pathway, however it often overestimates the height of the molecules due to the lack of molecule-molecule interaction. On the other hand, a (1 x 1) periodic DFT study often overestimates the molecule-molecule interaction and the result is suspicious. A (2 x 1) periodic DFT, where locally the linear packing of molecules on Si(111) is approximated by periodically tethering every other surface silicon to one molecule, better simulates the structures of SAMs/Si(111). Due to the nature of chain reaction growth, an initial orientation where the molecules are aligned along the molecular rows is suggested in the (2 x 1) periodic DFT. Overall, our study suggests a sp^3-sp^2 or sp^3-sp^3 alignment respectively at the molecule/substrate interface for the tethered alkenyl (sp^2) or alkyl (sp^3) organic adlayers on Si(111).

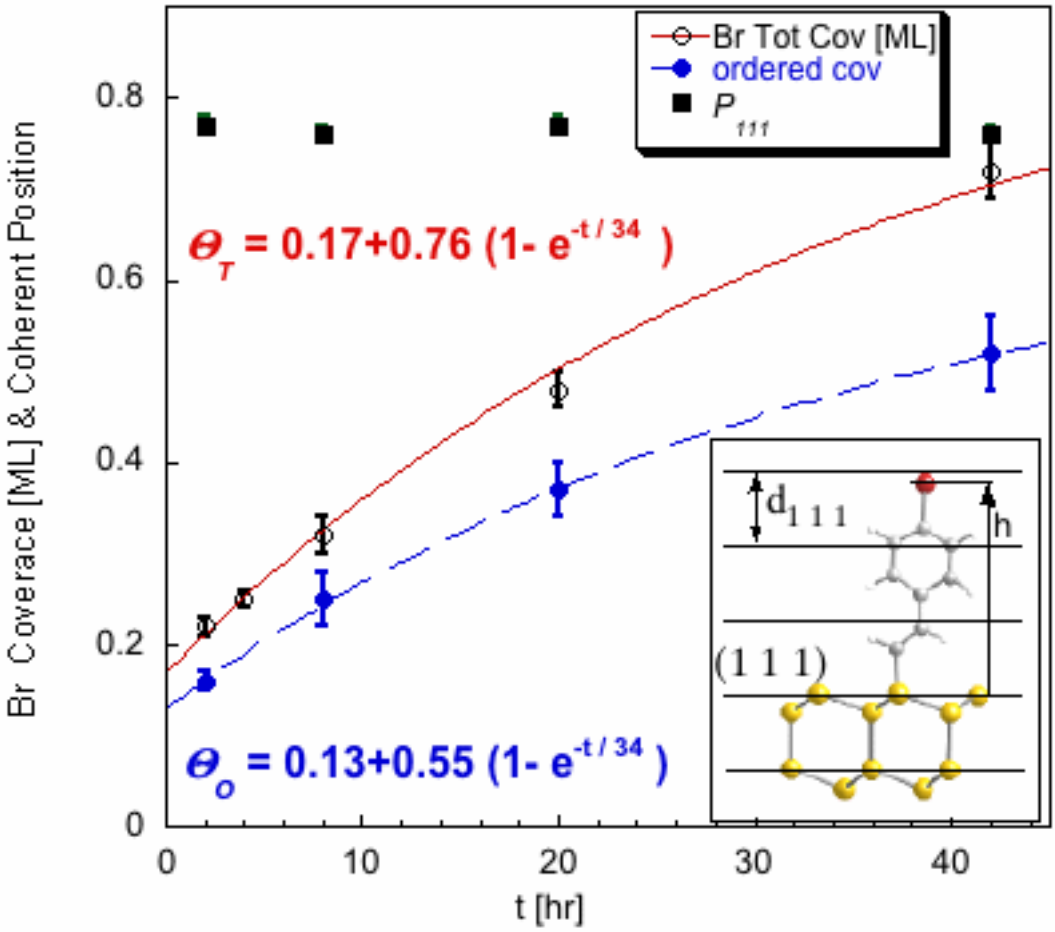

Figure 7.29 For a set of BPA-derived SAMs this shows the UV reaction time dependence for the measured Br total coverage Θ_T (open circles), ordered coverage Θ_O (filled circles), and coherent position P_{111} (filled squares). f_{111} = 0.68(3). The inset shows a side view of the BPA molecule covalently attached to the T_1 site on the Si(111) surface. For a single Br height P_{111} = Mod [h/d_{111}].

Chaper 8 : Extending Conjugated Organic Structures on Si

8.1 Introduction

It has been demonstrated that aryl-substituted acetylenes (BPA, BPPA, and BPEPA) can be used to functionalize Si(111) surface under mild UV irradiation, forming a fully conjugated monolayer structure with sp^2-conjugated moieties directly connected to surface Si atoms. When bromide terminated aromatic alkynes are used as the modifier in this chemistry, the halogen is preserved at the top of the monolayer, in contrast to previous deployment of monolayers based on undec-10-enoic acid 2-bromo-ethyl ester,[41] providing a ready handle for sequential substitution chemistry through Pd-based couplings such as the Sonogashira reaction.[42,43]

A microwave-assisted Sonogashira coupling to a Si(111) surface possessing an sp^2-conjugated monolayer is discussed in this chapter. Specifically, (4-bromophenyl)acetylene (BPA) is coupled to a (4-iodophenyl)acetylene (IPA)-derived monolayer on Si(111) to form a (*p*-(4-bromophenylethynyl)phenyl)vinylene layer on a Si surface (Fig 8.1). The increased thickness of the Si-supported molecular layer can be clearly observed by XRR analysis, confirming the successful conjugation. The extent of coupling is directly assessed via XSW and XRF measurements of the iodine and bromine contents of the surface. Since alkyne handles can be readily incorporate into a wide range of bioactive compounds,[44,45] the present Sonogashira coupling chemistry may provide a facile strategy for coupling Si-based electronic devices to a wide range of biomedical applications.

In a typical Sonogashira reaction, the sp-sp^2 coupling between the aryl-halide and alkynes usually takes place in the presence of a base.[42] Since thermal Sonogashira reaction often requires

extended reaction time[46,47] or high reaction temperature[46,48] (T > 100˚C), this basic condition could potentially corrode the Si surface. As such, we employed microwave-assisted conditions[49] in our study to minimize the reaction time and maximize the coupling yield between the IPA-derived film on Si(111) (IPA/Si(111), sample **S1**) and BPA (Fig 8.1). For comparison, a (*p*-(4-bromophenylethynyl)-phenyl)vinylene monolayer film on Si(111) surface (BPEPA/Si(111), sample **S3**) via the photo-induced hydrosilylation of (*p*-(4-bromophenylethynyl)phenyl)acetylene (BPEPA) by H-passivated Si(111) (H-Si(111)) is also separately prepared. This **S3** sample, which is prepared in only a single step, has the same monolayer composition as the **S2** Sonogashira-prepared sample and therefore serves as a standard for evaluating our Sonogashira-coupling chemistry method.

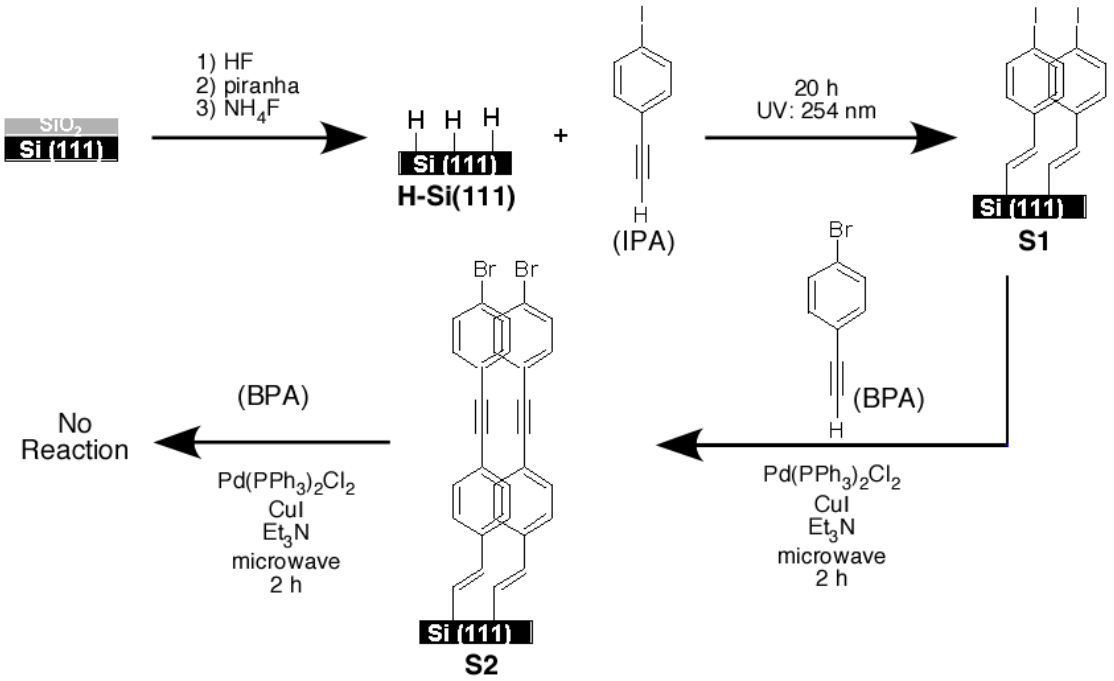

Figure 8.1 *p*-(4-iodophenyl)acetylene-based monolayer is first grown on a H-passivated Si(111) surface and subsequently coupled to *p*-(4-bromophenyl)acetylene *via* microwave-assisted Sonogashira reaction.

8.2 Experimental results and discussion

Fig 8.2 shows the XRR analysis of the film after each step in our Sonigashira-based organic film growth process, as well as the standard **S3**. In contrast to the smooth Fresnel-like decay of the H-Si(111) interface, the IPA/Si(111) (**S1**) and the Sonogashira-prepared (**S2**) films show clear interference thickness oscillations. In addition, the antireflection dip in the Sonogashira-prepared sample is shifted to a lower value (Q = 0.17 $Å^{-1}$) compared to **S1** (Q = 0.23 $Å^{-1}$). Since the antireflection dip in the XRR measurement is sensitive to the thickness of the organic film on Si and a smaller Q for the dip corresponds to a thicker film,[18] the initial organic layer in **S1** has clearly been extended outward from the Si surface in **S2** (i.e., after the reaction). The observation that the antireflection dips occur at the same Q for samples **S2 and S3** serves to confirm the expected final BPEPA-derived (*p*-(4-bromophenylethynyl)-phenyl)vinylene monolayer structure for **S2** as shown in Fig 8.1. Referring to the XRR analysis[19] in Table 8.1, monolayers **S2** and **S3** have equivalent thicknesses (defined as the height of the center of the halogen layer, $t_3 + ½ t_2 = 14.6$ Å), as would be expected for isostructural films.

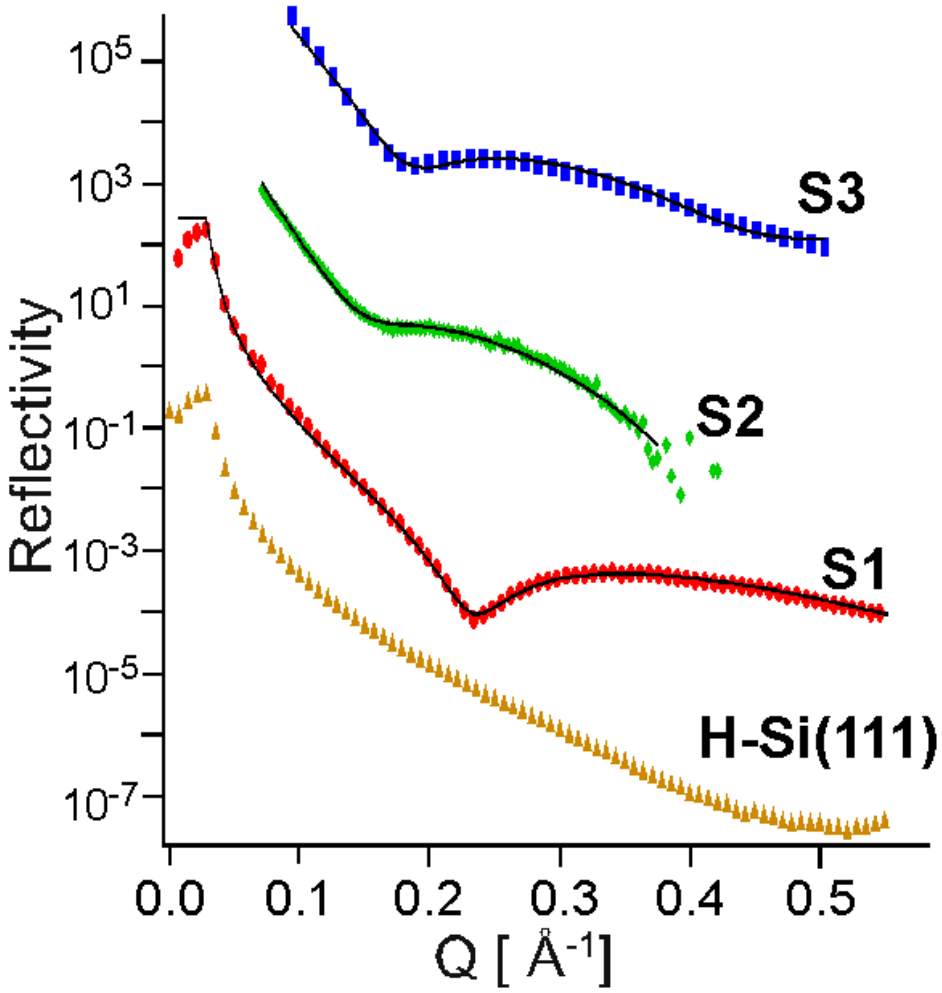

Figure 8.2 XRR data for the respective H-Si(111), IPA/Si(111) (**S1**), [IPA/Si(111) + BPA] Sonogashira-prepared (**S2**), and standard BPEPA/Si(111) (**S3**) thin films (triangles, circles, diamonds, and squares, respectively). The solid lines are theoretical fits based on Parratt's recursion method[19] using a two-layer/Si model (i.e., halogen and hydrocarbon layers). The structural parameters from the fits are listed in Table 8.1. For purposes of clarity, **S1**, **S2**, and **S3** are vertically offset by 10^3, 10^6, and 10^9, respectively.

	t_3 (Å)	ρ_3	t_2 (Å)	ρ_2	$\sigma_{1,2}$ (Å)	$\sigma_{2,3}$ (Å)	$\sigma_{3,4}$ (Å)
S1	8.6	0.5	0.7	2.1	3.2	1.8	2.4
S2	14.4	0.6	0.3	2.2	6.7	5.1	3.7
S3	14.1	0.7	0.9	2.5	4.0	2.5	2.0

Table 8.1 XRR two-layer/Si model determined relative electron density ($\rho = \rho_{layer} / \rho_{Si}$), thickness (t), and interfacial roughness (σ) of each layer. Layers 1 through 4 are air, halogen, hydrocarbon, and Si, respectively.

Under our surface Sonogashira coupling scheme (Fig 8.1), it is possible that the Sonogashira-formed (*p*-(4-bromophenylethynyl)phenyl)vinylene monolayer could have undergone further coupling with BPA. In addition, BPA could have undergone self-coupling in solution to generate BPEPA. Given that the Sonogashira couplings between phenylacetylene and iodo-aromatics are much faster than the analogous reactions with bromo-aromatics, the coupling between BPA and the iodine-terminated monolayer on **S1** should occur in a more facile fashion over both of the aforementioned possibilities during our short reaction time. Further support for this hypothesis was provided by our observation that BPA did not couple to a Br-styrene-derived monolayer on Si(111) under identical microwave-assisted Sonogashira coupling conditions and BPEPA was not found as a side product in the synthesis of **S2**. These results suggest that selective patterning of organic molecules on a Si(111) surface via surface Sonogashira coupling may be possible via judicious deployment of organic monolayers with different halide termination.

In contrast to XRR, which measures the "averaged electron density" profile for the organic/Si interface structures,[18] the 111 XSW analysis, with the XRF modulation observed while scanning through the Si(111) Bragg reflection (Fig. 8.3), directly measures the spatial distribution of the fluorescence marker atoms (Br and/or I) with respect to the lattice of the single crystal substrate (i.e., d_{111} spacing, Figure 8.4). As a result, XSW is element-specific and has sub-angstrom resolution.[20-23] The XSW results for the IPA/Si(111) starting film (**S1**), the Sonogashira-prepared film (**S2**), and the standard BPEPA/Si(111) film (**S3**) are shown in Fig 8.3 and Table 8.2. The differences between the Br Kα (**S2**) and I $L\beta_1$ (**S1**) XSW modulations indicate the variance in the vertical distributions of the halogen atoms before and after the Sonogashira reaction. The coherent fraction f_{111} and coherent position P_{111} in the XSW analysis measures the distribution width of the XRF-selected fluorescence species and the location of the distribution center, respectively.[24,25] The smaller coherent fraction f_{111} from **S2** compared to **S1** (Table 8.2) suggests a broader vertical distribution of the Br atoms in the Sonogashira-prepared sample **S2** than the I atoms in the IPA/Si(111) monolayer **S1**. This is consistent with the fact that the Br atoms in the former are set further away from the Si surface than the I atoms in the latter by an extended spacer group post Sonogashira coupling (Fig. 8.4).

The agreement in the XSW-obtained f_{111} and P_{111} values for Br in **S2** and **S3** is consistent with the previously discussed XRR results, which found an identical film thickness (and hence molecular structure) on the Si surface regardless of the growth method. In conjunction with the longer-length scale XRR measurement,[26] the XSW analysis yields the height of the Br in the Sonogashira-prepared sample **S2** to be $h_{Br} = [4 + P_{111}]d_{111} = 14.8$ Å. Whereas before the coupling

reaction, the height of the I atom in sample **S1** is $h_I = [2 + P_{111}]d_{111} = 8.7$ Å (See Fig 8.4). For **S3** $h_{Br} = 14.7$ Å.

In our surface Sonogashira coupling scheme shown in Fig 8.1, the terminal iodide from the IPA/Si(111) monolayer in sample **S1** is replaced by a BPA group in creating sample **S2**. Hence, the coupling reaction yield can be determined by measuring both the loss in iodide coverage and gain in bromide coverage. The XRF-calibrated iodide and bromide coverages (Table 8.2) show an iodide loss equivalent to a bromide gain of 0.14 monolayers (ML) after the Sonogashira coupling. Compared to the initial 0.15 ML of iodide, this amounts to an approximately 93 % yield for the Sonogashira reaction.

	Iodide			Bromide		
	Cov (ML)	f_{111}	P_{111}	Cov (ML)	f_{111}	P_{111}
S1	0.15(1)	0.44(5)	0.77(3)	--	--	--
S2	0.010(5)	--	--	0.14(3)	0.19(4)	0.73(3)
S3	--	--	--	0.22(2)	0.17(4)	0.70(2)

Table 8.2 XSW and XRF results for IPA/Si(111) film (**S1)**, Sonogashira-prepared film (**S2**), and the standard BPEPA/Si(111) film (**S3**).

8.3 Summary

We have demonstrated that a microwave-assisted surface Sonogashira coupling reaction can be employed to construct extended conjugated organic structures on Si(111) surfaces. In this manner, halide-terminated alkenyl monolayers on silicon can be systematically functionalized with a wide range of substituted alkynes, providing an entry point for integrating biosensing with Si-based electronics.

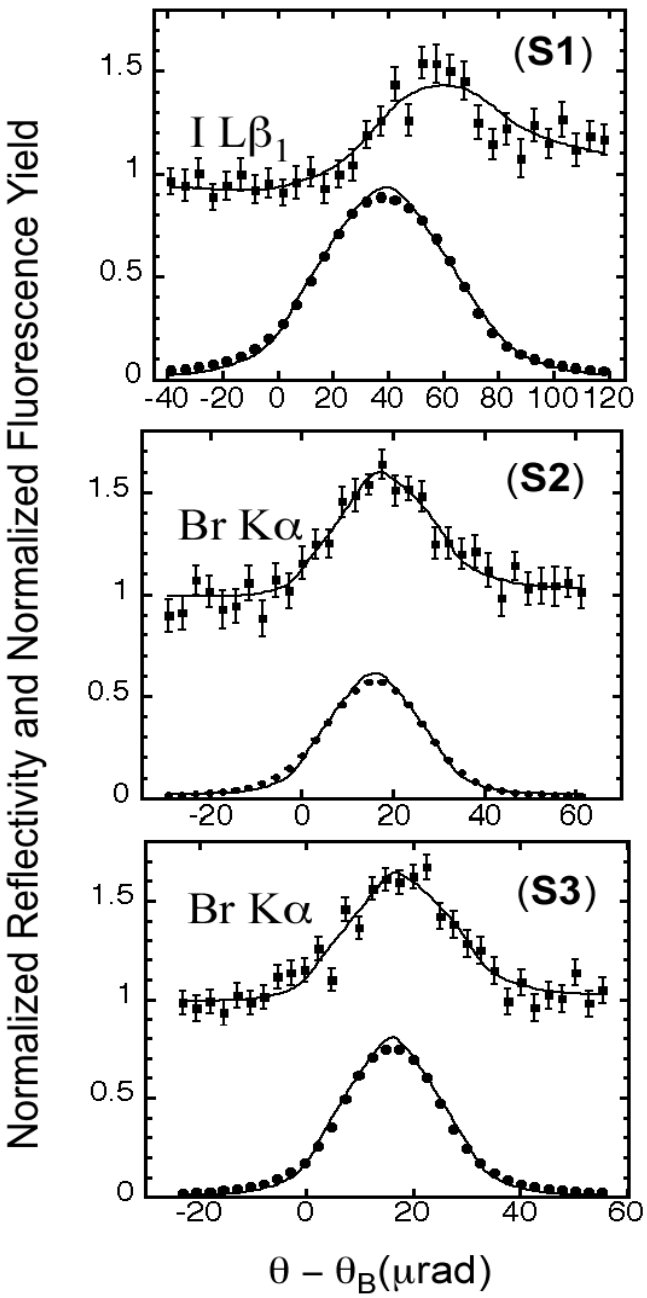

Figure 8.3 The 111 XSW analyses showing the experimental and theoretical angular dependence for the X-ray reflectivity and the X-ray fluorescence for IPA/Si(111) film (**S1**), [IPA/Si(111) + BPA] Sonogashira-prepared film (**S2**), and the standard BPEPA/Si(111) (**S3**) film.

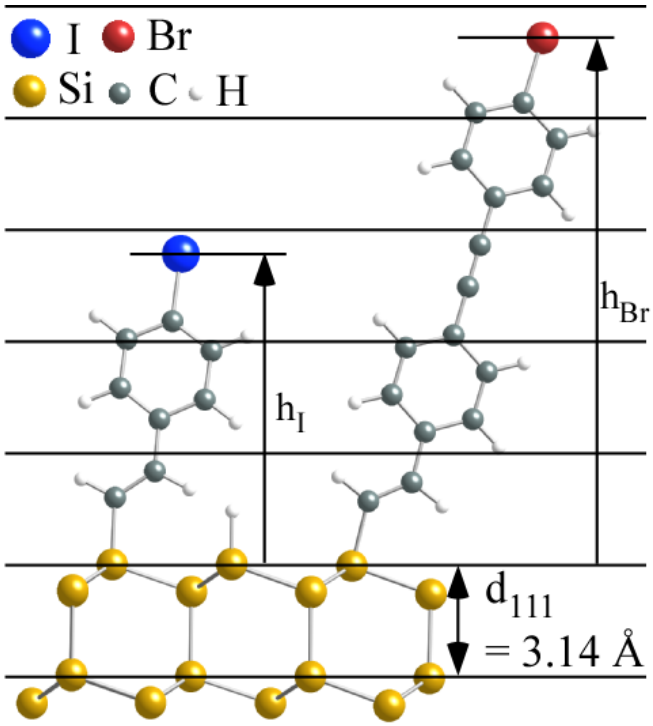

Figure 8.4 Ball-and-stick models for IPA-derived (left) and BPEPA-derived (right) covalent monolayer on Si(111) surfaces. The XSW determined heights of iodide (h_I) and bromide (h_{Br}) are measured with respect to the Si substrate d_{111} spacing. P_{111} = Mod[h/d_{111}].

Chaper 9 : Structural Characterization of Brominated SAMs on Si(001)

9.1 Introduction

The growth of organic molecules on Si(001) surfaces has gained special interests for the realization of molecule-based miniature devices.[53] Self-assembled lines of absorbed molecules, in contrast to the irregular islands of molecules on Si(111), have been shown on anisotropic Si(001)-2x1 surfaces[21,53] via chain reaction growth (Fig 9.1). Although such one-dimensional growth has so far only been demonstrated using alkenes, alkynes are also expected to grow linearly on the monohydride terminated Si dimers based on the reaction schemes in Fig 2.2. To confirm this hypothesis, *p*-bromostyrene (BrSty) and (4-bromophenyl)acetylene (BPA), two aromatic molecules that are identical with the exception of their respective terminal groups (a C=C bond for BrSty and a C≡C bond for the BPA molecule before the hydrosilylation step), are identically grown on Si(001)-2x1:H surfaces in a STM-UHV (ultra high vacuum) chamber,[10] and the structures are side-by-side compared. The STM topography in Fig 9.2 shows that the adsorbed BPA molecules form nanoscale molecular lines on the Si(001)-2x1 surface identical to the BrSty case.[21] In order to further explore the intrinsic structures of the molecular chains, the characterization strategy developed in the study of SAMs on Si(111), including DFT, XRR, XRF, and XSW, was applied on both BrSty- and BPA- based SAMs on Si(001) and the results will be discussed in the following chapters.

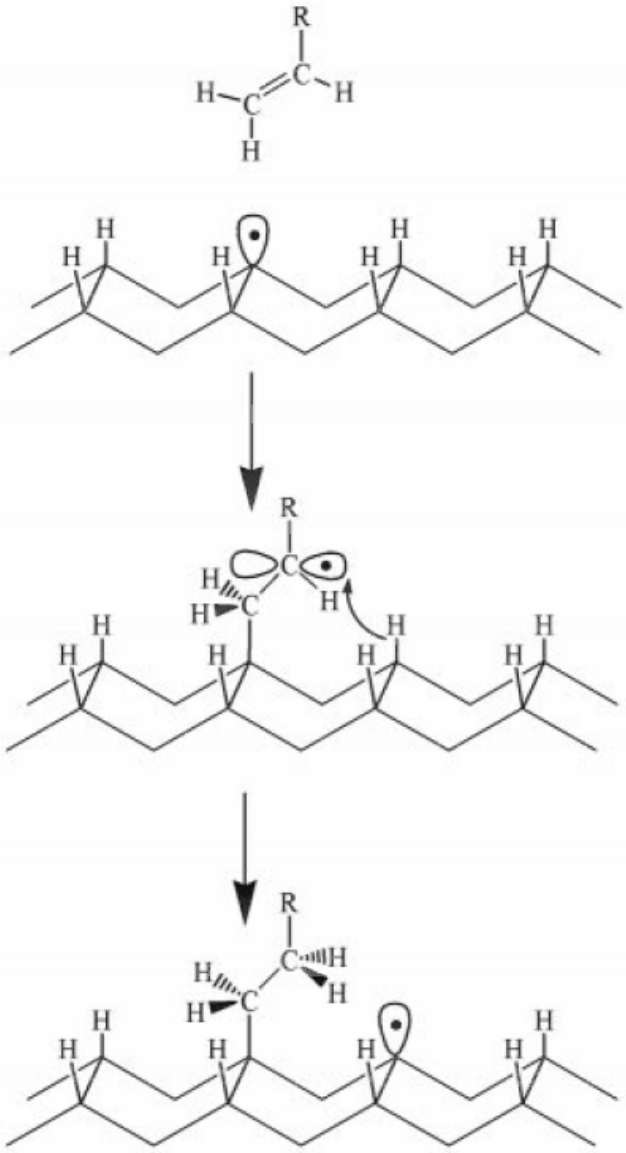

Figure 9.1 Chain reaction growth mechanism for self-directed growth of alkenes on Si(001)-2x1:H proposed by Lopinski et al. The initial reaction involves formation of a carbon-centered radical that can then abstract a hydrogen from an adjacent dimer along a row, creating a new Si dangling bond.[53] The figure is reproduced from Ref. [53].

(a)

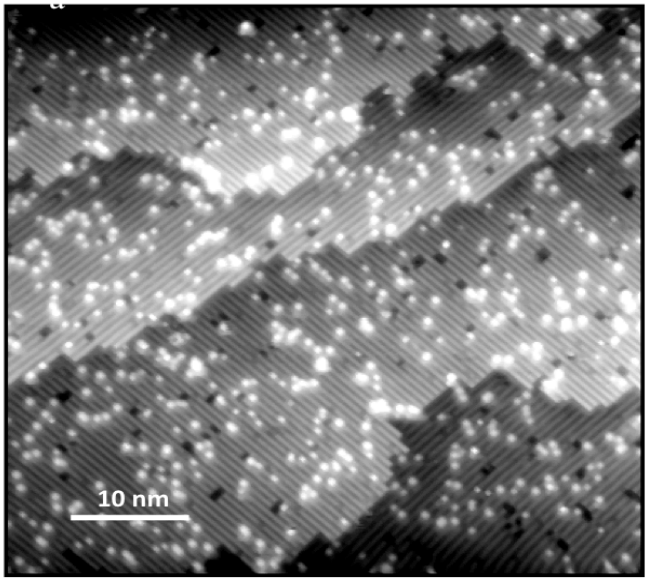

(b)

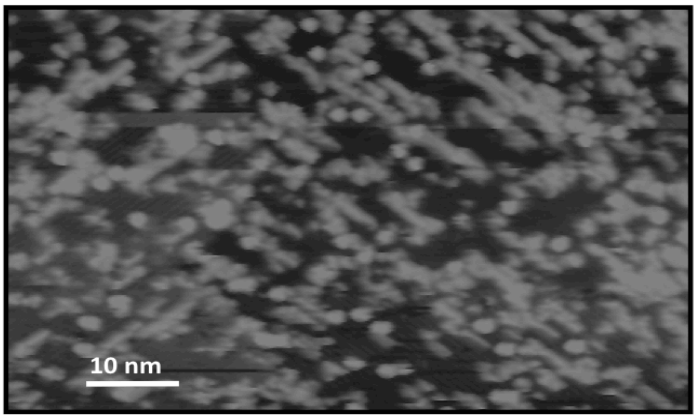

Figure 9.2 (a) STM image of a Si(001)-2x1:H surface with dangling bonds created by elevating the surface temperature to 400˚C. (b) The surface of (a) after being exposed to BPA molecules. STM images are from Michael Walsh in the Hersam group.

9.2 DFT modeling

Ball-and-stick models for an isolated BrSty / BPA molecule on a Si dimer, based on the single molecule cluster DFT calculation results, are respectively shown in Fig 9.3 and 9.4. The coordinates are listed in appendix C.3. For the case of BPA, the molecular bonding with alkene- (Fig 9.3a), double-bridge- (Fig 9.4a), and single-bridge- (Fig 9.4b) like linkages at the molecule/substrate interface are considered in the computation. The heights of the terminal Br atoms, with respect to the bulk-terminated surfaces, are shown in Table 9.1.

SAMs	BrSty	BPA		
Bonding type	Alkyne	Alkene	Double bridge	Single bridge
Height (Å)	9.7	10.0	7.4	7.5

Table 9.1 The heights of the terminal Br atoms with respect to the bulk-terminated surfaces for the models shown in Fig 9.3 and 9.4.

According to the earlier study of brominated SAMs on Si(111), a cluster DFT calculation with an isolated molecule provides the azimuthal orientation of the molecule with respect to the Si substrate, but the overall tilting of the molecule is also being underestimated due to the lack of molecule-molecule interaction. As the result, the single molecule cluster DFT predicted configurations in Fig 9.3 and 9.4 are further optimized using (2 x 1) periodic DFT and the results

are shown in Fig 9.5 to 9.13. The XYZ coordinates for the DFT models are listed in appendix C.8 for BrSty and C.9 for BPA, respectively. Referring to the model structures in Fig 9.3, the pre-relaxed (2 x 1) packed SAMs in Fig 9.5, 9.6, 9.9, and 9.10 have the molecules either away from the Si dimers (Or1) or directly over the Si dimers (Or2). The pre-relaxed Or1 and Or2 types configurations for BrSty-derived SAMs are shown in Fig 9.5 and 9.6, respectively, and Fig 9.9 and 9.10 for BPA-derived SAMs. Four different molecular tilts (t0 - t3) are also studied in each type of orientation. The relaxed results for BrSty and BPA are respectively shown in Fig 9.7, 9.8, and Fig 9.11, 9.12. The results for the two alternative bridge-like types of bonding for BPA on Si(001) are shown in Fig 9.13. The heights of the terminal Br atoms with respect to the bulk-terminated surfaces, after the structure relaxation, are listed in Table 9.2, 9.3, and 9.4. The total energies are also listed in the tables.

BrSty/Si(001)	Or1				Or2			
	Away from the Si dimer				Over the Si dimer			
	t0	t1	t2	t3	t0	t1	t2	t3
Heights (Å)	8.7	8.4	8.2	8.5	8.7	9.3	9.1	9.1
$E_{Tot.}$	-3105.168	-3105.275	-3105.274	-3105.274	-3105.120	-3105.018	-3105.129	-3105.126

Table 9.2 The heights of the terminal Br atoms (with respect to the bulk-terminated surfaces) and the calculated total energies for the models of BrSty/Si(001)-2x1 shown in Fig 9.7 and 9.8.

BPA/Si(001)	Or1				Or2			
	Away from the Si dimer				Over the Si dimer			
	t0	t1	t2	t3	t0	t1	t2	t3
Heights (Å)	8.6	8.6	8.5	8.6	9.0	9.3	9.0	9.0
$E_{Tot.}$	-3072.565	-3072.568	-3072.596	-3072.569	-3072.442	-3072.398	-3072.411	-3072.413

Table 9.3 The heights of the terminal Br atoms (with respect to the bulk-terminated surfaces) and the calculated total energies for the models of BPA/Si(001)-2x1 shown in Fig 9.11 and 9.12.

	Heights (Å)	$E_{Tot.}$
Double-Bridge	6.0	-3073.116
Single-Bridge	8.9	-3071.810

Table 9.4 The heights of the terminal Br atoms (with respect to the bulk-terminated surfaces) and the calculated total energies for the models of alternative bridge-like types of bonding shown in Fig 9.13.

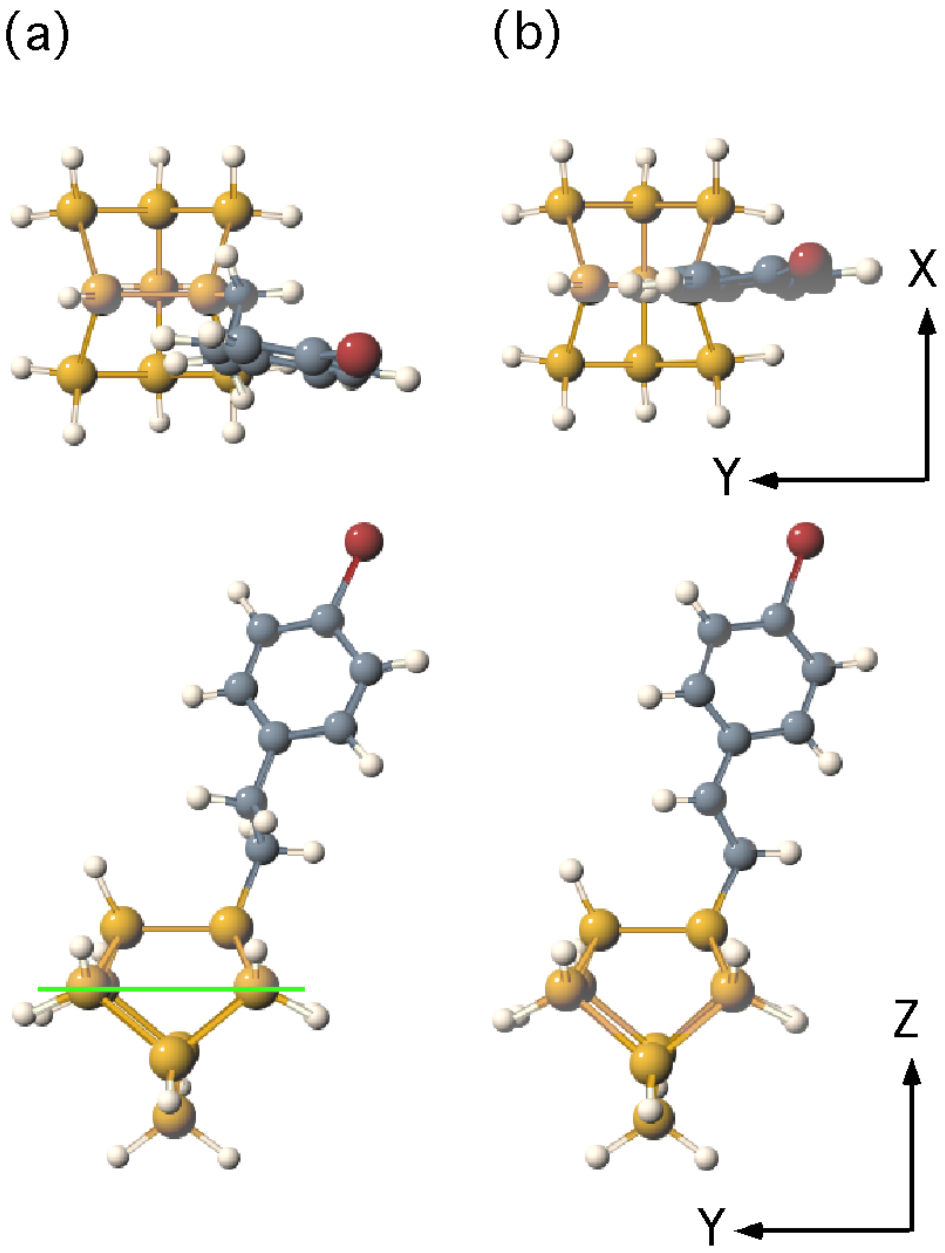

Figure 9.3 Top views (upper images) and side views (lower images) of binding geometry configurations for an isolated (a) BrSty and (b) BPA molecule on a Si_9H_{12} cluster. The calculation for BPA assumes the alkenyl-like linkage at the molecule/substrate interface. The green line in (a) indicates the bulk-terminated Si(001) surface.

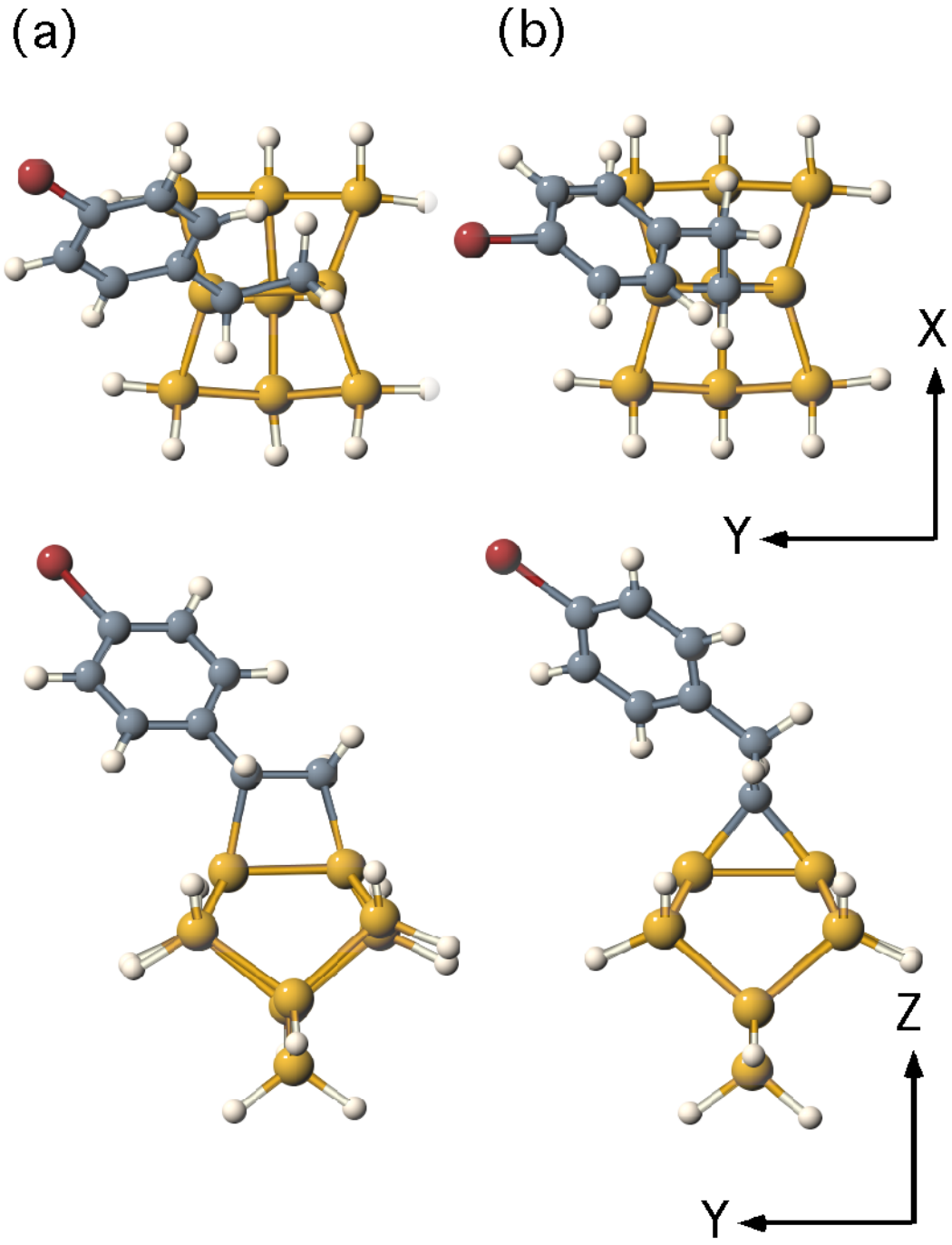

Figure 9.4 Top views (upper images) and side views (lower images) of binding geometry configurations for a (a) double-bridge- and (b) single-bridge- like bound BPA molecule on a Si_9H_{12} cluster.

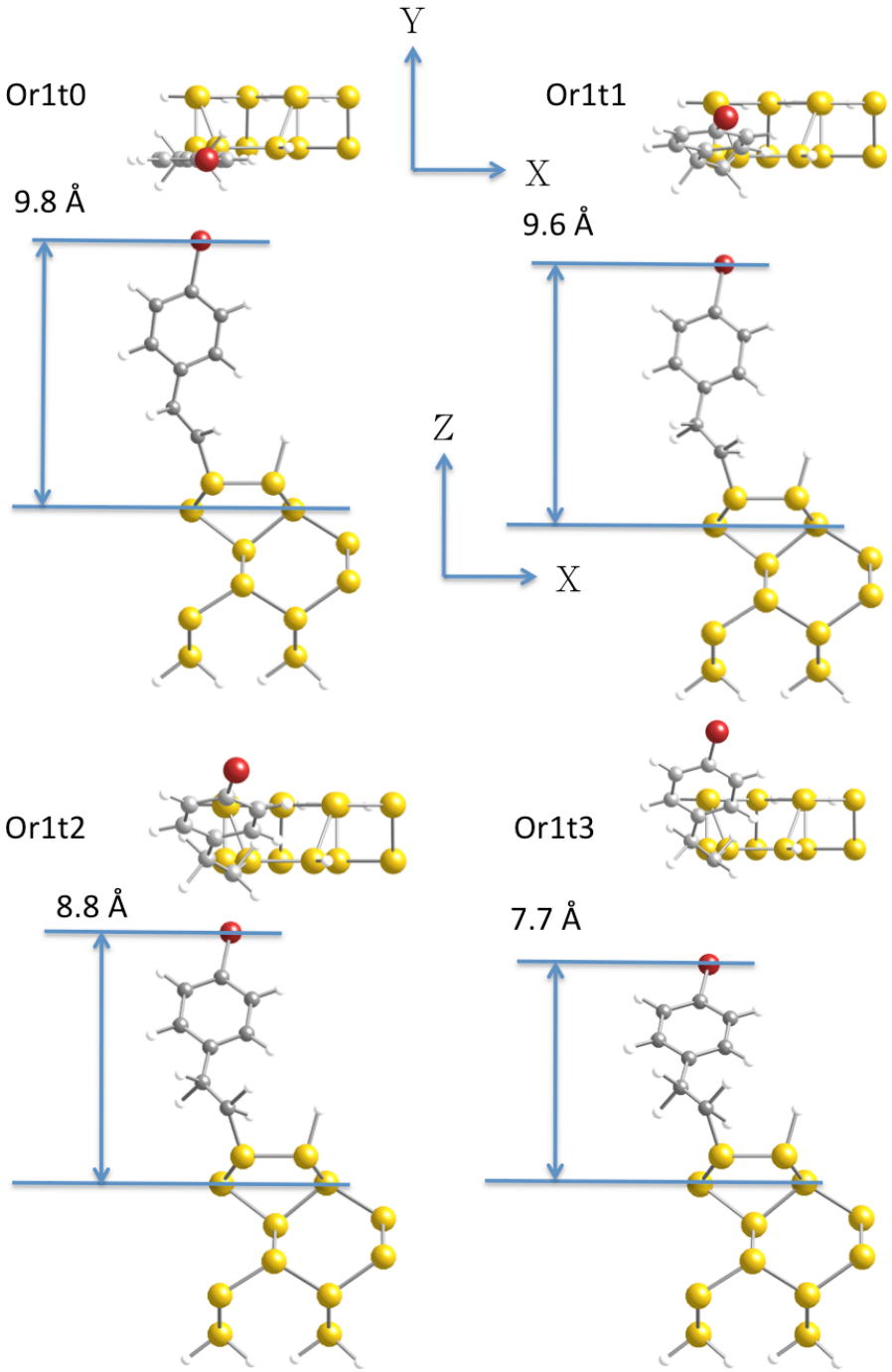

Figure 9.5 Top and side views of the four pre-relaxed BrSty/Si(001) unit structures studied in the (2 x 1) periodic DFT calculations. The four models are commonly having the bottom alkyl C-C bonds of the molecules "away" from the Si dimers. The four molecules are tilted differently in order to explore the effect of the molecular tilt within the one-dimensional molecular rows.

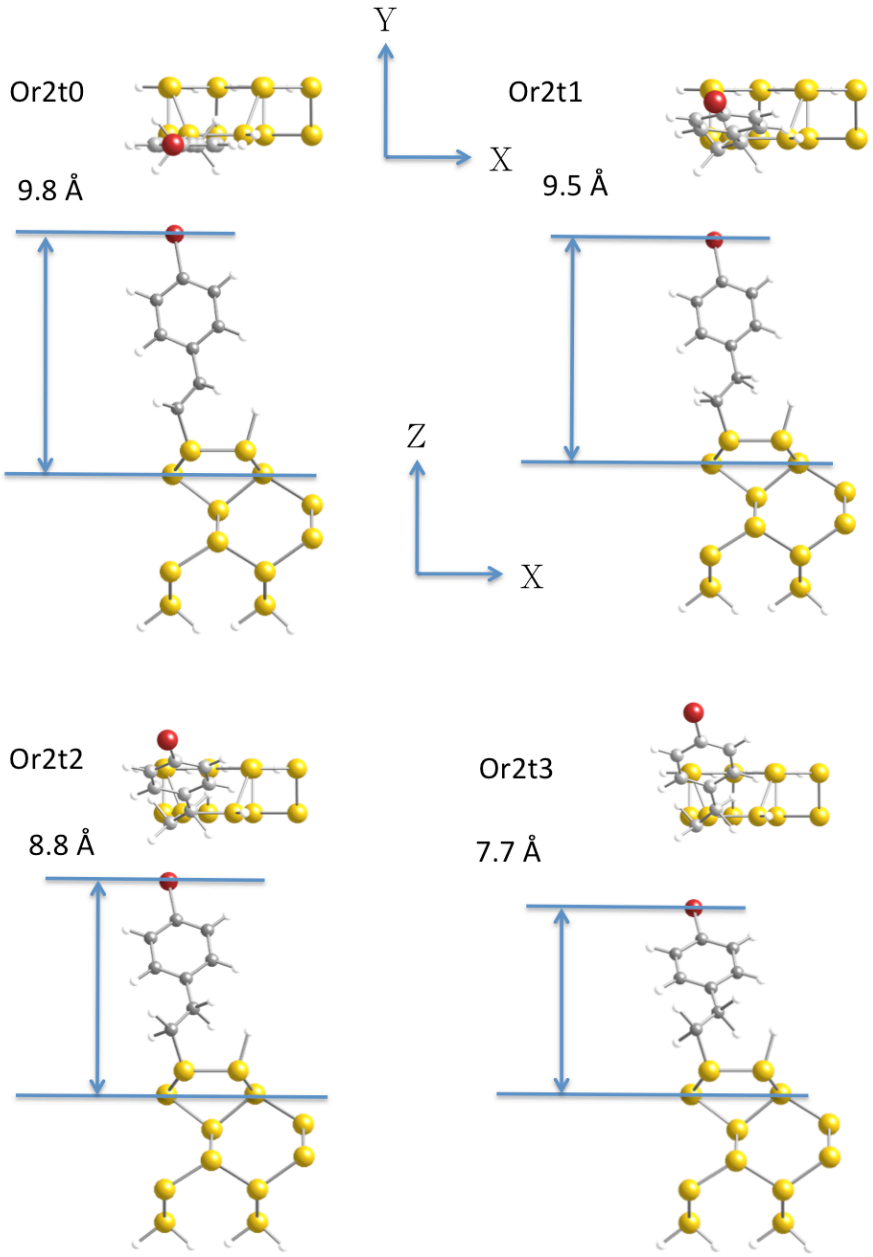

Figure 9.6 Top and side views of another four pre-relaxed BrSty/Si(001) unit structures studied in the (2 x 1) periodic DFT calculations. In contrast to Figure 9.5, the four models are commonly having the bottom alkyl C-C bonds "over" the Si dimers. The four molecules are tilted differently in order to explore the effect of the molecular tilt within the one-dimensional molecular rows.

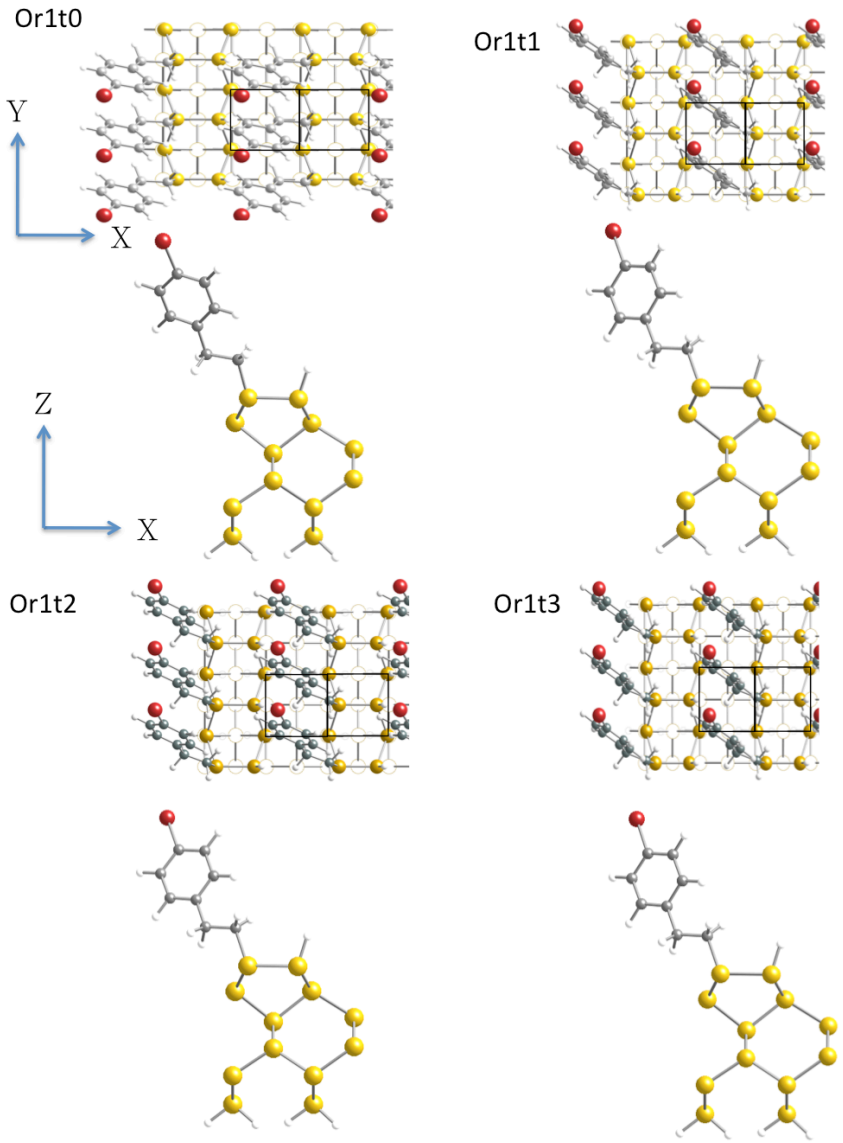

Figure 9.7 Top and side views of the relaxed BrSty/Si(001) super-cells based on the (2 x 1) periodic DFT calculation results of the four configurations in Figure 9.5. The (1 x 1) unit cells of the bulk-terminated Si surfaces are illustrated by the black squares. The heights of the terminal Br atoms, with respect to the bulk-terminated Si surfaces, are listed in Table 9.2. The four structures commonly show the bottom alkyl C-C bonds away from the Si dimers. Besides the orientation Or1t2, which has the Br near the middle of the sides of the (1 x 1) unit cells, all the orientations have the Br atoms close to the corners of the (1 x 1) unit cells.

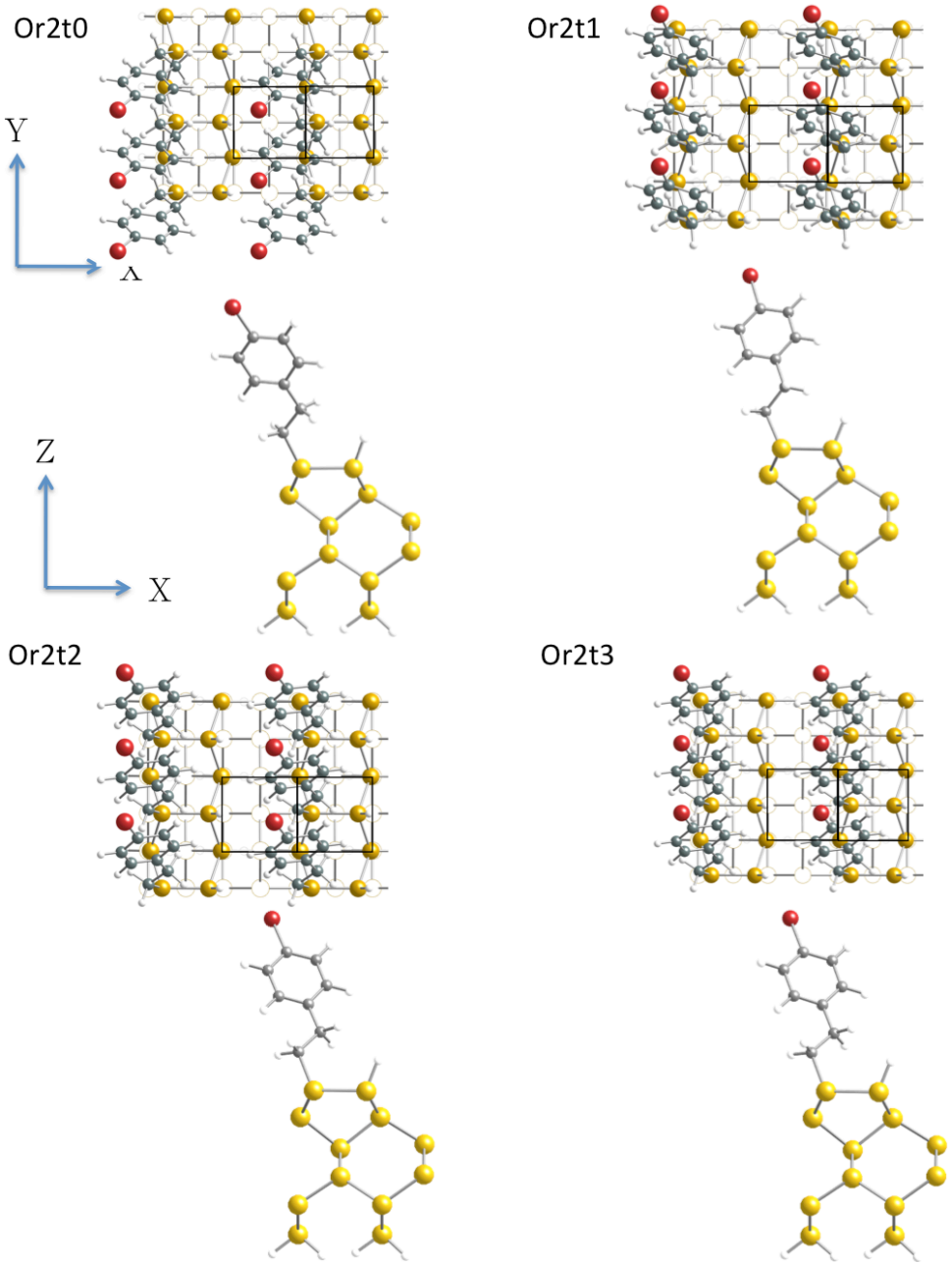

Figure 9.8 Top and side views of the relaxed BrSty/Si(001) super-cells based on the (2 x 1) periodic DFT calculation results of the four configurations in Figure 9.6. The (1 x 1) unit cells of the bulk-terminated Si are illustrated by the black squares. The heights of the terminal Br atoms, with respect to the bulk-terminated Si surfaces, are listed in Table 9.2. In contrast to Figure 9.7, the four structures commonly show the bottom alkyl C-C bonds over the Si dimers. Besides the orientation Or2t1, all the others have the Br atoms close to the centers of the (1 x 1) unit cells.

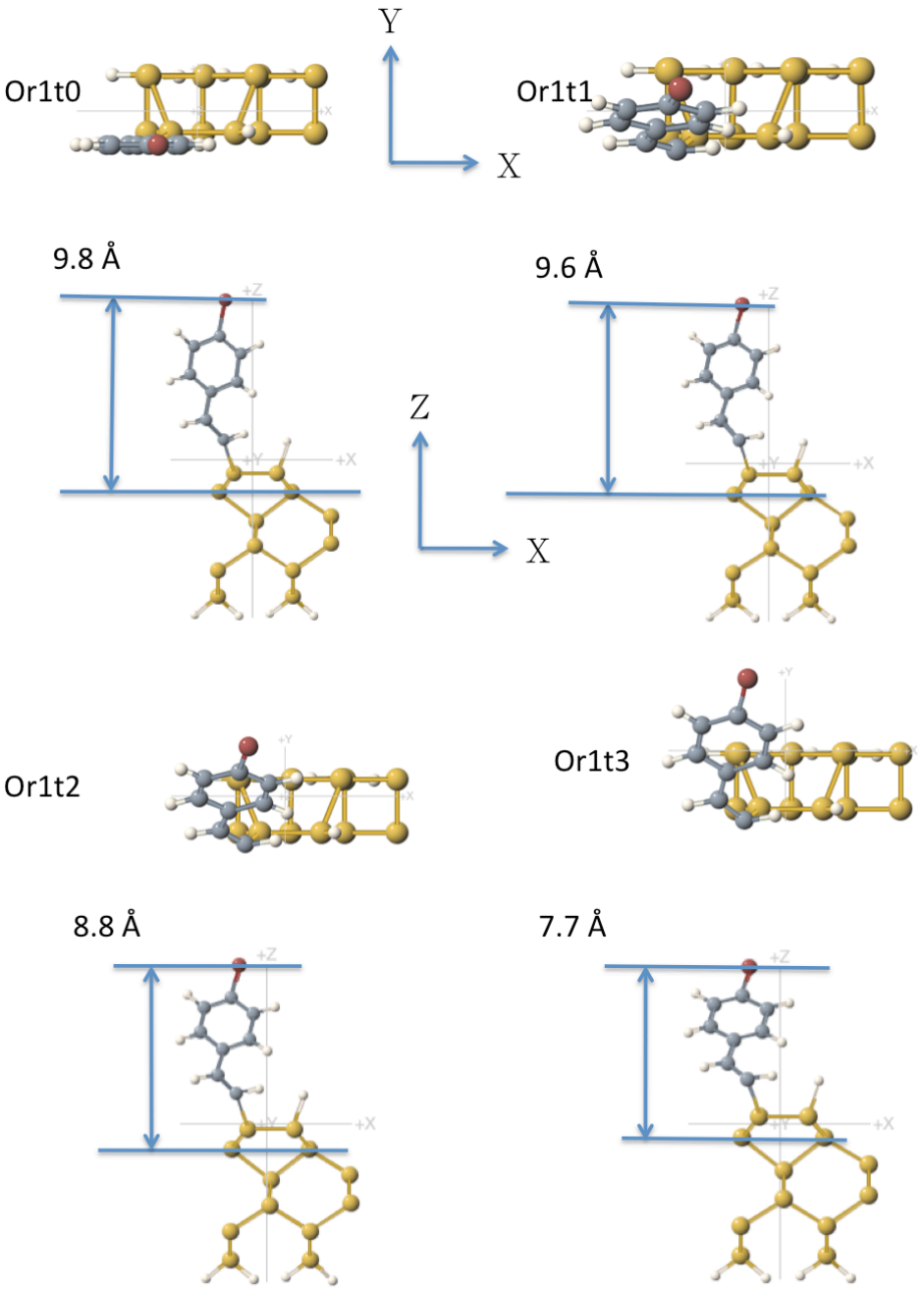

Figure 9.9 Top and side views of the four pre-relaxed BPA/Si(001) unit structures studied in the (2 x 1) periodic DFT calculations. The four models are commonly having the bottom alkenyl C=C bonds of the covalently bonded molecules “away” from the Si dimers. The four molecules are tilted differently to explore the effect of the molecular tilt within the one-dimensional molecular rows.

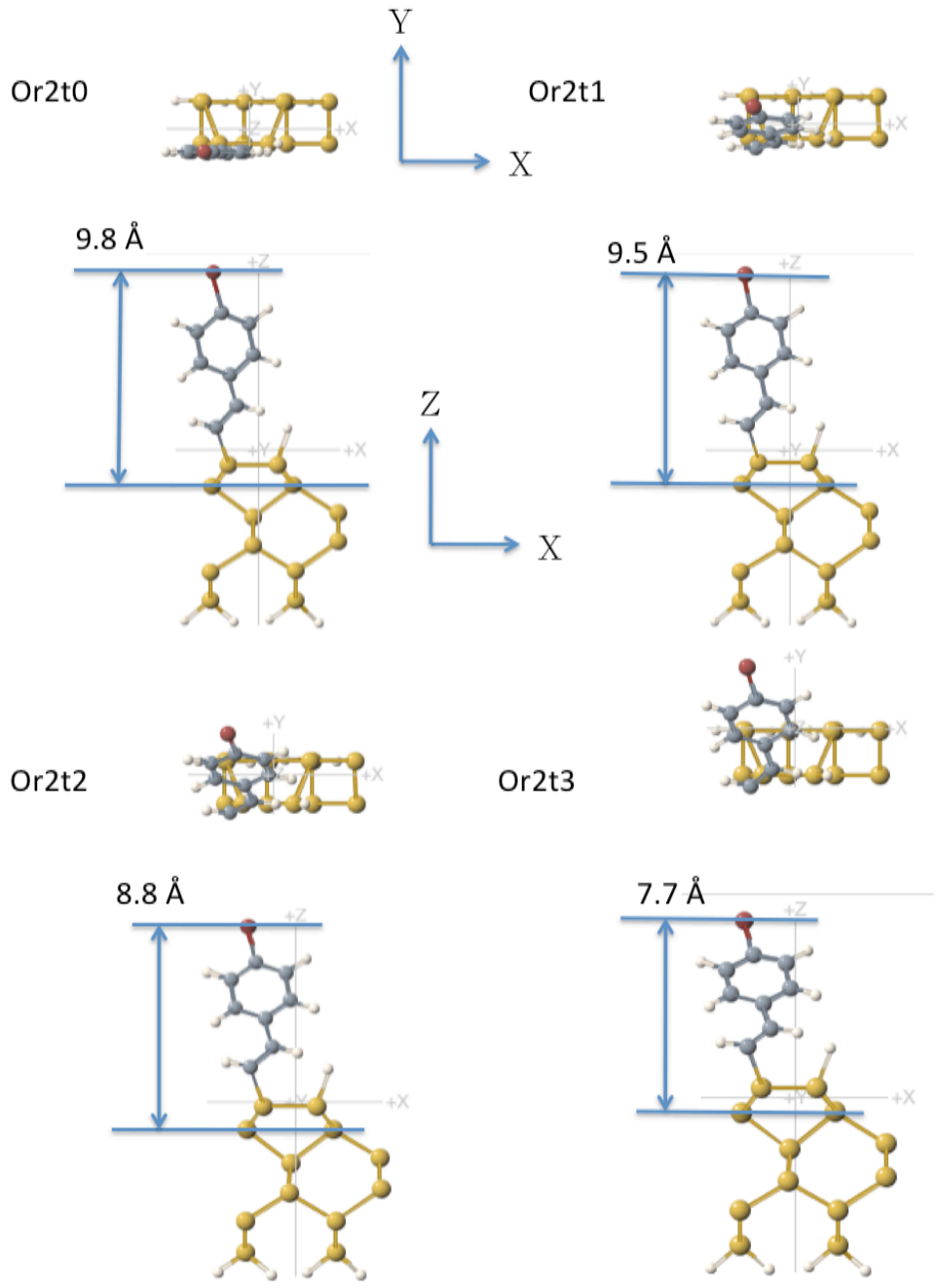

Figure 9.10 Top and side views of another four pre-relaxed BPA/Si(001) unit structures studied in the (2 x 1) periodic DFT calculations. In contrast to Figure 9.9, the four models are commonly having the bottom alkenyl C=C bonds of the covalently bonded molecules "over" the Si dimers. The four molecules are tilted differently to explore the effect of the molecular tilt within the one-dimensional molecular rows.

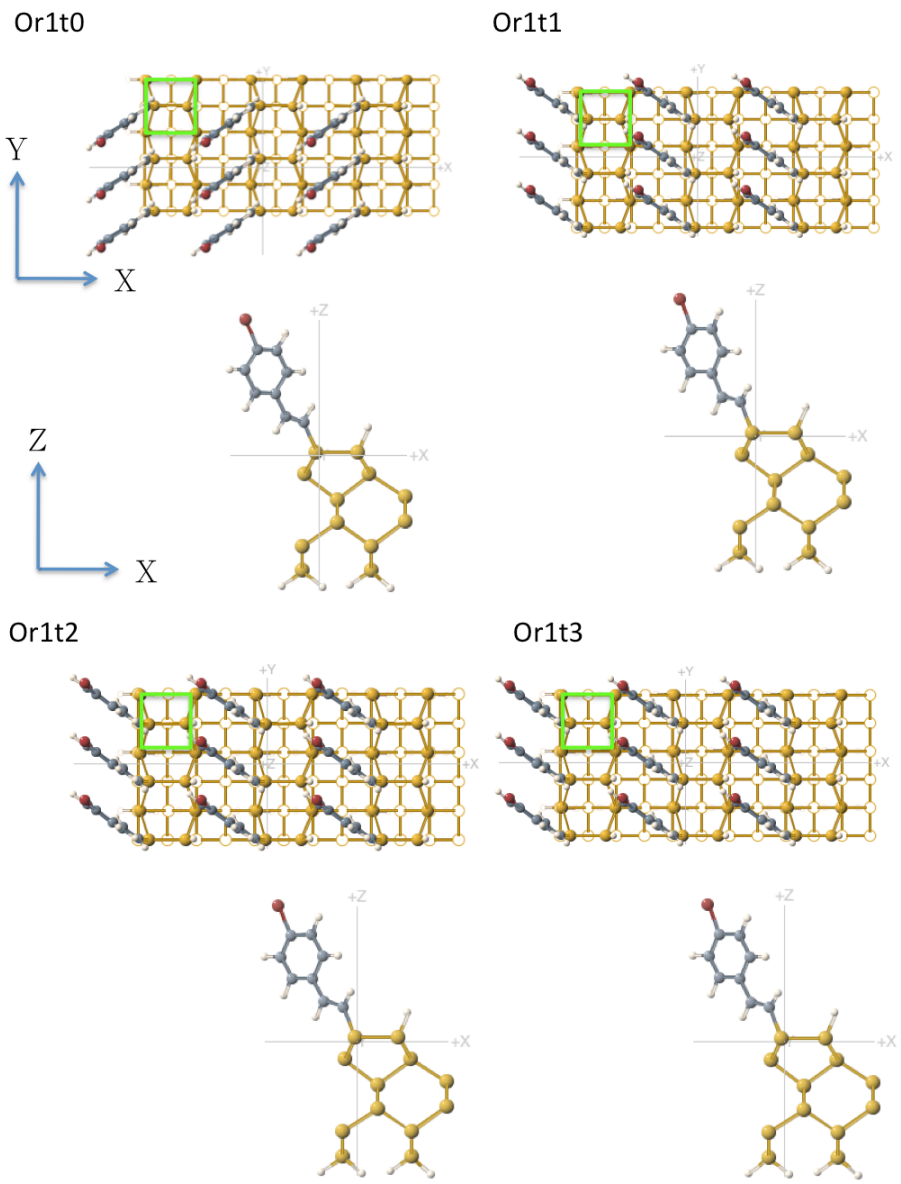

Figure 9.11 Top and side views of the relaxed BPA/Si(001) super-cells based on the (2 x 1) periodic DFT calculation results of the four configurations in Figure 9.9. The (1 x 1) unit cells of the bulk-terminated Si surfaces are illustrated by the green squares. The heights of the terminal Br atoms, with respect to the bulk-terminated Si surfaces, are listed in Table 9.3. The four structures commonly show the bottom alkenyl C=C bonds of the covalently bound molecules away from the Si dimers. All the orientations have the Br atoms near the corners of the (1 x 1) unit cells.

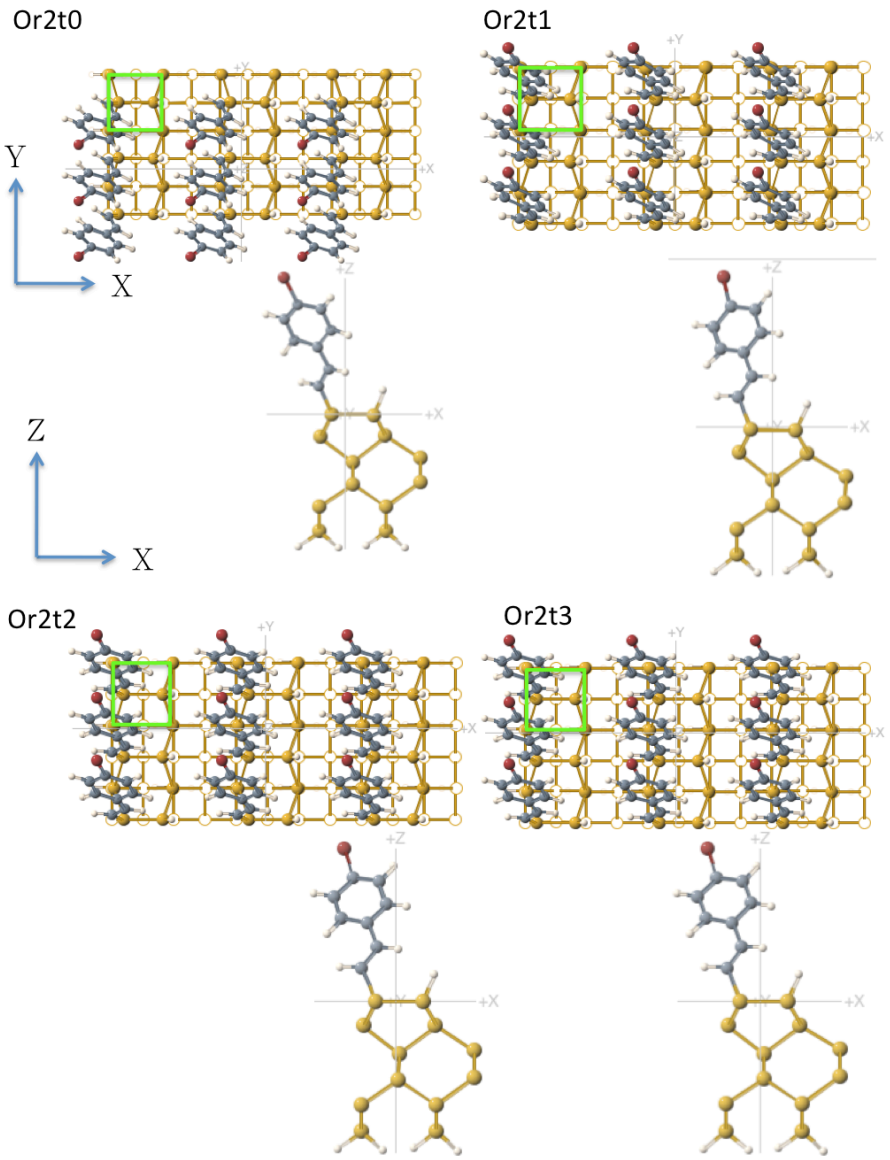

Figure 9.12 Top and side views of the relaxed BPA/Si(001) super-cells based on the (2 x 1) periodic DFT calculation results of the four configurations in Figure 9.10. The (1 x 1) unit cells of the bulk-terminated Si surfaces are illustrated by the green squares. The heights of the terminal Br atoms, with respect to the bulk-terminated Si surfaces, are listed in Table 9.3. In contrast to Figure 9.11, the four structures commonly show the bottom alkenyl C-C bonds of the covalently bound molecules over the Si dimers. All the orientations have the Br atoms near the centers of the (1 x 1) unit cells.

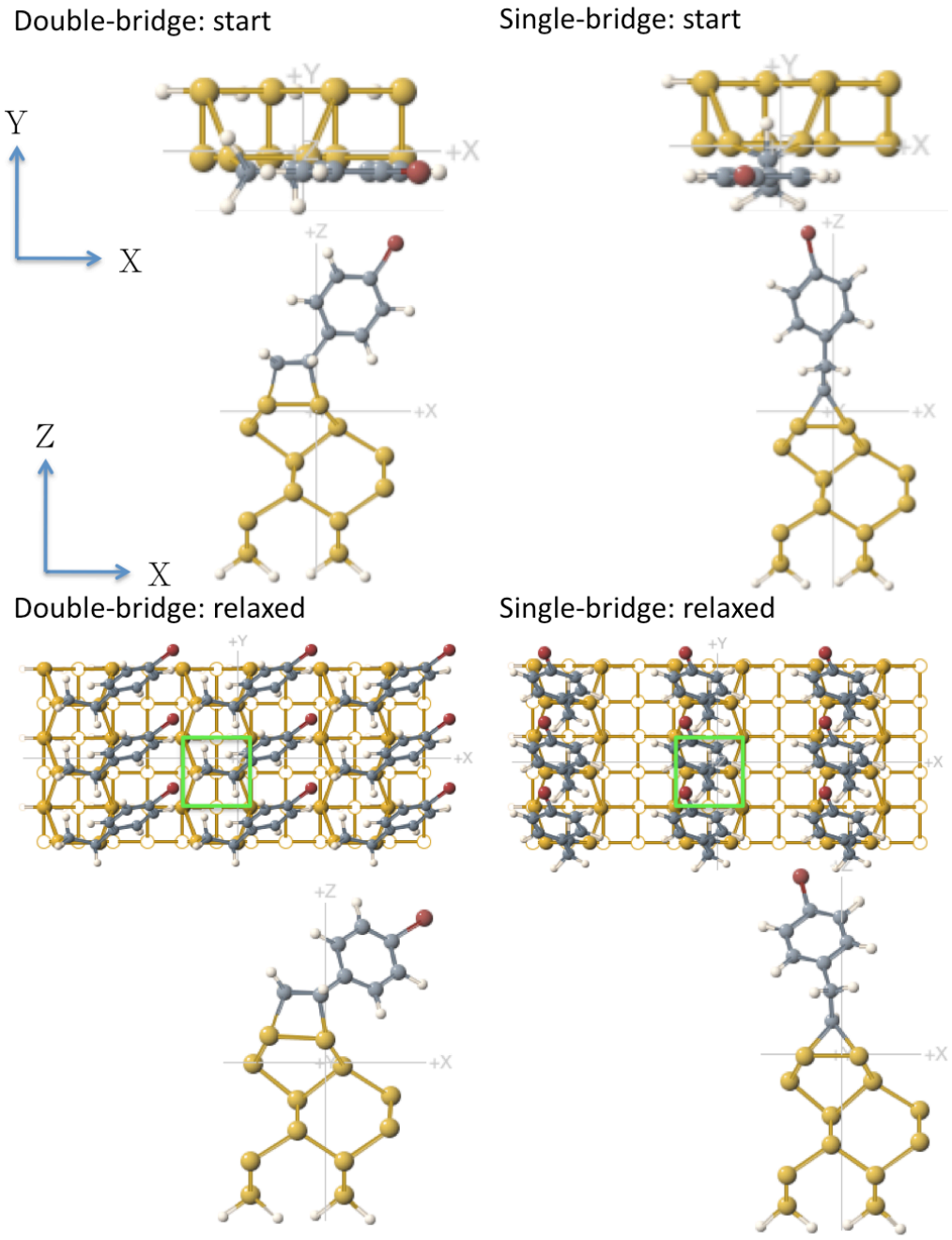

Figure 9.13 Top and side views of the structures of (2 x 1) packed BPA-based SAMs on Si(001)-2x1:H based on the alternative bridge-like bonding, before (upper images) and after (lower images) the relaxation of the models in the periodic DFT calculations. The green squares indicate the (1 x 1) unit cells of the bulk-terminated surfaces.

9.3 XRR analysis

Comparing the Br heights from orientation Or1 to Or2 in Table 9.2 and 9.3, the Or2 orientation has a greater Br height of the Br atoms than the other due to the interaction between the molecules and the Si dimers. Additionally, for the three types of possible bonding configurations of BPA-derived SAMs (Fig 9.11 to 9.13), the terminal Br atoms are locating at different heights. If the absolute heights of the Br atoms can be determined by the XRR analysis, or even more accurately by the combination of XRR and XSW analyses, the accurate configurations for BrSty- and BPA- based SAMs on Si(001) may be directly determined. However, our XRR results suggest that the organic films on our two samples are thicker than 10 Å, which is not consistent with the DFT models. It is possible that due to the existence of very low coverage SAMS on the UHV prepared samples, the XRR experiments, instead of measuring the structures of the brominated SAMs, sensing the physisorbed hydrocarbon contaminants on the surfaces. An in-situ XRR measurement in an UHV chamber may be necessary to prevent the problem. Since structurally the vertical profiles of the SAMs are not available from the XRR analysis, the characterization of the structures will be performed via the XSW 3D imaging technique.

9.4 XSW analysis

The specular and off-specular XSW results for BrSty- and BPA- based SAMs on Si(001) are respectively shown in Fig 9.14 and 9.15. The XRF measured Br coverage as well as the coherent fractions and coherent positions are summarized in Table 9.5. As a point of reference, a

1x1 bulk-like terminated Si(001) surface has 6.78 Si / nm^2. The XSW experiments for the BrSty/Si(001) and BPA/Si(001) were performed at 12 ID-D and 5 ID-C, respectively.

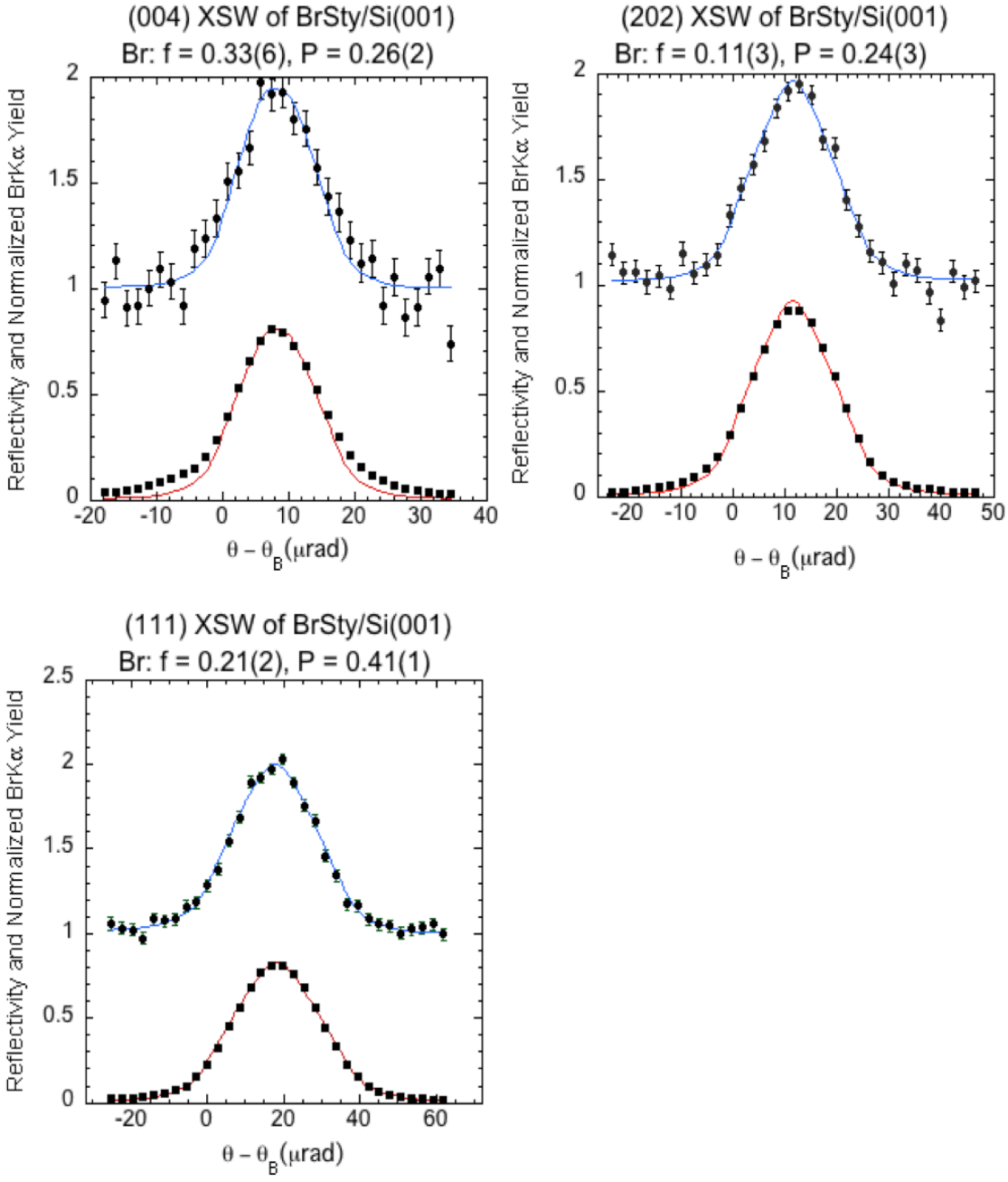

Figure 9.14 The single-crystal XSW results for the *p*-(4-bromophenyl)styrene (**BrSty**)-derived SAM on a Si(001)-2x1 surface. Shown are the angle dependences of the *h k l* Si Bragg reflectivity (bottom) and the Br Kα XRF yield data (top). Symbols are measured data, and solid lines are the best-fits of theory to the data.

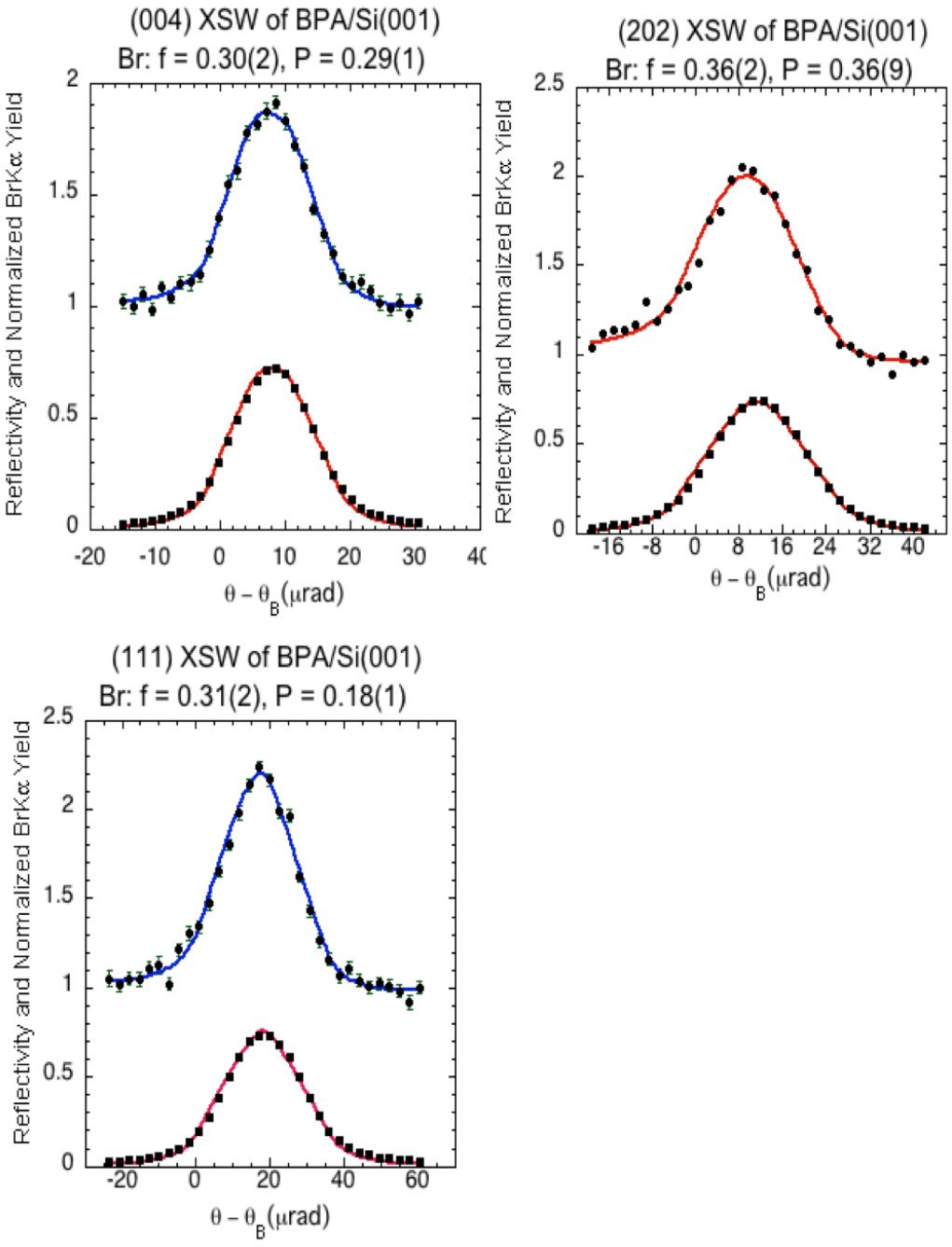

Figure 9.15 The single-crystal XSW results for the (4-bromophenyl)acetylene (**BPA**)-derived SAM on a Si(001)-2x1 surface. Shown are the angle dependences of the *h k l* Si Bragg reflectivity (bottom) and the Br Kα XRF yield data (top). Symbols are measured data, and solid lines are the best-fits of theory to the data.

	Cov.	(004)		(202)		(111)	
	Br / nm^2	f_{004}	P_{004}	f_{202}	P_{202}	f_{111}	P_{111}
BrSty	0.78	0.33(6)	0.26(2)	0.11(3)	0.24(3)	0.21(2)	0.41(1)
BPA	0.88	0.30(2)	0.29(1)	0.36(2)	0.36(9)	0.31(2)	0.18(1)

Table 9.5 The XRF measured Br coverage together with the specular and off-specular XSW results (Fig 9.14 and 9.15) for BrSty- and BPA- based SAMs on Si(001)

The XSW-measured Fourier components listed in Table 9.5 (and their 4-fold symmetry equivalents) are summed to produce Br 3D atomic density maps shown in Fig 9.16. The origin is chosen at the bulk-terminated Si.

For the case of the BrSty-derived SAM, the comparison of the DFT models with XSW Br density map shows that the Or1 orientation, where the alkyl C-C bond is away from the Si dimer, better fits the XSW result. Additionally, the relaxed Or1t3 orientations, having the Br at the height about 8.5 Å (above the bulk-terminated surface) and laterally near the corners of the (1 x 1) unit cells, best fit the XSW measured density map. (Or1t1 result has the almost identical structure and total energy as that for Or1t3 so the two configurations are essentially identical). On the other hand, for the case of BPA SAM, the Or2 (t0, t2, and t3), double-bridge and single-bridge orientations have the height of Br fit with the XSW density map within 0.3 Å. (The match of the double-bridge structure with the density map is through the hot spot at 6.28 Å high). However, since the double-bridge bonding has the Br near the middles of the sides of the (1 x 1)

unit cells, and the single-bridge bonding has the Br near the corners of the (1 x 1) unit cells, the comparison of the BPA Br density map in Fig 9.16 to the simulated Br density maps in Fig 9.17 clearly shows that the Or2t0 model better fits the data (Or2t0 is chosen because its energy is lower than Or2t2 and Or2t3). The alignment of the alkenyl C=C bond over the Si dimer for BPA/Si(001) is consistent with the earlier proposed sp^3-sp^2 alignment in the case of alkenyl SAMs on Si(111). Further study of the effect of the molecular orientation to the electronic property may contribute to the development of nano-scale molecular electronics.

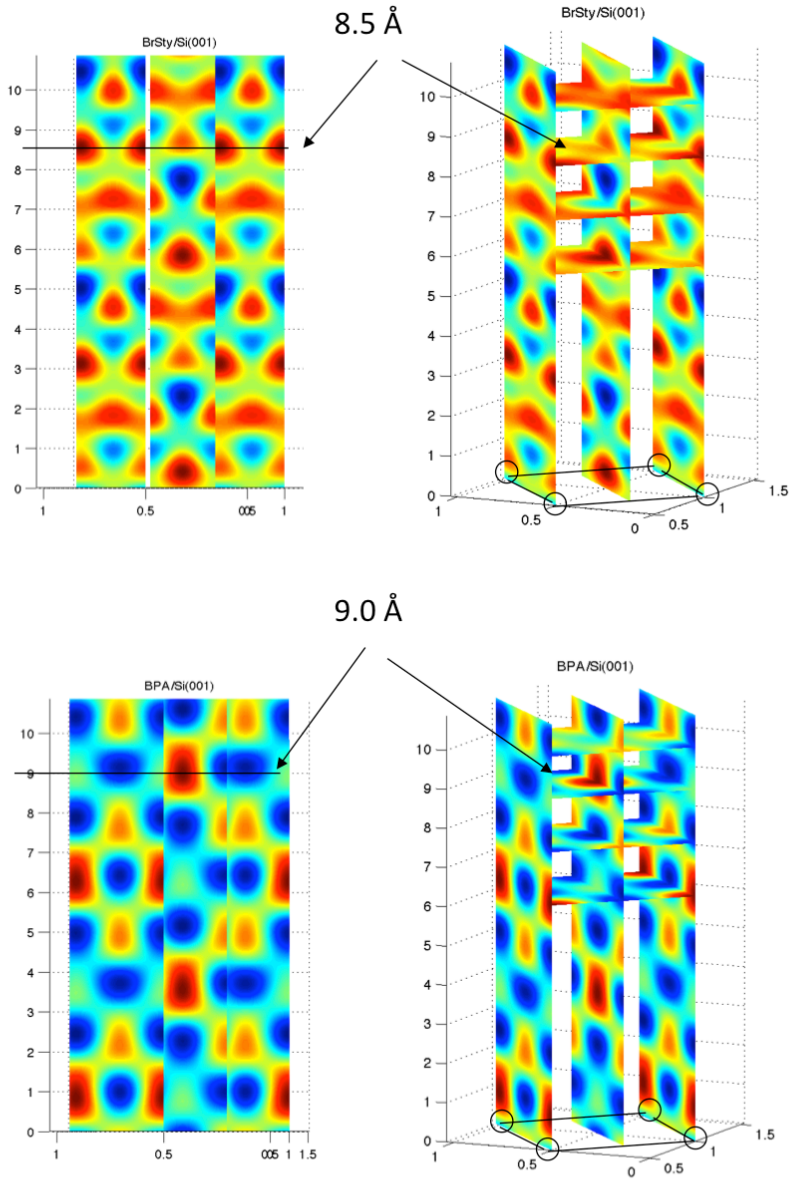

Figure 9.16 XSW generated Br atomic maps from two different viewing angles for BrSty- (upper images) and BPA- (lower images) based SAMs on Si(001)-2x1:H surfaces. The 2D cuts through the 3D Br atomic density maps coincide with the Br maxima in the 3D maps. Because of the intrinsic periodicity of XSW imaging, the hot spots show up at (8.5 – n x 1.36) Å, n = 0 to 6 for BrSty, and (9.0 – n x 1.36) Å , n = 0 to 6 for BPA. The origin is at the bulk-terminated Si.

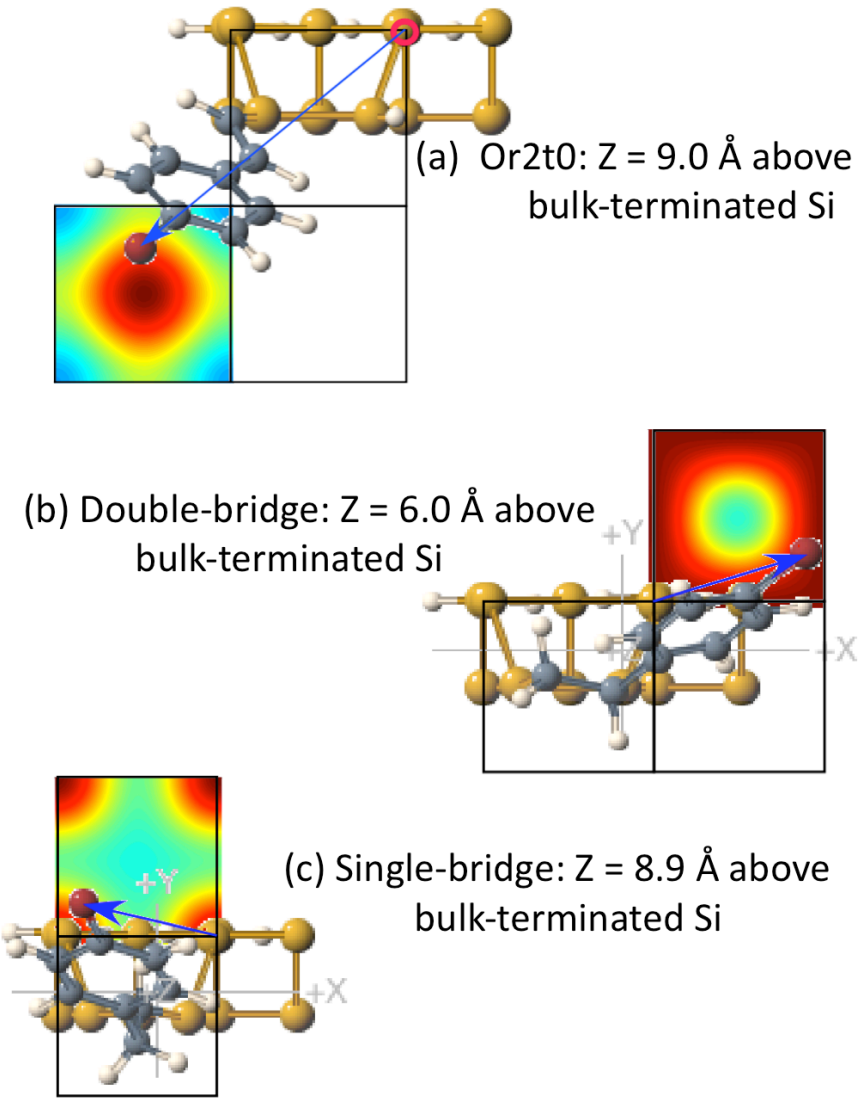

Figure 9.17 Projected ball-and-stick models for (a) Or2t3, (b) Double-bridge, and (c) Single-bridge types of bonding for BPA-derived SAM on Si(001)-2x1, based on the (2 x 1) periodic DFT calculation results, in conjunction with the corresponding XSW Br density maps (model simulations).

9.5 Summary

By combining DFT modeling and XSW atomic imaging techniques, atomic-scale structures for BrSty- and BPA- derived SAMs on Si(001)-2x1:H are studied. The alkyl C-C bonds at the molecule/substrate interface for BrSty molecules after the surface hydrosilylation, are away from the Si dimers. In contrast, the alkenyl C=C bonds for a tethered BPA molecule on Si(001)-2x1:H are directly over the Si dimers. Complementary infrared technique may be useful to confirm these results.

Chaper 10 : X-ray induced desorption

In the XRR and XSW experiments the SAM/Si samples were sealed within a dry nitrogen flow cell with a thin Kapton X-ray window to avoid air exposure and oxidation. With no X-ray flux on the sample there were no significant changes to the SAMs. However, under the full undulator intensity of 1 x 10^{11} photons/sec/mm^2 of radiated surface area, the Br coverage showed an X-ray induced desorption effect corresponding to an exponential decay with a half-life of 10 min for BrSty/Si(111). For all the data presented in this thesis work, the X-ray radiation effects were closely monitored and minimized during exposure to the X-ray beam. This was done by using incident beam transmission filters, a fast-shutter, and by moving the footprint of the beam on the sample to a fresh unradiated spot before any significant damage occurred. However, the radiation induced desorption mechanism is still worth studying because an understanding of the mechanism will contribute to a control of the desorption process and knowledge of the limitations of the technique.

10.1 Determination of the X-ray induced desorption rate

A preliminary study of X-ray induced Br desorption from a BPA/Si(111) sample using E = 16.00 keV X-rays was performed at the 5ID-C station with an incident flux ~ 3.7 x 10^{11} photons per second (p/s) . The relative decrease in the Br coverage as a function of accumulated X-ray flux incident on the sample (dose D in p/mm^2) was measured at five incident angles near the total external reflection (TER) condition. This was at normalized incident angles of $X = \theta/\theta_c$,

= 0.5, 1.0, 1.2, 2.0, and 3.0; where the critical angle θ_c = 0.112˚ for 16.00 keV X-rays reflecting from a Si mirror (See Fig 10.1a - 10.1e). In sequential time periods the Br Kα counts and the incident beam ion chamber counts were collected at each fixed incident angle. Since the vertical size of the incident beam slit (SS = 0.2 mm) was always larger then the projected height of the sample length (SL), the ion chamber counts were reduced by the factor (SL x Sin(θ) / SS) to give the effective ion chamber counts I_e, The "normalized" Br Kα yield (Br Kα yield = Br Kα counts / I_e), which is normalized to unity at the first time interval, was used to monitor the relative decrease in the Br coverage. The results shown in Fig 10.1 suggests that the X-ray induced desorption process is angle dependent and is greatly enhanced near the critical angle.

10.2 Dependence of the desorption rate on the incident angle of X-rays

The strong increase in the Br desorption rate in Fig 10.1f at the Si critical angle can be used to determine the primary mechanism for the X-ray induced desorption process. Is it caused by the primary E-field intensity at the surface or by the secondary electron emission from the Si substrate or by some other mechanism? To understand how the X-ray incident angle affects the desorption rate, the E-field intensity profile along the surface normal direction is calculated using Eq. 10.1 and 10.2 at each incident angle and the results are shown in Fig 10.2a.

$$EFI(\theta,z) = |E_0|^2[1+R+2\sqrt{R}\,Cos(\upsilon-Q_z)] \qquad z \geq 0 \qquad (10.1)$$

$$EFI(\theta,z) = |E_0|^2[1+R+2\sqrt{R}\,Cos(\upsilon-Q_z)] \times Exp(\mu(\theta)\, z) \qquad z < 0 \qquad (10.2)$$

Where $\mu(\theta) = (4\pi/\sqrt{2}\lambda)\{[(\theta_c^2 - \theta^2)^2 + 4\beta^2]^{1/2} + \theta_c^2 - \theta^2\}^{1/2}$ is the attenuation depth, θ_c is the critical angle, $Q = 4\pi Sin\theta/\lambda$ is the magnitude of the wavevector transfer, R is the reflectivity, υ is the phase and E_0 is the electric field amplitude of the incident beam.

In our case the generation of the emitted electrons is primarily related to the X-ray induced photoelectric effect within the Si substrate and is proportional to the E-field intensity (EFI) within the substrate, whereas the flux of X-ray interacting with the molecules is related to the EFI at the surface. As the result, the integrated EFI within the substrate (from Z = 0 at the surface to Z = - 5.4 x 10^6 x Sin(θ) Å at the depth of 16.00 keV electrons. 5.4 x 10^6 Å is the attenuation length for 16.00 keV electrons) and the EFI at the substrate surface are separately calculated and plotted together as functions of normalized incident angle $X = \theta/\theta_c$ in Fig 10.2b. A comparison with Fig 10.1f indicates that the Br desorption is primarily induced by an interaction with the primary X-rays as opposed to being induced by the secondary electron emission.

In order to further explore the first order interaction between the "X-rays" and the brominated SAMs on Si, an X-ray induced desorption experiment was performed on a BPA/Si(111) sample with the incident X-rays E = 16.00 keV and straight-through-beam (STB) flux F ~1.5 x 10^{10} p/s at the 33 BM-C station. Since at 16.00 keV the X-ray absorption cross

section for the hydrocarbon part (H: 0.67 barns/atom, C: 12.84 barns/atom) of the BPA molecule is much smaller than that for Br (12,400 barns/atom), (data from http://csrri.iit.edu/periodic-table.html), our study focused on the X-rays–Br interaction. The desorption of the Br was monitored at the incident angle $\theta = 4^\circ$ (which is much greater than the critical angle). On the A = 0.26 mm^2 radiated footprint (the whole footprint is smaller than the surface area of the sample), the X-ray photon density was $F/A \sim 5.8 \times 10^{10}$ $p/s/mm^2$. At time t = 0, the radiated footprint, with the coverage $\Theta = 0.14$ Br/nm^2, yielded a Br Kα count-rate into the detector of 23 cps. With a detector active area of 50 mm^2 and a detector distance of 58 mm we were collecting $50/(4\pi 58^2) = 0.00118$ of the entire solid-angle of emission with a 0.788 detector efficiency. Therefore the collected 23 cps represents a total Br Ka emission rate of 25,000 p/s. The yield of the Br Kα + Br Kβ photons together was therefore ~ 30,000 cps. Since W_K^{Br} (the fluorescence yield for the K-shell for a Br atom) ~ 0.62 (based on the X-ray data booklet), the photoelectric effect absorption rate for the incident 16.00 keV X-rays is then ~50,000 p/s. Assuming (1) the first order photoelectric effect caused the Br desorbed and (2) the Br Kα yield is 25,000 p/s and is independent of time (as an extreme case), the 3.6×10^{10} Br on the 0.26 mm^2 footprint (at t = 0) will have a half-life ~100 hr. However, our XRF measurement shows a much shorter half-life of ~70 min (Fig 10.3). Therefore there must be some other X-ray induced reaction at the surface that induces Br desorption. It is possible that besides the first order X-ray-Br interaction, secondary interactions with near-surface molecules in the condensed or gas phases may also play important roles in the desorption process. Quantitative determination of the contribution from each factor will be useful to truly understand the desorption mechanism and the result may provide a better strategy to increase the lifetime for the X-ray measurements on

organic SAMs/Si. See Chapter 11 for suggested future experiments that may help in discovery the X-ray induced desorption mechanism.

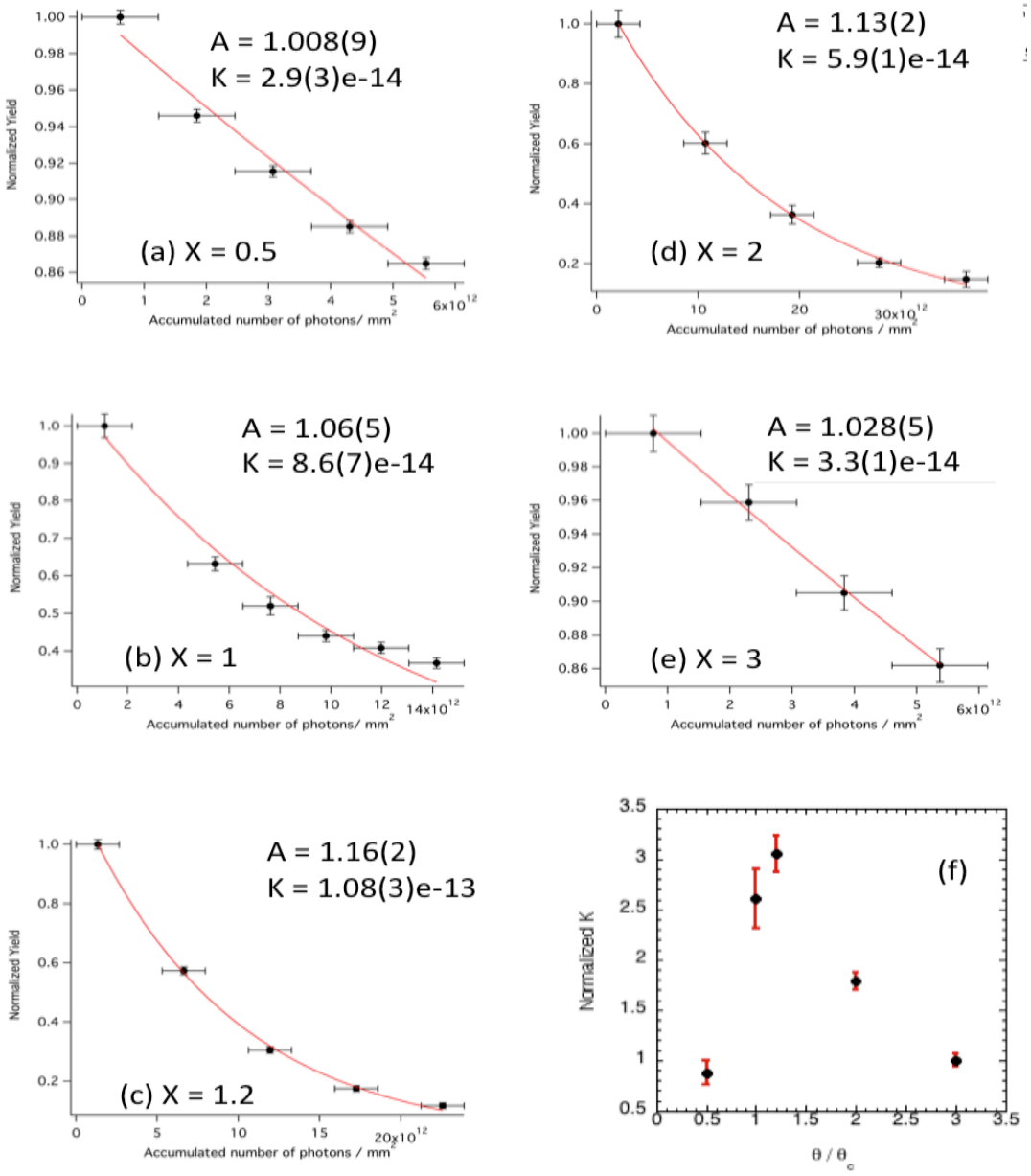

Figure 10.1 X-ray induced Br desorption study for the BPA/Si(111) surface: (a) to (e) Normalized Br XRF yield as a function of accumulated dose of incident photons/mm^2 radiated footprint (D) measured at normalized incident angles X = θ/θ_c = 0.5, 1.0, 1.2, 2.0, and 3.0, respectively. Each plot is fitted with a function Y = A exp(-KD) where the value K is proportional to the probability of the radiation induced Br desorption from a single incident photon. (f) is the normalized K (normalized by the K at X = 3) at X =0.5, 1.0, 1.2, 2.0, and 3.0.

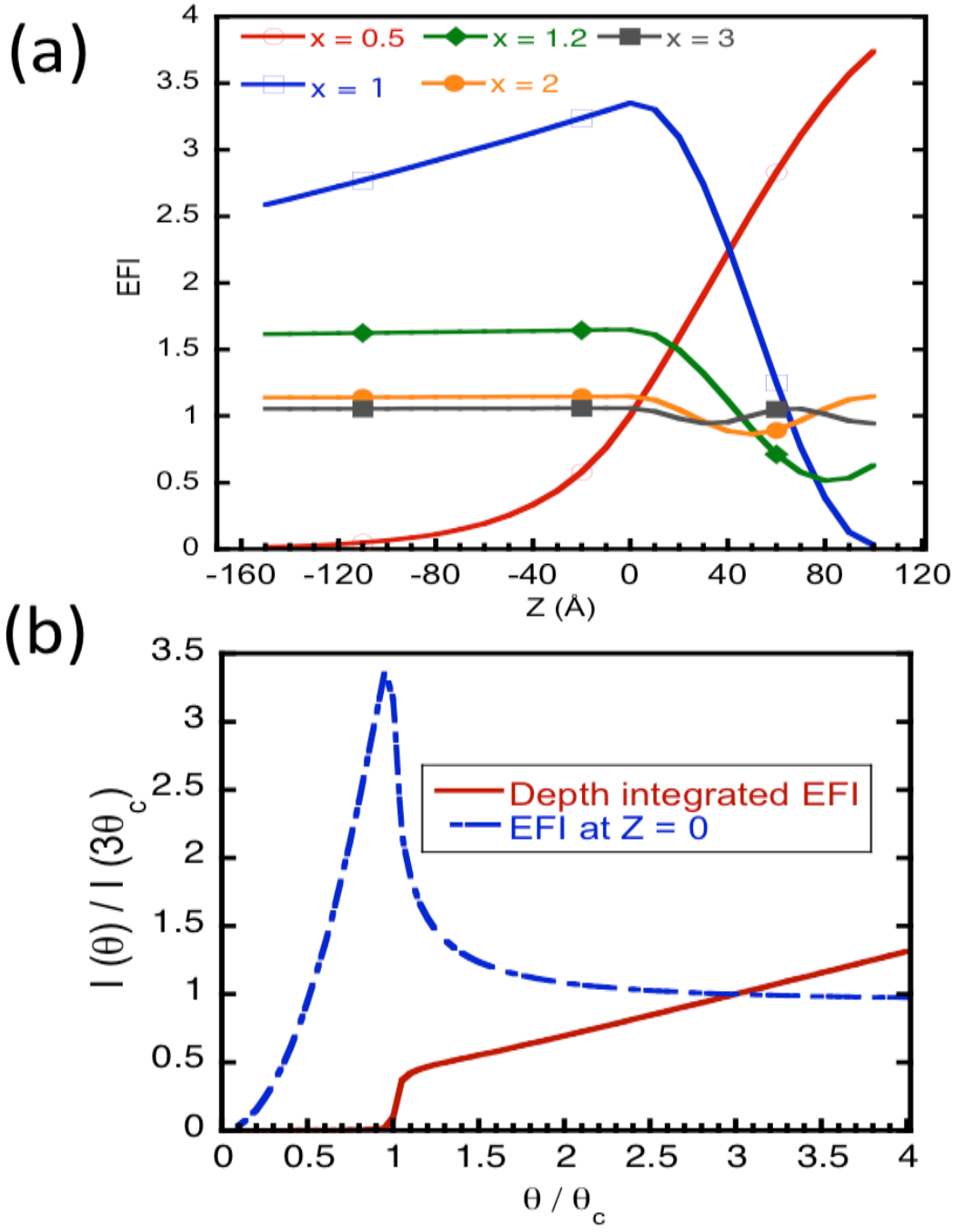

Figure 10.2 (a) The depth (z) dependent E-field intensity (EFI) profiles at X = 0.5 (red), 1.0 (blue), 1.2 (green), 2.0 (orange), and 3.0 (black). (b) The depth integrated EFI within the substrate (red) and the EFI at the surface (blue) as functions of normalized incident angle $X = \theta/\theta_c$ Each curve is normalized to unity at X = 3.

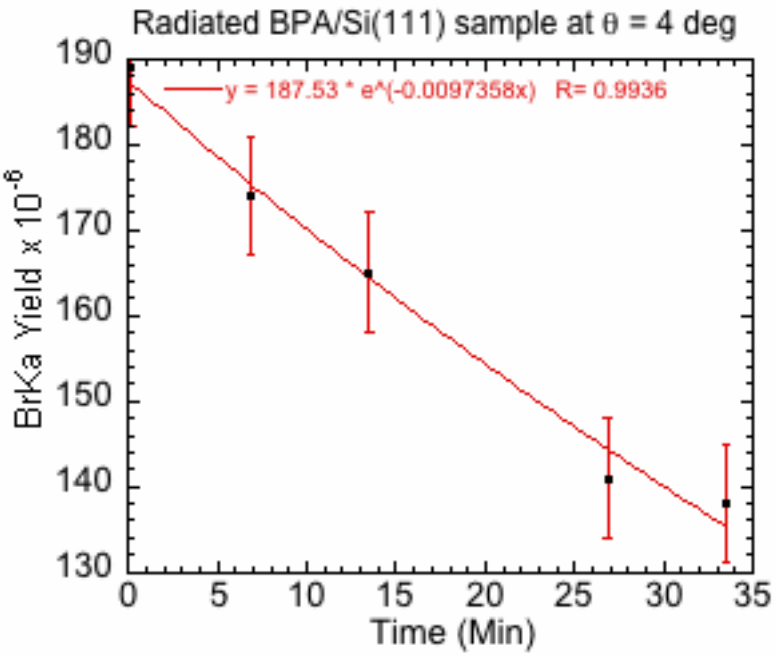

Figure 10.3 The X-ray induced desorption of Br from BPA/Si(111) under E = 16.00 keV, STB flux = 1.5 x 10^{10} cps radiation at θ = 4° . The half life = -ln(0.5) / -0.0097358 = 71 min. The sample was sealed within a 0.0 % R. H. (relative humidity) nitrogen flow cell during the radiation.

Chaper 11 : Summary and Outlook

11.1 Thesis summary

This thesis work has employed a variety of surface-sensitive characterization tools together with DFT modeling to study the atomic-scale structures of the self-assembly of π-conjugated molecules on silicon surfaces. Through the study of six different aromatic self-assembled monolayers (SAMs) on H-Si(111) and two on H-Si(001), a structure characterization strategy for SAMs/Si was developed. In each case DFT calculations predicted several possible atomic-scale models from which the most correct structure was experimentally determined. XPS provided the chemical bonding state for Br atoms to legitimate the use of Br as the XRF marker at the top end of the molecule for XSW structural analysis. Specular XRR measurements sensed the electron density profile along the surface normal direction and the results were used to determine the thickness of the film, the packing density of the molecules, and the roughness at each interface. The direct comparison of the x-ray fluorescence yield from the sample with that from a calibrated reference standard provided the atomic coverage of the sample. By using the generated XSW from the Si substrate, the 3D lattice location(s) of the XRF selected atom (i.e. Br) was measured. The XSW determined atomic density map, in conjunction with the coarser-length-scale XRR analysis (to rule out the subsidiary images of Br attributed to the intrinsic periodicity of XSW technique) and DFT modeling, provided the atomic-scale structure of a SAM on Si.

In the AFM study, the comparisons of the three alkyl SAMs/Si(111) with the three alkenyl SAMs/Si(111) show a higher dependence of the surface's uniformity with the molecular

length for those having alkyl linkage at the molecule/substrate interface. The higher degree of order for the alkenyl SAMs relative to alkyl SAMs was also confirmed by the 111 XSW measurements of the Br coherent fraction. The effect of the alkyl or alkenyl linkage at the molecule/substrate interface also shows up in the azimuthal orientation of the covalently bound molecules with respect to the Si substrate. Based on the DFT studies, a sp^2 alkenyl C=C bond at the surface will azimuthally align over the sp^3 Si-Si bond from the substrate, whereas the sp^3 alkyl C-C bond at the surface will azimuthally bisect two sp^3 Si-Si bonds. These configurational differences should affect the electronic properties of the hybrid structures and be of importance for the development of molecule-based devices.

Through the comparison of various DFT models (i.e. single molecule DFT, (1 x 1) periodic DFT and (2 x 1) periodic DFT) to the XSW measured Br density maps, the (2 x 1) periodic DFT was found to best simulate the structures of the SAMs on Si(111). In this (2 x 1) periodic DFT the linear packing of molecules on Si(111) is approximated by a periodic attachment to every other surface silicon. Qualitatively, the azimuthanl orientation of the molecule to the Si substrate and the tilting of the molecules within the organic adlayers, which respectively are attributed to molecule-substrate and molecule-molecule interactions, were correctly reflected in the (2 x 1) DFT calculations. However, an initial orientation, where the molecules are aligned along the molecular rows, was suggested in the (2 x 1) periodic DFT calculations due to the nature of chain reaction growth.

Overall, the thesis work demonstrates a characterization strategy that is powerful in the determination of the atomic-scale structures of SAMs on Si. The method was successfully applied in the development of the microwave-assisted Sonogashira coupling chemistry. The

microwave-assisted Sonogashira coupling reaction provides the strategy to extend the conjugated organic structures on Si surfaces and tailor the electronic property of the hybrid materials.

11.2 Outlook

11.2.1 Brominated SAMs on Si(001)-2x1:H

In the study of the BPA-derived SAM on Si(001)-2x1:H surfaces, the correct hot spot which corresponds to the Br marker of the molecule was not able to be exclusively determined from the XSW atomic-density map therefore the correct bonding configuration was not directly decided. Although the bridge-like bonding geometries were indirectly ruled out by the comparison of the XSW images generated from the data with that from the model simulations based on the DFT structures, a direct determination of the Br height is still worthy of further investigation. The XRR measurement did not sense the SAM's structure due to the combination of low SAM coverage and physisorbed hydrocarbon contaminants on the surface. The problem may be solved by two different approaches: (1) Remove the hydrocarbon contaminants: An in-situ XRR measurement in an STM-UHV chamber will be ideal because STM topography can serve as a tool to monitor the physisorbtion on the surfaces. The excess contaminants can also be removed by annealing the surfaces and examined again with STM if necessary. (2) Increase the coverage of the SAM: All of our brominated SAMs on Si(001) were prepared in a UHV chamber due to the desire of STM imaging. The surface reaction speed is limited to the pressure of the gas and is much smaller than that in the solution based reaction. To increase the SAM coverage, one can follow the same procedure that used UV to initiate a solution based hydrosilylation reaction.

With a higher SAM coverage, it is expected that the XRR measurement to be less affected by the contamination. Also, with a higher coverage, infrared (IR) technique such as FT-IR, which is sensitive to the hydrocarbon bonding, will be very informative in the determination of the atomic-scale structures. However, the surfaces prepared by wet chemistry method will need to be extensively cleaned in order to uncover the nanoscale structures in STM imaging.

11.2.2 X-ray induced damage

As was described in chapter 10, some experiments were performed to study the X-ray induced desorption of SAMs on Si but the desorption mechanism is still not clear. The understanding of the mechanism will contribute to a control of the desorption process, knowledge of the limitations of the technique, and even the X-ray lithography applications. Quantitative determination of the contribution from the primary and secondary interactions attributed to the X-rays will be useful to truly understand the desorption mechanism and the result may provide a better strategy to increase the lifetime for the X-ray measurements on organic SAMs/Si. This will require performing the Br desorption rate studies in UHV, as well as gas controlled environments, and consequently better control of physisorbed molecules. It is also important to combine XRR analysis into the XRF and XSW desorption analysis to determine if a Br atom desorbs as an atom or as part of a molecular fragment. In other words, is the XRR determined molecular packing density commensurate with the Br coverage during the X-ray induced desorption process or is the molecular packing density unaffected.

References

(1) Horowitz, G. *Adv. Mater.* **1980**, *10*, 365.

(2) Kovac, J.; Peternai, L.; Lengyel, O. *Thin Solid Films* **2003**, *433*, 22-26.

(3) Wagner, P. N., S.; Spudich, J. A.; Volkmuth, W. D.; Chu, S.; Cicero, R. L.; Wade, C. P.; Linford, M. R.; Chidsey, C. E.D. *Journal of Structural Biology* **1997**, *119*, 189-201.

(4) Yu, G.; Gao, J.; Hummelen, J. C.; Wudl, F.; Heeger, A. J. *Sci* **1995**, *270*, 1789-1791.

(5) Burroughes, J. H.; Bradley, D. D. C.; Brown, A. R.; Marks, R. N.; Mackay, K.; Friend, R. H.; Burns, P. L.; Holmes, A. B. *Natur* **1990**, *347*, 539.

(6) Dimitrakopoulos, C. D.; Malenfant, P. R. L. *Adv. Mater.* **2002**, *14*, 99-117.

(7) Molina, L. M.; Hammer, B. *Chem. Phys. Lett.* **2002**, *360*, 264-271.

(8) Ramachandran, G. K.; Hopson, T. J.; Rawlett, A. M.; Nagahara, L. A.; Primak, A.; Lindsay, S. M. *Sci* **2003**, *300*, 1413-1416.

(9) J., W. A.; R., C. S.; C., V.; H., F. D. *Langmuir* **2002**, *18*, 1542.

(10) Basu, R.; Lin, J.-C.; Kim, C.-Y.; Schmitz, M. J.; Yoder, N. L.; Kellar, J. A.; Bedzyk, M. J.; Hersam, M. C. *Langmuir* **2007**, *23*, 1905-1911.

(11) Kellar, J. A.; Lin, J.-C.; Kim, J.-H.; Yoder, N. L.; Bevan, K. H.; Stokes, G. Y.; Geiger, F.; Nguyen, S. T.; Bedzyk, M. J.; Hersam, M. C. *The Journal of Physical Chemistry C* **2009**, 2919-2927.

(12) Lin, J.-C.; Kellar, J. A.; Kim, J.-H.; Yoder, N. L.; Bevan, K. H.; Nguyen, S. T.; Hersam, M. C.; Bedzyk, M. J. *European Journal of Physics Special Topics* **2009**, *168*, 33-39.

(13) Yeganeh, M. S.; Dougal, S. M.; Polizzotti, R. S.; Rabinowitz, P. *Phys. Rev. Lett.* **1995**, *74*, 1811.

(14) Linford, M. R.; Chidsey, C. E. D. *J. Am. Chem. Soc.* **1993**, *115*, 12631-12632.

(15) Buriak, J. M. *Chem. Rev.* **2002**, *102*, 1271-1308.

(16) Cicero, R. L.; Linford, M. R.; Chidsey, C. E. D. *Langmuir* **2000**, *16*, 5688-5695.

(17) J., T.; R., L. M.; C., W.; Y., C. R.; P., P.; D., C. C. E. *Appl. Phys. Lett.* **1997**, *71*, 1056.

(18) Eves, B. J.; Sun, Q. Y.; Lopinski, G. P.; Zuilhof, H. *J. Am. Chem. Soc.* **2004**, *126*, 14318-14319.

(19) Cicero, R. L. C., C. E. D.; Lopinski, G. P.; Wayner, D. D. M.; Wolkow, R. A. *Langmuir* **2002**, *18*, 305-307.

(20) Schlier, R. E.; Farnsworth, H. E. *The Journal of Chemical Physics* **1959**, *30*, 917-926.

(21) Basu, R.; Guisinger, N. P.; Greene, M. E.; Hersam, M. C. *Appl. Phys. Lett.* **2004**, *85*, 2619-2621.

(22) Martinez-Guerra, E.; Takeuchi, N. Physical Review B (Condensed Matter and Materials Physics) **2007**, 75, 205338-7.

(23) Jin, H.; Kinser, C. R.; Bertin, P. A.; Kramer, D. E.; Libera, J. A.; Hersam, M. C.; Nguyen, S. T.; Bedzyk, M. J. *Langmuir* **2004**, *20*, 6252.

(24) Batterman, B. W. *Phys. Rev.* **1964**, *133*, A759.

(25) Cowan, P. L.; Golovchenko, J. A.; Robbins, M. F. *Phys. Rev. Lett.* **1980**, *44*, 1680.

(26) Golovchenko, J. A.; Patel, J. R.; Kaplan, D. R.; Cowan, P. L.; Bedzyk, M. J. *Phys. Rev. Lett.* **1982**, *49*, 560-563.

(27) Bedzyk, M. J.; Materlik, G. *Phys. Rev. B* **1985**, *31*, 4110-4112.

(28) Zegenhagen, J. *Surf. Sci. Rep.* **1993**, *18*, 199-271.

(29) Bedzyk, M. J.; Cheng, L. W. Applications of Synchrotron Radiation in Low-Temperature Geochemistry and Environmental Sciences, Rev Mineral Geochem **2002**, 49, 221-266.

(30) Bedzyk, M. J. *Scattering: X-Ray Standing Wave Techniques*; Elsevier: Oxford, 2005; Vol. 6.

(31) Batterman, B. W.; Cole, H. *RvMP* **1964**, *36*, 681.

(32) Bedzyk, M. J.; Fenter, P.; Zhang, Z.; Cheng, L.; Okasinski, J. S.; Sturchio, N. C. *Synchrotron Radiation News (Technical Review)* **2004**, *17*, 5-10.

(33) Cheng, L.; Fenter, P.; Bedzyk, M. J.; Sturchio, N. C. *Phys. Rev. Lett.* **2003**, *90*, 255503.

(34) Okasinski, J. S.; Kim, C.; Walko, D. A.; Bedzyk, M. J. *Phys. Rev. B* **2004**, *69*, 0414041.

(35) Fenter, P. “Applications of Synchrotron Radiation in Low-Temperature Geochemistry and Environmental Science”, 2002.

(36) Robinson, I. K.; Tweet, D. J. *Rep. Prog. Phys.* **1992**, *55*, 599-651.

(37) Kohanoff, J.; Gidopoulos, N. I. *Density Functional Theory: Basics, New Trends and Applications*; John Wiley & Sons, Ltd: Chichester, 2003; Vol. 2.

(38) Nelson, A. *J. Appl. Crystallogr.* **2006**, *39*, 273-276.

(39) Eves, B. J.; Sun, Q. Y.; Lopinski, G. P.; Zuilhof, H. *J. Am. Chem. Soc.* **2004**, *126*, 14318.

(40) Cicero, R. L.; Linford, M. R.; Chidsey, C. E. D. *Langmuir* **2000**, *16*, 5688.

(41) Jin, H.; Kinser, C. R.; Bertin, P. A.; Kramer, D. E.; Libera, J. A.; Hersam, M. C.; Nguyen, S. T.; Bedzyk, M. J. *Langmuir* **2004**, *20*, 6252-6258.

(42) Chinchilla, R.; Najera, C. *Chem. Rev.* **2007**, *107*, 874-922.

(43) Sonogashira, K.; Tohda, Y.; Hagihara, N. *Tetrahedron Lett.* **1975**, *16*, 4467-4470.

(44) Bohlmann, F.; Burkhardt, T.; Zdero, C. *Naturally occurring acetylenes*; London, New York, Academic Press: New York, 1973.

(45) Lam, J.; Breteler, H.; Arnason, T.; Hansen, L. *Chemistry and Biology of Naturally Occurring Acetylenes and Related Compounds*; Elsevier Science Ltd: New York, 1989.

(46) Thakur, K. G.; Jaseer, E. A.; Naidu, A. B.; Sekar, G. *Tetrahedron Lett.* **2009**, *50*, 2865-2869.

(47) Eckhardt, M.; Fu, G. C. *J. Am. Chem. Soc.* **2003**, *125*, 13642-13643.

(48) Stein, A. L.; Alves, D.; da Rocha, J. T.; Nogueira, C. W.; Zeni, G. *Org. Lett.* **2008**, *10*, 4983-4986.

(49) Erdelyi, M.; Gogoll, A. *The Journal of Organic Chemistry* **2003**, *68*, 6431-6434.

(50) Pangborn, A. B.; Giardello, M. A.; Grubbs, R. H.; Rosen, R. K.; Timmers, F. J. *Organometallics* **1996**, *15*.

(51) Lavastre, O.; Cabioch, S.; Dixneuf, P. H.; Vohlidal, J. *Tetrahedron* **1997**, *53*, 7595-7604.

(52) Holmes, B. T.; Pennington, W. T.; Hanks, T. W. *Synth. Commun.* **2003**, *33*, 2447-2461.

(53) Lopinsky, G. P.; Wayner, D. D. M.; Wolkow, R. A. *Natur* **2000**, *406*.

(54) Dahl, P. K. *Macromol. Rep.* **1992**, *A29*, 39-45.

(55) Denmark, S. E.; Neuville, L.; Christy, M. E. L.; Tymonko, S. A. *J. Org. Chem.* **2006**, *71*, 8500-8509.

(56) Malkoch, M.; Thibault, R. J.; Drockenmuller, E.; Messerschmidt, M.; Voit, B.; Russell, T. P.; Hawker, C. J. *J. Am. Chem. Soc* **2005**, *127*, 14942-14949.

(57) Maya, F.; Tour, J. M. *Tetrahedron* **2004**, *60*, 81-92.

(58) McIlroy, S. P.; Clo, E.; Nikolajsen, L.; Frederiksen, P. K.; Nielsen, C. B.; Mikkelsen, K. V.; Gothelf, K. V.; Ogilby, P. R. *J. Org. Chem.* **2005**, *70*, 1134-1146.

(59) Kamikawa, T.; Hayashi, T. *J. Org. Chem.* **1998**, *63*, 8922-8925.

(60) Hreha, R. D.; Zhang, Y.-D.; Domercq, B.; Larribeau, N.; Haddock, J. N.; Kippelen, B.; Marder, S. R. *Synthesis* **2002**, *9*, 1201-1212.

(61) Nitschke, J. R.; Tilley, T. D. *J. Am. Chem. Soc* **2001**, *123*, 10183-10190.

(62) Trumbo, D. L.; Marvel, C. S. *J. Polym. Sci. Part A: Polym. Chem.* **1987**, *25*, 839-846.

(63) Orita, A.; Taniguchi, H.; Otera, J. *Chem. Asian J.* **2006**, *1*, 430-437.

(64) Higashi, G. S.; Chabal, Y. J.; Trucks, G. W.; Raghavachari, K. *Appl. Phys. Lett.* **1990**, *56*, 656-658.

(65) Zhang, Z., Ph.D. thesis, Northwestern University, 2004.

(66) Cheng, L., Ph.D. thesis, Northwestern University, 1998.

(67) Escuadro, A. A., Ph.D. thesis, Northwestern University, 2005.

(68) Libera, J. A., Ph.D. thesis, Northwestern University, 2005.

Appendix A : Syntheses of Vinyl- and Acetylene-Terminated Organic Molecules

Six brominated molecules were studied in this thesis: (a) *p*-bromostyrene (BrSty), (b) *p*-(4-bromophenyl)styrene (BPS), (c) *p*-(4-bromophenylethynyl)styrene (BPES), (d) (4-bromophenyl)acetylene (BPA), (e) (*p*-(4-bromophenyl)phenyl)acetylene (BPPA), and (f) (*p*-(4-bromophenylethynyl)phenyl)acetylene (BPEPA). Besides *p*-bromostyrene was obtained from Aldrich Chemicals, all the other molecules were synthesized by Dr. Jun-hyun Kim in the Nguyen group at NU. FT-NMR and GC-MS were used to confirm the structures of the synthesized molecules and the procedures are detailed in chapter A.1. The chemicals used in the synthesis are listed in chapter A.2 and the reaction processes are stated in chapter A.3.

A.1 Instrumentation

Fourier-transformed nuclear magnetic resonance (FT-NMR) spectra were recorded on a Varian Inova spectrometer 500 (499.773 MHz for ^{1}H and 125.669 MHz for ^{13}C). ^{1}H chemical shifts are referenced to the proton resonance resulting from protic residue in deuterated solvent and ^{13}C chemical shifts recorded downfield in ppm relative to the carbon resonance of the deuterated solvents. ^{1}H NMR data are reported as follows: chemical shift [multiplicity (s = singlet, d = doublet, t = triplet, q = quartet, and m = multiplet), integration, assignments].

GC-MS analyses were carried out on a computer-interfaced Agilent 6890 GC/MSD interfaced to an Agilent 5973 Mass Selective Detector Quadrupole Mass Spectrometer. The column used was a 30-m HP-5 capillary column with a 0.32-mm inner diameter and a 0.25-μm

film thickness (flow rate = 1.8 mL/min for He carrier gas). Temp program: initial time = 1 min., initial temperature = 60 ^{o}C, rate = 20 ^{o}C/min; final time = 10 min., final temperature = 260 ^{o}C.

A.2 Materials

Tetrabutylammonium fluoride (TBAF, 1 M solution in THF, Aldrich), 1-bromo-4-iodobenzene (98%, Aldrich), 4-bromostyrene (98%, Aldrich), 4-bromobiphenyl (98%, Aldrich), titanium(IV) tetrachloride (99%, Aldrich), trimethylsilylacetylene (GFS Chemicals), potassium tert-butoxide (95%, Aldrich), 18-crown-6 (99%, Aldrich), copper(I) iodide (CuI, Aldrich), (4-iodophenylethynyl)trimethylsilane (97%, Aldrich), trans-dichloro(triphenylphosphine)palladium(II) ($PdCl_2(PPh_3)_2$, Alfa Aesar) were purchased from commercial sources and used as received, (4-iodophenylethynyl)trimethylsilane (97%, Aldrich),. Triethylamine (400 mL, Fischer Scientific) was stirred with CaH_2 (~15 g, +4 mesh, Aldrich) for 24 h, vacuum-transferred into a Strauss flask, and subjected to three freeze-pump-thaw cycles.

Anhydrous benzene (99.8%, Aldrich) was further dried over 3-Å molecular sieves (W. R. Grace Grade 564, 3A, 8-12 mesh beads, preactivated in a 500-^{o}C furnace overnight) overnight before use. Chloroform (99.9%, EMD Chemical, Inc. Omnisolv grade) was washed with water (1:1 v/v) to remove any ethanol, dried over anhydrous Na_2SO_4 (Fischer Scientific) overnight, vacuum-transferred to a vacuum flask, subjected to three freeze-pump-thaw cycles, and further dried over 3-Å activated molecular sieves overnight before use. All other anhydrous solvents were dried over neutral alumina via the Dow-Grubbs solvent system. Deuterated solvents (Cambridge Isotope Laboratories) were purchased from commercial sources and used as

received. All flash chromatography were carried out using silica gel (230-400 mesh, purchased from Sorbent Technologies; Atlanta, GA) under a positive pressure of lab air. Si(111) substrates (0.25˚ miscut in the <110> ± 0.1˚ direction, phosphorous doped, resistivity = 0.04-0.1 Ω·cm) were obtained from Virginia Semiconductor.

A.3 Synthesis of Vinyl- and Acetylene-Terminated Organic Molecules

The procedures for synthesizing *p*-(4-bromophenyl)styrene, *p*-(4-bromophenylethynyl)styrene, (4-bromophenyl)acetylene, (*p*-(4-bromophenyl)phenyl)acetylene, (*p*-(4-bromophenylethynyl)phenyl)acetylene, *p*-iodostyrene, and (4-iodophenyl)acetylene are summarized in Fig A.1.

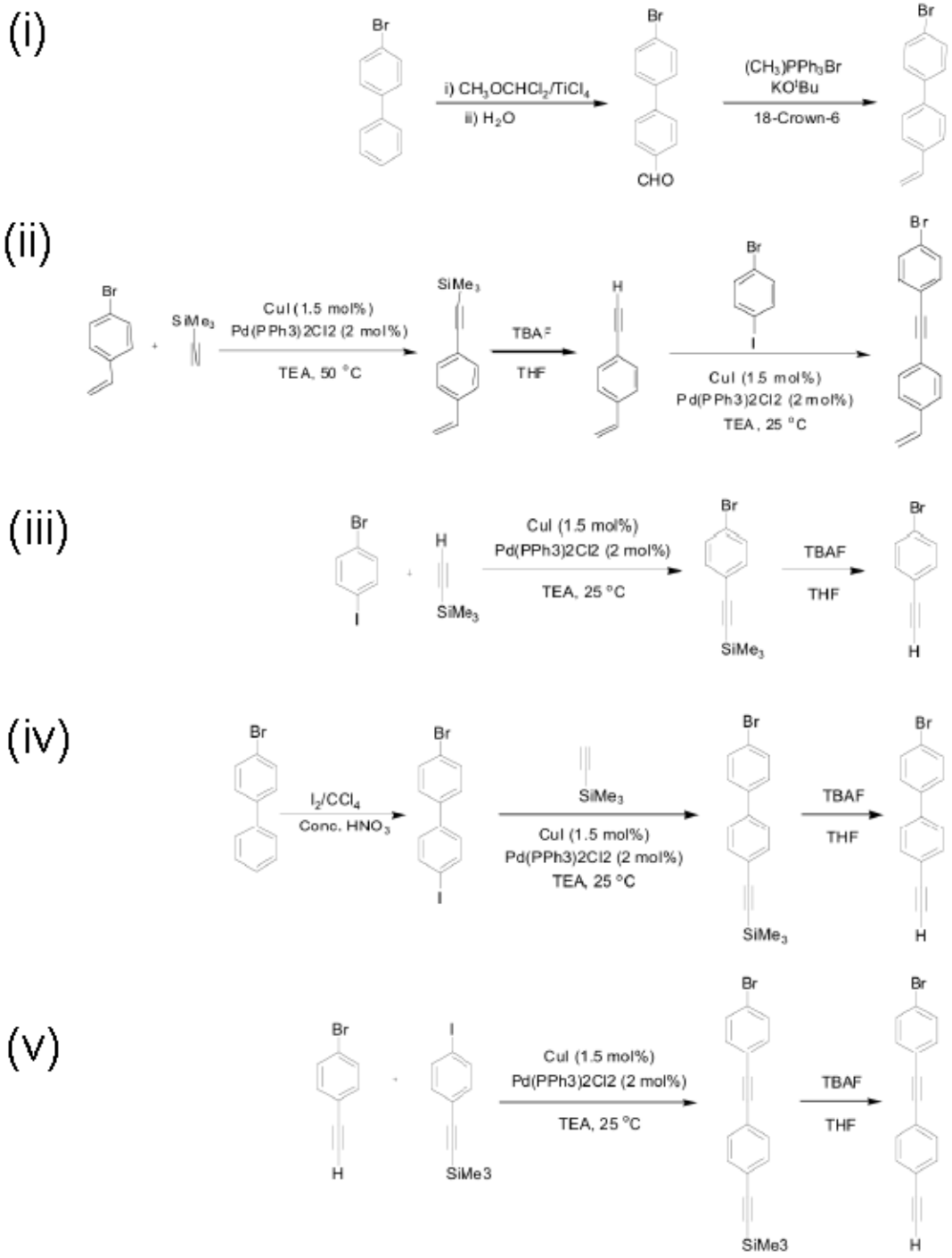

Figure A.1 The synthesis of (i) *p*-(4-bromophenyl)styrene (BPS), (ii) *p*-(4-bromophenylethynyl)styrene (BPES), (iii) (4-bromophenyl)acetylene (BPA), (iV) (*p*-(4-bromophenyl)phenyl)acetylene (BPPA), and (v) (*p*-(4-bromophenylethynyl)phenyl)acetylene (BPEPA).

(i) Synthesis of *p*-(4-bromophenyl)styrene

Step 1: Synthesis of (4-bromo-4'-formyl)biphenyl. Under dry nitrogen environment, to a 250-mL Kjeldahl-style Schlenk flask equipped with magnetic stir bar were added 4-bromobiphenyl (1.0 g, 4.3 mmol) and anhydrous dichloromethane (5 mL). The temperature was cooled down to 0 ^{o}C, followed by the addition of $TiCl_4$ (1.76g, 9.4 mmol). To this reaction flask dichloromethyl methyl ether (0.6g, 5.2 mmol) was added dropwise. The final mixture was slowly warmed up to room temperature and stirred for 24 h. The mixture was then poured into ice water (50 mL) with rapid stirring. The organics was then extracted with diethyl ether (4 × 10 mL) and dried over anhydrous sodium sulfate before being filtered and evaporated to dryness under vacuum. The residue was flash-column chromatographed with silica gel (5.5 cm × 30 cm) using benzene as eluent. The combined organics was evaporated to dryness and the remaining crude product was crystallized from absolute ethanol to give a final product as a shiny brown color powder (0.81 g, 3.1 mmol, 72%). Spectroscopic data for (4-bromo-4'-formyl)biphenyl was in good agreement with literature data. ^{1}H NMR (500 MHz, $CDCl_3$,): δ 7.4 -7.8 (m, 8H, aromatic), 10.5 (s, 1H, -CHO). GC-MS(EI): m/z = 260 and 262 ($C_{13}H_9Br_1O_1$)

Step 2: (4-bromo-4'-formyl)biphenyl -> *p*-(4-bromophenyl)styrene. This step involved the Wittig methylenation of (4-bromo-4'-formyl)biphenyl with methyltriphenyl phosphonium bromide and potassium tert-butoxide in anhydrous tetrahydrofuran. Under dry nitrogen environment, a suspension of potassium tert-butoxide (0.32 g, 2.9 mmol) and methyltriphenylphosphonium bromide (1.0 g, 2.8 mmol) in anhydrous THF (7.5 mL) was cooled to 0 ^{o}C. To increase the solubility of the base, a catalytic amount of 18-crown-6 (0.02 g, 75.8 μmol, 2.7 mol%) was also added. It is important that the phosphonium salt and base are allowed

to react together under these conditions for ~ 1 h to form the ylide prior to the addition of the aldehyde. After the ylide has formed, a solution of 4-bromo-4'-formyl biphenyl (0.67 g, 2.6 mmol) in anhydrous THF (2 mL) was added dropwise to the cooled reaction mixture. The reaction mixture was then stirred for additional 2 h at room temperature before being filtered off. The solid residue was further rinsed with THF (1 mL) and the combined filtrate was evaporated to dryness. The crude product was treated with anhydrous ether (~5 mL), stirred for 5 min, and filtered off. The filtrate was further passed through a pad of neutral alumina with ether eluent. Evaporation of the combined organics to dryness and recrystallizing the resulting solid from isopropanol yield pure p-(4-bromophenyl)styrene as a light yellow powder (0.37 g, 1.6 mmol, 60 %). Spectroscopic data for p-(4-bromophenyl)styrene was in good agreement with literature data.[54] ^{1}H NMR (500 MHz, $CDCl_3$,): δ 5.2-5.8 (2d, 2H, CH_2=CH-), 6.7 (m, 1H, -CH=CH_2), and 7.3-7.6 (m, 8H, aromatic). ^{13}C NMR (125 MHz, CD Cl_3): δ 114.5, 120.8, 121.8, 127.0, 127.2, 128.7, 130.6, 132.1, 136.4, 137.2. GC-MS(EI): m/z = 258 and 260 ($C_{14}H_{11}Br_1$).

(ii) Synthesis of p-(4-bromophenylethynyl)styrene

Step 1: Synthesis of 4-(trimethylsilylethynyl)styrene. Modified from a published procedure. In a N_2-filled glovebox and into a 150-mL Kjeldahl-style Schlenk flask equipped with magnetic stir bar were added p-bromostyrene (1.86 g, 10.2 mmol), $PdCl_2(PPh_3)_2$ (0.15 g, 0.21 mmol), trimethylsilylacetylene (2.28 g, 23.3 mmol), and anhydrous triethylamine (40 mL). After 5 min stirring, CuI (0.03 g, 0.16 mmol) was then added to the reaction flask to give a dark brown solution. The reaction flask was capped, taken out from the glovebox, covered with aluminum foil, and allowed to stir overnight at 50 ^{o}C under N_2 environment. The reaction flask was cooled

to room temperature. The mixture was then filtered over a Buchner funnel and the solid residue remained on the filter was rinsed with HPLC grade triethylamine (2 × 10 mL). The combined organics were concentrated to a minimum on a rotary evaporator to give a viscous dark gray solid, which was subjected to column chromatography (5.5 cm × 30 cm, hexanes). The isolated product is a light yellow solid (1.76 g, 8.7 mmol, 86%). Spectroscopic data for 4-(trimethylsilylethynyl)styrene was in good agreement with literature data.[55,56] ^{1}H NMR (500 MHz, $CDCl_3$,): δ 0.26 (s, 9H, $(CH_3)_3$-Si-), 5.2-5.8 (2d, 2H, CH_2=CH-), 6.7 (m, 1H, -CH=CH_2), and 7.3-7.6 (m, 8H, aromatic). GC-MS(EI): m/z = 200 ($C_{13}H_{16}Si_1$).

Step 2: 4-(trimethylsilylethynyl)styrene -> 4-ethynylstyrene. Modified from a published procedure.[55,56] In a N_2-filled glovebox and into a 150-mL Kjeldahl-style Schlenk flask equipped with magnetic stir bar were added 4-(trimethylsilylethynyl)styrene (0.98 g, 4.9 mmol), anhydrous THF (5 mL), and TBAF (7.5 mL of a 1-M solution in THF, 15 mmol). The reaction flask was capped and allowed to stir at room temperature for 2 h before being removed from the glovebox. The reaction mixture was concentrated on a rotary evaporator to give a purple residue, which was dissolved in deionized water (8 mL) and extracted with methylene chloride (3 × 8 mL). The combined organics was concentrated to a minimum on a rotary evaporator to give a viscous oil, which was subjected to column chromatography (5.5 cm × 30 cm, hexanes). The isolated product is a light yellow liquid (0.57 g, 4.4 mmol, 90%). Spectroscopic data for 4-ethynylstyrene was in good agreement with literature data.[55,56] ^{1}H NMR (500 MHz, $CDCl_3$): δ 3.1 (s, 1H, CH≡C-), 5.2-5.8 (2d, 2H, CH_2=CH-), 6.7 (m, 1H, -CH=CH_2), and 7.3-7.6 (m, 4H, aromatic). GC-MS(EI): m/z = 128 (C_{10}H8).

Step 3: 4-ethynylstyrene -> *p*-(4-bromophenylethynyl)styrene. In a N_2-filled glovebox and into a 150-mL Kjeldahl-style Schlenk flask equipped with magnetic stir bar were added 1-bromo-4-iodobenzene (1.1 g, 3.88 mmol), $PdCl_2(PPh_3)_2$ (0.05 g, 0.07 mmol), 4-ethynyl styrene (0.5 g, 3.88 mmol), and anhydrous triethylamine (15 mL). After 5 min stirring, CuI (0.01 g, 0.05 mmol) was then added to the reaction flask to give a dark brown solution. The reaction flask was capped, covered with aluminum foil, and allowed to stir overnight at room temperature under N_2 environment. The mixture was taken out from the glovebox, and then filtered over a Buchner funnel and the solid residue remained on the filter was rinsed with HPLC grade triethylamine (2 × 10 mL). The combined organics were concentrated to a minimum on a rotary evaporator to give a viscous dark gray solid, which was subjected to column chromatography (5.5 cm × 30 cm, hexanes eluent). The isolated product is a light yellow solid (1.06 g, 0.36 mmol, 96%). Spectroscopic data for p-(4-bromophenylethynyl)styrene ^{1}H NMR (500 MHz, $CDCl_3$,): δ 5.2-5.8 (2d, 2H, CH_2=CH-), 6.7 (m, 1H, -CH=CH_2), and 7.4-7.6 (m, 8H, aromatic). ^{13}C NMR (125 MHz, CD Cl_3): δ 89.2, 90.8, 115.2, 122.4, 122.7, 126.4, 131.8, 132.0, 133.2, 136.4. GC-MS(EI): m/z = 282 and 284 ($C_{16}H_{11}Br_1$).

(iii) Synthesis of (4-bromophenyl)acetylene.

Step 1: Synthesis of ((4-bromophenyl)ethynyl)trimethylsilane. In a N_2-filled glovebox and into a 150-mL Kjeldahl-style Schlenk flask equipped with magnetic stir bar were added 4-bromo-1-iodobenzene (2.83 g, 10 mmol), $PdCl_2(PPh_3)_2$ (0.15 g, 0.21 mmol), trimethylsilylacetylene (2.28 g, 23 mmol), and anhydrous triethylamine (35 mL). After 5 min stirring, CuI (0.03 g, 0.16 mmol) was then added to the reaction flask to give a bright yellow

solution. The reaction flask was capped, covered with aluminum foil and allowed to stir overnight at room temperature during which time its color turned gray. The reaction flask was then removed from the glovebox. The reaction mixture was filtered over a Buchner funnel and the solid residue remained on the filter was rinsed with HPLC grade triethylamine (2 × 20 mL). The combined organics were concentrated to a minimum on a rotary evaporator to give a viscous oil, which was subjected to column chromatography (5.5 cm × 30 cm, hexanes:methylene chloride 9:1 v/v). The isolated product is a light yellow solid (2.47 g, 9.8 mmol, 98%). Spectroscopic data for ((4-bromophenyl)ethynyl)trimethylsilane was in good agreement with literature data.[57] ^{1}H NMR (500 MHz, $CDCl_3$,): δ 0.26 (s, 9H, $(CH_3)_3$-Si-) and 7.3-7.6 (m, 4H, aromatic). ^{13}C NMR (125 MHz, $CDCl_3$): δ 0.2, 95.5, 103.8, 122.0, 122.7, 131.4, 133.4. GC-MS: m/z = 252 and 254 ($C_{11}H_{13}Br_1Si_1$).

Step 2: ((4-bromophenyl)ethynyl)trimethylsilane -> (4-bromophenyl)acetylene. Modified from a published procedure.[58,59] In a N_2-filled glovebox and into a 150-mL Kjeldahl-style Schlenk flask equipped with magnetic stir bar were added ((4-bromophenyl)ethynyl)trimethylsilane (2.53 g, 10 mmol), anhydrous THF (10 mL), and TBAF (15 mL of a 1-M solution in THF, 15 mmol). The reaction flask was capped and allowed to stir at room temperature for 2 h before being removed from the glovebox. The reaction mixture was concentrated on a rotary evaporator to give a purple residue, which was dissolved in deionized water (15 mL) and extracted with methylene chloride (3 × 15 mL). The combined organics was concentrated to a minimum on a rotary evaporator to give a viscous oil, which was subjected to column chromatography (5.5 cm × 30 cm, hexanes:methylene chloride 9:1 v/v). The isolated product is a light yellow solid (1.44 g, 8 mmol, 80%). Spectroscopic data for (4-

bromophenyl)acetylene was in good agreement with literature data.[58,59] ^{1}H NMR (500 MHz, $CDCl_3$): δ 3.13 (s, 1H, CH≡C-) and 7.3-7.6 (m, 4H, aromatic). ^{13}C NMR (125 MHz, $CDCl_3$): δ 78.3, 82.5, 121.0, 123.1, 131.6, 133.5. GC-MS(EI): m/z = 180 and 182 ($C_8H_5Br_1$).

(iv) Synthesis of (p-(4-bromophenyl)phenyl)acetylene.

Step 1: Synthesis of 4-bromo-4'-iodobiphenyl. In a 50-mL round bottom flask equipped with magnetic stir bar and reflux condenser were added 4-bromobiphenyl (4.98 g, 21.4 mmol), iodine (3.25 g, 12.8 mmol), and anhydrous carbon tetrachloride (10 mL). The temperature was heated to 50 ^{o}C and stirred while concentrated nitric acid (1.7 mL, 38.5 mmol) was added over 3 min. After all the nitric acid was added, the mixture was gently refluxed for 16 h. After cooling down to room temperature, the purple-colored reaction mixture was successively washed with concentrated nitric acid (3 × 2 mL) and 10% aqueous sodium hydroxide (25 mL), which decolorized it to light pink color. This organic was dried over magnesium sulfate, filtered, and evaporated under vacuum giving light pink powder. The pink powder was recrystallized from hexane to give a white crystal of 4-bromo-4'-iodobiphenyl (5.2 g, 14.5 mmol, 68%). Spectroscopic data for 4-bromo-4'-iodobiphenyl was in good agreement with literature data.[60] ^{1}H NMR (500 MHz, $CDCl_3$): δ 7.3-7.6 (m, 8H, aromatic). ^{13}C NMR (125 MHz, $CDCl_3$): δ 93.5, 121.8, 127.9, 129.1, 132.1, 138.0, 139.0, 139.5. GC-MS(EI): m/z = 358 and 360 ($C_{12}H_8Br_1I_1$).

Step 2: 4-bromo-4'-iodobiphenyl. -> 4-bromo-4'-[(trimethylsilyl)-ethynyl]biphenyl. In a N_2-filled glovebox and into a 150-mL Kjeldahl-style Schlenk flask equipped with magnetic stir bar were added 4-bromo-4'-iodobiphenyl (3.65 g, 10.2 mmol), $PdCl_2(PPh_3)_2$ (0.15 g, 0.21 mmol), trimethylsilylacetylene (2.28 g, 23.3 mmol), and anhydrous triethylamine (40 mL). After 5 min

stirring, CuI (0.03 g, 0.16 mmol) was then added to the reaction flask to give a bright yellow solution. The reaction flask was capped, covered with aluminum foil and allowed to stir overnight at room temperature during which time its color turned green. The reaction flask was removed from the glovebox. The reaction mixture was filtered over a Buchner funnel and the solid residue remained on the filter was rinsed with HPLC-grade triethylamine (2 × 20 mL). The combined organics were concentrated to a minimum on a rotary evaporator to give a green powder, which was subjected to column chromatography (5.5 cm × 30 cm, hexanes:methylene chloride 9:1 v/v). The isolated product is a light yellow solid (3.19 g, 9.69 mmol, 95%). Spectroscopic data for 4-bromo-4'-[(trimethylsilyl)ethynyl]biphenyl was in good agreement with literature data.[61] ^{1}H NMR (500 MHz, $CDCl_3$,): δ 0.26 (s, 9H, $(CH_3)_3$-Si-) and 7.3-7.6 (m, 8H, aromatic). ^{13}C NMR (125 MHz, CD Cl_3): δ 0.2, 95.5, 106.0, 122.4, 123.1, 127.4, 129.2, 132.3, 132.9, 139.0, 140.9. GC-MS(EI): m/z = 328 and 330 ($C_{17}H_{17}Br_1Si_1$).

Step 3: 4-bromo-4'-[(trimethylsilyl)ethynyl]biphenyl -> (p-(4-bromophenyl)phenyl)acetylene. In a N_2-filled glovebox and into a 150-mL Kjeldahl-style Schlenk flask equipped with magnetic stir bar were 4-bromo-4'-[(trimethylsilyl)ethynyl]biphenyl (3.04 g, 9.24 mmol), anhydrous THF (10 mL), and TBAF (15 mL of a 1-M solution in THF, 15 mmol). The reaction flask was capped and allowed to stir at room temperature for 2 h before being removed from the glovebox. The reaction mixture was concentrated on a rotary evaporator to give a purple residue, which was subjected to filter through a silica column (3.5 cm diameter × 7 cm length) using a mixture of hexanes:methylene chloride (9:1 v/v) as the eluent. The filtrate was collected and evaporated to dryness on a rotary evaporator to yield the product as a light yellow solid (2.26 g, 8.78 mmol, 95%). Spectroscopic data for (p-(4-

bromophenyl)phenyl)acetylene was in good agreement with literature data.[62] ^{1}H NMR (500 MHz, $CDCl_3$): δ 3.13 (s, 1H, CH≡C-) and 7.3-7.6 (m, 8H, aromatic). ^{13}C NMR (125 MHz, $CDCl_3$): δ 78.4, 83.6, 121.6, 122.3, 127.0, 128.9, 132.2, 132.9, 139.3, 140.5. GC-MS(EI): m/z = 256 and 258 ($C_{14}H_9Br_1$).

(v) Synthesis of (p-(4-bromophenylethynyl)phenyl) acetylene.

Step 1: Synthesis of (*p*-(4-bromophenylethynyl)phenylethynyl)-trimethylsilane. In a N_2-filled glovebox and into a 150-mL Kjeldahl-style Schlenk flask equipped with magnetic stir bar were added (4-iodophenylethynyl) trimethylsilane (2.33 g, 7.76 mmol), $PdCl_2(PPh_3)_2$ (0.11 g, 0.16 mmol), p-(4-bromophenyl)acetylene (1.41 g, 7.76 mmol), and anhydrous triethylamine (30 mL). After 5 min stirring, CuI (0.23 g, 0.12 mmol) was then added to the reaction flask to give a bright yellow solution. The reaction flask was capped, covered with aluminum foil and allowed to stir overnight at room. The reaction flask was removed from the glovebox. The reaction mixture was filtered over a Buchner funnel and the solid residue remained on the filter was rinsed with HPLC-grade triethylamine (2 × 20 mL). The combined organics were concentrated to a minimum on a rotary evaporator to give a bright yellow powder, which was subjected to column chromatography (5.5 cm × 30 cm, hexanes:methylene chloride 9:1 v/v). The isolated product is a very light yellow powder (2.40 g, 6.8 mmol, 88%). Spectroscopic data for (p-(4-bromophenylethynyl)phenylethynyl)trimethylsilane was in good agreement with literature data.[63] ^{1}H NMR (500 MHz, $CDCl_{3,}$): δ 0.26 (s, 9H, $(CH_3)_3$-) and 7.3-7.6 (m, 8H, aromatic). ^{13}C NMR (125 MHz, $CDCl_3$): δ 0.2, 90.3, 96.7, 104.7, 122.1, 122.9, 123.1, 123.5, 131.6, 131.9, 132.2, 133.2. GC-MS(EI): m/z = 352 and 354 ($C_{19}H_{17}Br_1Si_1$).

Step 2: (*p*-(4-bromophenylethynyl)phenylethynyl)trimethylsilane -> (*p*-(4-bromophenylethynyl)phenyl)acetylene. In a N_2-filled glovebox and into a 150-mL Kjeldahl-style Schlenk flask equipped with magnetic stir bar were (p-(4-bromophenylethynyl)phenylethynyl)trimethylsilane (1.6 g, 2.27 mmol), anhydrous THF (5 mL), and TBAF (7.5 mL of a 1-M solution in THF, 15 mmol). The reaction flask was capped and allowed to stir at room temperature overnight before being removed from the glovebox. The reaction mixture was concentrated on a rotary evaporator to give a purple residue, which was subjected to filter through a silica column (3.5 cm diameter × 7 cm length) using a mixture of hexanes:methylene chloride (9:1 v/v) as the eluent. The filtrate was collected and evaporated to dryness on a rotary evaporator to yield the product as a very light yellow solid (1.22 g, 2.17 mmol, 96%). ^{1}H NMR (500 MHz, $CDCl_3$): δ 3.13 (s, 1H, CH≡C-) and 7.3-7.6 (m, 8H, aromatic). ^{13}C NMR (125 MHz, $CDCl_3$): δ 79.3, 83.4, 90.1, 90.5, 122.1, 122.3, 123.0, 123.6, 131.7, 131.9, 132.3, 133.3. GC-MS(EI): m/z = 280 and 282 ($C_{16}H_9Br_1$).

Appendix B : Preparation of H-Si(111) Surfaces

The hydrogen passivation of the 111 silicon surfaces was achieved by following the procedure described by Higashi et al.[64] Samples were cut (with typical lateral dimensions of 5-by-10-mm^2) from single-side-polished Si(111) wafers (Virginia Semiconductors, 0.50-mm-thick, 0.25º miscut towards the <110>±0.1º direction, phosphorous doped, resistivity = 0.05-0.07 Ω−cm). Prior to passivation, each substrate was rinsed with acetone and methanol. Initial passivation was accomplished by submerging the samples in a 0.5% solution of HF for 30 sec. They were then submerged in argon sparged ultrapure 18 MΩ−cm water for 5 sec. To remove organic contaminants the samples were next immersed in a solution of 4:1 (v/v) H_2SO_4/30% H_2O_2 (aq) for 10 min at 90ºC. Following this treatment, the samples were again submerged in argon sparged 18 MΩ−cm water for 5 sec. To create an atomically flat terraced surface, the samples were subsequently immersed in argon-sparged, clean-room-grade, 40% NH_4F (aq) for 30 min. During this time, the tube used for argon sparging was held over the NH_4F solution to minimize the amount of oxygen that could dissolve into the solution and cause surface pitting. A final 1 min immersion in argon sparged 18 MΩ−cm water was performed, following which the samples were blown dry with a N_2 gun and stored in an inert atmosphere glove box (Nexus, Vacuum Atmospheres) maintained at a slightly positive pressure of N_2 (99.999 % purity, < 1.5 ppm O_2, < 0.5 ppm H_2O). The purpose of this final rinse was to minimize the amount of residual fluorine atoms on the silicon surface and in turn decrease the rate of adsorption of organic contaminants on the surface. The passivated samples were stored in the glove box until subsequent SAM growth and surface analysis.

Appendix C : Density Functional Theory Calculation Results

C.1 Cluster DFT results for SAMs/Si(111) (Molecule-$Si_{26}H_{30}$)

(a) BrSty-Relaxed

//brsty_631Gs_fgeo_w_rotated.xyz//
74

C	-1.066071	0.501447	2.714336
C	-0.945700	0.286670	4.209001
H	-1.147047	1.574331	2.505272
C	-1.365511	-0.918398	4.788137
H	-1.791800	-1.695089	4.156838
C	-0.408732	1.271376	5.046858
H	-0.082788	2.219099	4.624111
C	-1.264297	-1.140537	6.160881
H	-1.601536	-2.075517	6.595195
C	-0.732222	-0.136072	6.967847
Br	-0.624443	-0.408185	8.863402
C	-0.297896	1.070475	6.423670
H	0.112046	1.845180	7.062509
C	0.118969	-0.089143	1.919043
Si	3.879288	2.236854	-0.804266
Si	3.905624	2.213125	-3.165298
Si	1.938055	3.346412	-0.041477
Si	-0.005822	2.236559	-0.819654
Si	-1.970656	3.402696	-0.191829
Si	3.847426	0.012731	-0.010747
Si	0.000000	0.000000	0.000000
Si	-0.023855	-4.481909	-0.803878
Si	-1.962762	-3.351278	-0.065865
Si	-1.945621	-1.106351	-0.819654
Si	-3.935135	0.015002	-0.185255
Si	-3.902167	2.256033	-0.931151
Si	-3.855966	2.218999	-3.288836
Si	1.988140	1.104275	-4.001084
Si	0.035076	2.182250	-3.195674
Si	0.018080	-4.491001	-3.164765
Si	0.029057	-2.275968	-3.997958
Si	-1.877382	-1.112117	-3.195871
Si	-1.907241	1.106774	-4.038645
Si	1.933977	-1.123957	-0.819654
Si	1.936943	-1.122924	-3.187140
H	-4.122001	-0.039294	1.294104
H	-2.037987	-3.384040	1.426780
H	3.813258	0.012700	1.483337
Si	0.066638	-2.267226	-6.364008
Si	1.987619	1.074754	-6.366950
Si	-1.861406	1.051785	-6.403122
Si	0.076403	-0.050644	-7.178849
H	-1.172494	-5.215168	-3.701399
H	1.235540	-5.211413	-3.642542
H	-0.028714	-5.886915	-0.288951
H	-1.122919	-3.001000	-6.889480
H	1.284564	-2.996560	-6.826065
H	-2.000629	0.044634	2.366816
H	1.052193	0.404532	2.222492
H	0.245281	-1.147392	2.185251

(b) BPS-Relaxed

br2peth_631Gs_fgeo_rotated.xyz
84

Br	0.790717	0.518724	13.131160
C	0.011190	0.523175	8.469951
C	0.570731	-0.595616	9.110047
H	0.846037	-1.466522	8.522095
C	-0.300699	1.643252	9.258429
H	-0.759301	2.513190	8.797253
C	0.808248	-0.604890	10.483630
H	1.248095	-1.474640	10.960575
C	0.483381	0.523703	11.234118
C	-0.068429	1.652351	10.632330
H	-0.325647	2.522080	11.226633
C	-1.031147	0.531788	2.723739
C	-0.773675	0.530972	4.216009
H	-1.231097	1.557998	2.395124
C	-0.963697	-0.625648	4.984348
H	-1.332379	-1.532278	4.508906
C	-0.313347	1.681257	4.868652
H	-0.151290	2.592594	4.297646
C	-0.705931	-0.631593	6.352404
H	-0.894798	-1.534457	6.926270
C	-0.247993	0.523470	7.008909
C	-0.055485	1.680315	6.237301
H	0.317523	2.585061	6.708940
C	0.150460	-0.051603	1.916665
Si	3.879153	2.238963	-0.785949
Si	3.893827	2.237670	-3.147419
Si	1.934658	3.355966	-0.040207
Si	-0.007442	2.242847	-0.811855
Si	-1.970359	3.399074	-0.149749
Si	3.857812	0.006030	-0.013441
Si	0.000000	0.000000	0.000000
Si	-0.018227	-4.483706	-0.815562
Si	-1.953233	-3.354417	-0.063028
Si	-1.949740	-1.106539	-0.811855
Si	-3.925878	0.028140	-0.151606
Si	-3.899380	2.266892	-0.913485
Si	-3.849939	2.240537	-3.271232
Si	1.986973	1.113296	-3.985799
Si	0.030800	2.193014	-3.186894
Si	0.003420	-4.482278	-3.176212
Si	0.026602	-2.261974	-3.996575
Si	-1.880963	-1.103590	-3.189055
Si	-1.910578	1.117601	-4.027306
Si	1.934855	-1.123173	-0.811855
Si	1.937402	-1.118343	-3.179248
H	-4.071849	-0.011104	1.334380
H	-2.001915	-3.387332	1.429645
H	3.861123	-0.012131	1.479503
Si	0.030529	-2.236752	-6.363067
Si	1.975213	1.109695	-6.352242

(c) BPES-Relaxed

br2pc3eth_631Gs_fgeo_rotated.xyz
86

Br	1.717201	0.240194	15.581829
C	0.806311	0.356893	10.958021
C	0.440399	-0.759429	11.736212
H	-0.063322	-1.596042	11.262272
C	1.462229	1.432611	11.589649
H	1.750058	2.297924	11.001044
C	0.713715	-0.799596	13.099860
H	0.426739	-1.662262	13.690576
C	1.358148	0.283024	13.697786
C	1.738661	1.399922	12.953349
H	2.241298	2.233796	13.431904
C	0.512068	0.397667	9.566134
C	0.252485	0.431814	8.378125
C	-0.970212	0.608773	2.744161
C	-0.681317	0.572160	4.229871
H	-1.086072	1.650552	2.423930
C	-1.066918	-0.522248	5.016796
H	-1.618597	-1.341444	4.560454
C	0.020497	1.617848	4.846111
H	0.323626	2.476995	4.251722
C	-0.762221	-0.575845	6.372575
H	-1.070000	-1.428242	6.970431
C	-0.056030	0.476502	6.988866
C	0.331154	1.578254	6.200569
H	0.872070	2.398147	6.663151
C	0.149236	-0.065991	1.918713
Si	3.878638	2.241547	-0.795748
Si	3.883074	2.245151	-3.156706
Si	1.933775	3.344325	-0.026857
Si	-0.005598	2.235741	-0.813422
Si	-1.973436	3.399040	-0.182606
Si	3.867185	0.005309	-0.035736
Si	0.000000	0.000000	0.000000
Si	-0.014637	-4.479640	-0.798966
Si	-1.936946	-3.338831	-0.028866
Si	-1.947060	-1.105825	-0.813422
Si	-3.926397	0.023694	-0.157400
Si	-3.904609	2.257694	-0.925305
Si	-3.864992	2.217999	-3.284146
Si	1.984301	1.105324	-3.991557
Si	0.026831	2.181888	-3.189878
Si	0.007156	-4.485754	-3.160479
Si	0.021791	-2.271415	-3.994743
Si	-1.886057	-1.108801	-3.190533
Si	-1.914747	1.107350	-4.035284
Si	1.935864	-1.125223	-0.813422
Si	1.932237	-1.123446	-3.181043
H	-4.074465	-0.014925	1.327976
H	-1.952240	-3.336518	1.465237
H	3.893799	-0.021328	1.457270

(d) BPPA-Relaxed

br2pac_631Gs_fgeo_rotated.xyz
82

Br	0.959127	0.819789	13.209512
C	0.463029	0.862706	8.511482
C	0.667793	-0.339271	9.209718
H	0.761170	-1.271158	8.659816
C	0.379009	2.050463	9.258000
H	0.186320	2.990290	8.749559
C	0.801960	-0.359481	10.596538
H	0.977486	-1.294075	11.118032
C	0.729874	0.840013	11.302895
C	0.512839	2.048956	10.645099
H	0.442910	2.975184	11.204623
C	0.211352	0.936919	2.722539
C	0.225323	0.892339	4.190864
C	-0.338277	-0.156119	4.940882
H	-0.859101	-0.964310	4.435522
C	0.836488	1.943261	4.896049
H	1.284389	2.764605	4.342068
C	-0.270729	-0.159351	6.328312
H	-0.745886	-0.965308	6.880353
C	0.364265	0.880977	7.032270
C	0.913169	1.935237	6.284072
H	1.433929	2.741416	6.792117
C	-0.027100	-0.087958	1.876918
Si	0.005940	-4.498318	-0.786200
Si	0.014399	-4.506149	-3.147849
Si	1.927407	-3.360360	-0.013325
Si	1.941817	-1.127255	-0.800057
Si	3.858487	0.024454	-0.021617
Si	-1.910783	-3.360384	-0.005490
Si	0.000000	0.000000	0.000000
Si	-3.878888	2.233593	-0.817167
Si	-1.948209	3.383343	-0.088547
Si	0.002814	2.244173	-0.800057
Si	1.960018	3.407229	-0.141193
Si	3.890846	2.241984	-0.841320
Si	3.896503	2.182712	-3.200362
Si	0.006406	-2.289611	-3.977821
Si	1.914912	-1.130671	-3.172622
Si	-3.874432	2.201962	-3.178743
Si	-1.948882	1.089325	-3.990564
Si	0.000108	2.171761	-3.175905
Si	1.950614	1.094157	-3.993903
Si	-1.936190	-1.129468	-0.800057
Si	-1.905054	-1.136876	-3.171758
H	1.979253	3.597036	1.340248
H	-1.948725	3.529518	1.396445
H	-1.912489	-3.350892	1.489241
Si	-1.917331	1.067479	-6.356899
Si	0.018846	-2.267699	-6.344436
Si	1.927007	1.072342	-6.359221

(e) BPEPA-Relaxed

br2pc3ac_631Gs_fgeo_rotated.xyz
84

Br	-0.978783	0.661650	15.788703
C	-0.437499	0.714272	11.108013
C	-0.340512	-0.492452	11.829552
H	-0.153521	-1.417519	11.293465
C	-0.675912	1.907964	11.818324
H	-0.750781	2.844694	11.275241
C	-0.489876	-0.511505	13.213068
H	-0.420297	-1.445708	13.759999
C	-0.736030	0.685323	13.886937
C	-0.826248	1.896582	13.201167
H	-1.017153	2.818566	13.738725
C	-0.318739	0.729827	9.690243
C	-0.245093	0.754936	8.475855
C	-0.089516	0.902256	2.753458
C	-0.097529	0.822716	4.219628
C	0.085762	-0.377093	4.935018
H	0.263793	-1.305166	4.400574
C	-0.311186	2.000381	4.960054
H	-0.453946	2.939717	4.432513
C	0.044827	-0.401832	6.319893
H	0.186640	-1.337135	6.851931
C	-0.182047	0.781848	7.055925
C	-0.355171	1.987022	6.347593
H	-0.528348	2.905633	6.899388
H	-0.202030	1.916571	2.368759
C	0.022341	-0.116835	1.874614
Si	3.881339	2.233025	-0.817698
Si	3.873780	2.199757	-3.179131
Si	1.951926	3.383878	-0.088680
Si	-0.001515	2.245282	-0.795055
Si	-1.957030	3.390633	-0.105870
Si	3.861785	0.009342	-0.019777
Si	0.000000	0.000000	0.000000
Si	0.001271	-4.502143	-0.772850
Si	-1.924468	-3.365745	-0.008895
Si	-1.940964	-1.132195	-0.795055
Si	-3.859388	0.014069	-0.014958
Si	-3.886965	2.234776	-0.824187
Si	-3.890273	2.183537	-3.184077
Si	1.947894	1.084149	-3.985963
Si	-0.000117	2.167942	-3.170677
Si	-0.004634	-4.512665	-3.134337
Si	-0.003717	-2.297247	-3.968777
Si	-1.913063	-1.137717	-3.166270
Si	-1.950928	1.088479	-3.985219
Si	1.937934	-1.131397	-0.795055
Si	1.907997	-1.142003	-3.165993
H	-3.866715	0.011549	1.477202
H	-1.950173	-3.363276	1.484362
H	3.882306	0.000605	1.472044

(f) BPA (Alkenyl)-start

bpa_631Gs_starting_geo_original_orientation.
72

C	3.548917	-0.305909	-0.011492
C	5.014226	-0.166952	-0.016898
C	5.676106	1.074203	-0.037644
H	5.105319	1.995153	-0.049457
C	5.798779	-1.333720	0.006174
H	5.310517	-2.302225	0.017806
C	7.065958	1.141508	-0.034734
H	7.568169	2.099738	-0.050131
C	7.818379	-0.029211	-0.008417
Br	9.743945	0.063492	0.005299
C	7.189685	-1.267463	0.011641
H	7.783354	-2.171315	0.032024
H	3.208612	-1.338409	0.038205
C	2.627060	0.674122	-0.056587
Si	0.304464	-1.416523	4.129168
Si	-2.050224	-1.744735	4.168509
Si	1.176833	-2.727691	2.349653
Si	0.303290	-1.956636	0.279008
Si	1.157184	-3.285194	-1.502105
Si	0.734819	0.895760	3.794947
Si	0.757077	0.355615	-0.031741
Si	-0.715455	4.648101	-0.654992
Si	0.246342	3.370998	-2.415137
Si	-0.203229	1.061537	-2.089229
Si	0.779091	-0.202686	-3.845496
Si	0.293611	-2.511953	-3.574588
Si	-2.060769	-2.824384	-3.539611
Si	-3.011381	-1.050778	2.108372
Si	-2.049477	-2.277060	0.319110
Si	-3.062331	4.278559	-0.611708
Si	-3.516878	1.971499	-0.281923
Si	-2.547573	0.708142	-2.042547
Si	-3.013375	-1.596994	-1.740337
Si	-0.217433	1.609969	1.738704
Si	-2.561385	1.252009	1.767237
H	2.264147	0.007465	-3.830898
H	1.732563	3.589533	-2.432449
H	2.211002	1.162663	3.791073
Si	-5.863695	1.601647	-0.235372
Si	-5.356578	-1.426137	2.141005
Si	-5.362510	-1.946529	-1.685780
Si	-6.328548	-0.704751	0.096173
H	-3.669986	4.725323	-1.909699
H	-3.686349	5.064479	0.505197
H	-0.432007	6.112316	-0.864807
H	-6.458441	2.056311	-1.536716
H	-6.471495	2.406751	0.876764

(g) BPA (Alkenyl2)-Start

bpac_631Gs_dirH_starting_geo.xyz

72

C	1.07330	-0.02247	2.63674
C	1.06966	-0.02464	4.10670
C	-0.10220	-0.03203	4.88532
H	-1.07427	-0.07208	4.40334
C	2.30422	0.01187	4.77754
H	3.22411	0.01577	4.19845
C	-0.04663	0.01314	6.27449
H	-0.95888	0.01132	6.86178
C	1.19855	0.06414	6.90519
Br	1.28235	0.15639	8.82161
C	2.37936	0.05917	6.16738
H	3.34130	0.09605	6.66604
H	2.07530	-0.06642	2.20885
C	0.01559	0.05558	1.80221
H	-0.98532	0.10688	2.23681
Si	3.88638	2.23999	-0.82449
Si	3.88658	2.18913	-3.18569
Si	1.95349	3.39326	-0.10844
Si	0.00028	2.24094	-0.79707
Si	-1.95344	3.38869	-0.10850
Si	3.86159	0.01926	-0.01796
Si	0.00000	0.00000	0.00000
Si	0.00406	-4.49303	-0.79485
Si	-1.91254	-3.35935	-0.00699
Si	-1.94093	-1.12698	-0.79707
Si	-3.85636	0.01345	0.00060
Si	-3.88862	2.23138	-0.81136
Si	-3.89808	2.18441	-3.17222
Si	1.94804	1.09688	-3.99351
Si	-0.00266	2.17248	-3.17236
Si	-0.02302	-4.49647	-3.15662
Si	-0.00869	-2.27823	-3.97887
Si	-1.92001	-1.12771	-3.16974
Si	-1.95795	1.09836	-3.98422
Si	1.94149	-1.12419	-0.79707
Si	1.90297	-1.12746	-3.17131
H	-3.84787	0.02034	1.49283
H	-1.91186	-3.35058	1.48708
H	3.86881	0.01596	1.47424
Si	-0.03103	-2.25792	-6.34574
Si	1.92187	1.06047	-6.36011
Si	-1.93600	1.07608	-6.35092
Si	-0.01329	-0.03848	-7.15077
H	-1.24770	-5.19405	-3.64894
H	1.15710	-5.24007	-3.68795
H	0.01217	-5.89827	-0.27672
H	-1.25666	-2.96087	-6.82825

(h) BPA (Alkenyl3)-start

bpac_631Gs_dirT_starting_geo.xyz

72

C	1.01377	0.48182	2.63457
C	1.06934	0.39968	4.10118
C	0.12738	-0.29589	4.88123
H	-0.67931	-0.84096	4.40066
C	2.10409	1.07688	4.76916
H	2.84581	1.61959	4.18875
C	0.20303	-0.30162	6.27017
H	-0.53316	-0.83881	6.85888
C	1.23706	0.39564	6.89902
Br	1.33084	0.41657	8.81708
C	2.19489	1.08370	6.15885
H	2.99554	1.61966	6.65589
H	1.85621	1.02208	2.20162
C	0.05681	0.00638	1.81027
H	-0.78851	-0.52753	2.25039
Si	3.88638	2.23999	-0.82449
Si	3.88658	2.18913	-3.18569
Si	1.95349	3.39326	-0.10844
Si	0.00028	2.24094	-0.79707
Si	-1.95344	3.38869	-0.10850
Si	3.86159	0.01926	-0.01796
Si	0.00000	0.00000	0.00000
Si	0.00406	-4.49303	-0.79485
Si	-1.91254	-3.35935	-0.00699
Si	-1.94093	-1.12698	-0.79707
Si	-3.85636	0.01345	0.00060
Si	-3.88862	2.23138	-0.81136
Si	-3.89808	2.18441	-3.17222
Si	1.94804	1.09688	-3.99351
Si	-0.00266	2.17248	-3.17236
Si	-0.02302	-4.49647	-3.15662
Si	-0.00869	-2.27823	-3.97887
Si	-1.92001	-1.12771	-3.16974
Si	-1.95795	1.09836	-3.98422
Si	1.94149	-1.12419	-0.79707
Si	1.90297	-1.12746	-3.17131
H	-3.84787	0.02034	1.49283
H	-1.91186	-3.35058	1.48708
H	3.86881	0.01596	1.47424
Si	-0.03103	-2.25792	-6.34574
Si	1.92187	1.06047	-6.36011
Si	-1.93600	1.07608	-6.35092
Si	-0.01329	-0.03848	-7.15077
H	-1.24770	-5.19405	-3.64894
H	1.15710	-5.24007	-3.68795
H	0.01217	-5.89827	-0.27672
H	-1.25666	-2.96087	-6.82825

(i) BPA (Alkenly1)-Relaxed

bpac_631Gs_fgeo_rotated.xyz

72

C	-0.063995	0.974903	2.715827
C	-0.194925	0.970174	4.179938
C	-0.240659	-0.202042	4.956719
H	-0.142672	-1.173037	4.480921
C	-0.310393	2.203549	4.844004
H	-0.275500	3.123721	4.266381
C	-0.412303	-0.148197	6.336047
H	-0.450121	-1.060774	6.921640
C	-0.538721	1.095601	6.958810
Br	-0.805420	1.176562	8.858938
C	-0.484499	2.276917	6.223792
H	-0.580696	3.237816	6.716494
H	0.003638	1.977757	2.293086
C	-0.050393	-0.083223	1.878279
Si	3.886375	2.239994	-0.824492
Si	3.886583	2.189130	-3.185688
Si	1.953492	3.393256	-0.108439
Si	0.000279	2.240938	-0.797065
Si	-1.953439	3.388690	-0.108496
Si	3.861591	0.019258	-0.017956
Si	0.000000	0.000000	0.000000
Si	0.004064	-4.493029	-0.794851
Si	-1.912543	-3.359351	-0.006991
Si	-1.940933	-1.126978	-0.797065
Si	-3.856363	0.013445	0.000598
Si	-3.888619	2.231383	-0.811357
Si	-3.898077	2.184407	-3.172217
Si	1.948041	1.096879	-3.993514
Si	-0.002656	2.172480	-3.172361
Si	-0.023017	-4.496468	-3.156619
Si	-0.008686	-2.278233	-3.978867
Si	-1.920013	-1.127712	-3.169740
Si	-1.957945	1.098355	-3.984220
Si	1.941491	-1.124193	-0.797065
Si	1.902974	-1.127464	-3.171308
H	-3.847866	0.020339	1.492834
H	-1.911856	-3.350577	1.487084
H	3.868805	0.015956	1.474239
Si	-0.031031	-2.257924	-6.345742
Si	1.921873	1.060467	-6.360111
Si	-1.936000	1.076076	-6.350920
Si	-0.013292	-0.038485	-7.150770
H	-1.247704	-5.194052	-3.648937
H	1.157097	-5.240071	-3.687948
H	0.012170	-5.898274	-0.276718
H	-1.256655	-2.960867	-6.828247
H	1.148453	-3.009414	-6.867553

(j) BPA (Alkenly2)-Relaxed

bpac_dirH_631Gs_fgeo.xyz
72

C	3.568963	-0.401892	0.223139
C	5.028277	-0.229709	0.192689
C	5.669795	1.020046	0.271139
H	5.082458	1.924650	0.395780
C	5.832392	-1.373037	0.045436
H	5.361134	-2.350600	-0.015336
C	7.054102	1.127930	0.187106
H	7.534507	2.099116	0.243370
C	7.818898	-0.029504	0.024761
Br	9.728840	0.114145	-0.128906
C	7.219471	-1.284383	-0.041352
H	7.821690	-2.177486	-0.163928
H	3.258126	-1.446274	0.182019
C	2.616488	0.553369	0.263958
H	2.927947	1.599792	0.298815
Si	0.463548	-1.599740	-3.975193
Si	-1.880071	-1.826619	-4.151525
Si	0.999851	0.677019	-3.651072
Si	-0.043152	1.496679	-1.690655
Si	0.479205	3.784438	-1.370050
Si	1.180943	-2.881788	-2.125565
Si	0.762039	0.254376	0.175767
Si	-0.032077	-2.491372	3.734250
Si	0.505456	-0.205988	4.001182
Si	-0.282717	1.055930	2.159727
Si	0.224632	3.352158	2.433494
Si	-0.559371	4.600851	0.587769
Si	-2.897918	4.346684	0.372340
Si	-2.933900	-1.053869	-2.178335
Si	-2.395530	1.231786	-1.849309
Si	-2.378693	-2.698545	3.565068
Si	-3.184899	-1.493032	1.694439
Si	-2.634392	0.801073	1.941336
Si	-3.453026	2.062555	0.104803
Si	0.241389	-2.047665	-0.117413
Si	-2.120985	-2.243078	-0.291111
H	1.703807	3.523566	2.555539
H	1.983256	-0.036285	4.121632
H	2.671441	-2.892691	-2.038069
Si	-5.532599	-1.719283	1.492237
Si	-5.282876	-1.305467	-2.328814
Si	-5.794107	1.782699	-0.107259
Si	-6.328113	-0.502578	-0.368859
H	-3.027633	-2.168241	4.801092
H	-2.771074	-4.133872	3.436407
H	0.459550	-3.269423	4.914529
H	-6.185005	-1.220008	2.739912

(k) BPA (Alkenly3)-Relaxed

bpac_dirT_631Gs_fgeo.xyz
72

C	3.569887	-0.401012	-0.212685
C	5.029372	-0.229158	-0.184795
C	5.670767	1.020690	-0.263146
H	5.083255	1.925678	-0.383519
C	5.833615	-1.372710	-0.039928
H	5.362114	-2.350156	0.020750
C	7.055318	1.128213	-0.182714
H	7.535858	2.099365	-0.238444
C	7.820201	-0.029514	-0.023724
Br	9.729915	0.114181	0.125594
C	7.221006	-1.284462	0.043113
H	7.823605	-2.177612	0.163407
H	3.258839	-1.444427	-0.154159
C	2.617506	0.553374	-0.271607
H	2.927945	1.599166	-0.326115
Si	0.461723	-1.541428	3.997762
Si	-1.881594	-1.771187	4.174489
Si	1.185485	-2.847514	2.167707
Si	0.244232	-2.044187	0.147159
Si	0.938270	-3.355920	-1.700948
Si	0.995428	0.731164	3.641441
Si	0.763122	0.253863	-0.179527
Si	-0.563896	4.594439	-0.651611
Si	0.220003	3.320626	-2.480526
Si	-0.282418	1.027414	-2.173978
Si	0.501185	-0.258744	-4.000788
Si	-0.026419	-2.541933	-3.697407
Si	-2.372601	-2.754046	-3.523436
Si	-2.934821	-1.025237	2.190782
Si	-2.118170	-2.239352	0.321422
Si	-2.902250	4.341222	-0.429064
Si	-3.456092	2.059961	-0.135479
Si	-2.634312	0.773141	-1.953061
Si	-3.182236	-1.517807	-1.674567
Si	-0.045163	1.522001	1.667757
Si	-2.397745	1.255891	1.829385
H	1.977123	-0.083559	-4.135953
H	1.698604	3.493605	-2.606575
H	2.474800	0.890152	3.527990
Si	-5.796780	1.781262	0.084291
Si	-5.283773	-1.278045	2.342506
Si	-5.529491	-1.746844	-1.468933
Si	-6.328857	-0.501442	0.371542
H	-3.604863	4.888270	-1.627008
H	-3.378255	5.112476	0.757607
H	-0.221464	6.035534	-0.868316
H	-6.490448	2.337672	-1.114632

(l) BPA (Double-Bridge)-Relaxed

bpac_1molr_alt1_631Gs_fgeo_rotated.xyz
72

C	-0.371446	-0.374964	1.884746
C	0.557184	0.309191	2.864418
C	1.830806	-0.189015	3.176579
H	2.174090	-1.118604	2.731680
C	0.163417	1.512490	3.470134
H	-0.818475	1.924375	3.250726
C	2.684212	0.485898	4.050399
H	3.667354	0.086552	4.272519
C	2.260910	1.681198	4.627173
Br	3.432099	2.629253	5.820274
C	1.000669	2.203189	4.345164
H	0.672673	3.131053	4.800578
H	-1.362229	0.076777	2.025144
C	-0.539522	-1.913888	2.096734
H	-1.119675	-2.083648	3.013906
Si	3.898563	2.344290	-1.043051
Si	3.763171	2.239199	-3.396593
Si	1.986371	3.428493	-0.182093
Si	0.022470	2.246936	-0.779244
Si	-1.921476	3.399968	-0.071029
Si	4.003274	0.117487	-0.270185
Si	0.000000	0.000000	0.000000
Si	0.126115	-4.333101	-0.433652
Si	-1.410833	-2.880919	0.646683
Si	-1.960059	-1.093118	-0.779244
Si	-3.854169	0.076104	0.029356
Si	-3.879598	2.288211	-0.788222
Si	-3.932903	2.171614	-3.145219
Si	1.840656	1.030618	-4.058417
Si	-0.075195	2.104038	-3.166477
Si	-0.169805	-4.507588	-2.778259
Si	-0.059445	-2.386458	-3.836667
Si	-1.989609	-1.221841	-3.120225
Si	-2.036056	1.004437	-3.942249
Si	2.004998	-1.055668	-0.779244
Si	1.854316	-1.159768	-3.146330
Si	2.218447	-3.309639	-0.081187
Si	-0.094387	-2.495574	-6.199599
Si	1.728540	0.907319	-6.419504
Si	-2.061720	0.874017	-6.305828
Si	-0.176716	-0.308308	-7.098995
H	-3.831466	0.082962	1.523714
H	4.298450	0.064197	1.190195
H	-1.491722	-5.122416	-3.101176
H	0.881952	-5.418006	-3.321178
H	0.093558	-5.702242	0.170147
H	-1.282392	-3.284499	-6.644808

(m) BPA (Single-Bridge)-Relaxed

bpac_1molr_alt2_631Gs_fgeo_rotated.xyz
72

C	0.221499	1.002765	2.881990
C	0.961916	-0.193808	3.452243
C	0.268613	-1.295532	3.975421
H	-0.818714	-1.292853	3.995977
C	2.360305	-0.230831	3.470425
H	2.924628	0.617744	3.093458
C	0.942919	-2.409596	4.473826
H	0.390744	-3.255582	4.868449
C	2.337449	-2.422065	4.454185
Br	3.277342	-3.977094	5.085274
C	3.056738	-1.337250	3.962928
H	4.141104	-1.350635	3.953248
H	-0.376342	1.468600	3.679063
C	-0.722724	0.650534	1.705692
H	-1.466778	-0.065454	2.074811
H	0.951058	1.759568	2.575253
Si	0.357920	-4.579839	-1.067254
Si	0.156758	-4.393612	-3.411769
Si	2.246738	-3.393601	-0.297237
Si	1.989938	-1.087225	-0.776124
Si	4.027529	0.046141	-0.327918
Si	-1.534044	-3.586803	-0.076197
Si	0.000000	0.000000	0.000000
Si	-3.699306	1.762838	-0.060270
Si	-1.572178	2.228853	0.900790
Si	0.081198	2.252930	-0.776124
Si	2.071953	3.337859	-0.091780
Si	3.962254	2.298493	-1.037876
Si	3.715247	2.426244	-3.376694
Si	-0.038492	-2.126326	-4.063767
Si	1.798312	-0.913791	-3.177350
Si	-3.869863	2.225702	-2.386433
Si	-2.171153	1.167685	-3.668050
Si	-0.198369	2.354013	-3.100664
Si	1.726410	1.315291	-4.013868
Si	-1.827541	-1.343830	-0.776124
Si	-1.965971	-1.137670	-3.114016
Si	-2.410892	1.274281	-6.019163
Si	-0.202730	-1.943204	-6.417170
Si	1.478196	1.410300	-6.365738
Si	-0.500551	0.313693	-7.043790
Si	-3.871089	-0.569737	0.130723
H	2.183250	3.319393	1.397800
H	-1.393516	-3.609533	1.411430
H	-3.791939	3.696461	-2.639011
H	-5.223407	1.776690	-2.831073
H	-4.779975	2.507867	0.657760

C.2 Cluster DFT results for SAMs/Si(111) (Molecule-$Si_{38}H_{45}$)

(a) BPA (Alkenly)-Relaxed

BPA_c2_std_631Gs_fgeo_rotated.xyz
92

Br	0.369328	1.247838	8.882400
C	0.008614	0.971022	2.711348
C	0.085434	0.976609	4.178425
C	0.296742	-0.177813	4.953995
C	-0.042647	2.205733	4.848123
C	0.377886	-0.110074	6.341340
C	0.043751	-0.088930	1.878097
C	0.245512	1.128624	6.971951
C	0.033026	2.291952	6.235482
H	0.410018	-1.143989	4.471410
H	-0.203663	3.110894	4.267946
H	0.546253	-1.007405	6.926718
H	-0.069084	3.248606	6.735834
H	0.129143	-1.089568	2.307358
H	-0.083672	1.966702	2.279943
Si	-1.925284	5.629345	-0.896891
Si	1.933720	5.625204	-0.867775
Si	-1.941979	-1.130774	-0.791327
Si	0.001179	2.247464	-0.791327
Si	-1.961070	3.402664	-0.093743
Si	-3.861206	0.024551	-0.025871
Si	-3.876348	2.236230	-0.854291
Si	3.907424	-4.480537	-0.741441
Si	5.830515	-1.141166	-0.750308
Si	1.944336	-1.128941	-0.791327
Si	1.942847	-3.373706	-0.014679
Si	-1.926153	-3.361758	-0.005325
Si	-0.001015	-4.486916	-0.785409
Si	1.952717	3.397119	-0.067645
Si	3.887048	-0.001315	-0.019044
Si	3.874353	2.228824	-0.811900
Si	0.000000	0.000000	0.000000
Si	5.818984	-3.354476	0.071999
Si	-1.917357	1.090854	-3.950228
Si	0.027783	4.451810	-3.978639
Si	-1.933685	5.571174	-3.262689
Si	-3.859690	2.234128	-3.221248
Si	-3.853803	4.443639	-4.053593
Si	3.935042	-2.286460	-3.893286
Si	5.848913	1.070283	-3.944373
Si	1.975791	1.092128	-3.923429
Si	1.975144	-1.155842	-3.167800
Si	-1.895152	-1.137754	-3.162997
Si	0.030230	-2.285009	-3.926532
Si	1.974195	5.574793	-3.231956
Si	3.928215	2.225340	-3.184069
Si	3.899691	4.443988	-4.001141
Si	0.021984	2.217855	-3.174537
Si	5.855408	-1.139989	-3.117000
Si	-0.000628	6.736417	-0.089822
Si	1.984923	-5.631383	-3.923426
Si	0.047524	-4.522019	-3.151401
Si	3.904111	-4.520419	-3.109276

(b) BPA (Double-Bridge)-Relaxed

BPA_c2_alt1_631Gs_fgeo_rotated2.xyz
92

Br	-0.084680	3.439452	6.396728
C	0.131636	-0.804850	1.817817
C	0.121990	0.202551	2.951497
C	1.242331	0.977981	3.287096
C	-1.051813	0.402450	3.695174
C	1.195484	1.924755	4.310192
C	0.007831	2.106746	5.015472
C	-1.121129	1.348276	4.718514
C	1.256425	-1.900787	1.949892
H	2.172246	0.853675	2.740217
H	-1.935879	-0.190156	3.471714
H	2.071481	2.519599	4.544596
H	-2.042353	1.489878	5.273723
H	0.968010	-2.597168	2.747633
H	2.189748	-1.431297	2.281158
H	-0.821632	-1.339299	1.883996
Si	-1.928731	5.741417	-0.860734
Si	1.913479	5.749475	-0.832602
Si	-1.994559	-0.993378	-0.878448
Si	-0.022695	2.321896	-0.623309
Si	-1.987057	3.524926	-0.024009
Si	-3.885333	0.177543	-0.073384
Si	-3.888673	2.392352	-0.867248
Si	3.689756	-4.072776	-0.066607
Si	5.838860	-0.934336	-0.627206
Si	1.943475	-0.897472	-0.961506
Si	1.689092	-2.846863	0.298590
Si	-2.152599	-3.205444	-0.061207
Si	-0.078661	-4.204961	-0.524367
Si	1.936302	3.531193	-0.005105
Si	3.854235	0.211150	-0.073384
Si	3.859275	2.429270	-0.833342
Si	0.000000	0.000000	0.000000
Si	5.705686	-2.990177	0.526843
Si	-0.015549	6.880766	-0.073384
Si	-1.881633	1.213683	-3.943905
Si	0.037796	4.503597	-3.891790
Si	-1.911284	5.667212	-3.225402
Si	-3.834518	2.357031	-3.234100
Si	-3.825132	4.567556	-4.061693
Si	3.981733	-2.315700	-3.661501
Si	5.836881	1.128548	-3.892837
Si	1.964677	1.219932	-3.940546
Si	1.999086	-1.061978	-3.292685
Si	-1.898329	-1.039519	-3.237783
Si	0.035924	-2.252401	-3.898756
Si	1.972500	5.671057	-3.196844
Si	3.921847	2.344311	-3.201377
Si	3.900231	4.567149	-4.009688
Si	0.030936	2.282199	-3.035031
Si	5.873096	-1.061837	-2.985739
Si	2.052369	-5.577040	-3.376408
Si	0.071255	-4.400642	-2.881129

(c) BPA (Single-Bridge)-Relaxed

BPA_c2_alt2_631Gs_fgeo_rotated.xyz
92

Br	-1.152707	3.772284	6.124576
C	-0.117931	-1.385494	2.764468
C	-0.380873	-0.141842	3.590974
C	0.663061	0.483072	4.288981
H	1.664069	0.058354	4.253553
C	-1.658318	0.426350	3.668071
H	-2.490405	-0.045985	3.151518
C	0.448498	1.639520	5.036707
H	1.265691	2.109019	5.573896
C	-0.835973	2.180766	5.088890
C	-1.895681	1.585201	4.411528
H	-2.892385	2.008980	4.465683
C	0.723837	-1.085222	1.506160
H	1.618238	-0.540328	1.827728
H	0.419945	-2.119745	3.381255
H	-1.071589	-1.850803	2.496936
Si	-2.018303	5.767467	-0.918339
Si	1.817734	5.813604	-0.863834
Si	-2.055483	-0.962066	-0.776285
Si	-0.078454	2.345688	-0.604716
Si	-2.057659	3.556145	-0.063019
Si	-3.997885	0.221922	-0.127058
Si	-3.959181	2.433530	-0.919575
Si	3.484126	-3.776330	0.266638
Si	5.764225	-0.803154	-0.532958
Si	1.891756	-0.777347	-1.135478
Si	1.450176	-2.524084	0.337331
Si	-2.308176	-3.176549	-0.008142
Si	-0.187464	-4.078298	-0.406570
Si	1.865590	3.599166	-0.031787
Si	3.748073	0.333366	-0.127058
Si	3.781173	2.531772	-0.908901
Si	0.000000	0.000000	0.000000
Si	5.529700	-2.724284	0.817473
Si	-1.929035	1.188423	-3.922763
Si	-0.025844	4.490535	-3.906837
Si	-1.979745	5.666815	-3.281412
Si	-3.889538	2.357203	-3.283144
Si	-3.876318	4.556172	-4.139215
Si	3.970664	-2.334850	-3.540726
Si	5.789532	1.139785	-3.865253
Si	1.901390	1.246611	-4.019307
Si	1.970523	-1.054486	-3.435612
Si	-1.934832	-1.043015	-3.145937
Si	-0.023603	-2.277238	-3.860269
Si	1.894421	5.689647	-3.226536
Si	3.853857	2.379891	-3.271493
Si	3.822205	4.603953	-4.074125
Si	-0.020737	2.274137	-3.028240
Si	5.833042	-1.023879	-2.884478
Si	2.057852	-5.559139	-3.032930
Si	0.040234	-4.379404	-2.745458
Si	3.757946	-4.227587	-2.086841

C.3 Cluster DFT results for SAMs/Si(001) (Molecule - Si_9H_{12})

(a) BrSty – Relaxed

bsafgnc.xyz
39

Si	-1.884181	2.974798	1.292668
Si	-0.000000	3.589663	0.000000
Si	-3.769320	3.585923	-0.000000
Si	-3.831896	1.798485	-1.542369
Si	0.080512	1.795952	-1.534093
Si	-1.872588	1.819533	-2.872034
Si	0.000000	0.000000	0.000000
Si	-1.879125	0.575313	1.328146
Si	-3.741888	-0.008846	-0.024430
H	-1.888393	3.582659	2.659216
H	1.248860	3.623871	0.817001
H	1.301414	1.790467	-2.394303
H	1.259305	-0.011653	0.804796
C	-1.866118	-0.183449	3.090760
C	-3.111756	0.139509	3.949535
H	-1.757663	-1.272156	2.995887
H	-3.231337	1.227041	4.030955
C	-3.028370	-0.456722	5.340434
C	-3.241075	-1.826647	5.549370
C	-3.134866	-2.393485	6.818573
C	-2.815397	-1.573557	7.900201
C	-2.606241	-0.207716	7.730312
C	-2.712400	0.337218	6.449300
H	-2.548393	1.403875	6.317277
H	-2.371633	0.424578	8.579555
H	-3.302835	-3.455392	6.963739
H	-3.494795	-2.467871	4.708206
H	-0.162803	4.925329	-0.646553
H	-3.620822	4.927632	-0.634771
H	-5.018603	3.599330	0.817544
H	-5.050145	1.789226	-2.407062
H	-1.875566	0.635224	-3.780720
H	-1.871056	3.038814	-3.734202
H	-0.141699	-1.341827	-0.636796
H	-5.011581	-0.054094	0.761229
H	-3.571169	-1.341083	-0.676073
Br	-2.663346	-2.347462	9.653413
H	-0.962886	0.167928	3.606173
H	-4.011315	-0.234527	3.444146

(b) BPA-(Alkenly)-Relaxed

bpaafgnc.xyz
37

Si	-0.009739	2.400352	-0.035098
Si	1.877810	3.009113	-1.328084
Si	-1.901934	2.987766	-1.328084
Si	-1.955023	1.196923	-2.866907
Si	1.965772	1.210450	-2.856596
Si	0.008986	1.225803	-4.192821
Si	1.877810	-0.587286	-1.328084
Si	0.000000	0.000000	0.000000
Si	-1.861370	-0.606839	-1.344175
H	-0.009622	3.009455	1.330451
H	3.120824	3.056199	-0.503670
H	3.182230	1.211780	-3.723152
H	3.129766	-0.620112	-0.514329
C	0.022613	-0.783313	1.705530
C	-0.050618	-0.109696	2.871568
H	0.127499	-1.869364	1.735127
H	-0.151770	0.975075	2.838767
C	0.013754	-0.661977	4.232658
C	0.108522	-2.038648	4.506419
C	0.207907	-2.511594	5.810170
C	0.214099	-1.600759	6.868901
C	0.105017	-0.231587	6.637601
C	0.002831	0.223574	5.324236
H	-0.077128	1.292015	5.141283
H	0.104977	0.469468	7.465137
H	0.286302	-3.575903	6.002327
H	0.114255	-2.757181	3.692494
H	1.698881	4.341736	-1.975353
H	-1.760010	4.331764	-1.959302
H	-3.144657	2.992924	-0.500066
H	-3.167468	1.188844	-3.739011
H	0.012636	0.036405	-5.095046
H	0.005975	2.441626	-5.059374
H	1.726805	-1.922541	-1.979447
H	-3.120389	-0.664976	-0.542845
H	-1.681721	-1.934217	-2.005108
Br	0.410430	-2.250263	8.659234

(c) BPA (Double-Bridge)-Relaxed

bpabfgnc.xyz
37

Si	-1.938551	3.037664	1.185129
Si	-0.000000	3.668113	0.000000
Si	-3.889832	3.648677	0.000000
Si	-3.994968	1.726354	-1.377890
Si	0.015476	1.827710	-1.500818
Si	-2.028404	1.737768	-2.714921
Si	0.000000	0.000000	0.000000
Si	-1.879379	0.681057	1.252329
Si	-3.892918	-0.004620	0.241648
H	1.233509	3.662944	0.838809
H	1.154139	1.839217	-2.470064
H	1.235841	-0.024376	0.838177
C	-1.626271	1.157701	3.121984
C	-2.065371	2.658932	3.119761
H	-2.128276	0.556858	3.888427
C	-1.430505	3.580149	4.139783
C	-0.557875	3.114028	5.131118
C	-0.009813	3.974514	6.085868
C	-0.340090	5.324005	6.052737
C	-1.204498	5.826143	5.079224
C	-1.737386	4.952130	4.135475
H	-2.410613	5.347402	3.377110
H	-1.457564	6.881199	5.058342
H	0.659565	3.589394	6.847053
H	-0.302683	2.060427	5.178819
H	-0.093882	4.991012	-0.682061
H	-3.789982	4.924339	-0.765865
H	-5.074892	3.740812	0.904247
H	-5.190951	1.658351	-2.273106
H	-2.009015	0.511728	-3.568361
H	-2.100177	2.910503	-3.637956
H	-0.133625	-1.326695	-0.667468
H	-5.062971	0.090702	1.163666
H	-3.872086	-1.378963	-0.335955
Br	0.390300	6.515762	7.377795
H	-0.546403	1.074958	3.296139
H	-3.153940	2.681219	3.279618

(d) BPA (Single-Bridge)-Relaxed

bpacfgnc.xyz
37

Si	-1.976500	2.956308	1.131644
Si	-0.000000	3.512729	0.000000
Si	-3.944727	3.533106	0.000000
Si	-4.009260	1.769172	-1.566335
Si	0.052306	1.758257	-1.573879
Si	-1.980743	1.795323	-2.809293
Si	0.000000	0.000000	0.000000
Si	-1.981179	0.533510	1.131894
Si	-3.940458	-0.021291	-0.028545
H	1.201045	3.483775	0.887023
H	1.201811	1.760262	-2.538668
H	1.198895	0.045125	0.887665
C	-2.011164	1.750800	2.625893
C	-0.885566	1.735136	3.676881
H	-2.998575	1.762676	3.096978
H	0.090740	1.679389	3.180698
C	-0.911817	2.939517	4.596085
C	-1.820892	3.010860	5.660636
C	-1.873283	4.124958	6.499067
C	-0.996827	5.183440	6.266352
C	-0.075804	5.141465	5.222693
C	-0.041745	4.018278	4.395960
H	0.684345	3.981520	3.587502
H	0.605217	5.968729	5.057774
H	-2.582989	4.167336	7.318811
H	-2.497694	2.179454	5.845495
H	-0.108628	4.878289	-0.590261
H	-3.823825	4.886990	-0.613066
H	-5.139245	3.525551	0.896913
H	-5.167197	1.774359	-2.519676
H	-1.984424	0.631986	-3.747678
H	-1.969660	3.026195	-3.658828
H	-0.090193	-1.365757	-0.590280
H	-5.143777	-0.026748	0.856347
H	-3.814413	-1.366934	-0.658185
Br	-1.049465	6.738366	7.400031
H	-0.982451	0.815729	4.270618

C.4 Periodic DFT calculations: BrSty/Si(111)

(1 x 1). Starting Configurations

(a) Si111BromoStyrene1x1Opt2Start

```
26
C  -6.2414447e+00  -1.1851708e+01  2.1222872e+01
C  -6.6516000e+00  -1.1520800e+01  2.3808902e+01
C  -6.9115928e+00  -1.0539844e+01  2.4753812e+01
C  -6.3182609e+00  -1.2751997e+01  2.4319791e+01
C  -6.8443960e+00  -1.0736733e+01  2.6154232e+01
C  -6.2449599e+00  -1.2975012e+01  2.5714933e+01
C  -6.5091298e+00  -1.1977615e+01  2.6620253e+01
C  -6.9529524e+00  -1.1194329e+01  2.2378674e+01
H  -6.8670899e+00  -1.0097517e+01  2.2284249e+01
H  -8.0361656e+00  -1.1370617e+01  2.2231139e+01
H  -5.1564874e+00  -1.1658603e+01  2.1282888e+01
H  -6.3284678e+00  -1.2951712e+01  2.1283992e+01
H  -7.0411531e+00  -9.9682421e+00  2.6902974e+01
H  -5.9869601e+00  -1.3947075e+01  2.6092735e+01
Br  -6.3856793e+00  -1.2355690e+01  2.8440222e+01
H  -7.1681977e+00  -9.5579616e+00  2.4398166e+01
H  -6.1340466e+00  -1.3573256e+01  2.3642779e+01
Si  -6.6207510e+00  -1.1546456e+01  1.9367897e+01
Si  -7.7324430e+00  -9.6284660e+00  1.8583672e+01
Si  -7.6652950e+00  -9.6966510e+00  1.6253833e+01
Si  -5.4499490e+00  -9.6986530e+00  1.5493878e+01
Si  -5.4478300e+00  -9.7016270e+00  1.3161253e+01
Si  -6.5563070e+00  -1.1621993e+01  1.2394467e+01
Si  -6.5558290e+00  -1.1620414e+01  1.0062556e+01
Si  -7.6644930e+00  -9.7002340e+00  9.3186160e+00
H  -7.6626750e+00  -9.6999310e+00  7.8175600e+00
```

(b) Si111BromoStyrene1x1Opt3Start

```
26
C  -6.3410658e+00  -1.1946589e+01  2.1222872e+01
C  -6.6516000e+00  -1.1520800e+01  2.3808902e+01
C  -6.6488436e+00  -1.0505978e+01  2.4753812e+01
C  -6.6482762e+00  -1.2796319e+01  2.4319791e+01
C  -6.6348952e+00  -1.0713550e+01  2.6154232e+01
C  -6.6351937e+00  -1.3030707e+01  2.5714933e+01
C  -6.6322166e+00  -1.1998923e+01  2.6620253e+01
C  -6.8581872e+00  -1.1127458e+01  2.2378674e+01
H  -6.4913745e+00  -1.0090241e+01  2.2284249e+01
H  -7.9501174e+00  -1.1017382e+01  2.2231139e+01
H  -5.2430982e+00  -1.2040871e+01  2.1282888e+01
H  -6.7098255e+00  -1.2986588e+01  2.1283992e+01
H  -6.6260479e+00  -9.9203205e+00  2.6902974e+01
H  -6.6375732e+00  -1.4036423e+01  2.6092735e+01
Br  -6.6108256e+00  -1.2396067e+01  2.8440222e+01
H  -6.6425751e+00  -9.4911384e+00  2.4398166e+01
H  -6.6828966e+00  -1.3637273e+01  2.3642779e+01
Si  -6.6207510e+00  -1.1546456e+01  1.9367897e+01
Si  -7.7324430e+00  -9.6284660e+00  1.8583672e+01
Si  -7.6652950e+00  -9.6966510e+00  1.6253833e+01
Si  -5.4499490e+00  -9.6986530e+00  1.5493878e+01
Si  -5.4478300e+00  -9.7016270e+00  1.3161253e+01
Si  -6.5563070e+00  -1.1621993e+01  1.2394467e+01
Si  -6.5558290e+00  -1.1620414e+01  1.0062556e+01
Si  -7.6644930e+00  -9.7002340e+00  9.3186160e+00
H  -7.6626750e+00  -9.6999310e+00  7.8175600e+00
```

(c) Si111BromoStyrene1x1Opt4Start

```
26
C  -6.4618493e+00  -1.2012453e+01  2.1222872e+01
C  -6.6516000e+00  -1.1520800e+01  2.3808902e+01
C  -6.3862822e+00  -1.0541270e+01  2.4753812e+01
C  -6.9785181e+00  -1.2753717e+01  2.4319791e+01
C  -6.4265329e+00  -1.0745380e+01  2.6154232e+01
C  -7.0265455e+00  -1.2983505e+01  2.5714933e+01
C  -6.7566244e+00  -1.1987648e+01  2.6620253e+01
C  -6.7493434e+00  -1.1087392e+01  2.2378674e+01
H  -6.1265782e+00  -1.0180456e+01  2.2284249e+01
H  -7.7755773e+00  -1.0698455e+01  2.2231139e+01
H  -5.4256960e+00  -1.2387697e+01  2.1282888e+01
H  -7.0872153e+00  -1.2921572e+01  2.1283992e+01
H  -6.2126840e+00  -9.9814688e+00  2.6902974e+01
H  -7.2891423e+00  -1.3954336e+01  2.6092735e+01
Br  -6.8387507e+00  -1.2376796e+01  2.8440222e+01
H  -6.1175675e+00  -9.5626332e+00  2.4398166e+01
H  -7.2296138e+00  -1.3557056e+01  2.3642779e+01
Si  -6.6207510e+00  -1.1546456e+01  1.9367897e+01
Si  -7.7324430e+00  -9.6284660e+00  1.8583672e+01
Si  -7.6652950e+00  -9.6966510e+00  1.6253833e+01
Si  -5.4499490e+00  -9.6986530e+00  1.5493878e+01
Si  -5.4478300e+00  -9.7016270e+00  1.3161253e+01
Si  -6.5563070e+00  -1.1621993e+01  1.2394467e+01
Si  -6.5558290e+00  -1.1620414e+01  1.0062556e+01
Si  -7.6644930e+00  -9.7002340e+00  9.3186160e+00
H  -7.6626750e+00  -9.6999310e+00  7.8175600e+00
```

(d) Si111BromoStyrene1x1Opt5Start

```
26
C  -6.5955640e+00  -1.2044811e+01  2.1222872e+01
C  -6.6516000e+00  -1.1520800e+01  2.3808902e+01
C  -6.1418018e+00  -1.0643316e+01  2.4753812e+01
C  -7.2864810e+00  -1.2627094e+01  2.4319791e+01
C  -6.2335085e+00  -1.0830054e+01  2.6154232e+01
C  -7.3923454e+00  -1.2836621e+01  2.5714933e+01
C  -6.8738750e+00  -1.1944558e+01  2.6620253e+01
C  -6.6338385e+00  -1.1076862e+01  2.2378674e+01
H  -5.7975612e+00  -1.0362013e+01  2.2284249e+01
H  -7.5244401e+00  -1.0435569e+01  2.2231139e+01
H  -5.6918373e+00  -1.2675446e+01  2.1282888e+01
H  -7.4349185e+00  -1.2761096e+01  2.1283992e+01
H  -5.8292315e+00  -1.0147520e+01  2.6902974e+01
H  -7.8972639e+00  -1.3706407e+01  2.6092735e+01
Br  -7.0539217e+00  -1.2299190e+01  2.8440222e+01
H  -5.6289534e+00  -9.7675739e+00  2.4398166e+01
H  -7.7369403e+00  -1.3338071e+01  2.3642779e+01
Si  -6.6207510e+00  -1.1546456e+01  1.9367897e+01
Si  -7.7324430e+00  -9.6284660e+00  1.8583672e+01
Si  -7.6652950e+00  -9.6966510e+00  1.6253833e+01
Si  -5.4499490e+00  -9.6986530e+00  1.5493878e+01
Si  -5.4478300e+00  -9.7016270e+00  1.3161253e+01
Si  -6.5563070e+00  -1.1621993e+01  1.2394467e+01
Si  -6.5558290e+00  -1.1620414e+01  1.0062556e+01
Si  -7.6644930e+00  -9.7002340e+00  9.3186160e+00
H  -7.6626750e+00  -9.6999310e+00  7.8175600e+00
```

(e) Si111BromoStyrene1x1Opt6Start

```
26
C  -6.7330975e+00  -1.2041459e+01  2.1222872e+01
C  -6.6516000e+00  -1.1520800e+01  2.3808902e+01
C  -5.9320633e+00  -1.0805161e+01  2.4753812e+01
C  -7.5511779e+00  -1.2425078e+01  2.4319791e+01
C  -6.0689763e+00  -1.0961800e+01  2.6154232e+01
C  -7.7076647e+00  -1.2600067e+01  2.5714933e+01
C  -6.9759779e+00  -1.1872590e+01  2.6620253e+01
C  -6.5195441e+00  -1.1096586e+01  2.2378674e+01
H  -5.5267456e+00  -1.0622539e+01  2.2284249e+01
H  -7.2138202e+00  -1.0246639e+01  2.2231139e+01
H  -6.0233847e+00  -1.2884507e+01  2.1282888e+01
H  -7.7292400e+00  -1.2516097e+01  2.1283992e+01
H  -5.5018220e+00  -1.0407158e+01  2.6902974e+01
H  -8.4204956e+00  -1.3309532e+01  2.6092735e+01
Br  -7.2416752e+00  -1.2168539e+01  2.8440222e+01
H  -5.2100309e+00  -1.0091994e+01  2.4398166e+01
H  -8.1703027e+00  -1.2995243e+01  2.3642779e+01
Si  -6.6207510e+00  -1.1546456e+01  1.9367897e+01
Si  -7.7324430e+00  -9.6284660e+00  1.8583672e+01
Si  -7.6652950e+00  -9.6966510e+00  1.6253833e+01
Si  -5.4499490e+00  -9.6986530e+00  1.5493878e+01
Si  -5.4478300e+00  -9.7016270e+00  1.3161253e+01
Si  -6.5563070e+00  -1.1621993e+01  1.2394467e+01
Si  -6.5558290e+00  -1.1620414e+01  1.0062556e+01
Si  -7.6644930e+00  -9.7002340e+00  9.3186160e+00
H  -7.6626750e+00  -9.6999310e+00  7.8175600e+00
```

(f) Si111BromoStyrene1x1Opt7Start

```
26
C  -6.8650770e+00  -1.2002625e+01  2.1222872e+01
C  -6.6516000e+00  -1.1520800e+01  2.3808902e+01
C  -5.7713600e+00  -1.1015776e+01  2.4753812e+01
C  -7.7545700e+00  -1.2161438e+01  2.4319791e+01
C  -5.9441490e+00  -1.1131642e+01  2.6154232e+01
C  -7.9510150e+00  -1.2289962e+01  2.5714933e+01
C  -7.0559750e+00  -1.1776648e+01  2.6620253e+01
C  -6.4142490e+00  -1.1145219e+01  2.2378674e+01
H  -5.3325870e+00  -1.0944280e+01  2.2284249e+01
H  -6.8648860e+00  -1.0144542e+01  2.2231139e+01
H  -6.3977440e+00  -1.3000634e+01  2.1282888e+01
H  -7.9501220e+00  -1.2203269e+01  2.1283992e+01
H  -5.2527680e+00  -1.0742689e+01  2.6902974e+01
H  -8.8231800e+00  -1.2790759e+01  2.6092735e+01
Br  -7.3892160e+00  -1.1993745e+01  2.8440222e+01
H  -4.8893490e+00  -1.0513785e+01  2.4398166e+01
H  -8.5001680e+00  -1.2551933e+01  2.3642779e+01
Si  -6.6207510e+00  -1.1546456e+01  1.9367897e+01
Si  -7.7324430e+00  -9.6284660e+00  1.8583672e+01
Si  -7.6652950e+00  -9.6966510e+00  1.6253833e+01
Si  -5.4499490e+00  -9.6986530e+00  1.5493878e+01
Si  -5.4478300e+00  -9.7016270e+00  1.3161253e+01
Si  -6.5563070e+00  -1.1621993e+01  1.2394467e+01
Si  -6.5558290e+00  -1.1620414e+01  1.0062556e+01
Si  -7.6644930e+00  -9.7002340e+00  9.3186160e+00
H  -7.6626750e+00  -9.6999310e+00  7.8175600e+00
```

(g) Si111BromoStyrene1x1Opt8Start

```
26
C  -6.9825084e+00  -1.1930955e+01  2.1222872e+01
C  -6.6516000e+00  -1.1520800e+01  2.3808902e+01
C  -5.6706436e+00  -1.1260807e+01  2.4753812e+01
C  -7.8827965e+00  -1.1854139e+01  2.4319791e+01
C  -5.8675333e+00  -1.1328004e+01  2.6154232e+01
C  -8.1058123e+00  -1.1927440e+01  2.5714933e+01
C  -7.1084146e+00  -1.1663270e+01  2.6620253e+01
C  -6.3251290e+00  -1.1219448e+01  2.2378674e+01
H  -5.2283169e+00  -1.1305310e+01  2.2284249e+01
H  -6.5014167e+00  -1.0136234e+01  2.2231139e+01
H  -6.7894032e+00  -1.3015913e+01  2.1282888e+01
H  -8.0825119e+00  -1.1843932e+01  2.1283992e+01
H  -5.0990421e+00  -1.1131247e+01  2.6902974e+01
H  -9.0778748e+00  -1.2185440e+01  2.6092735e+01
Br  -7.4864895e+00  -1.1786721e+01  2.8440222e+01
H  -4.6887616e+00  -1.1004202e+01  2.4398166e+01
H  -8.7040564e+00  -1.2038353e+01  2.3642779e+01
Si  -6.6207510e+00  -1.1546456e+01  1.9367897e+01
Si  -7.7324430e+00  -9.6284660e+00  1.8583672e+01
Si  -7.6652950e+00  -9.6966510e+00  1.6253833e+01
Si  -5.4499490e+00  -9.6986530e+00  1.5493878e+01
Si  -5.4478300e+00  -9.7016270e+00  1.3161253e+01
Si  -6.5563070e+00  -1.1621993e+01  1.2394467e+01
Si  -6.5558290e+00  -1.1620414e+01  1.0062556e+01
Si  -7.6644930e+00  -9.7002340e+00  9.3186160e+00
H  -7.6626750e+00  -9.6999310e+00  7.8175600e+00
```

(2 x 1). Starting Configurations

(a) Si111BromoStyrene2x1OPT2oneMol_Start

```
36
C  -7.6805000e+00  -3.8403000e+00  2.1013249e+01
C  -6.1641770e+00  -4.0163110e+00  2.3033987e+01
C  -5.0793640e+00  -4.7937470e+00  2.3441438e+01
C  -7.1182170e+00  -3.6551670e+00  2.3989885e+01
C  -4.9608830e+00  -5.2384320e+00  2.4754646e+01
C  -7.0062630e+00  -4.0760360e+00  2.5308154e+01
C  -5.9368910e+00  -4.8867480e+00  2.5677891e+01
C  -6.3023180e+00  -3.5898910e+00  2.1607423e+01
H  -5.5267650e+00  -4.1098820e+00  2.1007356e+01
H  -6.0604170e+00  -2.5107010e+00  2.1509176e+01
H  -8.0459930e+00  -4.8469310e+00  2.1296726e+01
H  -8.4269670e+00  -3.1291080e+00  2.1413361e+01
H  -4.1527050e+00  -5.9064060e+00  2.5064077e+01
H  -7.7214550e+00  -3.7720630e+00  2.6077277e+01
Br  -5.8766980e+00  -5.5861440e+00  2.7400336e+01
H  -4.3243870e+00  -5.0876730e+00  2.2700393e+01
H  -7.9531380e+00  -3.0059470e+00  2.3703708e+01
H  -1.1527607e+01  -1.9918160e+00  2.0589350e+01
Si  -7.7029270e+00  -3.9206410e+00  1.9122610e+01
Si  -1.1552584e+01  -1.9938290e+00  1.9075458e+01
Si  -9.0287910e+00  -2.0020270e+00  1.8444076e+01
Si  -1.2880674e+01  -3.9146350e+00  1.8437937e+01
Si  -1.2889267e+01  -3.9155330e+00  1.6103689e+01
Si  -9.0509520e+00  -1.9946330e+00  1.6107951e+01
Si  -6.5314440e+00  -1.9963540e+00  1.5428573e+01
Si  -1.0373154e+01  -3.9161450e+00  1.5428446e+01
Si  -6.5680710e+00  -2.0027440e+00  1.3094600e+01
Si  -1.0410171e+01  -3.9233440e+00  1.3093500e+01
Si  -7.8906710e+00  -3.9233440e+00  1.2420500e+01
Si  -1.1731971e+01  -2.0037440e+00  1.2418500e+01
Si  -7.9146710e+00  -3.9237440e+00  1.0087500e+01
Si  -1.1755171e+01  -2.0040440e+00  1.0085600e+01
Si  -9.2376710e+00  -2.0036440e+00  9.4398000e+00
Si  -1.3078671e+01  -3.9241440e+00  9.4384000e+00
H  -9.2598710e+00  -2.0039440e+00  7.9376000e+00
H  -1.3104771e+01  -3.9246440e+00  7.9362000e+00
```

(1 x 1). Relaxed Configurations

(a) Si111BromoStyrene1x1Opt1.xyz

```
 26
C       -0.290197   -1.468933   21.222872
C       -0.772022   -1.255456   23.808902
C       -1.277046   -0.375216   24.753812
C       -0.131384   -2.358426   24.319791
C       -1.161180   -0.548005   26.154232
C       -0.002860   -2.554871   25.714933
C       -0.516174   -1.659831   26.620253
C       -1.147603   -1.018105   22.378674
H       -1.348542    0.063557   22.284249
H       -2.148280   -1.468742   22.231139
H        0.707812   -1.001600   21.282888
H       -0.089553   -2.553978   21.283992
H       -1.550133    0.143376   26.902974
H        0.497937   -3.427036   26.092735
Br      -0.299077   -1.993072   28.440222
H       -1.779037    0.506795   24.398166
H        0.259111   -3.104024   23.642779
Si      -0.741173   -1.281112   19.367897
Si      -1.852865    0.636878   18.583672
Si      -1.785717    0.568693   16.253833
Si       0.429629    0.566691   15.493878
Si       0.431748    0.563717   13.161253
Si      -0.676729   -1.356649   12.394467
Si      -0.676251   -1.355070   10.062556
Si      -1.784915    0.565110    9.318616
H       -1.783097    0.565413    7.817560
```

(b) Si111BromoStyrene1x1Opt2.xyz

```
 26
C        0.450809   -0.235540   21.230366
C       -0.047681   -0.037477   23.815841
C       -0.556851    0.837839   24.764050
C        0.590920   -1.142953   24.323197
C       -0.445772    0.658046   26.164254
C        0.714557   -1.346375   25.717969
C        0.198909   -0.455466   26.626521
C       -0.412311    0.211518   22.384276
H       -0.605617    1.295180   22.295971
H       -1.415080   -0.231064   22.228603
H        1.450300    0.226260   21.301249
H        0.645237   -1.322547   21.284076
H       -0.837705    1.345609   26.915949
H        1.214023   -2.220500   26.092461
Br       0.405111   -0.799805   28.446089
H       -1.056506    1.721952   24.411354
H        0.980387   -1.888077   23.644472
Si       0.013413   -0.035016   19.372669
Si      -1.096751    1.884282   18.587149
Si      -1.015142    1.823244   16.255901
Si       1.201700    1.822100   15.493900
Si       1.203800    1.819200   13.161300
Si       0.095300   -0.101200   12.394500
Si       0.095800   -0.099600   10.062600
Si      -1.012900    1.820600    9.318600
H       -1.011100    1.820900    7.817600
```

(c) Si111BromoStyrene1x1Opt4.xyz

```
 26
C        0.079142   -0.505615   21.224198
C        0.048093    0.021077   23.809706
C        0.553912    0.899005   24.756693
C       -0.588608   -1.084962   24.319210
C        0.457394    0.713781   26.156742
C       -0.699137   -1.292438   25.714737
C       -0.183622   -0.400608   26.621900
C        0.091684    0.463813   22.379236
H        0.952347    1.150420   22.296270
H       -0.774085    1.136343   22.219251
H        0.929010   -1.210138   21.275006
H       -0.816059   -1.147547   21.295416
H        0.860058    1.397033   26.905215
H       -1.205041   -2.161324   26.092770
Br      -0.372766   -0.753457   28.441301
H        1.068773    1.773758   24.402210
H       -1.037698   -1.799241   23.644264
Si       0.105197   -0.019417   19.368096
Si      -1.004261    1.903893   18.583990
Si      -1.014418    1.820623   16.253772
Si       1.201700    1.822100   15.493900
Si       1.203800    1.819200   13.161300
Si       0.095300   -0.101200   12.394500
Si       0.095800   -0.099600   10.062600
Si      -1.012900    1.820600    9.318600
H       -1.011100    1.820900    7.817600
```

(d) Si111BromoStyrene1x1Opt5.xyz

```
 26
C        0.056977   -0.517419   21.222764
C        0.017165    0.004457   23.809380
C        0.522299    0.880185   24.758922
C       -0.619888   -1.102607   24.316573
C        0.424010    0.691671   26.158432
C       -0.731823   -1.313978   25.711314
C       -0.217313   -0.423613   26.620949
C        0.064061    0.449841   22.379496
H        0.923872    1.138072   22.302199
H       -0.802324    1.120921   22.215934
H        0.905180   -1.223221   21.275711
H       -0.839816   -1.157666   21.289318
H        0.826618    1.374020   26.908057
H       -1.239193   -2.184482   26.083730
Br      -0.407424   -0.780339   28.440237
H        1.038666    1.755346   24.407775
H       -1.067698   -1.815603   23.639872
Si       0.089484   -0.028374   19.366808
Si      -1.019078    1.895326   18.582131
Si      -1.016074    1.819303   16.252277
Si       1.201700    1.822100   15.493900
Si       1.203800    1.819200   13.161300
Si       0.095300   -0.101200   12.394500
Si       0.095800   -0.099600   10.062600
Si      -1.012900    1.820600    9.318600
H       -1.011100    1.820900    7.817600
```

(e) Si111BromoStyrene1x1Opt6.xyz

```
 26
C        0.025419   -0.498658   21.229279
C       -0.037408    0.034237   23.814332
C        0.461335    0.912820   24.765212
C       -0.678249   -1.071316   24.319643
C        0.358019    0.725006   26.164504
C       -0.796754   -1.280895   25.714401
C       -0.284975   -0.390068   26.625106
C        0.024110    0.472913   22.382904
H        0.887978    1.156219   22.310440
H       -0.837478    1.147195   22.210101
H        0.868860   -1.209027   21.294716
H       -0.874779   -1.135191   21.288491
H        0.755872    1.409794   26.915099
H       -1.304443   -2.151960   26.085815
Br      -0.481704   -0.742702   28.444327
H        0.979049    1.787685   24.415158
H       -1.128408   -1.782661   23.642219
Si       0.075143   -0.018488   19.371731
Si      -1.031489    1.903957   18.586605
Si      -1.017070    1.820442   16.255131
Si       1.201700    1.822100   15.493900
Si       1.203800    1.819200   13.161300
Si       0.095300   -0.101200   12.394500
Si       0.095800   -0.099600   10.062600
Si      -1.012900    1.820600    9.318600
H       -1.011100    1.820900    7.817600
```

(f) Si111BromoStyrene1x1Opt8.xyz

```
 26
C       -0.268874   -0.315899   21.222723
C        0.124480    0.030221   23.810194
C        1.131447    0.031735   24.764296
C       -1.154806    0.029876   24.311797
C        0.912986    0.022817   26.162801
C       -1.400328    0.021316   25.705690
C       -0.375353    0.021432   26.619503
C        0.537332    0.214382   22.381356
H        1.573626   -0.161499   22.307384
H        0.660001    1.302262   22.217826
H       -0.381561   -1.409985   21.302848
H       -1.304671    0.070321   21.256984
H        1.702734    0.013725   26.915434
H       -2.409060    0.025589   26.075124
Br      -0.785830    0.010325   28.437066
H        2.148705    0.023397   24.417022
H       -1.993346    0.063370   23.631348
Si       0.155050   -0.051145   19.369546
Si      -0.949227    1.869661   18.584745
Si      -1.017571    1.822135   16.254027
Si       1.201700    1.822100   15.493900
Si       1.203800    1.819200   13.161300
Si       0.095300   -0.101200   12.394500
Si       0.095800   -0.099600   10.062600
Si      -1.012900    1.820600    9.318600
H       -1.011100    1.820900    7.817600
```

(2 x 1). Relaxed Configurations

(a)Si111BromoStyrene2x1OPT1oneMol

```
36
C  -1.1068627e+01  -7.4362558e+00  2.1013258e+01
C  -1.2584951e+01  -7.2602447e+00  2.3033998e+01
C  -1.3669764e+01  -6.4828085e+00  2.3441449e+01
C  -1.1630910e+01  -7.6213890e+00  2.3989996e+01
C  -1.3788245e+01  -6.0381234e+00  2.4754658e+01
C  -1.1742865e+01  -7.2005202e+00  2.5308166e+01
C  -1.2812237e+01  -6.3898071e+00  2.5677903e+01
C  -1.2446810e+01  -7.6866646e+00  2.1607433e+01
H  -1.3222363e+01  -7.1666734e+00  2.1007366e+01
H  -1.2688710e+01  -8.7658555e+00  2.1509186e+01
H  -1.0703134e+01  -6.4296240e+00  2.1296736e+01
H  -1.0322160e+01  -8.1474485e+00  2.1413371e+01
H  -1.4596424e+01  -5.3701490e+00  2.5064089e+01
H  -1.1027672e+01  -7.5044925e+00  2.6077289e+01
Br  -1.2872429e+01  -5.6904115e+00  2.7400349e+01
H  -1.4424742e+01  -6.1888824e+00  2.2700404e+01
H  -1.0795989e+01  -8.2706097e+00  2.3703719e+01
H  -1.4915736e+01  -5.5877713e+00  2.0589360e+01
Si  -1.1091054e+01  -7.5165965e+00  1.9122619e+01
Si  -1.4940713e+01  -5.5897836e+00  1.9075467e+01
Si  -1.2416918e+01  -5.5979820e+00  1.8444084e+01
Si  -1.6268804e+01  -7.5105904e+00  1.8437946e+01
Si  -1.6277396e+01  -7.5114888e+00  1.6103697e+01
Si  -1.2439079e+01  -5.5905880e+00  1.6107958e+01
Si  -9.9195701e+00  -5.5923086e+00  1.5428581e+01
Si  -1.3761282e+01  -7.5121007e+00  1.5428453e+01
Si  -9.9561975e+00  -5.5986990e+00  1.3094606e+01
Si  -1.3798299e+01  -7.5192999e+00  1.3093506e+01
Si  -1.1278798e+01  -7.5192999e+00  1.2420506e+01
Si  -1.5120100e+01  -5.5996990e+00  1.2418506e+01
Si  -1.1302798e+01  -7.5196999e+00  1.0087505e+01
Si  -1.5143300e+01  -5.5999990e+00  1.0085605e+01
Si  -1.2625799e+01  -5.5995990e+00  9.4398044e+00
Si  -1.6466801e+01  -7.5200999e+00  9.4384044e+00
H  -1.2647999e+01  -5.5998990e+00  7.9376037e+00
H  -1.6492901e+01  -7.5205999e+00  7.9362037e+00
```

(b) Si111BromoStyrene2x1OPT2oneMol

```
36
C  -1.5330843e+01  -7.8677749e+00  2.1035224e+01
C  -1.3852513e+01  -7.8421594e+00  2.3077394e+01
C  -1.2769835e+01  -8.6252423e+00  2.3478484e+01
C  -1.4794623e+01  -7.4652960e+00  2.4038917e+01
C  -1.2640520e+01  -9.0596803e+00  2.4793863e+01
C  -1.4673138e+01  -7.8783522e+00  2.5358639e+01
C  -1.3605269e+01  -8.6940684e+00  2.5723029e+01
C  -1.4005569e+01  -7.4388696e+00  2.1646805e+01
H  -1.3169636e+01  -7.8850812e+00  2.1070386e+01
H  -1.3871911e+01  -6.3430686e+00  2.1539407e+01
H  -1.5525599e+01  -8.9259601e+00  2.1295376e+01
H  -1.6175687e+01  -7.3007763e+00  2.1468933e+01
H  -1.1833467e+01  -9.7308321e+00  2.5099457e+01
H  -1.5377357e+01  -7.5627053e+00  2.6133468e+01
Br  -1.3531845e+01  -9.3822621e+00  2.7449369e+01
H  -1.2027031e+01  -8.9323522e+00  2.2730904e+01
H  -1.5625030e+01  -6.8088346e+00  2.3754186e+01
H  -1.9208337e+01  -5.8261150e+00  2.0579993e+01
Si  -1.5410454e+01  -7.7399093e+00  1.9135350e+01
Si  -1.9222427e+01  -5.8244288e+00  1.9065590e+01
Si  -1.6714126e+01  -5.8163807e+00  1.8431189e+01
Si  -2.0561806e+01  -7.7449806e+00  1.8437553e+01
Si  -2.0575881e+01  -7.7560243e+00  1.6103472e+01
Si  -1.6731248e+01  -5.8410656e+00  1.6098748e+01
Si  -1.4216142e+01  -5.8371300e+00  1.5427002e+01
Si  -1.8055938e+01  -7.7616850e+00  1.5426354e+01
Si  -1.4248599e+01  -5.8429991e+00  1.3094606e+01
Si  -1.8090701e+01  -7.7636000e+00  1.3093506e+01
Si  -1.5571200e+01  -7.7636000e+00  1.2420506e+01
Si  -1.9412502e+01  -5.8439991e+00  1.2418506e+01
Si  -1.5595200e+01  -7.7640000e+00  1.0087505e+01
Si  -1.9435702e+01  -5.8442991e+00  1.0085605e+01
Si  -1.6918201e+01  -5.8438991e+00  9.4398044e+00
Si  -2.0759203e+01  -7.7644000e+00  9.4384044e+00
H  -1.6940401e+01  -5.8441991e+00  7.9376037e+00
H  -2.0785303e+01  -7.7649000e+00  7.9362037e+00
```

C.5 Periodic DFT calculations: BPA/Si(111)

Si111BPA1x1Opt1Start.xyz

C	-6.50	-12.02	21.19
C	-6.65	-11.52	23.64
C	-6.92	-10.53	24.59
C	-6.32	-12.77	24.14
C	-6.86	-10.75	25.98
C	-6.26	-13.00	25.54
C	-6.53	-12.00	26.44
C	-6.73	-11.20	22.24
H	-7.01	-10.15	22.03
H	-6.22	-13.07	21.41
H	-7.07	-9.99	26.74
H	-6.00	-13.97	25.92
Br	-6.43	-12.38	28.26
H	-7.19	-9.55	24.22
H	-6.10	-13.56	23.44
Si	-6.51	-11.70	19.36
Si	-7.62	-9.79	18.59
Si	-7.59	-9.83	16.26
Si	-5.37	-9.82	15.49
Si	-5.37	-9.83	13.16
Si	-6.48	-11.75	12.39
Si	-6.48	-11.75	10.06
Si	-7.59	-9.83	9.32
H	-7.59	-9.83	7.82

Si111BPA1x1CGOpt1.xyz

C	0.27	-0.42	21.18
C	-0.05	0.10	23.62
C	-0.58	1.02	24.53
C	0.59	-1.00	24.17
C	-0.49	0.86	25.94
C	0.68	-1.17	25.58
C	0.14	-0.24	26.45
C	-0.18	0.35	22.21
H	-0.71	1.29	21.96
H	0.81	-1.35	21.43
H	-0.91	1.58	26.65
H	1.18	-2.03	25.98
Br	0.31	-0.52	28.28
H	-1.09	1.89	24.13
H	1.01	-1.74	23.50
Si	0.15	-0.18	19.36
Si	-0.96	1.73	18.59
Si	-0.94	1.69	16.26
Si	1.28	1.70	15.49
Si	1.28	1.69	13.16
Si	0.17	-0.23	12.39
Si	0.17	-0.23	10.06
Si	-0.94	1.69	9.32
H	-0.93	1.69	7.82

Si111BPA2x1Or1Tilt1Start

C	4.78	1.88	17.93
C	3.36	2.19	19.99
C	2.19	2.83	20.45
C	4.04	1.35	20.88
C	1.74	2.66	21.75
C	3.60	1.18	22.18
C	2.46	1.85	22.62
C	3.80	2.46	18.64
H	3.22	3.27	18.16
H	5.36	1.05	18.37
H	0.87	3.21	22.12
H	4.10	0.50	22.88
Br	1.97	1.78	24.41
H	1.66	3.50	19.76
H	4.93	0.80	20.54
H	1.89	4.37	17.65
Si	5.19	2.46	16.21
Si	1.86	4.37	16.14
Si	4.05	4.37	15.49
Si	0.70	2.45	15.51
Si	0.69	2.45	13.18
Si	4.03	4.37	13.16
Si	6.22	4.37	12.49
Si	2.88	2.45	12.49
Si	6.19	4.37	10.16
Si	2.84	2.45	10.16
Si	5.03	2.45	9.48
Si	1.70	4.37	9.48
Si	5.01	2.45	7.15
Si	1.67	4.37	7.15
Si	3.86	4.37	6.50
Si	0.52	2.45	6.50
H	3.84	4.37	5.00
H	0.50	2.45	5.00

Si111BPA2x1Or1Tilt3Start

C	5.41	3.85	17.34
C	3.50	3.32	18.91
C	2.22	3.76	19.29
C	3.99	2.13	19.49
C	1.47	3.08	20.23
C	3.24	1.44	20.43
C	1.99	1.93	20.81
C	4.24	4.12	17.97
H	3.76	5.09	17.76
H	5.91	2.88	17.51
H	0.50	3.45	20.58
H	3.59	0.50	20.87
Br	1.08	1.11	22.21
H	1.84	4.69	18.86
H	4.96	1.74	19.18
H	2.91	7.01	17.65
Si	6.20	5.09	16.21
Si	2.87	7.00	16.14
Si	5.06	7.00	15.49
Si	1.71	5.08	15.51
Si	1.70	5.08	13.18
Si	5.04	7.01	13.16
Si	7.23	7.00	12.49
Si	3.89	5.09	12.49
Si	7.20	7.00	10.16
Si	3.86	5.08	10.16
Si	6.05	5.08	9.48
Si	2.71	7.00	9.48
Si	6.02	5.08	7.15
Si	2.68	7.00	7.15
Si	4.87	7.00	6.50
Si	1.53	5.08	6.50
H	4.85	7.00	5.00
H	1.51	5.08	5.00

Si111BPA1x1Opt3Start.xyz

C	-6.77	-12.03	21.19
C	-6.65	-11.52	23.64
C	-6.39	-10.53	24.59
C	-6.99	-12.77	24.14
C	-6.45	-10.75	25.98
C	-7.05	-13.00	25.54
C	-6.78	-11.99	26.44
C	-6.56	-11.20	22.24
H	-6.27	-10.16	22.03
H	-7.05	-13.08	21.41
H	-6.25	-9.99	26.74
H	-7.31	-13.96	25.92
Br	-6.89	-12.38	28.26
H	-6.13	-9.55	24.22
H	-7.20	-13.56	23.44
Si	-6.51	-11.70	19.36
Si	-7.62	-9.79	18.59
Si	-7.59	-9.83	16.26
Si	-5.37	-9.82	15.49
Si	-5.37	-9.83	13.16
Si	-6.48	-11.75	12.39
Si	-6.48	-11.75	10.06
Si	-7.59	-9.83	9.32
H	-7.59	-9.83	7.82

Si111BPA1x1CGOpt3.xyz

C	0.05	-0.40	21.22
C	0.36	0.17	23.65
C	0.89	1.10	24.54
C	-0.27	-0.93	24.22
C	0.81	0.97	25.95
C	-0.36	-1.07	25.63
C	0.18	-0.14	26.49
C	0.50	0.39	22.23
H	1.04	1.32	21.97
H	-0.49	-1.32	21.50
H	1.23	1.69	26.65
H	-0.86	-1.93	26.05
Br	0.02	-0.39	28.32
H	1.40	1.97	24.13
H	-0.71	-1.67	23.55
Si	0.18	-0.19	19.38
Si	-0.93	1.73	18.60
Si	-0.94	1.70	16.26
Si	1.28	1.70	15.49
Si	1.28	1.69	13.16
Si	0.17	-0.23	12.39
Si	0.17	-0.23	10.06
Si	-0.94	1.69	9.32
H	-0.93	1.69	7.82

Si111BPA2x1Or1Tilt2Start

C	4.95	2.95	17.69
C	3.26	2.81	19.57
C	2.04	3.34	20.00
C	3.84	1.78	20.33
C	1.42	2.90	21.16
C	3.23	1.32	21.49
C	2.03	1.90	21.91
C	3.87	3.37	18.38
H	3.35	4.27	18.02
H	5.48	2.03	18.00
H	0.50	3.36	21.53
H	3.64	0.50	22.08
Br	1.32	1.43	23.56
H	1.59	4.16	19.42
H	4.77	1.31	19.99
H	2.27	5.80	17.65
Si	5.56	3.89	16.21
Si	2.23	5.80	16.14
Si	4.42	5.80	15.49
Si	1.07	3.88	15.51
Si	1.06	3.88	13.18
Si	4.41	5.81	13.16
Si	6.59	5.80	12.49
Si	3.25	3.88	12.49
Si	6.56	5.80	10.16
Si	3.22	3.88	10.16
Si	5.41	3.88	9.48
Si	2.07	5.80	9.48
Si	5.38	3.88	7.15
Si	2.05	5.80	7.15
Si	4.23	5.80	6.50
Si	0.90	3.88	6.50
H	4.21	5.80	5.00
H	0.87	3.88	5.00

Si111BPA2x1Or1Tilt1

C	4.91	2.33	18.15
C	3.42	2.22	20.17
C	2.08	2.42	20.57
C	4.25	1.48	21.02
C	1.58	1.87	21.74
C	3.77	0.94	22.21
C	2.43	1.12	22.56
C	3.83	2.73	18.88
H	3.14	3.46	18.44
H	5.58	1.56	18.57
H	0.54	2.03	22.04
H	4.43	0.34	22.86
Br	1.74	0.31	24.07
H	1.43	3.03	19.92
H	5.30	1.31	20.74
H	1.63	4.63	17.80
Si	5.03	2.64	16.33
Si	1.69	4.60	16.29
Si	3.92	4.56	15.56
Si	0.58	2.67	15.55
Si	0.57	2.63	13.22
Si	3.89	4.52	13.22
Si	6.11	4.55	12.45
Si	2.78	2.60	12.46
Si	6.11	4.54	10.12
Si	2.78	2.61	10.12
Si	5.00	2.62	9.35
Si	1.67	4.53	9.35
Si	5.00	2.62	7.02
Si	1.67	4.53	7.02
Si	3.89	4.54	6.28
Si	0.57	2.61	6.28
H	3.89	4.54	4.78
H	0.57	2.61	4.78

Si111BPA2x1Or1Tilt2

C	5.17	3.33	18.01
C	3.44	3.16	19.86
C	2.08	3.42	20.10
C	4.14	2.37	20.78
C	1.43	2.88	21.19
C	3.50	1.84	21.90
C	2.14	2.08	22.10
C	4.01	3.68	18.63
H	3.35	4.40	18.12
H	5.84	2.59	18.47
H	0.37	3.09	21.38
H	4.05	1.20	22.60
Br	1.24	1.30	23.51
H	1.53	4.06	19.39
H	5.20	2.13	20.60
H	1.94	5.69	17.63
Si	5.35	3.67	16.20
Si	2.02	5.65	16.13
Si	4.25	5.59	15.41
Si	0.90	3.72	15.40
Si	0.88	3.67	13.07
Si	4.21	5.55	13.08
Si	6.43	5.59	12.30
Si	3.10	3.63	12.31
Si	6.43	5.58	9.97
Si	3.10	3.65	9.98
Si	5.32	3.66	9.21
Si	2.00	5.57	9.21
Si	5.32	3.66	6.88
Si	2.00	5.57	6.88
Si	4.21	5.58	6.13
Si	0.89	3.65	6.13
H	4.21	5.58	4.63
H	0.89	3.65	4.63

Si111BPA2x1Or2Tilt0Start

C	5.02	1.21	18.05
C	3.87	2.00	20.16
C	2.76	2.74	20.61
C	4.67	1.37	21.12
C	2.48	2.88	21.96
C	4.40	1.50	22.47
C	3.32	2.28	22.89
C	4.12	1.96	18.74
H	3.48	2.64	18.17
H	5.66	0.50	18.59
H	1.66	3.51	22.31
H	5.00	0.99	23.24
Br	3.07	2.61	24.70
H	2.14	3.25	19.86
H	5.52	0.75	20.80
H	1.89	3.30	17.65
Si	5.19	1.39	16.21
Si	1.86	3.30	16.14
Si	4.05	3.30	15.49
Si	0.70	1.38	15.51
Si	0.69	1.38	13.18
Si	4.03	3.30	13.16
Si	6.22	3.30	12.49
Si	2.88	1.38	12.49
Si	6.19	3.30	10.16
Si	2.84	1.38	10.16
Si	5.03	1.38	9.48
Si	1.70	3.30	9.48
Si	5.01	1.38	7.15
Si	1.67	3.30	7.15
Si	3.86	3.30	6.50
Si	0.52	1.38	6.50
H	3.84	3.30	5.00
H	0.50	1.38	5.00

Si111BPA2x1Or2Tilt2Start

C	5.49	1.16	17.92
C	4.86	2.85	19.69
C	3.86	3.78	20.04
C	5.92	2.65	20.60
C	3.92	4.50	21.22
C	5.99	3.37	21.78
C	5.00	4.31	22.07
C	4.76	2.18	18.42
H	3.95	2.59	17.79
H	6.29	0.72	18.53
H	3.18	5.27	21.46
H	6.79	3.21	22.51
Br	5.19	5.41	23.56
H	3.04	3.95	19.33
H	6.69	1.91	20.37
H	1.89	2.43	17.65
Si	5.19	0.51	16.21
Si	1.86	2.42	16.14
Si	4.05	2.42	15.49
Si	0.70	0.50	15.51
Si	0.69	0.51	13.18
Si	4.03	2.43	13.16
Si	6.22	2.43	12.49
Si	2.88	0.51	12.49
Si	6.19	2.42	10.16
Si	2.84	0.50	10.16
Si	5.03	0.50	9.48
Si	1.70	2.42	9.48
Si	5.01	0.50	7.15
Si	1.67	2.42	7.15
Si	3.86	2.42	6.50
Si	0.52	0.50	6.50
H	3.84	2.42	5.00
H	0.50	0.50	5.00

Si111BPA2x1Or2Tilt0

C	4.84	1.13	18.08
C	4.24	2.36	20.20
C	3.24	3.13	20.80
C	5.35	2.00	20.98
C	3.34	3.55	22.12
C	5.48	2.42	22.29
C	4.47	3.22	22.86
C	4.10	2.02	18.80
H	3.32	2.59	18.28
H	5.60	0.52	18.58
H	2.57	4.20	22.57
H	6.35	2.15	22.89
Br	4.70	3.91	24.56
H	2.37	3.44	20.20
H	6.15	1.38	20.54
H	1.26	2.93	17.67
Si	4.68	1.00	16.24
Si	1.33	2.92	16.17
Si	3.57	2.91	15.47
Si	0.22	1.00	15.42
Si	0.24	0.99	13.09
Si	3.57	2.92	13.13
Si	5.78	2.91	12.34
Si	2.47	1.00	12.35
Si	5.78	2.91	10.01
Si	2.47	0.99	10.02
Si	4.68	0.99	9.24
Si	1.36	2.91	9.26
Si	4.68	0.99	6.91
Si	1.36	2.91	6.92
Si	3.57	2.91	6.17
Si	0.25	0.99	6.18
H	3.56	2.91	4.67
H	0.26	0.99	4.67

Si111BPA2x1Or1Tilt3

C	5.71	4.06	17.79
C	3.81	4.10	19.50
C	2.44	4.42	19.44
C	4.25	3.29	20.56
C	1.53	3.91	20.34
C	3.34	2.79	21.50
C	1.98	3.08	21.37
C	4.61	4.59	18.39
H	4.13	5.44	17.88
H	6.20	3.17	18.23
H	0.47	4.16	20.25
H	3.69	2.13	22.30
Br	0.72	2.31	22.50
H	2.09	5.08	18.63
H	5.31	3.01	20.66
H	2.56	6.51	17.36
Ge	5.98	4.41	15.99
Si	2.65	6.42	15.87
Si	4.89	6.34	15.18
Si	1.52	4.49	15.16
Si	1.50	4.44	12.83
Si	4.85	6.31	12.84
Si	7.05	6.35	12.06
Si	3.73	4.39	12.08
Si	7.06	6.34	9.73
Si	3.73	4.40	9.75
Si	5.95	4.42	8.97
Si	2.63	6.33	8.97
Si	5.95	4.41	6.64
Si	2.63	6.33	6.64
Si	4.84	6.33	5.89
Si	1.52	4.41	5.90
H	4.84	6.34	4.39
H	1.52	4.41	4.40

Si111BPA2x1Or2Tilt1Start

	5.26	1.09	18.05
C	4.38	2.34	20.06
C	3.33	3.18	20.47
C	5.31	1.93	21.02
C	3.22	3.62	21.78
C	5.22	2.36	22.34
C	4.19	3.23	22.70
C	4.45	1.98	18.66
H	3.73	2.53	18.04
H	5.98	0.50	18.64
H	2.45	4.33	22.08
H	5.92	2.03	23.11
Br	4.17	3.96	24.41
H	2.61	3.52	19.72
H	6.12	1.24	20.74
H	1.89	2.75	17.65
Si	5.19	0.84	16.21
Si	1.86	2.75	16.14
Si	4.05	2.75	15.49
Si	0.70	0.83	15.51
Si	0.69	0.83	13.18
Si	4.03	2.76	13.16
Si	6.22	2.75	12.49
Si	2.88	0.83	12.49
Si	6.19	2.75	10.16
Si	2.84	0.83	10.16
Si	5.03	0.83	9.48
Si	1.70	2.75	9.48
Si	5.01	0.83	7.15
Si	1.67	2.75	7.15
Si	3.86	2.75	6.50
Si	0.52	0.83	6.50
H	3.84	2.75	5.00
H	0.50	0.83	5.00

Si111BPA2x1Or2Tilt3Start

	5.70	1.53	17.67
C	5.28	3.58	19.09
C	4.32	4.57	19.34
C	6.45	3.57	19.87
C	4.52	5.54	20.32
C	6.66	4.54	20.85
C	5.70	5.53	21.05
C	5.02	2.64	18.02
H	4.14	2.91	17.43
H	6.58	1.22	18.26
H	3.81	6.35	20.47
H	7.55	4.53	21.49
Br	6.07	6.93	22.21
H	3.42	4.59	18.73
H	7.19	2.78	19.72
H	1.89	2.43	17.65
Si	5.19	0.51	16.21
Si	1.86	2.42	16.14
Si	4.05	2.42	15.49
Si	0.70	0.50	15.51
Si	0.69	0.51	13.18
Si	4.03	2.43	13.16
Si	6.22	2.43	12.49
Si	2.88	0.51	12.49
Si	6.19	2.42	10.16
Si	2.84	0.50	10.16
Si	5.03	0.50	9.48
Si	1.70	2.42	9.48
Si	5.01	0.50	7.15
Si	1.67	2.42	7.15
Si	3.86	2.42	6.50
Si	0.52	0.50	6.50
H	3.84	2.42	5.00
H	0.50	0.50	5.00

Si111BPA2x1Or2Tilt1

C	5.09	1.05	18.10
C	4.47	2.23	20.25
C	3.47	3.01	20.85
C	5.57	1.84	21.03
C	3.56	3.41	22.17
C	5.68	2.24	22.36
C	4.68	3.04	22.92
C	4.35	1.92	18.84
H	3.56	2.50	18.33
H	5.86	0.44	18.60
H	2.80	4.07	22.62
H	6.53	1.93	22.97
Br	4.90	3.72	24.63
H	2.62	3.34	20.23
H	6.35	1.21	20.59
H	1.52	2.88	17.70
Si	4.93	0.94	16.26
Si	1.58	2.88	16.19
Si	3.82	2.86	15.50
Si	0.47	0.95	15.45
Si	0.49	0.95	13.12
Si	3.82	2.87	13.16
Si	6.03	2.87	12.37
Si	2.72	0.95	12.38
Si	6.03	2.87	10.04
Si	2.72	0.95	10.05
Si	4.93	0.96	9.27
Si	1.60	2.87	9.28
Si	4.93	0.95	6.94
Si	1.61	2.87	6.95
Si	3.82	2.88	6.20
Si	0.50	0.95	6.20
H	3.81	2.87	4.70
H	0.51	0.95	4.70

Si111BPA2x1Or2Tilt2

C	5.27	1.14	17.90
C	4.80	2.35	20.05
C	3.84	3.12	20.73
C	5.98	2.01	20.73
C	4.04	3.54	22.04
C	6.20	2.43	22.03
C	5.24	3.21	22.68
C	4.57	2.02	18.66
H	3.75	2.59	18.19
H	6.06	0.53	18.37
H	3.31	4.17	22.55
H	7.13	2.17	22.56
Br	5.60	3.92	24.36
H	2.92	3.41	20.20
H	6.74	1.41	20.22
H	1.66	2.95	17.51
Si	5.07	1.02	16.07
Si	1.71	2.94	16.00
Si	3.95	2.93	15.31
Si	0.61	1.02	15.25
Si	0.63	1.02	12.93
Si	3.95	2.94	12.97
Si	6.16	2.94	12.18
Si	2.85	1.02	12.19
Si	6.16	2.94	9.85
Si	2.85	1.02	9.85
Si	5.06	1.02	9.08
Si	1.74	2.94	9.09
Si	5.06	1.02	6.75
Si	1.74	2.94	6.76
Si	3.95	2.94	6.01
Si	0.63	1.02	6.01
H	3.94	2.94	4.50
H	0.64	1.02	4.51

Si111BPA2x1Or2Tilt3

C	5.42	1.51	17.59
C	5.12	2.74	19.75
C	4.21	3.49	20.52
C	6.37	2.43	20.31
C	4.54	3.92	21.80
C	6.72	2.88	21.58
C	5.81	3.63	22.32
C	4.77	2.40	18.38
H	3.93	2.97	17.96
H	6.24	0.91	18.02
H	3.85	4.54	22.38
H	7.71	2.65	21.99
Br	6.33	4.36	23.94
H	3.23	3.75	20.10
H	7.10	1.86	19.72
H	1.78	3.31	17.22
Si	5.18	1.39	15.76
Si	1.83	3.31	15.71
Si	4.06	3.30	15.01
Si	0.72	1.39	14.95
Si	0.75	1.39	12.62
Si	4.07	3.31	12.67
Si	6.28	3.31	11.87
Si	2.97	1.39	11.88
Si	6.28	3.31	9.54
Si	2.97	1.39	9.55
Si	5.18	1.39	8.77
Si	1.86	3.31	8.79
Si	5.18	1.40	6.44
Si	1.86	3.32	6.45
Si	4.07	3.32	5.70
Si	0.75	1.40	5.71
H	4.06	3.32	4.20
H	0.76	1.40	4.20

C.6 Periodic DFT calculations: BPPA/Si(111)

Si111BPPA_1x1_Or1_StartR0

C	0.27	-0.47	27.87
C	-0.26	0.45	28.78
C	0.91	-1.58	28.42
C	-0.17	0.29	30.19
C	1.00	-1.74	29.83
C	0.47	-0.81	30.70
H	-0.59	1.01	30.90
H	1.50	-2.61	30.23
Br	0.63	-1.10	32.53
H	-0.76	1.32	28.38
H	1.34	-2.31	27.75
C	0.27	-0.42	21.18
C	-0.05	0.10	23.62
C	-0.58	1.02	24.53
C	0.59	-1.00	24.17
C	-0.49	0.86	25.94
C	0.68	-1.17	25.58
C	0.14	-0.24	26.45
C	-0.18	0.35	22.21
H	-0.71	1.29	21.96
H	0.81	-1.35	21.43
H	-0.91	1.58	26.65
H	1.18	-2.03	25.98
H	-1.09	1.89	24.13
H	1.01	-1.74	23.50
Si	0.15	-0.18	19.36
Si	-0.96	1.73	18.59
Si	-0.94	1.69	16.26
Si	1.28	1.70	15.49
Si	1.28	1.69	13.16
Si	0.17	-0.23	12.39
Si	0.17	-0.23	10.06
Si	-0.94	1.69	9.32
H	-0.93	1.69	7.82

Si111BPPA_1x1_Or1_StartR2

C	0.27	-0.47	27.87
C	1.33	-0.47	28.78
C	-1.00	-0.47	28.42
C	1.16	-0.46	30.19
C	-1.19	-0.46	29.83
C	-0.12	-0.46	30.70
H	1.99	-0.46	30.90
H	-2.19	-0.46	30.23
Br	-4.46	-0.46	32.53
H	2.34	-0.46	28.38
H	-1.85	-0.47	27.75
C	0.27	-0.42	21.18
C	-0.05	0.10	23.62
C	-0.58	1.02	24.53
C	0.59	-1.00	24.17
C	-0.49	0.86	25.94
C	0.68	-1.17	25.58
C	0.14	-0.24	26.45
C	-0.18	0.35	22.21
H	-0.71	1.29	21.96
H	0.81	-1.35	21.43
H	-0.91	1.58	26.65
H	1.18	-2.03	25.98
H	-1.09	1.89	24.13
H	1.01	-1.74	23.50
Si	0.15	-0.18	19.36
Si	-9.58	1.73	18.59
Si	-9.38	1.69	16.26
Si	1.28	1.70	15.49
Si	1.28	1.69	13.16
Si	0.17	-0.23	12.39
Si	0.17	-0.23	10.06
Si	-9.36	1.69	9.32
H	-0.93	1.69	7.82

Si111BPPA_1x1_Or2_StartR1

C	0.05	-0.34	27.91
C	1.12	-0.34	28.80
C	-1.22	-0.34	28.47
C	0.97	-0.34	30.21
C	-1.39	-0.34	29.89
C	-0.31	-0.34	30.74
H	1.80	-0.34	30.91
H	-2.38	-0.34	30.31
Br	-0.61	-0.33	32.58
H	2.13	-0.34	28.39
H	-2.08	-0.34	27.81
C	0.05	-0.40	21.22
C	0.36	0.17	23.65
C	0.89	1.10	24.54
C	-0.27	-0.93	24.22
C	0.81	0.97	25.95
C	-0.36	-1.07	25.63
C	0.18	-0.14	26.49
C	0.50	0.39	22.23
H	1.04	1.32	21.97
H	-0.49	-1.32	21.50
H	1.23	1.69	26.65
H	-0.86	-1.93	26.05
H	1.40	1.97	24.13
H	-0.71	-1.67	23.55
Si	0.18	-0.19	19.38
Si	-0.93	1.73	18.60
Si	-0.94	1.70	16.26
Si	1.28	1.70	15.49
Si	1.28	1.69	13.16
Si	0.17	-0.23	12.39
Si	0.17	-0.23	10.06
Si	-0.94	1.69	9.32
H	-0.93	1.69	7.82

Si111BPPA_1x1_Ori1_R0.xyz

C	0.26	-0.44	27.94
C	-0.27	0.47	28.86
C	0.89	-1.55	28.50
C	-0.18	0.31	30.27
C	0.99	-1.71	29.91
C	0.46	-0.79	30.79
H	-0.59	1.04	30.97
H	1.49	-2.58	30.31
Br	0.62	-1.08	32.61
H	-0.78	1.35	28.49
H	1.33	-2.29	27.85
C	0.27	-0.42	21.18
C	-0.04	0.10	23.62
C	-0.57	1.01	24.53
C	0.59	-1.00	24.18
C	-0.48	0.85	25.94
C	0.68	-1.16	25.59
C	0.15	-0.25	26.51
C	-0.18	0.35	22.20
H	-0.72	1.28	21.96
H	0.81	-1.36	21.42
H	-0.92	1.60	26.59
H	1.19	-2.04	25.95
H	-1.08	1.88	24.14
H	1.02	-1.74	23.52
Si	0.14	-0.19	19.35
Si	-0.97	1.73	18.59
Si	-0.94	1.69	16.25
Si	1.28	1.70	15.49
Si	1.28	1.69	13.16
Si	0.17	-0.23	12.39
Si	0.17	-0.23	10.06
Si	-0.94	1.69	9.32
H	-0.93	1.69	7.82

Si111BPPA_1x1_Or1_StartR1

C	0.27	-0.47	27.87
C	0.80	0.45	28.78
C	-0.37	-1.57	28.42
C	0.71	0.30	30.19
C	-0.46	-1.73	29.83
C	0.07	-0.81	30.70
H	1.13	1.02	30.90
H	-0.96	-2.60	30.23
Br	-0.09	-1.09	32.53
H	1.30	1.32	28.38
H	-0.79	-2.31	27.75
C	0.27	-0.42	21.18
C	-0.05	0.10	23.62
C	-0.58	1.02	24.53
C	0.59	-1.00	24.17
C	-0.49	0.86	25.94
C	0.68	-1.17	25.58
C	0.14	-0.24	26.45
C	-0.18	0.35	22.21
H	-0.71	1.29	21.96
H	0.81	-1.35	21.43
H	-0.91	1.58	26.65
H	1.18	-2.03	25.98
H	-1.09	1.89	24.13
H	1.01	-1.74	23.50
Si	0.15	-0.18	19.36
Si	-0.96	1.73	18.59
Si	-0.94	1.69	16.26
Si	1.28	1.70	15.49
Si	1.28	1.69	13.16
Si	0.17	-0.23	12.39
Si	0.17	-0.23	10.06
Si	-0.94	1.69	9.32
H	-0.93	1.69	7.82

Si111BPPA_1x1_Or2_StartR0

C	0.05	-0.34	27.91
C	0.59	0.59	28.80
C	-0.58	-1.44	28.47
C	0.51	0.45	30.21
C	-0.67	-1.59	29.89
C	-0.13	-0.65	30.74
H	0.92	1.18	30.91
H	-1.17	-2.45	30.31
Br	-0.29	-0.91	32.58
H	1.09	1.46	28.39
H	-1.01	-2.19	27.81
C	0.05	-0.40	21.22
C	0.36	0.17	23.65
C	0.89	1.10	24.54
C	-0.27	-0.93	24.22
C	0.81	0.97	25.95
C	-0.36	-1.07	25.63
C	0.18	-0.14	26.49
C	0.50	0.39	22.23
H	1.04	1.32	21.97
H	-0.49	-1.32	21.50
H	1.23	1.69	26.65
H	-0.86	-1.93	26.05
H	1.40	1.97	24.13
H	-0.71	-1.67	23.55
Si	0.18	-0.19	19.38
Si	-0.93	1.73	18.60
Si	-0.94	1.70	16.26
Si	1.28	1.70	15.49
Si	1.28	1.69	13.16
Si	0.17	-0.23	12.39
Si	0.17	-0.23	10.06
Si	-0.94	1.69	9.32
H	-0.93	1.69	7.82

Si111BPPA_1x1_Or2_StartR2

C	0.05	-0.34	27.91
C	0.59	-1.27	28.80
C	-0.58	0.76	28.47
C	0.51	-1.13	30.21
C	-0.66	0.91	29.89
C	-0.12	-0.03	30.74
H	0.93	-1.85	30.91
H	-1.16	1.77	30.31
Br	-0.27	0.23	32.58
H	1.09	-2.14	28.39
H	-1.01	1.50	27.81
C	0.05	-0.40	21.22
C	0.36	0.17	23.65
C	0.89	1.10	24.54
C	-0.27	-0.93	24.22
C	0.81	0.97	25.95
C	-0.36	-1.07	25.63
C	0.18	-0.14	26.49
C	0.50	0.39	22.23
H	1.04	1.32	21.97
H	-0.49	-1.32	21.50
H	1.23	1.69	26.65
H	-0.86	-1.93	26.05
H	1.40	1.97	24.13
H	-0.71	-1.67	23.55
Si	0.18	-0.19	19.38
Si	-0.93	1.73	18.60
Si	-0.94	1.70	16.26
Si	1.28	1.70	15.49
Si	1.28	1.69	13.16
Si	0.17	-0.23	12.39
Si	0.17	-0.23	10.06
Si	-0.94	1.69	9.32
H	-0.93	1.69	7.82

Si111BPPA_1x1_Ori2_R0.xyz

C	0.06	-0.32	27.95
C	0.59	0.59	28.86
C	-0.57	-1.42	28.52
C	0.50	0.44	30.27
C	-0.67	-1.58	29.92
C	-0.13	-0.66	30.80
H	0.92	1.17	30.97
H	-1.17	-2.45	30.33
Br	-0.29	-0.93	32.63
H	1.10	1.47	28.49
H	-1.01	-2.18	27.87
C	0.05	-0.41	21.19
C	0.36	0.17	23.62
C	0.89	1.09	24.52
C	-0.27	-0.92	24.20
C	0.80	0.95	25.93
C	-0.36	-1.06	25.61
C	0.17	-0.14	26.52
C	0.50	0.39	22.20
H	1.04	1.32	21.94
H	-0.49	-1.33	21.48
H	1.24	1.71	26.57
H	-0.86	-1.94	25.98
H	1.39	1.97	24.11
H	-0.70	-1.67	23.54
Si	0.18	-0.20	19.36
Si	-0.92	1.73	18.58
Si	-0.94	1.70	16.25
Si	1.28	1.70	15.49
Si	1.28	1.69	13.16
Si	0.17	-0.23	12.39
Si	0.17	-0.23	10.06
Si	-0.94	1.69	9.32
H	-0.93	1.69	7.82

Si111BPPA_1x1_Ori2_R2.xyz

C	0.04	-0.17	27.99
C	0.53	-1.14	28.85
C	-0.58	0.91	28.61
C	0.46	-1.03	30.27
C	-0.70	1.00	30.02
C	-0.17	0.05	30.85
H	0.89	-1.78	30.94
H	-1.21	1.85	30.45
Br	-0.34	0.23	32.68
H	1.10	-1.97	28.46
H	-1.07	1.65	27.98
C	0.06	-0.49	21.20
C	0.41	0.09	23.62
C	0.95	1.03	24.50
C	-0.20	-1.00	24.24
C	0.84	0.92	25.91
C	-0.28	-1.11	25.65
C	0.22	-0.16	26.53
C	0.53	0.30	22.21
H	1.06	1.23	21.93
H	-0.47	-1.42	21.49
H	1.32	1.67	26.54
H	-0.83	-1.96	26.04
H	1.47	1.89	24.08
H	-0.65	-1.75	23.60
Si	0.18	-0.26	19.36
Si	-0.93	1.67	18.59
Si	-0.94	1.69	16.26
Si	1.28	1.70	15.49
Si	1.28	1.69	13.16
Si	0.17	-0.23	12.39
Si	0.17	-0.23	10.06
Si	-0.94	1.69	9.32
H	-0.93	1.69	7.82

Si111BPPA_2x1_StartOr1.xyz

C	-1.37	0.72	8.26
C	-2.46	1.37	8.85
C	-0.43	0.11	9.10
C	-2.60	1.44	10.23
C	-0.55	0.17	10.48
C	-1.63	0.86	11.04
H	-3.42	2.00	10.70
H	0.16	-0.32	11.15
Br	-1.70	1.10	12.88
H	-3.20	1.86	8.21
H	0.42	-0.43	8.66
C	-0.11	-0.30	1.82
C	-1.07	0.37	4.06
C	-2.16	1.02	4.65
C	-0.13	-0.24	4.90
C	-2.30	1.09	6.03
C	-0.26	-0.18	6.28
C	-1.33	0.51	6.84
C	-0.96	0.39	2.62
H	-1.65	1.10	2.13
H	0.57	-1.04	2.28
H	-3.12	1.65	6.49
H	0.46	-0.67	6.95
H	-2.90	1.51	4.00
H	0.72	-0.78	4.46
H	-3.41	1.94	1.44
Si	0.00	0.00	0.00
Si	-3.35	1.93	-0.07
Si	-1.11	1.92	-0.77
Si	-4.46	0.01	-0.81
Si	-4.44	0.01	-3.14
Si	-1.12	1.92	-3.10
Si	1.10	1.93	-3.89
Si	-2.22	0.00	-3.88
Si	1.10	1.93	-6.23
Si	-2.22	0.01	-6.22
Si	-0.01	0.01	-6.99
Si	-3.33	1.93	-6.98
Si	0.00	0.01	-9.32
Si	-3.33	1.93	-9.31
Si	-1.11	1.93	-10.07
Si	-4.43	0.01	-10.06
H	-1.12	1.93	-11.57
H	-4.42	0.01	-11.56

Si111BPPA_2x1_StartOr3.xyz

C	-0.06	1.55	8.26
C	-0.04	2.82	8.85
C	-0.12	0.42	9.10
C	-0.05	2.97	10.23
C	-0.13	0.56	10.48
C	-0.07	1.84	11.04
H	0.02	3.96	10.70
H	-0.20	-0.30	11.15
Br	0.10	2.02	12.88
H	0.01	3.70	8.21
H	-0.16	-0.58	8.66
C	-0.32	-0.06	1.82
C	-0.22	1.11	4.06
C	-0.20	2.38	4.65
C	-0.27	-0.01	4.90
C	-0.21	2.54	6.03
C	-0.29	0.13	6.28
C	-0.23	1.41	6.84
C	-0.14	1.02	2.62
H	0.12	1.98	2.13
H	-0.62	-1.02	2.28
H	-0.13	3.53	6.49
H	-0.35	-0.73	6.95
H	-0.14	3.27	4.00
H	-0.31	-1.02	4.46
H	-3.41	1.94	1.44
Si	0.00	0.00	0.00
Si	-3.35	1.93	-0.07
Si	-1.11	1.92	-0.77
Si	-4.46	0.01	-0.81
Si	-4.44	0.01	-3.14
Si	-1.12	1.92	-3.10
Si	1.10	1.93	-3.89
Si	-2.22	0.00	-3.88
Si	1.10	1.93	-6.23
Si	-2.22	0.01	-6.22
Si	-0.01	0.01	-6.99
Si	-3.33	1.93	-6.98
Si	0.00	0.01	-9.32
Si	-3.33	1.93	-9.31
Si	-1.11	1.93	-10.07
Si	-4.43	0.01	-10.06
H	-1.12	1.93	-11.57
H	-4.42	0.01	-11.56

Si111BPPA_2x1_StartOr5.xyz

C	1.31	0.83	8.26
C	2.42	1.45	8.85
C	0.30	0.32	9.10
C	2.55	1.53	10.23
C	0.42	0.40	10.48
C	1.56	0.99	11.04
H	3.44	1.96	10.70
H	-0.36	0.02	11.15
Br	1.80	0.92	12.88
H	3.21	1.84	8.21
H	-0.58	-0.15	8.66
C	-0.21	0.25	1.82
C	0.85	0.74	4.06
C	1.97	1.36	4.65
C	-0.15	0.23	4.90
C	2.10	1.45	6.03
C	-0.03	0.31	6.28
C	1.10	0.90	6.84
C	0.82	0.63	2.62
H	1.78	0.88	2.13
H	-1.19	0.03	2.28
H	2.99	1.88	6.49
H	-0.81	-0.06	6.95
H	2.76	1.75	4.00
H	-1.03	-0.24	4.46
H	-3.41	1.94	1.44
Si	0.00	0.00	0.00
Si	-3.35	1.93	-0.07
Si	-1.11	1.92	-0.77
Si	-4.46	0.01	-0.81
Si	-4.44	0.01	-3.14
Si	-1.12	1.92	-3.10
Si	1.10	1.93	-3.89
Si	-2.22	0.00	-3.88
Si	1.10	1.93	-6.23
Si	-2.22	0.01	-6.22
Si	-0.01	0.01	-6.99
Si	-3.33	1.93	-6.98
Si	0.00	0.01	-9.32
Si	-3.33	1.93	-9.31
Si	-1.11	1.93	-10.07
Si	-4.43	0.01	-10.06
H	-1.12	1.93	-11.57
H	-4.42	0.01	-11.56

Si111BPPA_2x1_StartOr0.xyz

C	-1.55	-0.06	8.26
C	-2.82	-0.04	8.85
C	-0.42	-0.12	9.10
C	-2.97	-0.05	10.23
C	-0.56	-0.13	10.48
C	-1.84	-0.07	11.04
H	-3.96	0.02	10.70
H	0.30	-0.20	11.15
Br	-2.02	0.10	12.88
H	-3.70	0.01	8.21
H	0.58	-0.16	8.66
C	0.06	-0.32	1.82
C	-1.11	-0.22	4.06
C	-2.38	-0.20	4.65
C	0.01	-0.27	4.90
C	-2.54	-0.21	6.03
C	-0.13	-0.29	6.28
C	-1.41	-0.23	6.84
C	-1.02	-0.14	2.62
H	-1.98	0.12	2.13
H	1.02	-0.62	2.28
H	-3.53	-0.13	6.49
H	0.73	-0.35	6.95
H	-3.27	-0.14	4.00
H	1.02	-0.31	4.46
H	-3.41	1.94	1.44
Si	0.00	0.00	0.00
Si	-3.35	1.93	-0.07
Si	-1.11	1.92	-0.77
Si	-4.46	0.01	-0.81
Si	-4.44	0.01	-3.14
Si	-1.12	1.92	-3.10
Si	1.10	1.93	-3.89
Si	-2.22	0.00	-3.88
Si	1.10	1.93	-6.23
Si	-2.22	0.01	-6.22
Si	-0.01	0.01	-6.99
Si	-3.33	1.93	-6.98
Si	0.00	0.01	-9.32
Si	-3.33	1.93	-9.31
Si	-1.11	1.93	-10.07
Si	-4.43	0.01	-10.06
H	-1.12	1.93	-11.57
H	-4.42	0.01	-11.56

Si111BPPA_2x1_StartOr2.xyz

C	-0.83	1.31	8.26
C	-1.45	2.42	8.85
C	-0.32	0.30	9.10
C	-1.53	2.55	10.23
C	-0.40	0.42	10.48
C	-0.99	1.56	11.04
H	-1.96	3.44	10.70
H	-0.02	-0.36	11.15
Br	-0.92	1.80	12.88
H	-1.84	3.21	8.21
H	0.15	-0.58	8.66
C	-0.25	-0.21	1.82
C	-0.74	0.85	4.06
C	-1.36	1.97	4.65
C	-0.23	-0.15	4.90
C	-1.45	2.10	6.03
C	-0.31	-0.03	6.28
C	-0.90	1.10	6.84
C	-0.63	0.82	2.62
H	-0.88	1.78	2.13
H	-0.03	-1.19	2.28
H	-1.88	2.99	6.49
H	0.06	-0.81	6.95
H	-1.75	2.76	4.00
H	0.24	-1.03	4.46
H	-3.41	1.94	1.44
Si	0.00	0.00	0.00
Si	-3.35	1.93	-0.07
Si	-1.11	1.92	-0.77
Si	-4.46	0.01	-0.81
Si	-4.44	0.01	-3.14
Si	-1.12	1.92	-3.10
Si	1.10	1.93	-3.89
Si	-2.22	0.00	-3.88
Si	1.10	1.93	-6.23
Si	-2.22	0.01	-6.22
Si	-0.01	0.01	-6.99
Si	-3.33	1.93	-6.98
Si	0.00	0.01	-9.32
Si	-3.33	1.93	-9.31
Si	-1.11	1.93	-10.07
Si	-4.43	0.01	-10.06
H	-1.12	1.93	-11.57
H	-4.42	0.01	-11.56

Si111BPPA_2x1_StartOr4.xyz

C	0.72	1.37	8.26
C	1.37	2.46	8.85
C	0.11	0.43	9.10
C	1.44	2.60	10.23
C	0.17	0.55	10.48
C	0.86	1.63	11.04
H	2.00	3.42	10.70
H	-0.32	-0.16	11.15
Br	1.10	1.70	12.88
H	1.86	3.20	8.21
H	-0.43	-0.42	8.66
C	-0.30	0.11	1.82
C	0.37	1.07	4.06
C	1.02	2.16	4.65
C	-0.24	0.13	4.90
C	1.09	2.30	6.03
C	-0.18	0.26	6.28
C	0.51	1.33	6.84
C	0.39	0.96	2.62
H	1.10	1.65	2.13
H	-1.04	-0.57	2.28
H	1.65	3.12	6.49
H	-0.67	-0.46	6.95
H	1.51	2.90	4.00
H	-0.78	-0.72	4.46
H	-3.41	1.94	1.44
Si	0.00	0.00	0.00
Si	-3.35	1.93	-0.07
Si	-1.11	1.92	-0.77
Si	-4.46	0.01	-0.81
Si	-4.44	0.01	-3.14
Si	-1.12	1.92	-3.10
Si	1.10	1.93	-3.89
Si	-2.22	0.00	-3.88
Si	1.10	1.93	-6.23
Si	-2.22	0.01	-6.22
Si	-0.01	0.01	-6.99
Si	-3.33	1.93	-6.98
Si	0.00	0.01	-9.32
Si	-3.33	1.93	-9.31
Si	-1.11	1.93	-10.07
Si	-4.43	0.01	-10.06
H	-1.12	1.93	-11.57
H	-4.42	0.01	-11.56

Si111BPPA_2x1_StartOr6.xyz

C	1.55	0.06	8.26
C	2.82	0.04	8.85
C	0.42	0.12	9.10
C	2.97	0.05	10.23
C	0.56	0.13	10.48
C	1.84	0.07	11.04
H	3.96	-0.02	10.70
H	-0.30	0.20	11.15
Br	2.02	-0.10	12.88
H	3.70	-0.01	8.21
H	-0.58	0.16	8.66
C	-0.06	0.32	1.82
C	1.11	0.22	4.06
C	2.38	0.20	4.65
C	-0.01	0.27	4.90
C	2.54	0.21	6.03
C	0.13	0.29	6.28
C	1.41	0.23	6.84
C	1.02	0.14	2.62
H	1.98	-0.12	2.13
H	-1.02	0.62	2.28
H	3.53	0.13	6.49
H	-0.73	0.35	6.95
H	3.27	0.14	4.00
H	-1.02	0.31	4.46
H	-3.41	1.94	1.44
Si	0.00	0.00	0.00
Si	-3.35	1.93	-0.07
Si	-1.11	1.92	-0.77
Si	-4.46	0.01	-0.81
Si	-4.44	0.01	-3.14
Si	-1.12	1.92	-3.10
Si	1.10	1.93	-3.89
Si	-2.22	0.00	-3.88
Si	1.10	1.93	-6.23
Si	-2.22	0.01	-6.22
Si	-0.01	0.01	-6.99
Si	-3.33	1.93	-6.98
Si	0.00	0.01	-9.32
Si	-3.33	1.93	-9.31
Si	-1.11	1.93	-10.07
Si	-4.43	0.01	-10.06
H	-1.12	1.93	-11.57
H	-4.42	0.01	-11.56

Si111BPPA_2x1_Or0.xyz

C	-1.80	0.28	8.31
C	-2.87	1.00	8.86
C	-0.92	-0.34	9.21
C	-3.02	1.16	10.23
C	-1.05	-0.19	10.58
C	-2.09	0.59	11.10
H	-3.83	1.78	10.63
H	-0.35	-0.68	11.27
Br	-2.18	0.95	12.91
H	-3.58	1.52	8.20
H	-0.11	-0.99	8.84
C	0.03	-0.19	1.85
C	-1.13	0.27	4.04
C	-2.32	0.78	4.60
C	-0.20	-0.31	4.92
C	-2.55	0.74	5.96
C	-0.43	-0.33	6.29
C	-1.60	0.21	6.85
C	-0.94	0.38	2.61
H	-1.70	1.00	2.11
H	0.78	-0.85	2.32
H	-3.49	1.16	6.34
H	0.34	-0.75	6.94
H	-3.06	1.23	3.93
H	0.74	-0.73	4.53
H	-3.38	1.95	1.44
Si	0.04	-0.06	0.01
Si	-3.31	1.92	-0.07
Si	-1.07	1.87	-0.77
Si	-4.42	-0.01	-0.80
Si	-4.43	-0.01	-3.13
Si	-1.10	1.88	-3.11
Si	1.11	1.91	-3.89
Si	-2.21	-0.03	-3.88
Si	1.10	1.93	-6.23
Si	-2.22	0.01	-6.22
Si	-0.01	0.01	-6.99
Si	-3.33	1.93	-6.98
Si	0.00	0.01	-9.32
Si	-3.33	1.93	-9.31
Si	-1.11	1.93	-10.07
Si	-4.43	0.01	-10.06
H	-1.12	1.93	-11.57
H	-4.42	0.01	-11.56

Si111BPPA_2x1_Or2.xyz

C	-0.64	2.23	8.17
C	-1.80	2.37	8.93
C	0.57	2.66	8.73
C	-1.78	2.99	10.18
C	0.61	3.29	9.97
C	-0.57	3.48	10.69
H	-2.70	3.11	10.76
H	1.55	3.68	10.37
Br	-0.55	4.41	12.29
H	-2.75	1.98	8.54
H	1.50	2.57	8.15
C	0.11	0.02	1.87
C	-0.68	1.04	4.04
C	-1.77	1.72	4.63
C	0.40	0.70	4.87
C	-1.78	2.04	5.98
C	0.40	1.04	6.22
C	-0.68	1.74	6.79
C	-0.71	0.81	2.61
H	-1.50	1.37	2.09
H	0.88	-0.59	2.37
H	-2.61	2.63	6.39
H	1.25	0.77	6.85
H	-2.61	2.02	3.98
H	1.25	0.15	4.45
H	-3.43	1.93	1.44
Si	-0.01	-0.04	0.02
Si	-3.36	1.91	-0.07
Si	-1.11	1.88	-0.75
Si	-4.47	-0.01	-0.81
Si	-4.45	-0.01	-3.14
Si	-1.12	1.90	-3.09
Si	1.09	1.91	-3.89
Si	-2.22	-0.02	-3.88
Si	1.10	1.93	-6.23
Si	-2.22	0.01	-6.22
Si	-0.01	0.01	-6.99
Si	-3.33	1.93	-6.98
Si	0.00	0.01	-9.32
Si	-3.33	1.93	-9.31
Si	-1.11	1.93	-10.07
Si	-4.43	0.01	-10.06
H	-1.12	1.93	-11.57
H	-4.42	0.01	-11.56

Si111BPPA_2x1_Or5.xyz

C	1.27	0.92	8.34
C	2.34	1.59	8.94
C	0.33	0.32	9.20
C	2.50	1.64	10.32
C	0.47	0.36	10.59
C	1.57	1.02	11.15
H	3.35	2.18	10.76
H	-0.25	-0.14	11.23
Br	1.78	1.07	12.99
H	3.08	2.11	8.32
H	-0.52	-0.24	8.80
C	-0.08	-0.06	1.84
C	0.91	0.63	4.05
C	2.01	1.26	4.65
C	-0.08	0.09	4.90
C	2.12	1.36	6.03
C	0.04	0.19	6.27
C	1.14	0.83	6.88
C	0.86	0.55	2.61
H	1.69	1.06	2.10
H	-0.93	-0.58	2.32
H	3.00	1.87	6.44
H	-0.75	-0.25	6.89
H	2.79	1.69	4.01
H	-0.94	-0.43	4.47
H	-3.23	1.94	1.45
Si	-0.01	-0.05	-0.01
Si	-3.29	1.92	-0.06
Si	-1.09	1.88	-0.82
Si	-4.44	0.00	-0.76
Si	-4.44	0.00	-3.11
Si	-1.11	1.91	-3.14
Si	1.11	1.92	-3.89
Si	-2.22	-0.01	-3.89
Si	1.10	1.93	-6.23
Si	-2.22	0.01	-6.22
Si	-0.01	0.01	-6.99
Si	-3.33	1.93	-6.98
Si	0.00	0.01	-9.32
Si	-3.33	1.93	-9.31
Si	-1.11	1.93	-10.07
Si	-4.43	0.01	-10.06
H	-1.12	1.93	-11.57
H	-4.42	0.01	-11.56

Si111BPPA_2x1_Or1.xyz

C	-1.48	0.57	8.35
C	-2.55	1.25	8.94
C	-0.52	0.02	9.22
C	-2.62	1.47	10.31
C	-0.57	0.22	10.59
C	-1.60	0.99	11.14
H	-3.43	2.07	10.74
H	0.19	-0.22	11.25
Br	-1.56	1.48	12.92
H	-3.35	1.68	8.32
H	0.30	-0.59	8.82
C	0.02	-0.13	1.84
C	-0.97	0.51	4.06
C	-2.08	1.12	4.66
C	-0.06	-0.14	4.91
C	-2.27	1.11	6.03
C	-0.24	-0.14	6.28
C	-1.34	0.49	6.89
C	-0.83	0.57	2.62
H	-1.53	1.27	2.14
H	0.70	-0.87	2.31
H	-3.13	1.64	6.44
H	0.51	-0.66	6.90
H	-2.80	1.65	4.02
H	0.82	-0.64	4.48
H	-3.41	1.94	1.44
Si	0.00	-0.03	0.00
Si	-3.35	1.92	-0.07
Si	-1.11	1.89	-0.77
Si	-4.45	-0.01	-0.81
Si	-4.44	-0.01	-3.14
Si	-1.12	1.90	-3.11
Si	1.09	1.91	-3.89
Si	-2.22	-0.02	-3.88
Si	1.10	1.93	-6.23
Si	-2.22	0.01	-6.22
Si	-0.01	0.01	-6.99
Si	-3.33	1.93	-6.98
Si	0.00	0.01	-9.32
Si	-3.33	1.93	-9.31
Si	-1.11	1.93	-10.07
Si	-4.43	0.01	-10.06
H	-1.12	1.93	-11.57
H	-4.42	0.01	-11.56

Si111BPPA_2x1_Or4.xyz

C	0.73	1.84	8.10
C	1.84	2.03	8.94
C	-0.52	2.30	8.56
C	1.72	2.68	10.16
C	-0.65	2.95	9.78
C	0.48	3.16	10.57
H	2.60	2.82	10.81
H	-1.63	3.34	10.11
Br	0.32	4.10	12.16
H	2.82	1.62	8.64
H	-1.40	2.18	7.92
C	-0.04	-0.04	1.83
C	0.98	0.41	4.06
C	2.10	0.98	4.70
C	-0.18	0.21	4.83
C	2.03	1.41	6.02
C	-0.24	0.64	6.15
C	0.85	1.28	6.76
C	1.03	0.14	2.64
H	2.04	0.16	2.19
H	-1.05	-0.03	2.29
H	2.89	1.94	6.45
H	-1.15	0.45	6.73
H	3.02	1.14	4.11
H	-1.04	-0.31	4.39
H	-3.25	1.87	1.46
Si	0.03	-0.11	-0.01
Si	-3.28	1.85	-0.05
Si	-1.06	1.82	-0.80
Si	-4.41	-0.07	-0.77
Si	-4.43	-0.04	-3.11
Si	-1.10	1.87	-3.13
Si	1.12	1.88	-3.89
Si	-2.21	-0.04	-3.88
Si	1.10	1.93	-6.23
Si	-2.22	0.01	-6.22
Si	-0.01	0.01	-6.99
Si	-3.33	1.93	-6.98
Si	0.00	0.01	-9.32
Si	-3.33	1.93	-9.31
Si	-1.11	1.93	-10.07
Si	-4.43	0.01	-10.06
H	-1.12	1.93	-11.57
H	-4.42	0.01	-11.56

Si111BPPA_2x1_Or6.xyz

C	2.17	-2.93	7.57
C	3.48	-3.28	7.91
C	1.15	-3.31	8.46
C	3.78	-4.01	9.05
C	1.42	-4.04	9.61
C	2.74	-4.41	9.90
H	4.81	-4.31	9.29
H	0.62	-4.34	10.29
Br	3.12	-5.40	11.41
H	4.30	-3.00	7.23
H	0.11	-3.01	8.26
C	-0.06	-0.38	1.79
C	1.31	-1.02	3.81
C	2.58	-0.93	4.40
C	0.32	-1.74	4.51
C	2.86	-1.53	5.62
C	0.59	-2.33	5.73
C	1.87	-2.24	6.32
C	1.09	-0.42	2.51
H	2.01	0.00	2.06
H	-0.98	-0.79	2.23
H	3.85	-1.40	6.07
H	-0.18	-2.95	6.21
H	3.36	-0.35	3.88
H	-0.67	-1.88	4.05
H	-3.31	1.89	1.46
Si	-0.05	-0.04	-0.02
Si	-3.35	1.90	-0.05
Si	-1.14	1.89	-0.81
Si	-4.48	-0.01	-0.78
Si	-4.47	-0.01	-3.11
Si	-1.14	1.89	-3.14
Si	1.08	1.91	-3.89
Si	-2.25	-0.03	-3.89
Si	1.10	1.93	-6.23
Si	-2.22	0.01	-6.22
Si	-0.01	0.01	-6.99
Si	-3.33	1.93	-6.98
Si	0.00	0.01	-9.32
Si	-3.33	1.93	-9.31
Si	-1.11	1.93	-10.07
Si	-4.43	0.01	-10.06
H	-1.12	1.93	-11.57
H	-4.42	0.01	-11.56

C.7 Periodic DFT calculations: BPEPA/Si(111)

Si111BPEPA_2x1_Or0_Start.xyz

C	-1.83	0.04	11.07
C	-3.11	0.06	11.66
C	-0.71	-0.02	11.91
C	-3.26	0.05	13.04
C	-0.85	-0.03	13.28
C	-2.13	0.03	13.84
H	-4.25	0.12	13.50
H	0.01	-0.10	13.96
Br	-2.31	0.21	15.68
H	-3.99	0.12	11.01
H	0.29	-0.06	11.47
C	-1.70	-0.13	9.64
C	-1.55	-0.18	8.24
C	0.06	-0.32	1.82
C	-1.11	-0.22	4.06
C	-2.38	-0.20	4.65
C	0.01	-0.27	4.90
C	-2.54	-0.21	6.03
C	-0.13	-0.29	6.28
C	-1.41	-0.23	6.84
C	-1.02	-0.14	2.62
H	-1.98	0.12	2.13
H	1.02	-0.62	2.28
H	-3.53	-0.13	6.49
H	0.73	-0.35	6.95
H	-3.27	-0.14	4.00
H	1.02	-0.31	4.46
H	-3.41	1.94	1.44
Si	0.00	0.00	0.00
Si	-3.35	1.93	-0.07
Si	-1.11	1.92	-0.77
Si	-4.46	0.01	-0.81
Si	-4.44	0.01	-3.14
Si	-1.12	1.92	-3.10
Si	1.10	1.93	-3.89
Si	-2.22	0.00	-3.88
Si	1.10	1.93	-6.23
Si	-2.22	0.01	-6.22
Si	-0.01	0.01	-6.99
Si	-3.33	1.93	-6.98
Si	0.00	0.01	-9.32
Si	-3.33	1.93	-9.31
Si	-1.11	1.93	-10.07
Si	-4.43	0.01	-10.06
H	-1.12	1.93	-11.57
H	-4.42	0.01	-11.56

Si111BPEPA_2x1_Or2_Start.xyz

C	-0.88	1.61	11.07
C	-1.50	2.72	11.66
C	-0.37	0.61	11.91
C	-1.59	2.85	13.04
C	-0.45	0.72	13.28
C	-1.04	1.86	13.84
H	-2.02	3.74	13.50
H	-0.08	-0.05	13.96
Br	-0.98	2.10	15.68
H	-1.89	3.51	11.01
H	0.10	-0.28	11.47
C	-0.96	1.41	9.64
C	-0.93	1.26	8.24
C	-0.25	-0.21	1.82
C	-0.74	0.85	4.06
C	-1.36	1.97	4.65
C	-0.23	-0.15	4.90
C	-1.45	2.10	6.03
C	-0.31	-0.03	6.28
C	-0.90	1.10	6.84
C	-0.63	0.82	2.62
H	-0.88	1.78	2.13
H	-0.03	-1.19	2.28
H	-1.88	2.99	6.49
H	0.06	-0.81	6.95
H	-1.75	2.76	4.00
H	0.24	-1.03	4.46
H	-3.41	1.94	1.44
Si	0.00	0.00	0.00
Si	-3.35	1.93	-0.07
Si	-1.11	1.92	-0.77
Si	-4.46	0.01	-0.81
Si	-4.44	0.01	-3.14
Si	-1.12	1.92	-3.10
Si	1.10	1.93	-3.89
Si	-2.22	0.00	-3.88
Si	1.10	1.93	-6.23
Si	-2.22	0.01	-6.22
Si	-0.01	0.01	-6.99
Si	-3.33	1.93	-6.98
Si	0.00	0.01	-9.32
Si	-3.33	1.93	-9.31
Si	-1.11	1.93	-10.07
Si	-4.43	0.01	-10.06
H	-1.12	1.93	-11.57
H	-4.42	0.01	-11.56

Si111BPEPA_2x1_Or5_Start.xyz

C	1.61	0.88	11.07
C	2.72	1.50	11.66
C	0.61	0.37	11.91
C	2.85	1.59	13.04
C	0.72	0.45	13.28
C	1.86	1.04	13.84
H	3.74	2.02	13.50
H	-0.05	0.08	13.96
Br	2.10	0.98	15.68
H	3.51	1.89	11.01
H	-0.28	-0.10	11.47
C	1.41	0.96	9.64
C	1.26	0.93	8.24
C	-0.21	0.25	1.82
C	0.85	0.74	4.06
C	1.97	1.36	4.65
C	-0.15	0.23	4.90
C	2.10	1.45	6.03
C	-0.03	0.31	6.28
C	1.10	0.90	6.84
C	0.82	0.63	2.62
H	1.78	0.88	2.13
H	-1.19	0.03	2.28
H	2.99	1.88	6.49
H	-0.81	-0.06	6.95
H	2.76	1.75	4.00
H	-1.03	-0.24	4.46
H	-3.41	1.94	1.44
Si	0.00	0.00	0.00
Si	-3.35	1.93	-0.07
Si	-1.11	1.92	-0.77
Si	-4.46	0.01	-0.81
Si	-4.44	0.01	-3.14
Si	-1.12	1.92	-3.10
Si	1.10	1.93	-3.89
Si	-2.22	0.00	-3.88
Si	1.10	1.93	-6.23
Si	-2.22	0.01	-6.22
Si	-0.01	0.01	-6.99
Si	-3.33	1.93	-6.98
Si	0.00	0.01	-9.32
Si	-3.33	1.93	-9.31
Si	-1.11	1.93	-10.07
Si	-4.43	0.01	-10.06
H	-1.12	1.93	-11.57
H	-4.42	0.01	-11.56

Si111BPEPA_2x1_Or1_Start.xyz

C	-1.57	0.95	11.07
C	-2.66	1.60	11.66
C	-0.63	0.34	11.91
C	-2.80	1.67	13.04
C	-0.75	0.40	13.28
C	-1.83	1.09	13.84
H	-3.62	2.23	13.50
H	-0.04	-0.09	13.96
Br	-1.90	1.33	15.68
H	-3.40	2.10	11.01
H	0.22	-0.20	11.47
C	-1.53	0.74	9.64
C	-1.43	0.62	8.24
C	-0.11	-0.30	1.82
C	-1.07	0.37	4.06
C	-2.16	1.02	4.65
C	-0.13	-0.24	4.90
C	-2.30	1.09	6.03
C	-0.26	-0.18	6.28
C	-1.33	0.51	6.84
C	-0.96	0.39	2.62
H	-1.65	1.10	2.13
H	0.57	-1.04	2.28
H	-3.12	1.65	6.49
H	0.46	-0.67	6.95
H	-2.90	1.51	4.00
H	0.72	-0.78	4.46
H	-3.41	1.94	1.44
Si	0.00	0.00	0.00
Si	-3.35	1.93	-0.07
Si	-1.11	1.92	-0.77
Si	-4.46	0.01	-0.81
Si	-4.44	0.01	-3.14
Si	-1.12	1.92	-3.10
Si	1.10	1.93	-3.89
Si	-2.22	0.00	-3.88
Si	1.10	1.93	-6.23
Si	-2.22	0.01	-6.22
Si	-0.01	0.01	-6.99
Si	-3.33	1.93	-6.98
Si	0.00	0.01	-9.32
Si	-3.33	1.93	-9.31
Si	-1.11	1.93	-10.07
Si	-4.43	0.01	-10.06
H	-1.12	1.93	-11.57
H	-4.42	0.01	-11.56

Si111BPEPA_2x1_Or4_Start.xyz

C	0.95	1.57	11.07
C	1.60	2.66	11.66
C	0.34	0.63	11.91
C	1.67	2.80	13.04
C	0.40	0.75	13.28
C	1.09	1.83	13.84
H	2.23	3.62	13.50
H	-0.09	0.04	13.96
Br	1.33	1.90	15.68
H	2.10	3.40	11.01
H	-0.20	-0.22	11.47
C	0.74	1.53	9.64
C	0.62	1.43	8.24
C	-0.30	0.11	1.82
C	0.37	1.07	4.06
C	1.02	2.16	4.65
C	-0.24	0.13	4.90
C	1.09	2.30	6.03
C	-0.18	0.26	6.28
C	0.51	1.33	6.84
C	0.39	0.96	2.62
H	1.10	1.65	2.13
H	-1.04	-0.57	2.28
H	1.65	3.12	6.49
H	-0.67	-0.46	6.95
H	1.51	2.90	4.00
H	-0.78	-0.72	4.46
H	-3.41	1.94	1.44
Si	0.00	0.00	0.00
Si	-3.35	1.93	-0.07
Si	-1.11	1.92	-0.77
Si	-4.46	0.01	-0.81
Si	-4.44	0.01	-3.14
Si	-1.12	1.92	-3.10
Si	1.10	1.93	-3.89
Si	-2.22	0.00	-3.88
Si	1.10	1.93	-6.23
Si	-2.22	0.01	-6.22
Si	-0.01	0.01	-6.99
Si	-3.33	1.93	-6.98
Si	0.00	0.01	-9.32
Si	-3.33	1.93	-9.31
Si	-1.11	1.93	-10.07
Si	-4.43	0.01	-10.06
H	-1.12	1.93	-11.57
H	-4.42	0.01	-11.56

Si111BPEPA_2x1_Or6_Start.xyz

C	1.83	-0.04	11.07
C	3.11	-0.06	11.66
C	0.71	0.02	11.91
C	3.26	-0.05	13.04
C	0.85	0.03	13.28
C	2.13	-0.03	13.84
H	4.25	-0.12	13.50
H	-0.01	0.10	13.96
Br	2.31	-0.21	15.68
H	3.99	-0.12	11.01
H	-0.29	0.06	11.47
C	1.70	0.13	9.64
C	1.55	0.18	8.24
C	-0.06	0.32	1.82
C	1.11	0.22	4.06
C	2.38	0.20	4.65
C	-0.01	0.27	4.90
C	2.54	0.21	6.03
C	0.13	0.29	6.28
C	1.41	0.23	6.84
C	1.02	0.14	2.62
H	1.98	-0.12	2.13
H	-1.02	0.62	2.28
H	3.53	0.13	6.49
H	-0.73	0.35	6.95
H	3.27	0.14	4.00
H	-1.02	0.31	4.46
H	-3.41	1.94	1.44
Si	0.00	0.00	0.00
Si	-3.35	1.93	-0.07
Si	-1.11	1.92	-0.77
Si	-4.46	0.01	-0.81
Si	-4.44	0.01	-3.14
Si	-1.12	1.92	-3.10
Si	1.10	1.93	-3.89
Si	-2.22	0.00	-3.88
Si	1.10	1.93	-6.23
Si	-2.22	0.01	-6.22
Si	-0.01	0.01	-6.99
Si	-3.33	1.93	-6.98
Si	0.00	0.01	-9.32
Si	-3.33	1.93	-9.31
Si	-1.11	1.93	-10.07
Si	-4.43	0.01	-10.06
H	-1.12	1.93	-11.57
H	-4.42	0.01	-11.56

Si111BPEPA_2x1_Or0.xyz

C	-2.00	-0.14	10.83
C	-3.12	0.60	11.28
C	-1.03	-0.53	11.78
C	-3.23	1.00	12.61
C	-1.14	-0.13	13.11
C	-2.22	0.66	13.51
H	-4.06	1.62	12.93
H	-0.38	-0.44	13.84
Br	-2.27	1.34	15.23
H	-3.87	0.91	10.55
H	-0.19	-1.14	11.46
C	-1.85	-0.40	9.46
C	-1.71	-0.47	8.24
C	-0.02	-0.20	1.83
C	-1.16	-0.01	4.06
C	-2.34	0.43	4.70
C	-0.20	-0.68	4.84
C	-2.53	0.25	6.06
C	-0.39	-0.87	6.20
C	-1.55	-0.39	6.84
C	-1.01	0.25	2.65
H	-1.80	0.88	2.21
H	0.76	-0.86	2.26
H	-3.44	0.62	6.55
H	0.37	-1.39	6.79
H	-3.09	0.97	4.11
H	0.72	-1.05	4.37
H	-3.41	1.97	1.45
Si	-0.02	0.01	0.00
Si	-3.36	1.95	-0.06
Si	-1.12	1.93	-0.77
Si	-4.47	0.03	-0.81
Si	-4.44	0.01	-3.14
Si	-1.12	1.92	-3.10
Si	1.10	1.93	-3.89
Si	-2.22	0.00	-3.88
Si	1.10	1.93	-6.23
Si	-2.22	0.01	-6.22
Si	-0.01	0.01	-6.99
Si	-3.33	1.93	-6.98
Si	0.00	0.01	-9.32
Si	-3.33	1.93	-9.31
Si	-1.11	1.93	-10.07
Si	-4.43	0.01	-10.06
H	-1.12	1.93	-11.57
H	-4.42	0.01	-11.56

Si111BPEPA_2x1_Or2.xyz

C	-0.59	2.92	10.62
C	-1.72	3.60	11.11
C	0.55	2.82	11.45
C	-1.71	4.17	12.38
C	0.56	3.40	12.71
C	-0.57	4.08	13.17
H	-2.58	4.73	12.75
H	1.46	3.33	13.34
Br	-0.52	4.91	14.83
H	-2.60	3.70	10.47
H	1.42	2.27	11.08
C	-0.60	2.39	9.32
C	-0.62	1.97	8.16
C	0.11	0.05	1.84
C	-0.63	1.08	4.02
C	-1.66	1.83	4.61
C	0.39	0.59	4.85
C	-1.69	2.08	5.97
C	0.39	0.85	6.21
C	-0.65	1.61	6.80
C	-0.65	0.89	2.59
H	-1.40	1.52	2.07
H	0.83	-0.62	2.34
H	-2.48	2.70	6.41
H	1.19	0.46	6.86
H	-2.45	2.24	3.96
H	1.21	0.00	4.42
H	-3.41	1.94	1.44
Si	0.00	-0.01	0.00
Si	-3.35	1.93	-0.07
Si	-1.11	1.91	-0.77
Si	-4.45	0.01	-0.81
Si	-4.44	0.01	-3.14
Si	-1.12	1.92	-3.10
Si	1.10	1.93	-3.89
Si	-2.22	0.00	-3.88
Si	1.10	1.93	-6.23
Si	-2.22	0.01	-6.22
Si	-0.01	0.01	-6.99
Si	-3.33	1.93	-6.98
Si	0.00	0.01	-9.32
Si	-3.33	1.93	-9.31
Si	-1.11	1.93	-10.07
Si	-4.43	0.01	-10.06
H	-1.12	1.93	-11.57
H	-4.42	0.01	-11.56

Si111BPEPA_2x1_Or5.xyz

C	1.15	2.81	10.48
C	2.33	3.38	10.98
C	-0.03	2.90	11.25
C	2.34	4.04	12.20
C	-0.03	3.57	12.46
C	1.16	4.15	12.94
H	3.25	4.51	12.58
H	-0.95	3.66	13.06
Br	1.15	5.08	14.54
H	3.25	3.32	10.38
H	-0.95	2.44	10.88
C	1.14	2.19	9.21
C	1.15	1.71	8.08
C	-0.04	0.03	1.83
C	1.08	0.50	4.02
C	2.22	1.11	4.58
C	0.00	0.22	4.87
C	2.26	1.48	5.91
C	0.03	0.57	6.21
C	1.15	1.24	6.75
C	1.05	0.25	2.60
H	2.03	0.34	2.10
H	-1.03	-0.01	2.32
H	3.14	2.01	6.32
H	-0.81	0.34	6.87
H	3.08	1.33	3.92
H	-0.87	-0.32	4.48
H	-3.29	1.95	1.45
Si	0.00	-0.04	-0.01
Si	-3.31	1.93	-0.06
Si	-1.09	1.89	-0.78
Si	-4.44	0.01	-0.79
Si	-4.44	0.01	-3.14
Si	-1.12	1.92	-3.10
Si	1.10	1.93	-3.89
Si	-2.22	0.00	-3.88
Si	1.10	1.93	-6.23
Si	-2.22	0.01	-6.22
Si	-0.01	0.01	-6.99
Si	-3.33	1.93	-6.98
Si	0.00	0.01	-9.32
Si	-3.33	1.93	-9.31
Si	-1.11	1.93	-10.07
Si	-4.43	0.01	-10.06
H	-1.12	1.93	-11.57
H	-4.42	0.01	-11.56

Si111BPEPA_2x1_Or1.xyz

	-1.35	-1.35	10.87
C	-2.48	-1.97	11.43
C	-0.43	-0.72	11.73
C	-2.71	-1.93	12.80
C	-0.66	-0.68	13.10
C	-1.81	-1.27	13.63
H	-3.60	-2.41	13.23
H	0.04	-0.15	13.77
Br	-2.14	-1.16	15.45
H	-3.19	-2.49	10.77
H	0.45	-0.22	11.31
C	-1.15	-1.34	9.48
C	-1.01	-1.28	8.25
C	0.10	-0.04	1.84
C	-0.68	-0.99	4.04
C	-1.73	-1.70	4.64
C	0.29	-0.40	4.88
C	-1.85	-1.80	6.02
C	0.19	-0.51	6.26
C	-0.89	-1.20	6.85
C	-0.66	-0.87	2.60
H	-1.37	-1.54	2.09
H	0.79	0.67	2.34
H	-2.66	-2.37	6.47
H	0.94	-0.03	6.90
H	-2.47	-2.19	3.99
H	1.12	0.16	4.44
H	-3.40	1.90	1.44
Si	0.01	0.00	0.00
Si	-3.34	1.91	-0.07
Si	-1.10	1.92	-0.76
Si	-4.45	-0.01	-0.81
Si	-4.44	0.01	-3.14
Si	-1.12	1.92	-3.10
Si	1.10	1.93	-3.89
Si	-2.22	0.00	-3.88
Si	1.10	1.93	-6.23
Si	-2.22	0.01	-6.22
Si	-0.01	0.01	-6.99
Si	-3.33	1.93	-6.98
Si	0.00	0.01	-9.32
Si	-3.33	1.93	-9.31
Si	-1.11	1.93	-10.07
Si	-4.43	0.01	-10.06
H	-1.12	1.93	-11.57
H	-4.42	0.01	-11.56

Si111BPEPA_2x1_Or4.xyz

C	0.76	2.79	10.51
C	1.87	3.43	11.09
C	-0.46	2.79	11.22
C	1.77	4.05	12.33
C	-0.57	3.43	12.45
C	0.55	4.06	13.00
H	2.63	4.57	12.76
H	-1.52	3.44	12.99
Br	0.39	4.95	14.62
H	2.82	3.45	10.54
H	-1.33	2.28	10.78
C	0.85	2.20	9.23
C	0.93	1.73	8.10
C	-0.06	0.02	1.83
C	1.01	0.53	4.04
C	2.11	1.17	4.62
C	-0.09	0.21	4.86
C	2.11	1.54	5.96
C	-0.10	0.57	6.20
C	0.99	1.27	6.77
C	1.01	0.28	2.61
H	2.00	0.40	2.13
H	-1.06	-0.06	2.31
H	2.96	2.09	6.39
H	-0.95	0.31	6.84
H	2.98	1.42	3.99
H	-0.94	-0.34	4.45
H	-3.29	1.95	1.45
Si	0.00	-0.04	-0.01
Si	-3.31	1.92	-0.06
Si	-1.09	1.88	-0.79
Si	-4.44	0.00	-0.79
Si	-4.44	0.01	-3.14
Si	-1.12	1.92	-3.10
Si	1.10	1.93	-3.89
Si	-2.22	0.00	-3.88
Si	1.10	1.93	-6.23
Si	-2.22	0.01	-6.22
Si	-0.01	0.01	-6.99
Si	-3.33	1.93	-6.98
Si	0.00	0.01	-9.32
Si	-3.33	1.93	-9.31
Si	-1.11	1.93	-10.07
Si	-4.43	0.01	-10.06
H	-1.12	1.93	-11.57
H	-4.42	0.01	-11.56

Si111BPEPA_2x1_Or6.xyz

C	1.96	0.00	10.78
C	3.07	-0.74	11.23
C	0.97	0.36	11.72
C	3.16	-1.16	12.55
C	1.06	-0.06	13.04
C	2.14	-0.84	13.45
H	4.00	-1.79	12.88
H	0.29	0.22	13.77
Br	2.18	-1.54	15.16
H	3.84	-1.03	10.50
H	0.12	0.97	11.39
C	1.83	0.31	9.42
C	1.73	0.46	8.20
C	0.01	0.20	1.83
C	1.28	0.27	3.99
C	2.44	-0.22	4.62
C	0.31	0.92	4.78
C	2.60	-0.13	6.00
C	0.47	1.02	6.16
C	1.60	0.47	6.79
C	1.13	0.07	2.57
H	2.06	-0.26	2.06
H	-0.94	0.49	2.33
H	3.48	-0.55	6.48
H	-0.28	1.54	6.76
H	3.20	-0.72	4.02
H	-0.56	1.37	4.30
H	-3.30	1.91	1.45
Si	0.00	0.04	-0.01
Si	-3.32	1.92	-0.06
Si	-1.10	1.95	-0.78
Si	-4.45	0.01	-0.80
Si	-4.44	0.01	-3.14
Si	-1.12	1.92	-3.10
Si	1.10	1.93	-3.89
Si	-2.22	0.00	-3.88
Si	1.10	1.93	-6.23
Si	-2.22	0.01	-6.22
Si	-0.01	0.01	-6.99
Si	-3.33	1.93	-6.98
Si	0.00	0.01	-9.32
Si	-3.33	1.93	-9.31
Si	-1.11	1.93	-10.07
Si	-4.43	0.01	-10.06
H	-1.12	1.93	-11.57
H	-4.42	0.01	-11.56

C.8 Periodic DFT calculations: BrSty/Si(001)

Si100BrSty2x1_Or1_StartTilt0

C	0.27	-0.42	19.18
C	-0.34	-0.44	21.62
C	-1.40	-0.44	22.53
C	0.94	-0.44	22.17
C	-1.22	-0.44	23.94
C	1.13	-0.44	23.58
C	0.06	-0.44	24.45
C	-0.62	-0.42	20.21
H	-1.40	0.58	19.96
H	-1.40	-1.42	19.96
H	1.05	0.58	19.43
H	1.05	-1.42	19.43
H	-2.05	-0.44	24.65
H	2.13	-0.44	23.98
Br	0.38	-0.44	26.28
H	-2.40	-0.44	22.13
H	1.79	-0.44	21.50
H	3.49	0.01	19.11
Si	0.80	0.00	17.48
Si	3.04	0.00	17.48
Si	0.07	1.92	16.50
Si	3.74	1.92	16.53
Si	1.95	1.92	15.04
Si	5.73	1.92	15.28
Si	1.91	0.00	13.77
Si	5.75	0.00	13.93
Si	0.00	0.00	12.57
Si	3.84	0.00	12.57
Si	0.00	1.92	11.21
Si	3.84	1.92	11.21
H	-1.17	1.94	10.32
H	1.10	1.88	10.24
H	4.91	1.91	10.21
H	2.65	1.95	10.36

Si100BrSty2x1_Or1_StartTilt2

C	0.27	-0.42	19.18
C	-0.34	0.79	21.30
C	-1.40	1.24	22.09
C	0.94	1.06	21.78
C	-1.22	1.94	23.31
C	1.13	1.76	23.00
C	0.06	2.20	23.76
C	-0.62	0.09	20.07
H	-1.40	0.84	19.36
H	-1.40	-0.89	20.36
H	1.05	0.57	18.90
H	1.05	-1.16	19.90
H	-2.05	2.29	23.93
H	2.13	1.96	23.35
Br	0.38	3.11	25.34
H	-2.40	1.04	21.75
H	1.79	0.72	21.20
H	3.49	0.01	19.11
Si	0.80	0.00	17.48
Si	3.04	0.00	17.48
Si	0.07	1.92	16.50
Si	3.74	1.92	16.53
Si	1.95	1.92	15.04
Si	5.73	1.92	15.28
Si	1.91	0.00	13.77
Si	5.75	0.00	13.93
Si	0.00	0.00	12.57
Si	3.84	0.00	12.57
Si	0.00	1.92	11.21
Si	3.84	1.92	11.21
H	-1.17	1.94	10.32
H	1.10	1.88	10.24
H	4.91	1.91	10.21
H	2.65	1.95	10.36

Si100BrSty2x1_Or1_Tilt0.xyz

C	0.24	-0.17	19.60
C	-1.70	-0.57	21.23
C	-2.99	-0.27	21.67
C	-0.88	-1.33	22.06
C	-3.47	-0.76	22.88
C	-1.34	-1.83	23.28
C	-2.65	-1.55	23.68
C	-1.25	-0.09	19.87
H	-1.60	0.96	19.73
H	-1.80	-0.67	19.09
H	0.80	0.55	20.24
H	0.63	-1.17	19.87
H	-4.48	-0.51	23.23
H	-0.70	-2.46	23.90
Br	-3.31	-2.30	25.24
H	-3.63	0.39	21.07
H	0.15	-1.57	21.76
H	3.59	-0.01	19.16
Si	0.73	0.02	17.79
Si	3.12	0.01	17.74
Si	0.10	1.94	16.59
Si	3.76	1.92	16.57
Si	1.92	1.92	15.13
Si	5.78	1.92	15.32
Si	1.92	0.00	13.85
Si	5.75	0.00	13.93
Si	0.00	0.00	12.57
Si	3.84	0.00	12.57
Si	0.00	1.92	11.21
Si	3.84	1.92	11.21
H	-1.17	1.94	10.32
H	1.10	1.88	10.24
H	4.91	1.91	10.21
H	2.65	1.95	10.36

Si100BrSty2x1_Or1_Tilt2.xyz

C	0.12	0.23	19.56
C	-1.74	1.35	20.93
C	-3.00	1.95	21.01
C	-0.92	1.38	22.06
C	-3.43	2.58	22.18
C	-1.34	2.01	23.23
C	-2.59	2.62	23.29
C	-1.31	0.75	19.62
H	-1.46	1.52	18.83
H	-2.01	-0.07	19.36
H	0.82	0.98	19.99
H	0.23	-0.69	20.16
H	-4.41	3.08	22.22
H	-0.68	2.04	24.11
Br	-3.12	3.51	24.82
H	-3.66	1.94	20.13
H	0.06	0.88	22.04
H	3.54	0.00	19.18
Si	0.71	0.00	17.78
Si	3.09	-0.01	17.75
Si	0.10	1.91	16.57
Si	3.76	1.91	16.58
Si	1.93	1.93	15.13
Si	5.77	1.92	15.32
Si	1.92	0.01	13.84
Si	5.75	0.00	13.93
Si	0.00	0.00	12.57
Si	3.84	0.00	12.57
Si	0.00	1.92	11.21
Si	3.84	1.92	11.21
H	-1.17	1.94	10.32
H	1.10	1.88	10.24
H	4.91	1.91	10.21
H	2.65	1.95	10.36

Si100BrSty2x1_Or1_StartTilt1

C	0.27	-0.42	19.18
C	-0.34	0.20	21.54
C	-1.40	0.43	22.42
C	0.94	0.34	22.07
C	-1.22	0.79	23.78
C	1.13	0.70	23.44
C	0.06	0.92	24.28
C	-0.62	-0.16	20.17
H	-1.40	0.75	19.68
H	-1.40	-1.18	20.19
H	1.05	0.61	19.16
H	1.05	-1.32	19.68
H	-2.05	0.97	24.47
H	2.13	0.80	23.83
Br	0.38	1.40	26.05
H	-2.40	0.32	22.04
H	1.79	0.16	21.42
H	3.49	0.01	19.11
Si	0.80	0.00	17.48
Si	3.04	0.00	17.48
Si	0.07	1.92	16.50
Si	3.74	1.92	16.53
Si	1.95	1.92	15.04
Si	5.73	1.92	15.28
Si	1.91	0.00	13.77
Si	5.75	0.00	13.93
Si	0.00	0.00	12.57
Si	3.84	0.00	12.57
Si	0.00	1.92	11.21
Si	3.84	1.92	11.21
H	-1.17	1.94	10.32
H	1.10	1.88	10.24
H	4.91	1.91	10.21
H	2.65	1.95	10.36

Si100BrSty2x1_Or1_StartTilt3

C	0.27	-0.42	19.18
C	-0.34	1.29	20.92
C	-1.40	1.93	21.56
C	0.94	1.68	21.31
C	-1.22	2.93	22.56
C	1.13	2.68	22.31
C	0.06	3.29	22.93
C	-0.62	0.30	19.91
H	-1.40	0.84	19.03
H	-1.40	-0.57	20.44
H	1.05	0.46	18.65
H	1.05	-0.95	20.07
H	-2.05	3.43	23.06
H	2.13	2.96	22.60
Br	0.38	4.58	24.22
H	-2.40	1.65	21.29
H	1.79	1.21	20.83
H	3.49	0.01	19.11
Si	0.80	0.00	17.48
Si	3.04	0.00	17.48
Si	0.07	1.92	16.50
Si	3.74	1.92	16.53
Si	1.95	1.92	15.04
Si	5.73	1.92	15.28
Si	1.91	0.00	13.77
Si	5.75	0.00	13.93
Si	0.00	0.00	12.57
Si	3.84	0.00	12.57
Si	0.00	1.92	11.21
Si	3.84	1.92	11.21
H	-1.17	1.94	10.32
H	1.10	1.88	10.24
H	4.91	1.91	10.21
H	2.65	1.95	10.36

Si100BrSty2x1_Or1_Tilt1.xyz

C	0.08	0.14	19.56
C	-1.83	1.13	20.93
C	-3.02	1.87	21.00
C	-1.15	0.88	22.12
C	-3.50	2.37	22.21
C	-1.61	1.37	23.34
C	-2.78	2.13	23.38
C	-1.35	0.64	19.60
H	-1.49	1.46	18.86
H	-2.02	-0.17	19.24
H	0.76	0.86	20.07
H	0.18	-0.82	20.09
H	-4.40	3.00	22.24
H	-1.07	1.16	24.27
Br	-3.34	2.89	24.98
H	-3.57	2.08	20.07
H	-0.23	0.27	22.11
H	3.52	0.03	19.19
Si	0.70	-0.01	17.78
Si	3.08	-0.01	17.75
Si	0.09	1.91	16.57
Si	3.75	1.91	16.58
Si	1.92	1.93	15.13
Si	5.76	1.92	15.32
Si	1.92	0.01	13.85
Si	5.75	0.00	13.93
Si	0.00	0.00	12.57
Si	3.84	0.00	12.57
Si	0.00	1.92	11.21
Si	3.84	1.92	11.21
H	-1.17	1.94	10.32
H	1.10	1.88	10.24
H	4.91	1.91	10.21
H	2.65	1.95	10.36

Si100BrSty2x1_Or1_Tilt3.xyz

C	0.11	0.13	19.56
C	-1.79	1.11	20.97
C	-2.97	1.84	21.06
C	-1.07	0.86	22.14
C	-3.42	2.35	22.28
C	-1.51	1.36	23.37
C	-2.68	2.11	23.43
C	-1.33	0.62	19.63
H	-1.48	1.44	18.89
H	-2.01	-0.19	19.28
H	0.79	0.84	20.07
H	0.22	-0.84	20.09
H	-4.33	2.96	22.33
H	-0.94	1.16	24.29
Br	-3.20	2.87	25.04
H	-3.55	2.05	20.15
H	-0.15	0.26	22.11
H	3.54	0.01	19.19
Si	0.71	-0.02	17.78
Si	3.10	-0.02	17.75
Si	0.10	1.90	16.57
Si	3.76	1.91	16.58
Si	1.93	1.92	15.13
Si	5.77	1.92	15.32
Si	1.92	0.00	13.85
Si	5.75	0.00	13.93
Si	0.00	0.00	12.57
Si	3.84	0.00	12.57
Si	0.00	1.92	11.21
Si	3.84	1.92	11.21
H	-1.17	1.94	10.32
H	1.10	1.88	10.24
H	4.91	1.91	10.21
H	2.65	1.95	10.36

Si100BrSty2x1_Or2_StartTilt0

C	0.27	-0.42	19.18
C	0.88	-0.40	21.62
C	1.94	-0.39	22.53
C	-0.39	-0.39	22.17
C	1.77	-0.39	23.94
C	-0.58	-0.39	23.58
C	0.49	-0.39	24.45
C	1.17	-0.41	20.21
H	1.94	-1.42	19.96
H	1.94	0.58	19.96
H	-0.50	-1.41	19.43
H	-0.50	0.59	19.43
H	2.60	-0.39	24.65
H	-1.58	-0.39	23.98
Br	0.16	-0.39	26.28
H	2.95	-0.39	22.13
H	-1.24	-0.40	21.50
H	3.49	0.01	19.11
Si	0.80	0.00	17.48
Si	3.04	0.00	17.48
Si	0.07	1.92	16.50
Si	3.74	1.92	16.53
Si	1.95	1.92	15.04
Si	5.73	1.92	15.28
Si	1.91	0.00	13.77
Si	5.75	0.00	13.93
Si	0.00	0.00	12.57
Si	3.84	0.00	12.57
Si	0.00	1.92	11.21
Si	3.84	1.92	11.21
H	-1.17	1.94	10.32
H	1.10	1.88	10.24
H	4.91	1.91	10.21
H	2.65	1.95	10.36

Si100BrSty2x1_Or2_StartTilt2

C	0.27	-0.42	19.18
C	0.88	0.82	21.28
C	1.94	1.28	22.07
C	-0.39	1.10	21.76
C	1.77	1.98	23.29
C	-0.58	1.80	22.98
C	0.49	2.24	23.73
C	1.17	0.10	20.07
H	1.94	-0.89	20.36
H	1.94	0.84	19.36
H	-0.50	-1.15	19.90
H	-0.50	0.58	18.90
H	2.60	2.34	23.90
H	-1.58	2.01	23.33
Br	0.16	3.16	25.32
H	2.95	1.08	21.73
H	-1.24	0.76	21.18
H	3.49	0.01	19.11
Si	0.80	0.00	17.48
Si	3.04	0.00	17.48
Si	0.07	1.92	16.50
Si	3.74	1.92	16.53
Si	1.95	1.92	15.04
Si	5.73	1.92	15.28
Si	1.91	0.00	13.77
Si	5.75	0.00	13.93
Si	0.00	0.00	12.57
Si	3.84	0.00	12.57
Si	0.00	1.92	11.21
Si	3.84	1.92	11.21
H	-1.17	1.94	10.32
H	1.10	1.88	10.24
H	4.91	1.91	10.21
H	2.65	1.95	10.36

Si100BrSty2x1_Or2_Tilt0.xyz

C	-0.19	-0.10	19.45
C	-0.14	-1.30	21.70
C	0.52	-2.03	22.70
C	-1.52	-1.10	21.83
C	-0.17	-2.57	23.78
C	-2.22	-1.63	22.91
C	-1.55	-2.38	23.87
C	0.64	-0.78	20.53
H	1.23	-1.62	20.09
H	1.41	-0.06	20.89
H	-1.10	-0.70	19.24
H	-0.55	0.88	19.81
H	0.35	-3.17	24.53
H	-3.30	-1.46	23.00
Br	-2.50	-3.17	25.25
H	1.61	-2.19	22.62
H	-2.05	-0.50	21.09
H	3.61	0.01	19.20
Si	0.67	0.02	17.77
Si	3.08	0.02	17.79
Si	0.11	1.94	16.54
Si	3.74	1.93	16.60
Si	1.94	1.92	15.12
Si	5.76	1.92	15.33
Si	1.92	0.00	13.84
Si	5.75	0.00	13.93
Si	0.00	0.00	12.57
Si	3.84	0.00	12.57
Si	0.00	1.92	11.21
Si	3.84	1.92	11.21
H	-1.17	1.94	10.32
H	1.10	1.88	10.24
H	4.91	1.91	10.21
H	2.65	1.95	10.36

Si100BrSty2x1_Or2_Tilt2.xyz

C	0.00	0.20	19.54
C	0.44	1.45	21.74
C	1.29	2.16	22.60
C	-0.90	1.29	22.11
C	0.81	2.73	23.77
C	-1.39	1.86	23.28
C	-0.54	2.59	24.11
C	1.00	0.89	20.46
H	1.81	0.17	20.71
H	1.52	1.71	19.92
H	-0.33	-0.76	19.98
H	-0.91	0.82	19.43
H	1.47	3.33	24.42
H	-2.44	1.72	23.57
Br	-1.21	3.41	25.63
H	2.35	2.29	22.33
H	-1.57	0.70	21.48
H	3.65	-0.01	19.17
Si	0.70	0.00	17.79
Si	3.11	-0.02	17.77
Si	0.11	1.92	16.57
Si	3.75	1.91	16.58
Si	1.93	1.93	15.12
Si	5.77	1.92	15.33
Si	1.92	0.01	13.84
Si	5.75	0.00	13.93
Si	0.00	0.00	12.57
Si	3.84	0.00	12.57
Si	0.00	1.92	11.21
Si	3.84	1.92	11.21
H	-1.17	1.94	10.32
H	1.10	1.88	10.24
H	4.91	1.91	10.21
H	2.65	1.95	10.36

Si100BrSty2x1_Or2_StartTilt1

C	0.27	-0.42	19.18
C	0.88	0.23	21.53
C	1.94	0.47	22.41
C	-0.39	0.38	22.06
C	1.77	0.84	23.77
C	-0.58	0.75	23.42
C	0.49	0.97	24.27
C	1.17	-0.14	20.17
H	1.94	-1.18	20.19
H	1.94	0.75	19.68
H	-0.50	-1.31	19.68
H	-0.50	0.62	19.16
H	2.60	1.02	24.45
H	-1.58	0.85	23.81
Br	0.16	1.45	26.03
H	2.95	0.37	22.03
H	-1.24	0.20	21.41
H	3.49	0.01	19.11
Si	0.80	0.00	17.48
Si	3.04	0.00	17.48
Si	0.07	1.92	16.50
Si	3.74	1.92	16.53
Si	1.95	1.92	15.04
Si	5.73	1.92	15.28
Si	1.91	0.00	13.77
Si	5.75	0.00	13.93
Si	0.00	0.00	12.57
Si	3.84	0.00	12.57
Si	0.00	1.92	11.21
Si	3.84	1.92	11.21
H	-1.17	1.94	10.32
H	1.10	1.88	10.24
H	4.91	1.91	10.21
H	2.65	1.95	10.36

Si100BrSty2x1_Or2_StartTilt3

C	0.27	-0.42	19.18
C	0.88	1.32	20.89
C	1.94	1.97	21.53
C	-0.39	1.71	21.28
C	1.77	2.97	22.53
C	-0.58	2.71	22.27
C	0.49	3.33	22.89
C	1.17	0.31	19.90
H	1.94	-0.57	20.44
H	1.94	0.84	19.02
H	-0.50	-0.94	20.06
H	-0.50	0.47	18.65
H	2.60	3.47	23.03
H	-1.58	3.00	22.56
Br	0.16	4.62	24.18
H	2.95	1.69	21.25
H	-1.24	1.24	20.80
H	3.49	0.01	19.11
Si	0.80	0.00	17.48
Si	3.04	0.00	17.48
Si	0.07	1.92	16.50
Si	3.74	1.92	16.53
Si	1.95	1.92	15.04
Si	5.73	1.92	15.28
Si	1.91	0.00	13.77
Si	5.75	0.00	13.93
Si	0.00	0.00	12.57
Si	3.84	0.00	12.57
Si	0.00	1.92	11.21
Si	3.84	1.92	11.21
H	-1.17	1.94	10.32
H	1.10	1.88	10.24
H	4.91	1.91	10.21
H	2.65	1.95	10.36

Si100BrSty2x1_Or2_Tilt1.xyz

C	-0.03	0.16	19.54
C	0.43	0.42	22.01
C	1.37	0.66	23.03
C	-0.89	0.83	22.24
C	1.02	1.31	24.20
C	-1.25	1.48	23.41
C	-0.29	1.74	24.39
C	0.87	-0.19	20.72
H	0.95	-1.29	20.83
H	1.90	0.15	20.51
H	-0.99	-0.41	19.57
H	-0.33	1.22	19.62
H	1.77	1.52	24.97
H	-2.28	1.82	23.57
Br	-0.75	2.69	25.91
H	2.41	0.33	22.87
H	-1.65	0.65	21.47
H	3.67	0.00	19.16
Si	0.70	-0.02	17.80
Si	3.11	0.00	17.76
Si	0.11	1.90	16.57
Si	3.75	1.92	16.58
Si	1.93	1.93	15.12
Si	5.77	1.92	15.33
Si	1.92	0.01	13.84
Si	5.75	0.00	13.93
Si	0.00	0.00	12.57
Si	3.84	0.00	12.57
Si	0.00	1.92	11.21
Si	3.84	1.92	11.21
H	-1.17	1.94	10.32
H	1.10	1.88	10.24
H	4.91	1.91	10.21
H	2.65	1.95	10.36

Si100BrSty2x1_Or2_Tilt3.xyz

C	0.05	0.21	19.57
C	0.57	1.46	21.75
C	1.44	2.18	22.57
C	-0.76	1.30	22.17
C	1.01	2.75	23.77
C	-1.20	1.86	23.37
C	-0.32	2.59	24.16
C	1.07	0.90	20.45
H	1.89	0.19	20.67
H	1.58	1.73	19.89
H	-0.26	-0.75	20.02
H	-0.87	0.83	19.47
H	1.69	3.34	24.39
H	-2.24	1.72	23.70
Br	-0.92	3.41	25.71
H	2.49	2.31	22.26
H	-1.45	0.71	21.56
H	3.68	-0.01	19.16
Si	0.71	0.00	17.80
Si	3.12	-0.01	17.76
Si	0.11	1.92	16.58
Si	3.76	1.91	16.57
Si	1.93	1.93	15.13
Si	5.77	1.92	15.33
Si	1.92	0.01	13.84
Si	5.75	0.00	13.93
Si	0.00	0.00	12.57
Si	3.84	0.00	12.57
Si	0.00	1.92	11.21
Si	3.84	1.92	11.21
H	-1.17	1.94	10.32
H	1.10	1.88	10.24
H	4.91	1.91	10.21
H	2.65	1.95	10.36

C.9 Periodic DFT calculations: BPA/Si(001)

Si100BPA2x1_Or1_StartTilt0

C	0.27	-0.42	19.18
C	-0.34	-0.44	21.62
C	-1.40	-0.44	22.53
C	0.94	-0.44	22.17
C	-1.22	-0.44	23.94
C	1.13	-0.44	23.58
C	0.06	-0.44	24.45
C	-0.62	-0.42	20.21
H	-1.70	-0.42	19.96
H	1.35	-0.42	19.43
H	-2.05	-0.44	24.65
H	2.13	-0.44	23.98
Br	0.38	-0.44	26.28
H	-2.40	-0.44	22.13
H	1.79	-0.44	21.50
H	3.49	0.01	19.11
Si	0.80	0.00	17.48
Si	3.04	0.00	17.48
Si	0.07	1.92	16.50
Si	3.74	1.92	16.53
Si	1.95	1.92	15.04
Si	5.73	1.92	15.28
Si	1.91	0.00	13.77
Si	5.75	0.00	13.93
Si	0.00	0.00	12.57
Si	3.84	0.00	12.57
Si	0.00	1.92	11.21
Si	3.84	1.92	11.21
H	-1.17	1.94	10.32
H	1.10	1.88	10.24
H	4.91	1.91	10.21
H	2.65	1.95	10.36

Si100BPA2x1_Or1_StartTilt2

C	0.27	-0.42	19.18
C	-0.34	0.79	21.30
C	-1.40	1.24	22.09
C	0.94	1.06	21.78
C	-1.22	1.94	23.31
C	1.13	1.76	23.00
C	0.06	2.20	23.76
C	-0.62	0.09	20.07
H	-1.70	-0.03	19.86
H	1.35	-0.30	19.40
H	-2.05	2.29	23.93
H	2.13	1.96	23.35
Br	0.38	3.11	25.34
H	-2.40	1.04	21.75
H	1.79	0.72	21.20
H	3.49	0.01	19.11
Si	0.80	0.00	17.48
Si	3.04	0.00	17.48
Si	0.07	1.92	16.50
Si	3.74	1.92	16.53
Si	1.95	1.92	15.04
Si	5.73	1.92	15.28
Si	1.91	0.00	13.77
Si	5.75	0.00	13.93
Si	0.00	0.00	12.57
Si	3.84	0.00	12.57
Si	0.00	1.92	11.21
Si	3.84	1.92	11.21
H	-1.17	1.94	10.32
H	1.10	1.88	10.24
H	4.91	1.91	10.21
H	2.65	1.95	10.36

Si100BPA2x1_Or1_Tilt0.xyz

C	0.04	-0.12	19.53
C	-1.55	-1.25	21.13
C	-2.71	-2.03	21.20
C	-0.95	-0.84	22.33
C	-3.24	-2.42	22.43
C	-1.46	-1.23	23.56
C	-2.60	-2.04	23.60
C	-0.99	-0.95	19.82
H	-1.46	-1.52	19.00
H	0.49	0.49	20.33
H	-4.11	-3.09	22.47
H	-0.99	-0.90	24.49
Br	-3.19	-2.71	25.23
H	-3.18	-2.37	20.27
H	-0.05	-0.20	22.30
H	3.63	-0.03	19.20
Si	0.70	0.01	17.81
Si	3.11	0.00	17.79
Si	0.12	1.93	16.59
Si	3.75	1.92	16.60
Si	1.93	1.92	15.13
Si	5.77	1.92	15.36
Si	1.92	0.00	13.84
Si	5.76	0.00	13.97
Si	0.00	0.00	12.57
Si	3.84	0.00	12.57
Si	0.00	1.92	11.21
Si	3.84	1.92	11.21
H	-1.17	1.94	10.32
H	1.10	1.88	10.24
H	4.91	1.91	10.21
H	2.65	1.95	10.36

Si100BPA2x1_Or1_Tilt2.xyz

C	0.00	0.11	19.52
C	-1.67	1.21	21.06
C	-2.83	1.99	21.07
C	-1.14	0.78	22.29
C	-3.44	2.37	22.26
C	-1.74	1.16	23.49
C	-2.88	1.97	23.47
C	-1.04	0.93	19.78
H	-1.48	1.50	18.94
H	0.44	-0.50	20.33
H	-4.32	3.03	22.25
H	-1.33	0.82	24.45
Br	-3.57	2.63	25.06
H	-3.25	2.34	20.11
H	-0.25	0.14	22.31
H	3.61	0.04	19.20
Si	0.70	-0.01	17.81
Si	3.09	0.00	17.78
Si	0.11	1.90	16.58
Si	3.75	1.92	16.60
Si	1.93	1.92	15.13
Si	5.77	1.92	15.36
Si	1.92	0.00	13.84
Si	5.76	0.00	13.97
Si	0.00	0.00	12.57
Si	3.84	0.00	12.57
Si	0.00	1.92	11.21
Si	3.84	1.92	11.21
H	-1.17	1.94	10.32
H	1.10	1.88	10.24
H	4.91	1.91	10.21
H	2.65	1.95	10.36

Si100BPA2x1_Or1_StartTilt1

C	0.27	-0.42	19.18
C	-0.34	0.20	21.54
C	-1.40	0.43	22.42
C	0.94	0.34	22.07
C	-1.22	0.79	23.78
C	1.13	0.70	23.44
C	0.06	0.92	24.28
C	-0.62	-0.16	20.17
H	-1.70	-0.22	19.93
H	1.35	-0.36	19.42
H	-2.05	0.97	24.47
H	2.13	0.80	23.83
Br	0.38	1.40	26.05
H	-2.40	0.32	22.04
H	1.79	0.16	21.42
H	3.49	0.01	19.11
Si	0.80	0.00	17.48
Si	3.04	0.00	17.48
Si	0.07	1.92	16.50
Si	3.74	1.92	16.53
Si	1.95	1.92	15.04
Si	5.73	1.92	15.28
Si	1.91	0.00	13.77
Si	5.75	0.00	13.93
Si	0.00	0.00	12.57
Si	3.84	0.00	12.57
Si	0.00	1.92	11.21
Si	3.84	1.92	11.21
H	-1.17	1.94	10.32
H	1.10	1.88	10.24
H	4.91	1.91	10.21
H	2.65	1.95	10.36

Si100BPA2x1_Or1_StartTilt3

C	0.27	-0.42	19.18
C	-0.34	1.29	20.92
C	-1.40	1.93	21.56
C	0.94	1.68	21.31
C	-1.22	2.93	22.56
C	1.13	2.68	22.31
C	0.06	3.29	22.93
C	-0.62	0.30	19.91
H	-1.70	0.13	19.73
H	1.35	-0.24	19.36
H	-2.05	3.43	23.06
H	2.13	2.96	22.60
Br	0.38	4.58	24.22
H	-2.40	1.65	21.29
H	1.79	1.21	20.83
H	3.49	0.01	19.11
Si	0.80	0.00	17.48
Si	3.04	0.00	17.48
Si	0.07	1.92	16.50
Si	3.74	1.92	16.53
Si	1.95	1.92	15.04
Si	5.73	1.92	15.28
Si	1.91	0.00	13.77
Si	5.75	0.00	13.93
Si	0.00	0.00	12.57
Si	3.84	0.00	12.57
Si	0.00	1.92	11.21
Si	3.84	1.92	11.21
H	-1.17	1.94	10.32
H	1.10	1.88	10.24
H	4.91	1.91	10.21
H	2.65	1.95	10.36

Si100BPA2x1_Or1_Tilt1.xyz

C	0.03	0.12	19.51
C	-1.58	1.23	21.10
C	-2.74	2.01	21.15
C	-1.01	0.81	22.31
C	-3.31	2.39	22.36
C	-1.56	1.18	23.53
C	-2.70	1.99	23.55
C	-1.00	0.95	19.80
H	-1.45	1.53	18.97
H	0.48	-0.50	20.31
H	-4.18	3.05	22.39
H	-1.11	0.85	24.47
Br	-3.33	2.64	25.17
H	-3.19	2.37	20.21
H	-0.11	0.18	22.30
H	3.63	0.05	19.20
Si	0.71	0.00	17.80
Si	3.11	0.01	17.78
Si	0.12	1.91	16.58
Si	3.76	1.93	16.60
Si	1.94	1.93	15.13
Si	5.78	1.93	15.35
Si	1.92	0.01	13.84
Si	5.76	0.00	13.97
Si	0.00	0.00	12.57
Si	3.84	0.00	12.57
Si	0.00	1.92	11.21
Si	3.84	1.92	11.21
H	-1.17	1.94	10.32
H	1.10	1.88	10.24
H	4.91	1.91	10.21
H	2.65	1.95	10.36

Si100BPA2x1_Or1_Tilt3.xyz

C	0.02	0.10	19.51
C	-1.62	1.19	21.09
C	-2.78	1.97	21.15
C	-1.07	0.74	22.30
C	-3.36	2.33	22.36
C	-1.63	1.09	23.52
C	-2.77	1.91	23.55
C	-1.03	0.92	19.80
H	-1.48	1.50	18.97
H	0.46	-0.51	20.32
H	-4.23	3.00	22.39
H	-1.21	0.73	24.47
Br	-3.41	2.54	25.17
H	-3.22	2.34	20.21
H	-0.18	0.09	22.29
H	3.62	0.03	19.20
Si	0.70	-0.01	17.81
Si	3.10	0.00	17.79
Si	0.11	1.90	16.58
Si	3.75	1.92	16.60
Si	1.94	1.92	15.13
Si	5.77	1.92	15.36
Si	1.92	0.00	13.85
Si	5.76	0.00	13.97
Si	0.00	0.00	12.57
Si	3.84	0.00	12.57
Si	0.00	1.92	11.21
Si	3.84	1.92	11.21
H	-1.17	1.94	10.32
H	1.10	1.88	10.24
H	4.91	1.91	10.21
H	2.65	1.95	10.36

Si100BPA2x1_Or2_StartTilt0

C	0.27	-0.42	1
C	0.88	-0.40	2
C	1.94	-0.39	2
C	-0.39	-0.39	2
C	1.77	-0.39	2
C	-0.58	-0.39	2
C	0.49	-0.39	2
C	1.17	-0.41	2
H	2.24	-0.42	1
H	-0.80	-0.41	1
H	2.60	-0.39	2
H	-1.58	-0.39	2
Br	0.16	-0.39	2
H	2.95	-0.39	2
H	-1.24	-0.40	2
H	3.49	0.01	1
Si	0.80	0.00	1
Si	3.04	0.00	1
Si	0.07	1.92	1
Si	3.74	1.92	1
Si	1.95	1.92	1
Si	5.73	1.92	1
Si	1.91	0.00	1
Si	5.75	0.00	1
Si	0.00	0.00	1
Si	3.84	0.00	1
Si	0.00	1.92	1
Si	3.84	1.92	1
H	-1.17	1.94	1
H	1.10	1.88	1
H	4.91	1.91	1
H	2.65	1.95	1

Si100BPA2x1_Or2_StartTilt2

C	0.27	-0.42	1
C	0.88	0.82	2
C	1.94	1.28	2
C	-0.39	1.10	2
C	1.77	1.98	2
C	-0.58	1.80	2
C	0.49	2.24	2
C	1.17	0.10	2
H	2.24	-0.03	1
H	-0.80	-0.29	1
H	2.60	2.34	2
H	-1.58	2.01	2
Br	0.16	3.16	2
H	2.95	1.08	2
H	-1.24	0.76	2
H	3.49	0.01	1
Si	0.80	0.00	1
Si	3.04	0.00	1
Si	0.07	1.92	1
Si	3.74	1.92	1
Si	1.95	1.92	1
Si	5.73	1.92	1
Si	1.91	0.00	1
Si	5.75	0.00	1
Si	0.00	0.00	1
Si	3.84	0.00	1
Si	0.00	1.92	1
Si	3.84	1.92	1
H	-1.17	1.94	1
H	1.10	1.88	1
H	4.91	1.91	1
H	2.65	1.95	1

Si100BPA2x1_Or2_Tilt0.xyz

C	-0.01	-0.11	1
C	-0.09	-1.30	2
C	0.65	-2.08	2
C	-1.41	-0.96	2
C	0.10	-2.52	2
C	-1.98	-1.40	2
C	-1.22	-2.19	2
C	0.51	-0.93	2
H	1.49	-1.41	2
H	-0.98	0.39	1
H	0.66	-3.18	2
H	-3.00	-1.13	2
Br	-2.01	-2.90	2
H	1.67	-2.38	2
H	-2.01	-0.34	2
H	3.64	0.00	1
Si	0.71	0.04	1
Si	3.11	0.00	1
Si	0.11	1.96	1
Si	3.75	1.92	1
Si	1.93	1.92	1
Si	5.77	1.92	1
Si	1.92	0.00	1
Si	5.76	0.00	1
Si	0.00	0.00	1
Si	3.84	0.00	1
Si	0.00	1.92	1
Si	3.84	1.92	1
H	-1.17	1.94	1
H	1.10	1.88	1
H	4.91	1.91	1
H	2.65	1.95	1

Si100BPA2x1_Or2_Tilt2.xyz

C	0.05	0.28	19.50
C	0.35	1.27	21.79
C	1.29	1.62	22.78
C	-0.99	1.63	22.01
C	0.92	2.32	23.92
C	-1.37	2.33	23.14
C	-0.41	2.69	24.09
C	0.81	0.65	20.57
H	1.91	0.55	20.49
H	-1.05	0.37	19.58
H	1.67	2.60	24.67
H	-2.41	2.63	23.29
Br	-0.91	3.68	25.58
H	2.34	1.34	22.62
H	-1.74	1.38	21.25
H	3.70	-0.01	19.19
Si	0.73	-0.03	17.82
Si	3.13	-0.01	17.79
Si	0.12	1.89	16.60
Si	3.76	1.91	16.59
Si	1.93	1.93	15.13
Si	5.78	1.91	15.36
Si	1.92	0.01	13.84
Si	5.76	0.00	13.97
Si	0.00	0.00	12.57
Si	3.84	0.00	12.57
Si	0.00	1.92	11.21
Si	3.84	1.92	11.21
H	-1.17	1.94	10.32
H	1.10	1.88	10.24
H	4.91	1.91	10.21
H	2.65	1.95	10.36

Si100BPA2x1_Or2_StartTilt1

C	0.27	-0.42	1
C	0.88	0.23	2
C	1.94	0.47	2
C	-0.39	0.38	2
C	1.77	0.84	2
C	-0.58	0.75	2
C	0.49	0.97	2
C	1.17	-0.14	2
H	2.24	-0.21	1
H	-0.80	-0.35	1
H	2.60	1.02	2
H	-1.58	0.85	2
Br	0.16	1.45	2
H	2.95	0.37	2
H	-1.24	0.20	2
H	3.49	0.01	1
Si	0.80	0.00	1
Si	3.04	0.00	1
Si	0.07	1.92	1
Si	3.74	1.92	1
Si	1.95	1.92	1
Si	5.73	1.92	1
Si	1.91	0.00	1
Si	5.75	0.00	1
Si	0.00	0.00	1
Si	3.84	0.00	1
Si	0.00	1.92	1
Si	3.84	1.92	1
H	-1.17	1.94	1
H	1.10	1.88	1
H	4.91	1.91	1
H	2.65	1.95	1

Si100BPA2x1_Or2_StartTilt3

C	0.27	-0.42	1
C	0.88	1.32	2
C	1.94	1.97	2
C	-0.39	1.71	2
C	1.77	2.97	2
C	-0.58	2.71	2
C	0.49	3.33	2
C	1.17	0.31	1
H	2.24	0.14	1
H	-0.80	-0.24	1
H	2.60	3.47	2
H	-1.58	3.00	2
Br	0.16	4.62	2
H	2.95	1.69	2
H	-1.24	1.24	2
H	3.49	0.01	1
Si	0.80	0.00	1
Si	3.04	0.00	1
Si	0.07	1.92	1
Si	3.74	1.92	1
Si	1.95	1.92	1
Si	5.73	1.92	1
Si	1.91	0.00	1
Si	5.75	0.00	1
Si	0.00	0.00	1
Si	3.84	0.00	1
Si	0.00	1.92	1
Si	3.84	1.92	1
H	-1.17	1.94	1
H	1.10	1.88	1
H	4.91	1.91	1
H	2.65	1.95	1

Si100BPA2x1_Or2_Tilt1.xyz

C	0.06	0.28	1
C	0.41	1.03	2
C	1.30	1.04	2
C	-0.84	1.64	2
C	0.98	1.65	2
C	-1.19	2.25	2
C	-0.27	2.26	2
C	0.83	0.46	2
H	1.90	0.22	2
H	-1.02	0.50	1
H	1.69	1.67	2
H	-2.15	2.76	2
Br	-0.69	3.15	2
H	2.28	0.55	2
H	-1.55	1.69	2
H	3.70	0.00	1
Si	0.73	-0.02	1
Si	3.13	-0.01	1
Si	0.12	1.90	1
Si	3.75	1.91	1
Si	1.93	1.93	1
Si	5.78	1.92	1
Si	1.92	0.01	1
Si	5.76	0.00	1
Si	0.00	0.00	1
Si	3.84	0.00	1
Si	0.00	1.92	1
Si	3.84	1.92	1
H	-1.17	1.94	1
H	1.10	1.88	1
H	4.91	1.91	1
H	2.65	1.95	1

Si100BPA2x1_Or2_Tilt3.xyz

C	0.02	0.27	19.49
C	0.29	1.27	21.78
C	1.22	1.62	22.77
C	-1.06	1.61	21.99
C	0.84	2.32	23.91
C	-1.45	2.31	23.12
C	-0.50	2.68	24.08
C	0.76	0.66	20.56
H	1.86	0.59	20.48
H	-1.08	0.32	19.56
H	1.57	2.61	24.67
H	-2.50	2.60	23.27
Br	-1.02	3.67	25.55
H	2.27	1.35	22.63
H	-1.81	1.35	21.23
H	3.68	0.00	19.19
Si	0.72	-0.03	17.82
Si	3.12	-0.01	17.79
Si	0.11	1.89	16.59
Si	3.75	1.92	16.59
Si	1.93	1.93	15.13
Si	5.77	1.92	15.35
Si	1.92	0.01	13.84
Si	5.76	0.00	13.97
Si	0.00	0.00	12.57
Si	3.84	0.00	12.57
Si	0.00	1.92	11.21
Si	3.84	1.92	11.21
H	-1.17	1.94	10.32
H	1.10	1.88	10.24
H	4.91	1.91	10.21
H	2.65	1.95	10.36

Si100BPA2x1_D-Bridge_Start.xyz

C	1.27	-0.42	19.18
C	3.43	-0.40	20.47
C	4.82	-0.39	20.37
C	2.92	-0.39	21.76
C	5.69	-0.39	21.49
C	3.78	-0.39	22.89
C	5.15	-0.39	22.76
C	2.63	-0.41	19.27
H	2.72	-1.42	19.34
H	0.69	-1.41	19.62
H	0.69	0.59	19.62
H	6.78	-0.39	21.40
H	3.36	-0.39	23.89
Br	6.22	-0.39	24.28
H	5.25	-0.39	19.37
H	1.84	-0.40	21.89
Si	0.80	0.00	17.48
Si	3.04	0.00	17.48
Si	0.07	1.92	16.50
Si	3.74	1.92	16.53
Si	1.95	1.92	15.04
Si	5.73	1.92	15.28
Si	1.91	0.00	13.77
Si	5.75	0.00	13.93
Si	0.00	0.00	12.57
Si	3.84	0.00	12.57
Si	0.00	1.92	11.21
Si	3.84	1.92	11.21
H	-1.17	1.94	10.32
H	1.10	1.88	10.24
H	4.91	1.91	10.21
H	2.65	1.95	10.36

Si100BPA2x1_S-Bridge_Start.xyz

C	1.97	-0.42	19.18
C	1.99	-1.03	21.62
C	3.05	-1.02	22.53
C	0.72	-1.02	22.17
C	2.88	-1.02	23.94
C	0.53	-1.02	23.58
C	1.60	-1.02	24.45
C	1.98	-1.31	20.21
H	0.98	-1.89	19.96
H	2.98	-1.89	19.96
H	1.98	0.66	19.43
H	3.70	-1.02	24.65
H	-0.47	-1.02	23.98
Br	1.27	-1.02	26.28
H	4.06	-1.02	22.13
H	-0.14	-1.03	21.50
Si	0.80	0.00	17.48
Si	3.04	0.00	17.48
Si	0.07	1.92	16.50
Si	3.74	1.92	16.53
Si	1.95	1.92	15.04
Si	5.73	1.92	15.28
Si	1.91	0.00	13.77
Si	5.75	0.00	13.93
Si	0.00	0.00	12.57
Si	3.84	0.00	12.57
Si	0.00	1.92	11.21
Si	3.84	1.92	11.21
H	-1.17	1.94	10.32
H	1.10	1.88	10.24
H	4.91	1.91	10.21
H	2.65	1.95	10.36

Si100BPA2x1_D-Bridge1.xyz

C	1.37	0.26	19.64
C	3.86	0.65	20.33
C	5.13	0.91	19.78
C	3.61	1.13	21.62
C	6.10	1.62	20.47
C	4.58	1.82	22.34
C	5.83	2.06	21.76
C	2.86	-0.10	19.52
H	2.99	-1.18	19.75
H	0.82	-0.26	20.45
H	1.26	1.35	19.83
H	7.06	1.84	19.99
H	4.38	2.20	23.35
Br	7.17	2.98	22.68
H	5.35	0.56	18.76
H	2.62	0.96	22.07
Si	0.78	0.02	17.80
Si	3.11	-0.04	17.62
Si	0.08	1.93	16.65
Si	3.79	1.89	16.52
Si	1.90	1.93	15.15
Si	5.80	1.92	15.33
Si	1.91	0.01	13.86
Si	5.77	0.00	13.95
Si	0.00	0.00	12.57
Si	3.84	0.00	12.57
Si	0.00	1.92	11.21
Si	3.84	1.92	11.21
H	-1.17	1.94	10.32
H	1.10	1.88	10.24
H	4.91	1.91	10.21
H	2.65	1.95	10.36

Si100BPA2x1_S-Bridge1.xyz

C	1.96	0.13	19.20
C	1.62	0.17	21.72
C	2.63	0.59	22.59
C	0.30	0.53	22.00
C	2.34	1.35	23.72
C	-0.01	1.30	23.12
C	1.01	1.71	23.98
C	1.94	-0.66	20.51
H	1.17	-1.46	20.46
H	2.90	-1.17	20.67
H	2.03	1.21	19.40
H	3.13	1.67	24.40
H	-1.04	1.58	23.34
Br	0.61	2.70	25.49
H	3.67	0.29	22.39
H	-0.50	0.18	21.33
Si	0.76	0.00	17.73
Si	3.11	-0.05	17.69
Si	0.13	1.92	16.61
Si	3.75	1.87	16.59
Si	1.93	1.91	15.13
Si	5.78	1.93	15.37
Si	1.92	-0.01	13.84
Si	5.76	0.00	13.97
Si	0.00	0.00	12.57
Si	3.84	0.00	12.57
Si	0.00	1.92	11.21
Si	3.84	1.92	11.21
H	-1.17	1.94	10.32
H	1.10	1.88	10.24
H	4.91	1.91	10.21
H	2.65	1.95	10.36

Appendix D: XSW data collection and analysis

D.1 X-ray fluorescence detector system

The energy dispersive X-ray fluorescence system is part of the equipment control and data acquisition systems. Parts of the experiments presented in this thesis work used a single element Ge UltraLEGe (Canberra) or multi-element Ultra Low Energy Ge (UltraLeGe) detectors, while the other measurements used a 50 mm^2 Vortex EX Si drift-diode (SDD) detector (SII NanoTechnology USA). For establishing the interface between the detector and the computer, the older Canberra detectors used a PCAIII card or a XIA DXP2X unit (details described in Zhan Zhang's thesis[12]) as a multichannel analyzer (MCA), while the newer Vortex detector (with its dedicated XIA unit) used "Experimental Physics and Industrial Control System (EPICS) " developed at APS at Argonne National Laboratory. The details of the EPICS system can be found from the website "http://www.aps.anl.gov/epics/". A typical XRF detector system setup is shown in Fig D.1.

Since the driver that came with the Vortex detector (from SII) is Windows-based, an EPICS program, START_IOC.bat, needs to run on a Windows computer to control the Vortex unit via a USB cable. The EPICS program, with its operating commands built in, can directly control the detector unit. This substitutes for the program that came from SII with its detector. The EPICS program also creates a communication channel so the commands sent out from the SPEC computer via the internet, e.g. ct or dscan, can arrive at the Windows computer and trigger data collection on the Vortex detector. The collected data are then sent back to the SPEC

computer via the Internet. A specific name has to be assigned to the detector in the EPICS program so it can be found on the network.

For the SPEC computer, in order to store the collected data from the detector, a pseudo counter called “vortot” has to be assigned within SPEC. Additional pseudo counters can also be set up in SPEC to store other useful information, such as input count rate (ICR), output count rate (OCR), livetime (LT), realtime (RT) and several single channel analyzers (SCA), but are not required for operating the detector. A SPEC macro “vortexnew.mac” contains a group of SPEC macros that can be individually used to control the Vortex detector (this ensemble macro has to be loaded into SPEC). Some of the important macros included in the vortexnew.mac are (1) vortex_add: to hook up vortex, (2) vortex_delete: to remove the vortex (it can save the scanning time if the XRF spectra are not necessary), (3) vortex_on: enable the counter vortot, (4) vortex_off: disable the counter vortot, (5) vortexfile_on: to save the XRF spectrum for each scan. Be aware that whenever the macro “vortex_add” is executed, the settings for the vortex detector (e.g. peaking time, threshold) will be changed back to the default values. More details can be found from the notes in the macro.

Although the macro vortexnew.mac handles all the communications between the LINUX-SPEC computer and the Windows-Vortex computer, an additional macro, xswdxp_Vortex.mac is required to simultaneously control the motors and record the readings from both the motors and counters (including the XRF spectra) for a XSW scan. Once the xswdxp_Vortex.mac macro is loaded, a SPEC command “xswdxp” will be able to initiate the XSW scan. The difference of this macro with the previous XSW macro (described in Zhang’s

thesis) is that the collection of the XRF spectra is changed from using the PCAIII/DXP2X interface to EPICS addresses. More details can be found in the macro file.

Because the control of the Vortex detector is through the internet, it is possible that the data collection time for each scan does not accurately correspond to the command due to the traffic in the network. Synchronizing the precise start and stop counting of the Vortex with all other counters is accomplished by sending a gate signal from the down-counter (Joerger VSC-16 VME unit) to the gate input of the Vortex control unit. A XRF spectrum is then only collected when the EPICS program receives the command from the SPEC computer and the gate voltage is on.

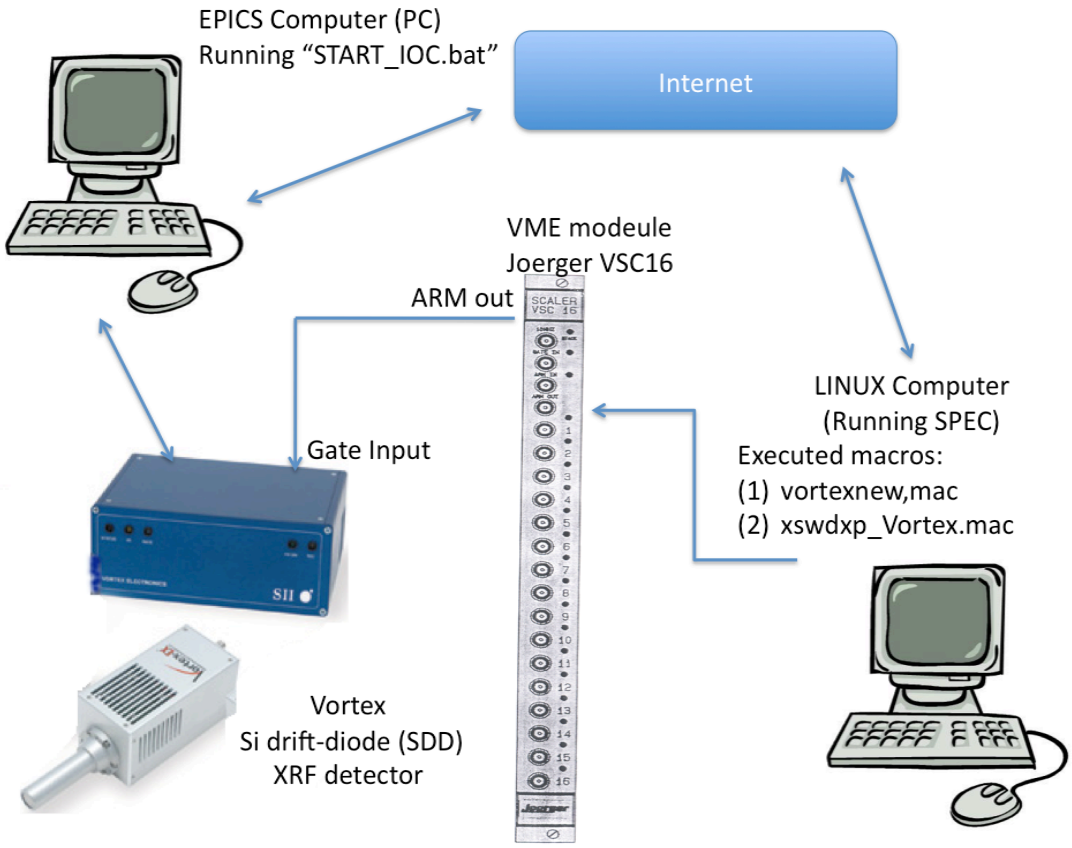

Figure D.1 A typical XRF detector system setup using EPICS.

D.2 XSW analysis

D.2.1 Data processing

Once the XSW file is saved, the raw data can be processed using a MATLAB GUI program SUGOM. The first version of SUGOM was developed by Joseph Libera in the group to handle the LSM and TER XSW data collected at ESRF, X15A (Brookhaven National Lab) and 5ID-C (APS). Three new versions of SUGOM were developed for this thesis work, based on the original version, to handle the single crystal XSW data collected at 5ID-C, 33ID-D and 33BM-C stations at APS (SUGOM program needs to be modified if the data file format is changed). The three programs are named SUGOM5IDC, SUGOM33IDD, and SUGOM33BMC, respectively, and stored in my thesis DVD. The difference between the three programs and the original Libera version is the part that handles the "read in" of the SPEC file. The details for the algorithm can be found in Libera's thesis.[68] The output from the SUGOM program is a spreadsheet file including motors' positions (first two columns). Columns 3 to 26 contain accumulated counts from single channel counters plus the calculated reflectivity and livetime fraction (LTF). After column 26 comes a set of 2N columns, which are the calculated XRF yield for a series of N selected XRF peaks along with their error. These yields are normalized to the incident beam monitor counts and are divided by the LTF. Lastly comes a set of 2N columns that hold the uncorrected XRF net counts paired with the corresponding uncertainty. Note that SUGOM labels the columns. There is no restriction on the number of rows, i.e. the number of steps in the scan

D.2.2 Single crystal XSW analysis

A Matlab program for analyzing Bragg-reflection XSW data was developed based on the previous Fortran program "SWAN" and Matlab program "sugomat" in the group. The program

SWAN was written by Likwan Cheng[13] based on the earlier program DARE (developed by M. Bedzyk and J. Zegenhagen in 1986) and further modified by Anathony Escuadro.[14] The program sugomat is an XSW analysis program developed by Zhan Zhang.

The program SWAM basically uses the identical algorithm as that used in the Fortran program SWAN. For better understanding the program, it may be helpful to study SWAM along with SWAN. Because computer power improvements, some of the codes were re-written (e.g. the use of loops was reduced) so it is easier to be understood and modified in the future. In the program SWAM, the atomic scattering factors are calculated analytically using the method presented by Wasmaier & Kirfel (Acta Crystallographica, 1995, A51, 416-431). SWAM can also calculate some physical parameters such as Bragg angles, structure factors, and ideal Darwin widths for a given crystal under a chosen dynamical diffraction condition. Most importantly, the program (currently version v2) calculates and convolutes the reflectivity curves from an ideal 2-bounce monochromator and a sample and fits the convolution result to the experimental rocking curve data. The result of the reflectivity fit is then used to perform a fit of the theoretical fluorescence yield to the experimental fluorescence yield data in order to obtain the resulting coherent position, coherent fraction, and off-Bragg normalized fluorescence yield. The previous version of SWAM (v1) used a 1-bounce monochromator in the calculation.

SWAM is a Matlab based program and is therefore independent of the operating system (Mac, PC, LINUX). Once Matlab is open, simply key in “SWAM” at the command line (when the working folder is at the SWAM program folder) and the program will start. The instructions are self-explanatory and are given step-by-step so no manuals will be needed. Both the formats of the input data files, an XRR file and an XRF file, are (X,Y,ΔY) three-column data, separated

by 'Tab', after the comments rows (begin with #, the number of comment rows are not limited). The first column is for the angular step number, the second column is for the experimental reflectivity (XRR) or XRF yield and the third column is the error. Examples for a XRR and a XRF file are shown in Fig D.2. The XRR and XRF files can be obtained by cutting the output spreadsheet file from SUGOM using the program KaleidaGraph. The three functions in SWAM are: (1) **cr**: Compute the physical parameters for a single crystal dynamical diffraction condition, (2) **r0**: Calculate and fit the rocking curve, and (3) **f1**: Calculate and fit the fluorescence yield. The computing algorithms for cr, r0 and f1 are shown in the flowcharts in Fig D.3, D.4 and D.5, respectively.

D.2.3 Guide to .ctl file

The crystal structure data input files for SWAM are exactly identical to that used in SWAN. Each file is given the extension name '.ctl' and contains the information of the crystal lattice. A crystal can have two different .ctl files depending on the choice of the origin, and the output coherent positions P_H from the program SWAM will be changed accordingly. As an example, two ctl files based on two different origins for Si are shown in Fig D.6. The format of the .ctl file is shown as the following:[13]

Line 1: Title of file (Comment line)

Line 2: a, b, c, α, β, γ. (Crystal lattice constants in Å and degree, at 293K)

Line 3: Crystal Debye temperature (K)

Line 4: Linear coefficients of thermal expansion along principle axes, in units of 10^{-6}/deg

Line 5: N N1 (N2 N3 …NN). (N: Number of basis in the unit cell, N1: Number of atom types occupying the first basis, .., NN: Number of atom types occupying the Nth

basis.)

Line 6: Comment line

Line (6 + 1): (Format specific: 2x, a4, 2x, i2, 2x, f5.3). Elemental symbol, (ionization state if ionized), atomic number, occupation fraction. (Write this line N1 times.)

Line (6 + 2): M (Number of atom sites for the current basis).

Line (6 + 2 + 1): to Line (6 + 2 + M): x(1), y(1), z(1); x(2), y(2), z(2); …; x(M), y(M), z(M). (Atomic coordinates for the current basis)

Continue with basis N2, N3, …, by repeating Line 6 through Line (6 + 2 + M)

D.2.4 Guides to some important subroutines

(a) leasqrpf.m

The subroutine leasqrpf.m performs the χ^2 fitting in both the programs SUGOM and SWAM. In SUGOM, leasqrpf.m fits the XRF spectrum using a single or multiple Gaussian functions simultaneously with a linear background. In SWAM, leasqrpf.m fits the theoretically calculated, convoluted, rocking curve and fluorescence yield functions to the experimental data. leasqrpf.m is a Matlab fitting routine initially developed by Dr. Richard I. Shrager and the version used in both SUGOM and SWAM is the version 3.beta, which was lastly modified by Dr. Ray Muzic. The program returns both the correlation matrix and the standard deviation of the parameter estimates. The later is used in both SUGOM and SWAM to determine the error bars of the fitting results. More details about the routine can be found in the file itself.

(b) RC.m and RC2bounce.m

The dynamical diffraction theory based subroutines RC.m and RC2bounce.m are respectively used to calculate the emittance functions from a one-bounce and a two-bounce crystal. In RC2bounce.m, it is assumed that the two crystals are identical and in perfect +/- nondispersive alignment, with no detune. It is used to calculate the emittance function from a double bounce channel-cut upstream. If in the future a more complicated system is considered, e.g. a monochromator with a pair of detuned two-bounce channel-cuts, the subroutine RC2bounce.m will need to be modified accordingly. SWAM also uses subroutine RC.m for calculating the sample crystal acceptance function, since it is a one-bounce case.

(c) calcref.m

The dynamical diffraction theory based subroutine calcref.m, which replaces WAR.f in SWAN, is a routine used to calculate the complex E-field amplitude ratio for a single crystal at a given normalized angle eta.

(d) calcf.m

Given the lattice structure, diffraction plane and energy, the structure factor of a single crystal is calculated accordingly. The database used to calculate the structure factors (e.g. f', f", …) for each individual atom is defined in the folder "Reference" and should never be modified.

(e) calcfluY.m

The program calcfluY.m is used to calculate the XRF yield for a XSW scan. The emittance function from the monochromator has to be pre-calculated and transferred into the routine through a global parameter RF. The information of the sample crystal (e.g. F_0, F_H, F_{-H},

…) is transferred into the routine via the input parameter “p” (which is an array) and the acceptance function of the sample crystal is calculated accordingly. The two functions are then convoluted in the routine and the result is used to calculate the XRF yield in the routine for a given set of off-bragg yield, coherent fraction and coherent position using Eq. 4.18.

(a)

#step	refl_norm	ERR
1.0000	0.028953	0.00017316
2.0000	0.033323	0.00019012
3.0000	0.039665	0.00021361
4.0000	0.049105	0.00024802
5.0000	0.061588	0.00029210
6.0000	0.080274	0.00035667
7.0000	0.10774	0.00044968
8.0000	0.15107	0.00059417
9.0000	0.21962	0.00082109
10.000	0.32519	0.0011674
11.000	0.46675	0.0016302
12.000	0.61608	0.0021186
13.000	0.73635	0.0025112
14.000	0.82393	0.0027972
15.000	0.87832	0.0029759
16.000	0.90170	0.0030508
17.000	0.88593	0.0029995
18.000	0.82313	0.0027941
19.000	0.70575	0.0024112
20.000	0.58086	0.0020026
21.000	0.45666	0.0015972
22.000	0.33971	0.0012147
23.000	0.23830	0.00088218
24.000	0.15674	0.00061279
25.000	0.10699	0.00044717
26.000	0.077505	0.00034688
27.000	0.058451	0.00028119
28.000	0.047127	0.00024057
29.000	0.038905	0.00021096
30.000	0.033103	0.00018924
31.000	0.028664	0.00017203
32.000	0.024450	0.00015548

(b)

#step	BrKa (1st10ss)	ERR
1.0000	0.0044804	9.3382e-05
2.0000	0.0046975	8.6562e-05
3.0000	0.0045514	8.7896e-05
4.0000	0.0047933	8.3497e-05
5.0000	0.0045132	9.5577e-05
6.0000	0.0045661	9.2177e-05
7.0000	0.0043753	8.8509e-05
8.0000	0.0043863	8.5517e-05
9.0000	0.0042291	8.4463e-05
10.000	0.0043081	0.00010587
11.000	0.0044211	9.1289e-05
12.000	0.0047949	8.9027e-05
13.000	0.0049225	7.8378e-05
14.000	0.0055161	0.00010223
15.000	0.0061901	0.00010405
16.000	0.0067463	8.8172e-05
17.000	0.0078812	0.00011421
18.000	0.0084148	0.00011373
19.000	0.0091050	0.00012006
20.000	0.0086299	0.00012335
21.000	0.0086679	0.00012869
22.000	0.0080305	0.00014254
23.000	0.0077278	0.00011228
24.000	0.0073368	0.00012223
25.000	0.0070723	0.00011032
26.000	0.0065223	0.00011180
27.000	0.0065847	0.00011289
28.000	0.0060635	0.00011504
29.000	0.0060998	0.00011154
30.000	0.0059907	0.00011106
31.000	0.0059532	9.5729e-05
32.000	0.0059042	9.1447e-05

Figure D.2 Formats for the input (a) XRR and (b) XRF files for SWAM. The columns are separated by a “Tab”. The symbol # at the beginning of a line indicates a comment line. At this point SWAM, like SWAN and DARE, assumes equal angular steps.

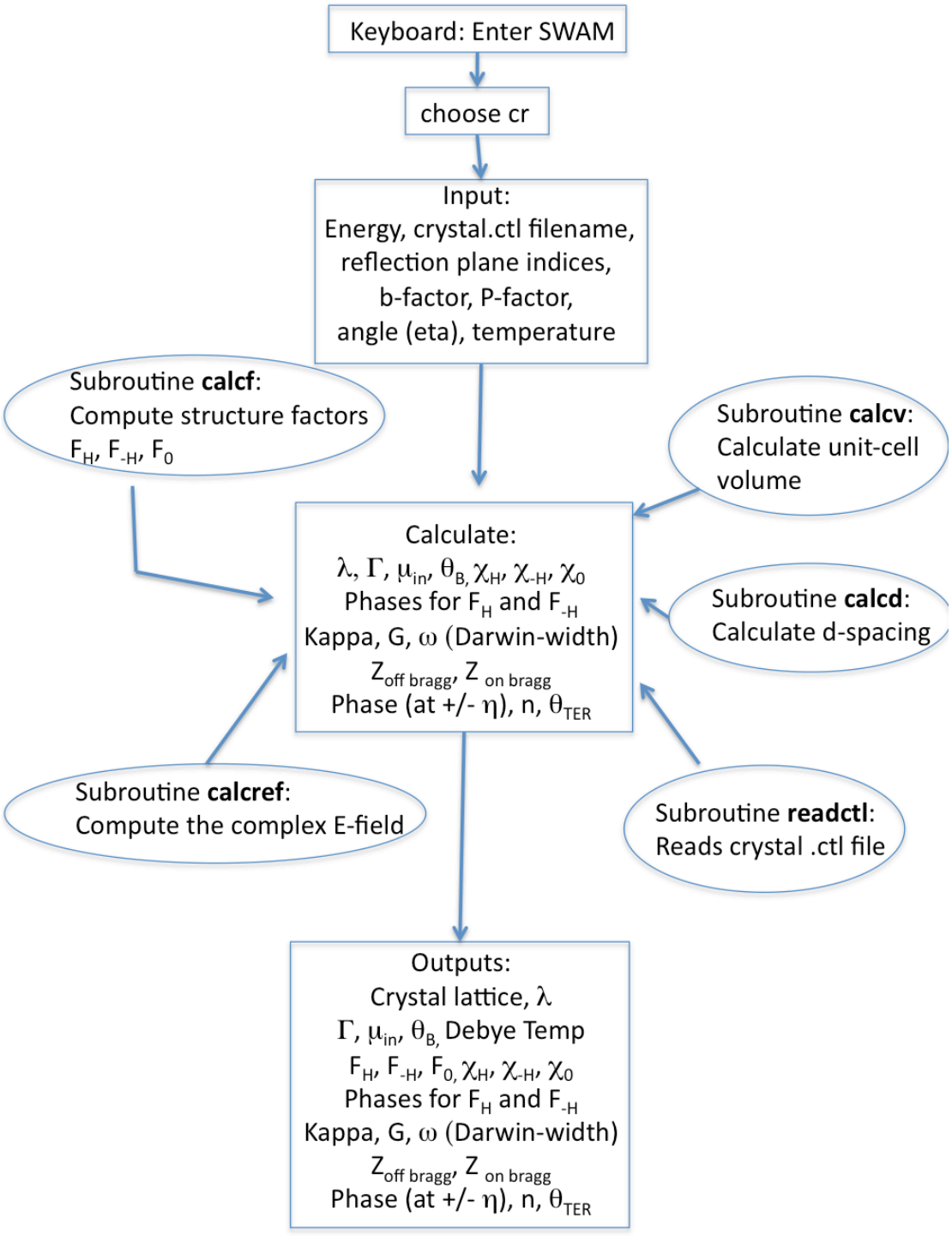

Figure D.3 Flowchart diagram showing the algorithm for computing physical parameters for a single crystal under dynamical diffraction condition.

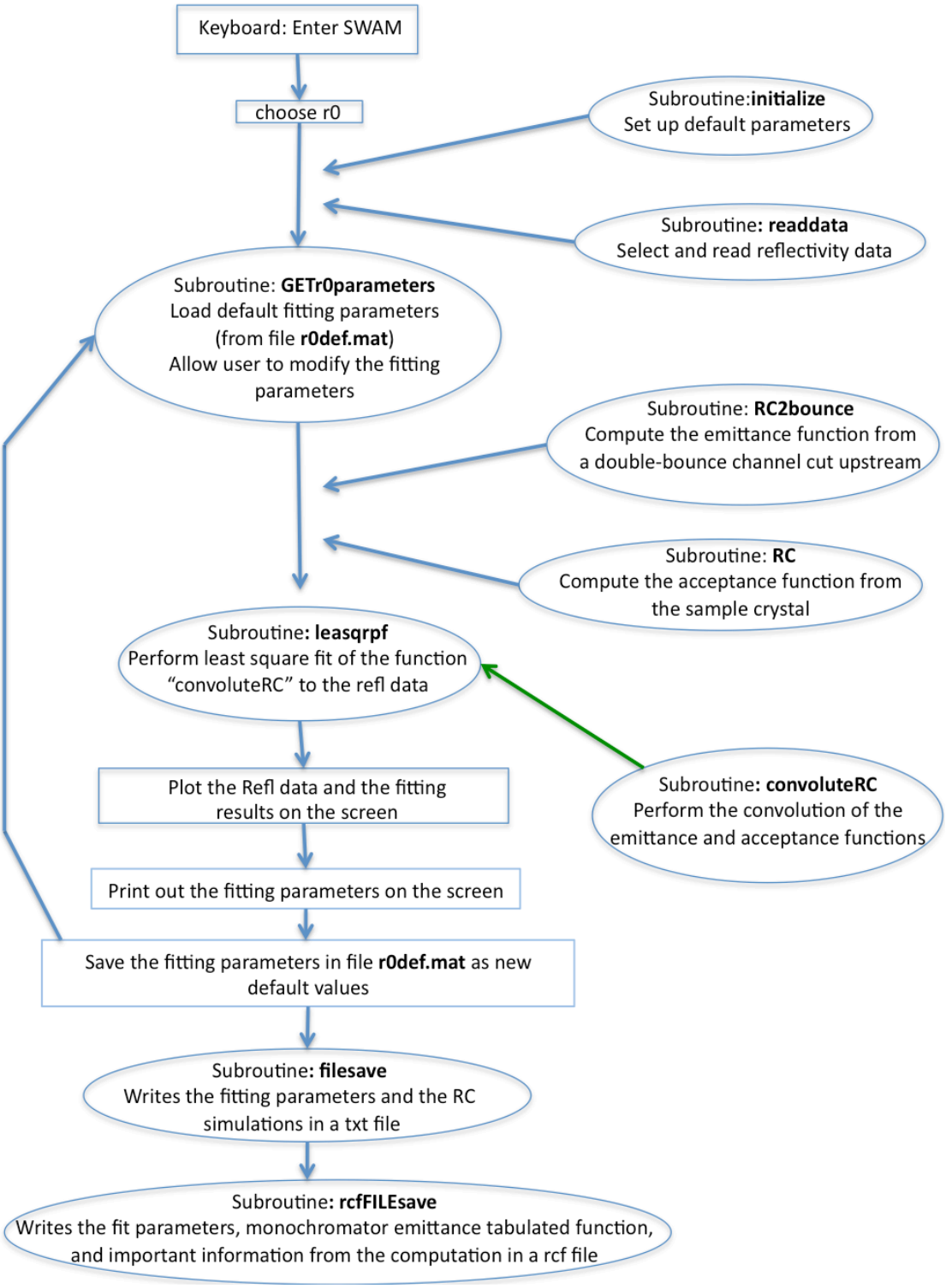

Figure D.4 Flowchart diagram showing the algorithm for rocking curve calculation and fitting in SWAM.

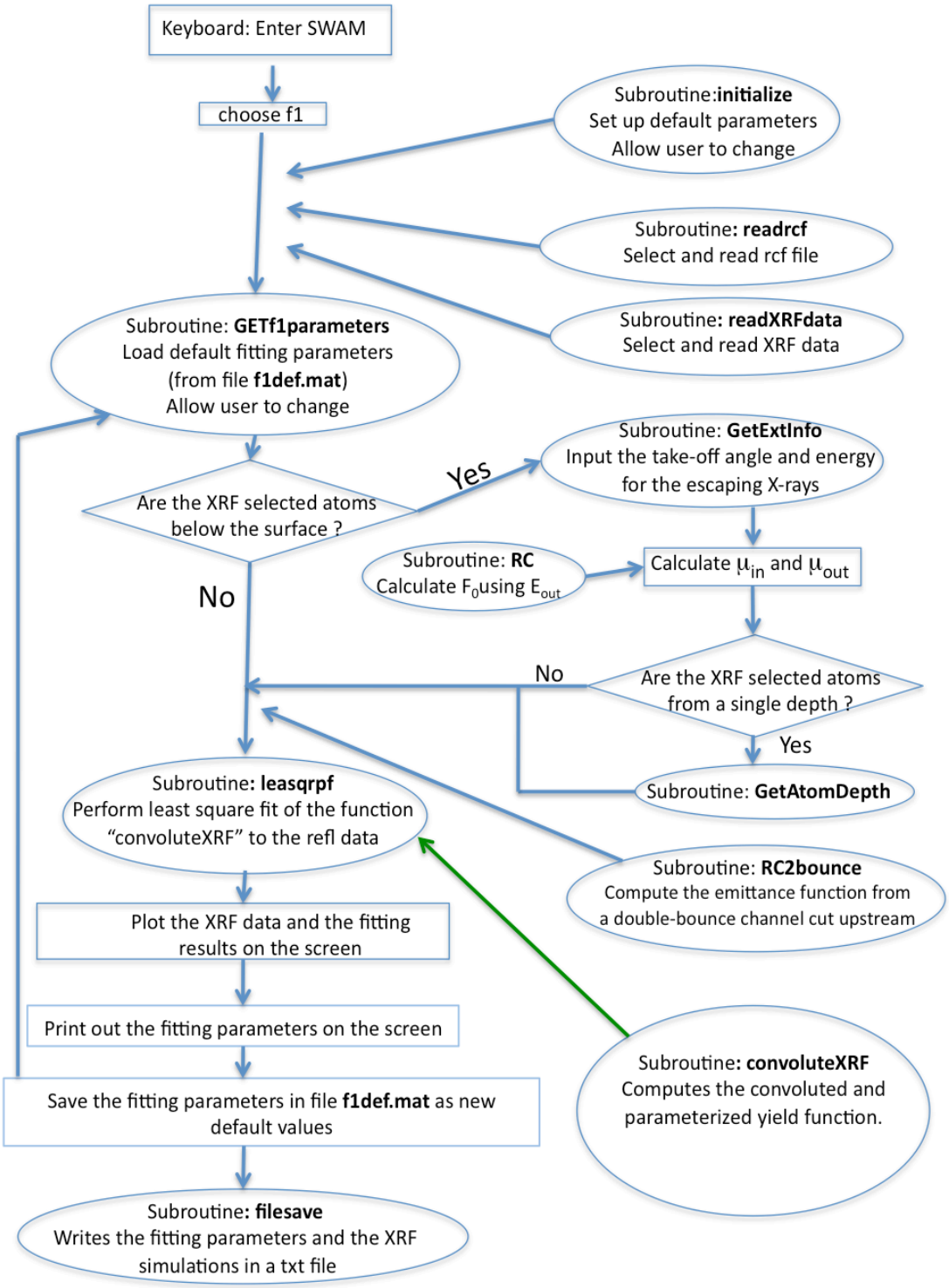

Figure D.5 Flowchart diagram showing the algorithm for fitting the fluorescence yield in SWAM

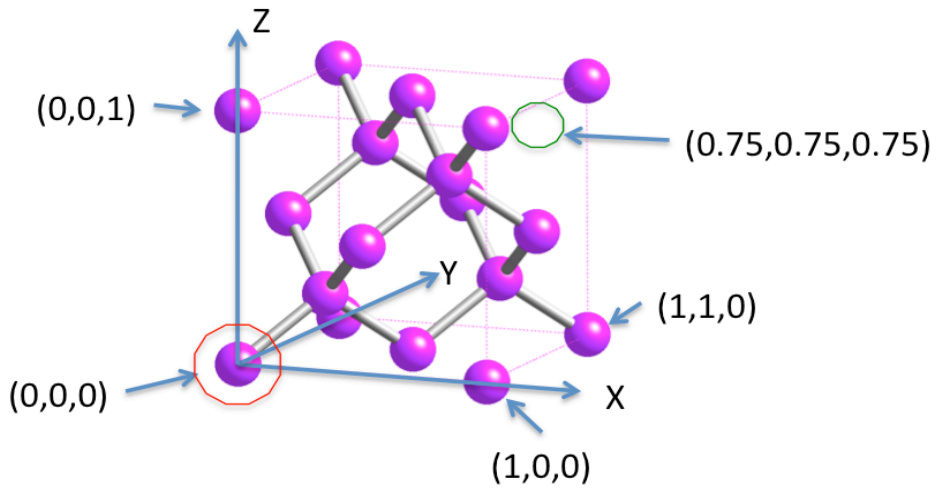

(a) Si.ctl

```
Si
  5.43072   5.43072   5.43072
90.00    90.00    90.00
  625
  4.68     4.68     4.68
  1   1
Atoms in basis # 1
 si    14  1.000
  8
  0.0  0.0  0.0
  0.5  0.5  0.0
  0.5  0.0  0.5
  0.0  0.5  0.5
  0.25  0.25  0.25
  0.75  0.75  0.25
  0.75  0.25  0.75
  0.25  0.75  0.75
```

(b) Si111.ctl

```
Si
  5.43072   5.43072   5.43072
90.00    90.00    90.00
  625
  4.68     4.68     4.68
  1   1
Atoms in basis # 1
 si    14  1.000
  8
  0.125  0.125  0.125
  0.625  0.625  0.125
  0.625  0.125  0.625
  0.125  0.625  0.625
  -.125  -.125  -.125
  -.625  -.625  -.125
  -.625  -.125  -.625
  -.125  -.625  -.625
```

Figure D.6 Two .ctl files for Si crystal. (a) The origin is at the red circle. (b) The origin is at the green circle.